GEOLOGY, STRUCTURE AND MINERALIZATION OF THE ONGUATI AREA, KARIBIB DISTRICT, CENTRAL NAMIBIA

A thesis submitted in fulfilment of the
requirements for the degree of

MASTER OF SCIENCE

in the Department of Geology,
Rhodes University, Grahamstown.

By

WAYNE VILJOEN

January 2005

A southwest-looking view of a large, mineralized sigmoidal-shaped quartz vein at Onguati Mine. This vein, like most in the marbles of the Onguati study area, is associated with a S-type flanking fold. The sheared and fractured marbles below the vein contain malachite staining and patches of gossanous material. Note the isoclinal, Z-shaped drag folds that have developed in the ductile calcitic marbles in the lower middle part of the image. In the upper, middle region of the plate, a series of metre-scale anticlines and synclines with near horizontal fold hinges can also be seen. (see Fig. 6.15 which includes an interpretive sketch of this photo).

ABSTRACT

The study area is situated in the Southern Central Zone of the intracontinental Pan-African Damara Orogen, approximately 20 km NNE of Navachab Gold Mine in the Karibib district of Namibia. Mesothermal vein systems with Cu-Fe±Au mineralization are hosted by amphibolite facies calcitic and dolomitic marbles belonging to the Navachab Member of the Karibib Formation, and are best developed around the defunct Onguati Copper Mine, Brown Mountain and Western Workings areas.

The Onguati study area is located in the saddle region of a moderately-to-gently inclined anticlinorium that experienced significant flattening during NNW–SSE-directed compression. The parallelogram arrangement of ENE- and NNE-trending thrusts and reverse faults that surround the Onguati study area may have developed when the direction of greatest principle subregional stress was oriented WSW-ESE. These structures define part of a Riedel shear system and later faults may have developed in the position of R and P shears respectively. Significant strain partitioning occurred between the ductile calcitic marbles which host the best developed, shear-related vein systems and the more competent dolomitic marbles.

The thickness distributions of veins in the marbles of the Onguati Mine, Brown Mountain and Western Workings areas conform to a fractal or power-law distribution. The most intensely mineralized vein systems in the Onguati Mine and Western Workings calcitic marbles share similar low fractal dimensions (D-values) of 0.41 and 0.37 respectively. Veins in the calcitic and dolomitic marbles of the Brown Mountain area and in the dolomitic marbles of Western Workings have elevated D-values (>0.60) and are poorly mineralized. The low D-values (<0.40) of the well mineralized vein systems reflect the higher degree of fracture connectivity. These vein systems were capable of efficiently draining and localizing large volumes of mineralizing fluids from crustal-scale structures.

A metamorphic devolatization model is proposed where the entire Damaran meta-sedimentary and meta-volcanic package is seen as a large source area of very low concentrations of Cu, Au and other metals. Localization of deformation into crustal-scale faults and shear zones led to regional-scale hydrothermal fluid flow and focussing into the upstream fracture networks of the Onguati study area. Strong mineralization resulted when fluids encountered the reactive marble lithologies.

"Big whorls have little whorls
Which feed on their velocity,
And little whorls have lesser whorls
And so on to viscosity"

– LEWIS F. RICHARDSON

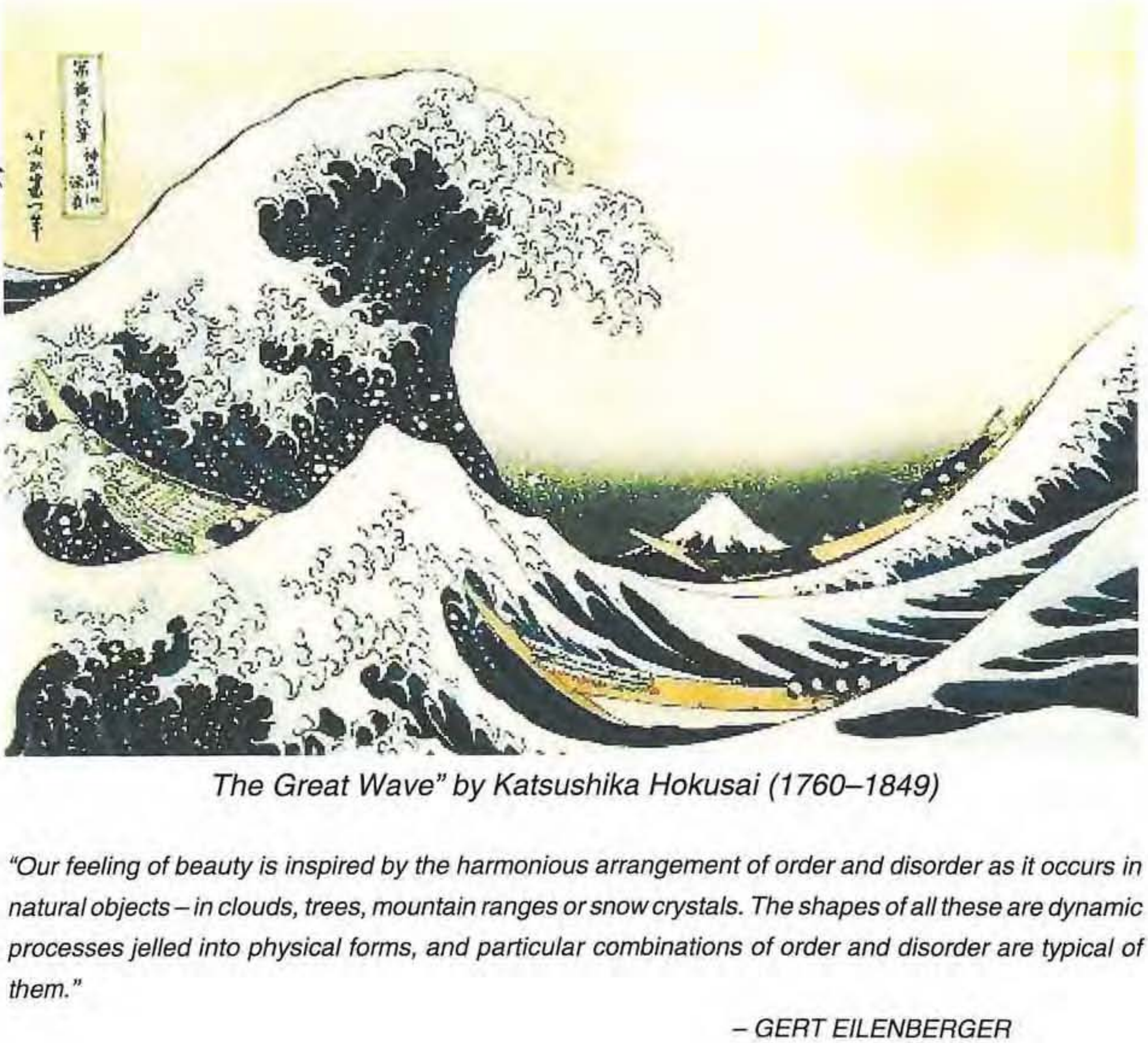

The Great Wave" by Katsushika Hokusai (1760–1849)

"Our feeling of beauty is inspired by the harmonious arrangement of order and disorder as it occurs in natural objects – in clouds, trees, mountain ranges or snow crystals. The shapes of all these are dynamic processes jelled into physical forms, and particular combinations of order and disorder are typical of them."

– GERT EILENBERGER

"What really interests me is whether God had any choice in the creation of the world"

– ALBERT EINSTEIN

CONTENTS

MAP POUCHES: *(*Digital copies of all the maps are provided on the CD at the back of this thesis)*

ILLUSTRATIONS

**High resolution digital copies of the photographs used in the illustrations are included on the CD at the back of the thesis.*

APPENDIX C:

PLATES

**High resolution digital copies of the photographs used in the plates are included on the CD at the back of the thesis.*

Page

TABLES

APPENDIX C:

ABBREVIATIONS USED IN TEXT AND DIAGRAMS

ZONE BOUNDARIES

AM	Areb Mylonite
OL	Okahandja Lineament
OML	Omaruru Lineament
WF	Waterberg Fault
AF	Autseib Fault/ Lineament
OT	Otjihorongo Thrust
PL	Purros Lineament
ST	Sesfontein Thrust

CRATONS

WC	West African craton
CC	Congo Craton
KC	Kalahari Craton

MAGNETIC LINEAMENTS

ABL(i)	Abbabis Lineament (Corner, 1983)
ABL(ii)	Abbabis Lineament (Corner, 2000)
WL	Welwitschia Lineament

DAMARA AND KAOKO BELT TECTONOSTRATIGRAPHIC ZONES

NCZ	Northern Central Zone	NP	Northern Platform and Foreland
SCZ	Southern Central Zone	NZ	Northern Zone
OLZ	Okahandja Lineament Zone	WKZ	Western Kaoko Zone
SZ	Southern Zone	CKZ	Central Kaoko Zone
SMZ	Southern Margin Zone	EKZ	Eastern Kaoko Zone
SF	Southern Foreland and Platform	SKZ	Southern Kaoko Zone
NNC	Naukluft Nappe Complex		

STUDY AREA

OBW	Onguati-Brown Mountain-Western Workings	ONG	Onguati Mine mapping area
BMD	Brown Mountain region diamond drill hole	BMT	Brown Mountain mapping area
BMP	Brown Mountain region percussion drill hole	WW	Western Workings mapping area

FRACTAL GEOMETRY

N/m	Number of veins with a thickness $\geq$t per metre transect
C	Frequency of veins $\geq$unit thickness (constant of proportionality or prefactor parameter)
t	Vein thickness
D	Fractal dimension or D-value (in terms of space filling it is also referred to as the Hausdorf-Besicovitch Dimension)

TOWNS

Kb	Karibib	Sw	Swakopmund
Ok	Okahandja	T	Tsumeb
Om	Omaruru	WB	Walvis Bay
Ot	Otavi	U	Usakos

COMPANY NAMES

AAPSN	Anglo American Prospecting Services Namibia
GFN	Gold Fields Namibia
GSN	Geological Survey of Namibia

MARBLES: **CM** Calcitic Marble **DM** Dolomitic Marble

1. INTRODUCTION

1.1 Location and Geography of the Onguati Study Area

The Onguati study area is located in central Namibia, about 15 km NNW of Karibib town and lies approximately 20 km to the NNE of the Navachab Gold Mine (Fig. 1.1). The field area is situated on the farm Onguati 52, and is less than 5 km from the foothills of the prominent Erongo Complex. Access to the study area is via unpaved roads, either through the farm Karibib 54 from the Windhoek-Swakopmund main road, or across the farm Daheim 106 from the Omaruru main road. The Walvis Bay-Tsumeb railway line lies a few kilometres to the west of the Onguati field area. A major set of power lines, running roughly north-south, cuts across part of the study area.

The Onguati study area consists of three known, closely-spaced mineralized zones, which include the areas over and immediately around the defunct Onguati Copper Mine, Brown Mountain and the dormant Western Workings (Digital Elevation Model, DEM, is shown in Fig. 1.2). The field area is located in the saddle of a doubly-plunging, anticlinorium and is entirely underlain by marbles of the Karibib Formation. The Onguati study area falls on the southeastern corner of the 1:250 000 scale, 2114-Omaruru Geological sheet.

The topography of the Onguati study area consists of well exposed, relatively steep-sided hills often capped by more resistant dolomitic marbles, and lower-lying calcrete and sand-covered plains (Fig. 1.2). The climate is arid and the vegetation is scrub-like and sparse. The region is drained by the ephemeral Khan River and its many streams and tributaries.

1.2. Exploration and Previous Study

The Onguati region has had a long history of mineral exploration and exploitation. Frommurze *et al.* (1942) provide some of the earliest accounts of the geology and mineral deposits of the Karibib region. In their accounts they describe stanniferous pegmatites in the western part of Onguati 52 with minor amounts of blue tourmaline and lepidolite They also refer to the "gossan deposit" found "3 miles south of the Etiro river along the Etiromund-Karibib road on Onguati 52" (Frommurze *et al.*, 1942, p.118). This zone of ferruginous material with jasper and chrysocolla infilling was to become the site of the Onguati Copper Mine years later, and eventually to be the focus of repeated gold exploration after the discovery of the Navachab

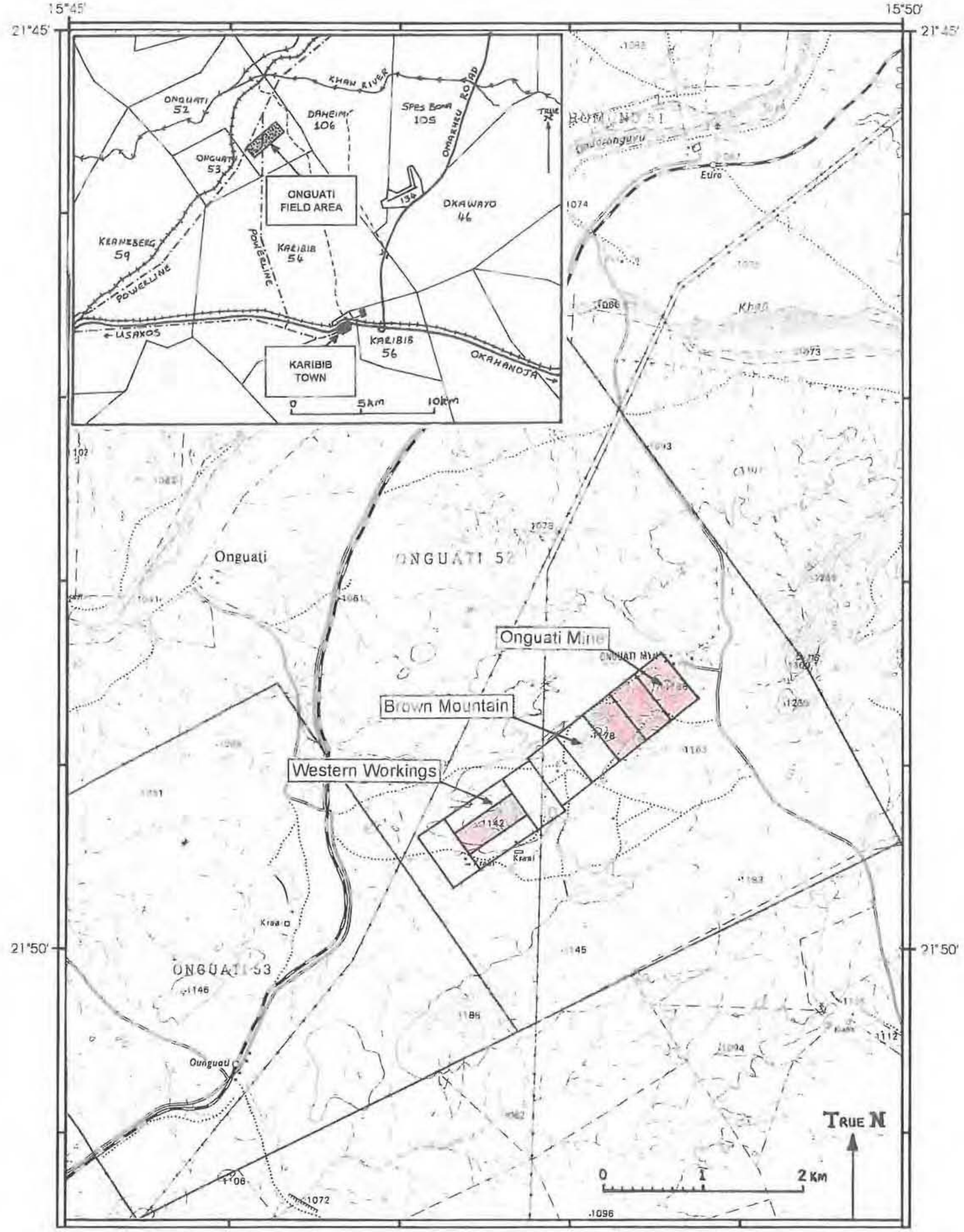

Fig. 1.1: Locality map of the Onguati study area, showing the position of the Western Workings and Onguati Mines, and Brown Mountain (scale 1:50 000). Shaded areas held by A.C. Maclaren; open areas J.S. Theron. Claim positions are based on Petzel, 1988, Fig. 2, p.3 and are marked on a portion of the 1:50 000 scale topographic map, Sheet 2115DD - KARIBIB (first edition).

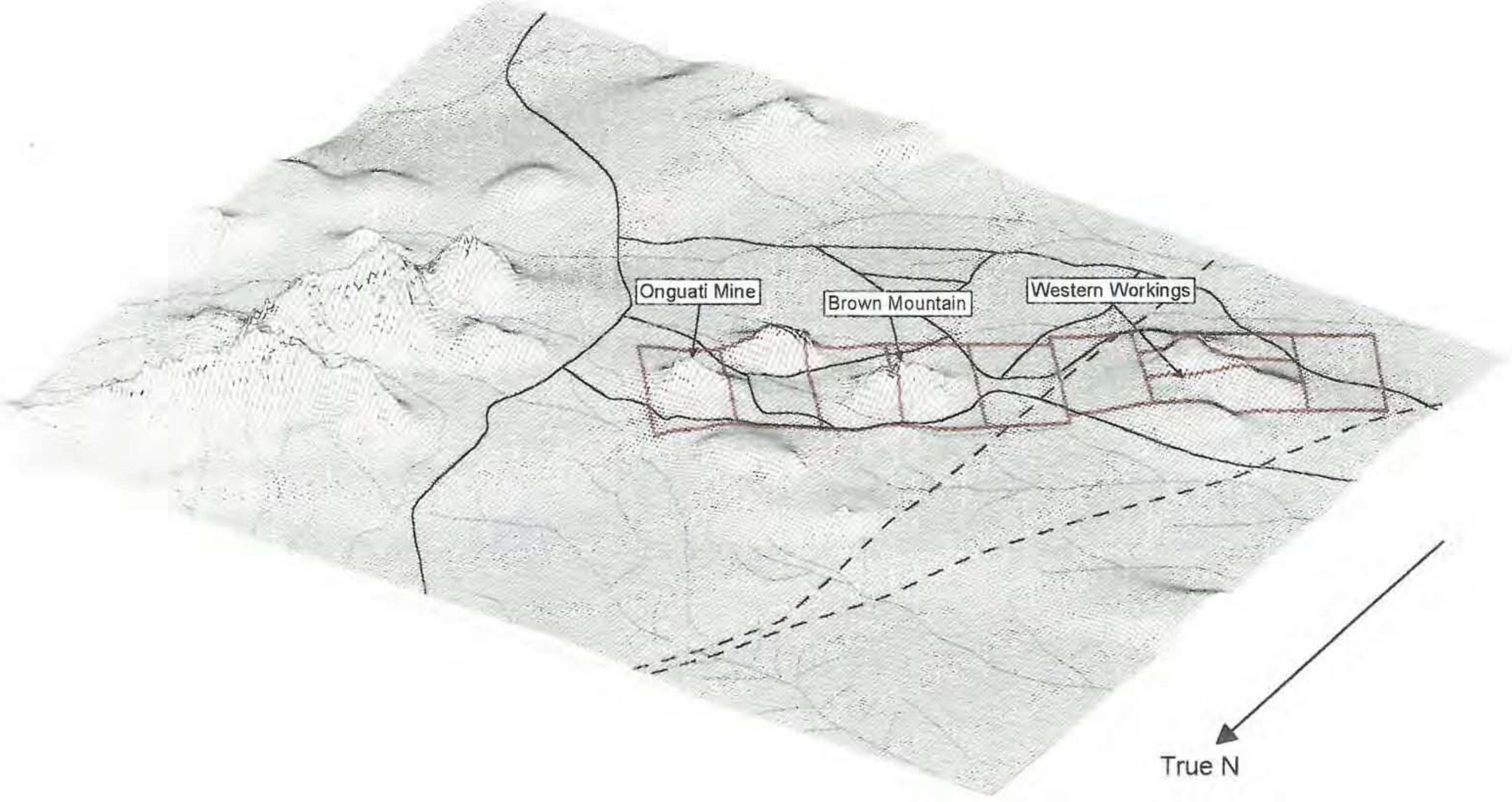

Fig. 1.2: DEM of the Onguati study area and surrounds constructed from the 1:50 000 scale, 2115DD topographic map of the Karibib region. The claim boundaries are shown in red, dirt roads as black lines, powerlines as dashed lines and ephemeral rivers and tributaries in blue.

gold skarn in the mid 1980s. Table 1.1 summarizes the history of mining and briefly describes the exploration strategies employed by companies in the region. Appendix A provides more detail on the mining history and gold exploration of the Onguati 52 area.

Recently, the Karibib region including the Onguati-Kranzberg anticlinorium, was remapped at 1:250 000 scale (sheets 2115B and D) by the Geological Survey of Namibia (Badenhorst, 1992). The Karibib Formation carbonates along this structure have also been examined for their potential use as fillers in the paper and paint industries, and for cement manufacture (Bessinger, 1994). Along with exploration in the vicinity of the Navachab gold-bearing skarn and vein system, there has been a significant amount of scientific interest in the various hydrothermal deposits of the region. Some of the earliest published work on the gold mineralization in this part of the Damara Orogen was by Pirajno & Jacob (1991). A comprehensive account of the epigenetic Au, W, Sn and rare earth element mineralization of the Usakos-Karibib-Omaruru region is also given by Steven (1993). Steven *et al.* (1994) review the main gold occurrences in the northern and central zones of the Damara Orogen, and emphasize the importance of structure in deposit formation. More recent research has centred on the possible genetic connection between mineralization and igneous rocks at Navachab (Meinert, 1998; Nörtemann *et al.*, 2000), and has made use of SHRIMP geochronology (Moore & Jacob, 1998; Jacob *et al.*, 2000a, b). The genetic aspects of gold mineralization at Navachab and in the surrounding region have yet to be resolved, and will probably require a thorough investigation of fluid inclusions and the compilation of an extensive stable isotope data base (Steven *et al.*, 1994).

Although some detailed geological mapping (including the underground workings) has been carried out by Gray (1988), and the geology of the Onguati study area described (Gray, 1988; Petzel, 1988a), very limited work has been done on the structural relationship to mineralization. Steven (2000) recommended that the Onguati Ridge should be reviewed with emphasis on detailed structural mapping and lineament interpretation of the existing aeromagnetic data. Steven (2000) also advocated renewed exploration at Onguati with 1:10,000 scale geological mapping of rock types, structure and superficial cover; a high-resolution bulk leach extractable gold (BLEG) survey in the surrounding drainage system; a rock-chip sampling exercise that includes host rock-vein selvedges, in addition to pure vein material; and a reverse circulation (RC) drilling programme for soil gold and metal anomalies. Following the motivation of Steven (2000), AngloGold commissioned a short study in May 2000 to assess the structural controls on Au mineralization in the Karibib district (Dirks & Mikhailov, 2000).

Table 1.1: History of mining and exploration techniques applied in the Onguati region.

	Copper mining	Mapping			Regional aeromagnetic survey	Stream sampling	Soil sampling	Chip sampling	Electromagnetic survey (EM)	Ground magnetic survey	Induced polarization survey (IP)	Direct current resistivity	Percussion drilling	Diamond drilling
		1:6500	1:2500	1:500										
Atlas Mining Company (1959-1961)	✓													✓
NV Billiton Maatschappij (1960s)									✓					✓
Cu Ventures (Pvt) Ltd. (1972-1973)	✓													
Anglo American Prospecting Services Namibia (1986-1989)						✓	✓							
Gold Fields Namibia (late 1986-1988)			✓	✓		✓	✓	✓		✓	✓	✓	✓	✓
Genmin (1990-1992)		✓	✓		✓	✓	✓	✓	✓	✓	✓			

1.3. Reasons for Undertaking this Study

The primary reason for undertaking this study was to address aspects of the Onguati geology that were poorly defined in previous research. Although many years of mining and exploration have been undertaken on the farm Onguati 52, specifically around the Western Workings and Onguati Mines and over Brown Mountain, very few accounts describe the structural geology in any detail. In fact many of the early Navachab skarn-type exploration models solely emphasized the importance of lithological control on mineralization. The most serious deficiency in the geological descriptions of the Onguati field area is the lack of vein orientation data for the three known mineralized areas, which show not only different styles of veining, but also starkly different mineralization. A clear understanding of vein orientation is also critical for the siting of effective exploration drill holes (at the time of writing a drilling programme was underway in the Onguati study area). There has also been a particular need for structural data on the quartz-tremolite veins in the dolomitic marbles of the field area, because similar style vein systems elsewhere in the Karibib district, have yielded irregular, but significant concentrations of gold (Steven, 2000, p.5)

The Onguati hydrothermal system appears to be related to the same regional mineralization event that resulted in the formation of the Navachab gold deposit. In light of this, it may be useful to compare the style and mineralization of the Onguati vein system to that of the Navachab Gold Mine, and thus elucidate the fundamental controls of economic Au deposition. In addition, better geochronological constraints on granite emplacement, deformation and mineralization have become available for the Navachab area, and as a consequence, new or refined mineralization models have been developed. Hence there is a need to review the genetic models suggested for the Onguati study area, relate them to regional mineralization, and develop holistic exploration models for the Usakos-Karibib-Omaruru region.

Finally, there is a dire need to understand the Au and metal hydrothermal mineralization of the Central Zone (see chapter 2) with respect to the geodynamic processes which shaped the Damara Belt. There is still debate on an ensialic or a plate tectonic origin for the Damara Belt, and until this issue is better resolved, exploration models will lack the ability to make predictions of other types of mineralization that have yet to be found, or of economic Au deposits in other zones of the orogen. The Mesoproterozoic through to the Neoproterozoic is also a period that appears devoid of gold-vein formation worldwide (Goldfarb *et al.*, 2001). Consequently, the Late Neoproterozoic Au mineralization of the

Damara Orogen is of particular interest, especially since many Pan-African terranes are assumed to have poor potential for Au mineralization.

1.4. Aims of this Study

The main aim of this thesis is therefore to describe and map the structural geology of the Onguati study area over a range of scale. Particular emphasis is placed on vein orientation, morphology and distribution, and the temporal and spatial relationship of veins to other structures in the Onguati Mine, Western Workings and Brown Mountain areas. Because mineralization is hosted in vein swarms over the study area, a related aim is to examine the relationship between structure and mineralization, and to determine which structures are important and at what scale they exert control.

A basic premise of this study, is that mineralizing fluids make use of interconnecting fracture systems to transport gold and sulphides from source to sink. This study aims to characterize the connectivity of these fracture or vein systems in terms of their fractal geometry. The purpose of this work is to better characterize the Onguati vein network so that a basic model can be developed which integrates structure and fluid flow along with previously recognised controls, such as lithology, on mineralization. This model should be able to explain the structural patterns, fluid dynamics and mineralization styles observed in the study area, and should have application to regional exploration.

1.5. Logistics and Methods Employed

This study is based on just over three months of fieldwork in the Onguati study area, undertaken by the author between April and July of 2001. Detailed 1:500 scale mapping was carried out within the existing Goldfields-Genmin grid, but was focussed primarily over the better exposed and mineralized parts of the Onguati Mine, Brown Mountain and Western Workings locales. For the most part the grid is composed of 20 x 20 m or 20 x 40 m cells but in areas with poor exposure or devoid of veining the grid spacing reduces to 20 x 120 m across strike. Basic lithological contacts and a variety of structures were measured and mapped. In addition, fresh samples were collected for the preparation of thin sections, probe sections and polished ore briquettes. Host-rock material was also sampled for X-ray fluorescence (XRF) analysis. A small, vehicle-mounted core drill was utilized to extract up to 50 cm lengths of fresh carbonate and vein material with unaltered sulphides.

Remote sensing techniques and airborne geophysics were used in combination with conventional field mapping to gain insight on the crustal structure of the region, and in more detail, to identify the lineaments and lithological contacts found in the Onguati-Kranzberg anticlinorium. Remote sensing relied on the interpretation of a series of 1:80 000 scale, black and white aerial photographs, as well as a mosaic of 1:10 000 scale aerial photographs commissioned by Navachab Mine. Access to high resolution airborne geophysics was granted by kind permission of the Geological Survey of Namibia (GSN), and a qualitative analysis carried out.

Samples collected from the Onguati study area were also analysed by X-ray diffraction (XRD) to confirm petrography. Carbonate and sulphide material was analysed by electron microprobe for geothermobarometry purposes, as well as to search for 'invisible' gold potentially held by sulphides, and to identify minor phases difficult to confirm optically. Preliminary carbon and oxygen stable isotope work was also carried out at the University of Cape Town on host rock material adjacent to veining.

2. GEOLOGY AND GEODYNAMIC EVOLUTION OF THE DAMARA OROGEN

2.1. Damara Orogen as part of the Pan-African Belt System

The Damara Orogen of Namibia forms an integral part of the extensive system of belts, known collectively as the Pan-African, that surround and transect the African continent (Fig. 2.1). The Damara Orogen is commonly described (e.g. Martin and Porada, 1977) as having a coastal branch which extends along the Atlantic continental margin, and an intracontinental branch which separates the Congo and Kalahari Cratons. Since Kennedy (1964, pg. 48) first defined the "Pan-African Thermo-Tectonic Episode" as a "major process of structural differentiation", there has been much progress in understanding the geodynamic evolution and subsequent history of the African continent. In this regard, research on the well exposed Damara Orogen has proved to be a cornerstone in understanding Late Precambrian sedimentation and tectonism.

The Pan-African event affected large parts of the African Platform, including the offshore Madagascar and Seychelle Islands, and also extended into adjoining, but now separated, areas of South America, Australia and Antarctica (Fig. 2.1). The Pan-African was one of the planet's most spectacular mountain-building events. It represented the final episode in a long history of spasmodic Precambrian instability, after which the African continent remained notably unaffected by widespread orogeny (Tankard *et al.*, 1982).

The development of this major belt system either commenced on a single supercontinent (Piper, 1982), or on two major continental fragments named "East Gondwana", constructed from Australia, India and Antarctica, and a united Africa-South America landmass named "West Gondwana", as is shown in Fig. 2.1 (McWilliams, 1981). East and West Gondwana subsequently collided along the Pan-African Mozambique Belt, which extends up the eastern margin of Africa to join with the Red Sea fold belt (Porada, 1989). Together with palaeomagnetic data, this situation implies that the majority of Pan-African belts must have evolved from continental rift structures, with wide ocean opening being the exception (McWilliams, 1981; Porada, 1989).

The Pan-African system of belts that developed in the southern parts of West Gondwana bears testimony to the assembly of the Congo, Kalahari and Rio de la Plata cratons (Miller, 1983c). Although at odds with the Pan-African palaeomagnetic data of

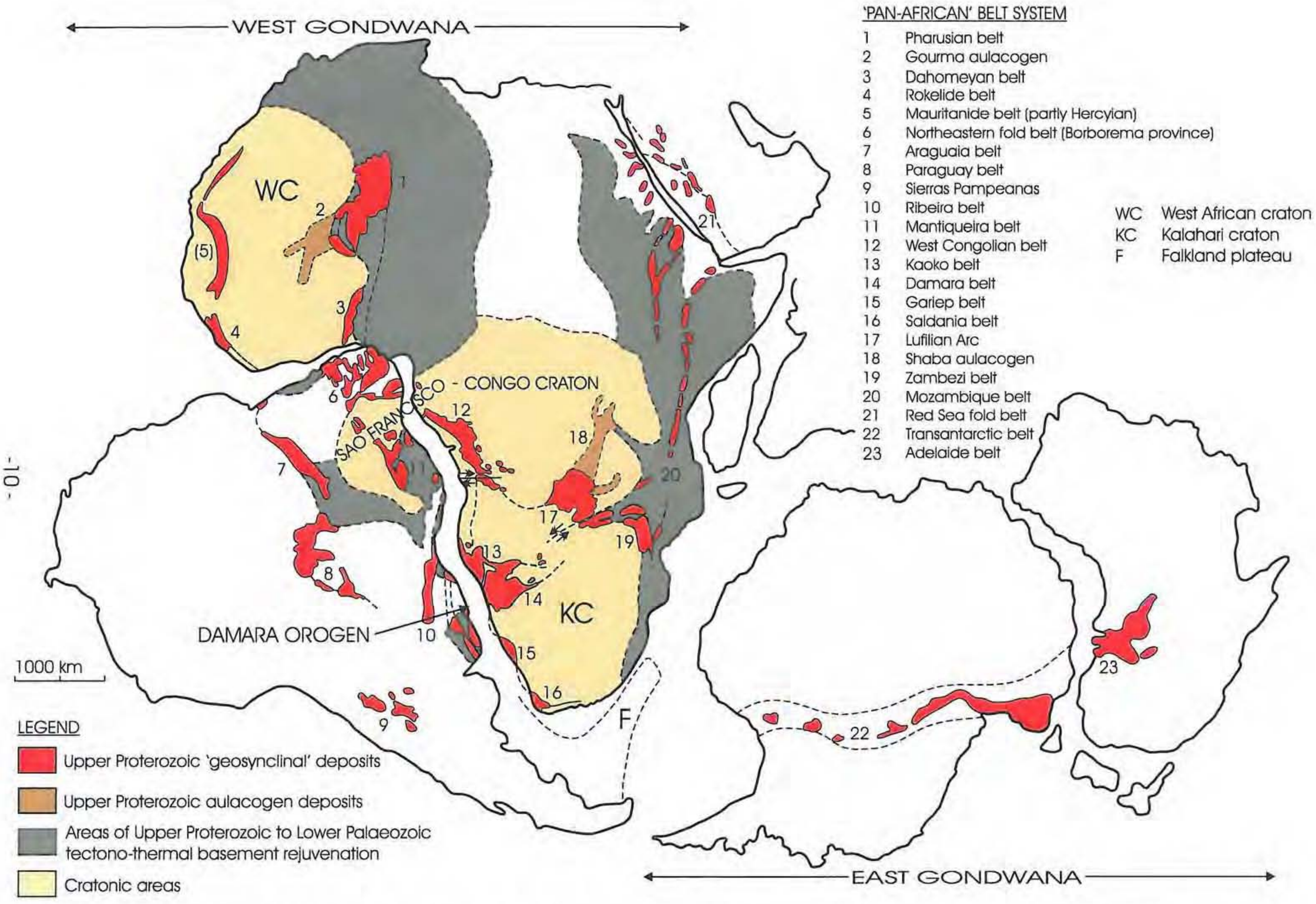

Fig. 2.1: Configuration of the upper Proterozoic Pan-African belt system with extensions into South America, Antarctica and Australia on a pre-drift assembly of the Gondwana continent (modified after Porada, 1985, Fig.1, p.240; Porada, 1989, Fig.1, p.105)

McWilliams (1981), there is significant evidence of ocean opening, subduction and continental collision along the Atlantic coastal regions of southern and equatorial Africa and Brazil. Porada (1989) reconciles these facts, and envisages that Africa and South America were never completely separated by an upper Proterozoic 'wide' ocean (as per Fig. 2.1). Instead, the Pan-African and Brasiliano belts may have evolved from continental rifts, with nominal contact maintained along the São Francisco-Congo cratonic bridge during the entire Pan-African cycle (Porada, 1989). Probably only in the southern half of this major rift system, where it was at its widest, was there creation of new oceanic crust (Porada, 1985, 1989).

2.2. General Features and Tectonostratigraphic Zones of the Damara Orogen

The Damara Orogen consists of two branches (Fig. 2.2), the coastal Kaoko Belt named after the province in Namibia where it is mainly exposed (Hoffmann, 1983), and the intracontinental, almost 400 km-wide Damara Belt *sensu stricto* (Porada, 1989). The coastal and inland branches of the Damara Orogen are thought to have evolved during scissor-like continental rifting between Africa and South America (Porada,1989). Porada (1983, 1985) suggests that rifting would have initially begun in the south, propagating northwards from the Gariep belt. An offshoot from this major rifting event may have deviated northeastwards between the Congo and Kalahari Cratons to form the inland branch of the Damara Orogen (Porada, 1989). If this is the case, then early models attempting to explain the apparent radiating structure of the Damara Orogen might be misleading. Perhaps then, it does not serve any useful purpose to group the coastal and intracontinental branches as the Damara Orogen, if they merely represent the welding and partial overprint of one Pan-African Belt over another. In the following, these possible, genetically distinct belts will be referred to as the Kaoko Belt and Damara Belt *sensu stricto*, and the use of the term Damara Orogen will be avoided where possible.

2.2.1. Kaoko Belt

The Kaoko Belt, formerly known as the Northern Coastal Branch, links southwards with the Gariep and Saldania Belts of South Africa, and may connect northwards with the West Congo Belt as shown in Fig. 2.1 (Martin and Porada, 1977). The relatively poorly exposed chain is thought to extend some 1200 km northwards along the Atlantic coastal margin of Africa (Miller, 1983c). Tentative correlations have even been proposed with the Dahomeyan and

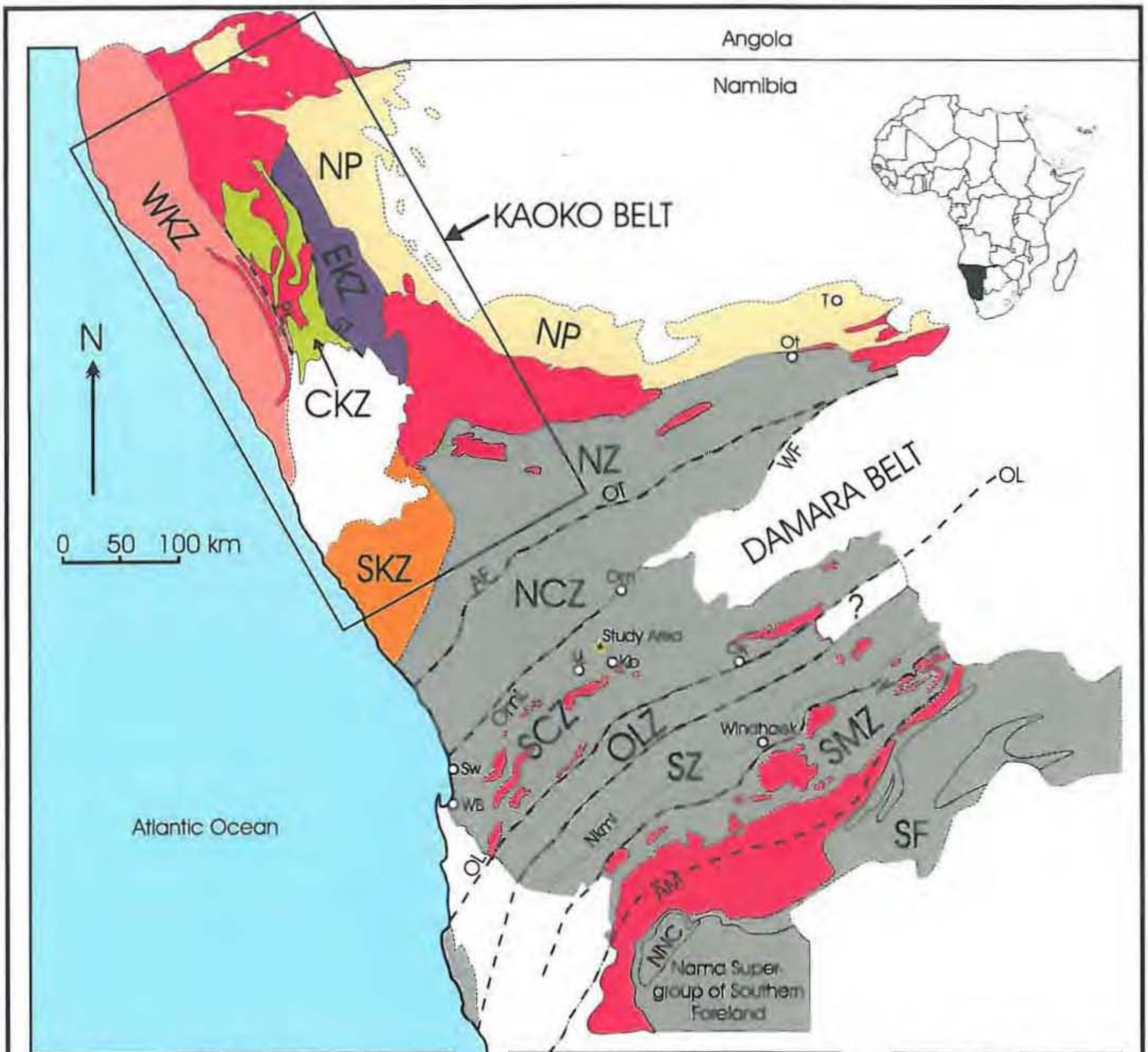

Geological Key

☐ Large areas of post-Damaran cover

🟥 Pre-Damara Basement

** Abbreviations and symbols for the Damara Belt sensu stricto are provided in Fig. 2.3. Details of the Damara Belt tectonostratigraphic zones are also provided in the text.*

Zone Boundaries

AM	Areb Mylonite
OL	Okahandja Lineament
OmL	Omaruru Lineament
WF	Waterberg Fault
AF	Autseib Fault
OT	Otjihorongo Thrust
PL	Purros Lineament
ST	Sesfontein Thrust

Towns

Kb	Karibib
Ok	Okahandja
Om	Omaruru
Ot	Otavi
Sw	Swakopmund
T	Tsumeb
WB	Walvis Bay
U	Usakos

Tectonostratigraphic Zones		Basic Geological Charateristics
WKZ	Western Kaoko Zone	High temperature, low pressure, cordierite-sillimanite-bearing rocks; mainly metagreywackes
CKZ	Central Kaoko Zone	Low temperature, high pressure, kyanite-bearing rocks; intense deformation
EKZ	Eastern Kaoko Zone	Low grade metamorphic rocks; stratigraphically similar to NP; fold intensity increases westwards
SKZ	Southern Kaoko Zone	Consists entirely of turbiditic rocks and underwent intense deformation and interference folding
NP	Northern Platform and Foreland	Overlies Congo craton edge; consists of low-grade platform carbonates; open folding

Fig. 2.2: Tectonostratigraphic zones of the Kaoko Belt and their relationship to the Damara Belt *sensu stricto* (modified after Miller, 1983c, Fig.2, p.434). See text and Fig. 2.3 for explanation of the Damara Belt *sensu stricto* symbols and abbreviations.

Pharusian Belts in north-west Africa, which are situated more than 3000 km away (Miller, 1983c). The Kaoko Belt has been divided into 4 main zones, which are illustrated and briefly described in Fig. 2.2, and are separated from one another by major lineaments and thrust zones (Hoffmann, 1983; Miller, 1983c).

2.2.2. Damara Belt *sensu stricto*

The "intracontinental" (Porada, 1985, p.239) or "intracratonic" (Martin and Porada, 1977, p.312) Damara Belt extends in a northeasterly direction between the Congo and Kalahari Cratons, and disappears beneath the post-Palaeozoic Kalahari basin in the continental interior (Tankard *et al.*, 1982). From here, the Damara Belt may connect with the Lufilian Arc and the Zambezi Belt (Porada, 1989), which continues eastwards to join with the Mozambique Belt (see Fig.2.1). The Damara Belt is exceptional because, unlike its adjoining Pan-African counterparts which have largely experienced basement tectono-thermal reworking, its enormous sediment pile was subjected to elevated metamorphism and voluminous granitic emplacement (Martin, 1983a).

Although it may be possible to correlate some formations across the original Damaran rift systems, there does appear to be asymmetry in the sedimentary facies of the Damara Supergroup. This is paralleled and accentuated by the strong structural and metamorphic asymmetry of the Damara Belt itself (Tankard *et al.*, 1982). It is therefore convenient to divide the northeast trending belt into several zones (Fig. 2.3., p.15) based on stratigraphy, structure, metamorphic grade, plutonic rocks, geochronology and aeromagnetic expression (Barnes and Sawyer, 1980; Miller and Hoffmann, 1981; Miller, 1983c). Based on Miller's (1983c) review of the Damara Belt (Fig. 2.3), these zones are as follows, from north to south:

(i) The *Northern Platform* (NP) is at least 80 km wide and largely overlies the rigid and stabilized Congo Craton (Tankard *et al.*,1982). This zone has consequently been shielded from orogeny and has only experienced weak metamorphism. The low-grade platform carbonates with their extensive marker units, and an overlying molasse succession, have experienced open folding which decreases in intensity, both northwards and eastwards.

(ii) The *Northern Zone* (NZ), also referred to as the Transitional Zone by Martin and Porada (1977), is approximately 40 km wide, and its boundary with the NP and the

Kaoko Belt is marked by a string of large basement inliers (Barnes and Sawyer, 1980). The NP-NZ boundary may also represent a geanticlinal ridge that acted as a hinge zone between the carbonate platforms in the north and the subsiding trough of the Central Zone (see below) to the south (Tankard *et al.*, 1982).

Major NE-trending thrusts make it impossible to correlate formations across the entire width of the NZ, and this, in effect, divides the zone into northern and southern parts. Miller (1983c) suggests that the northern belt should be called the Transitional Zone *sensu stricto* (TZ), as it exhibits both stratigraphic and tectonic resemblance to the NP, and the southern part as the Northern Zone *sensu stricto*. The southern part is characterized by the presence of alkaline volcanic rocks and displays a southward transition to deep-water facies sediments, stratigraphically similar to the Central Zone (see next). Both belts experienced greenschist metamorphism and polyphase deformation, which resulted in tight folds of variable axial trend.

(iii) The *Central Zone* (CZ) is the high-temperature, low-pressure zone of the Damara Belt, and measures approximately 160 km in width. It is characterized by a strong S_0-S_1 parallel-to-sub-parallel schistosity or banding, sillimanite-cordierite metamorphic assemblages, voluminous (more than 50 % of the area) intrusion of pre-, syn- and post-tectonic granitoids, polyphase deformation and complex dome structures (Barnes and Sawyer, 1980; Tankard *et al.*, 1982; Miller, 1983c).

The CZ is tectonically separated into the Northern Central Zone (NCZ) and the Southern Central Zone (SCZ) by the NE-trending Omaruru Lineament-Waterberg Fault. The SCZ, where this study is based, is characterized by several well-exposed basement inliers, its lower level stratigraphy and its different lithofacies to the NCZ, and the occurrence of the oldest Damaran granites *(see chapter 3 for more detail on the SCZ)*.

(iv) The *Okahandja Lineament Zone* (OLZ) takes its name from the distinctive linear feature which marks the southern edge of the CZ. The Okahandja Lineament is a major crustal, ENE-trending feature of the Damara belt, and can be clearly traced on Landsat images for at least 530 km along strike (Downing and Coward, 1981). Across the Okahandja Lineament from the CZ to the OLZ, there is a marked change in the stratigraphic succession, structural style, age of earliest deformation, aeromagnetic patterns and seismic characteristics of the lower crust. One of the most profound

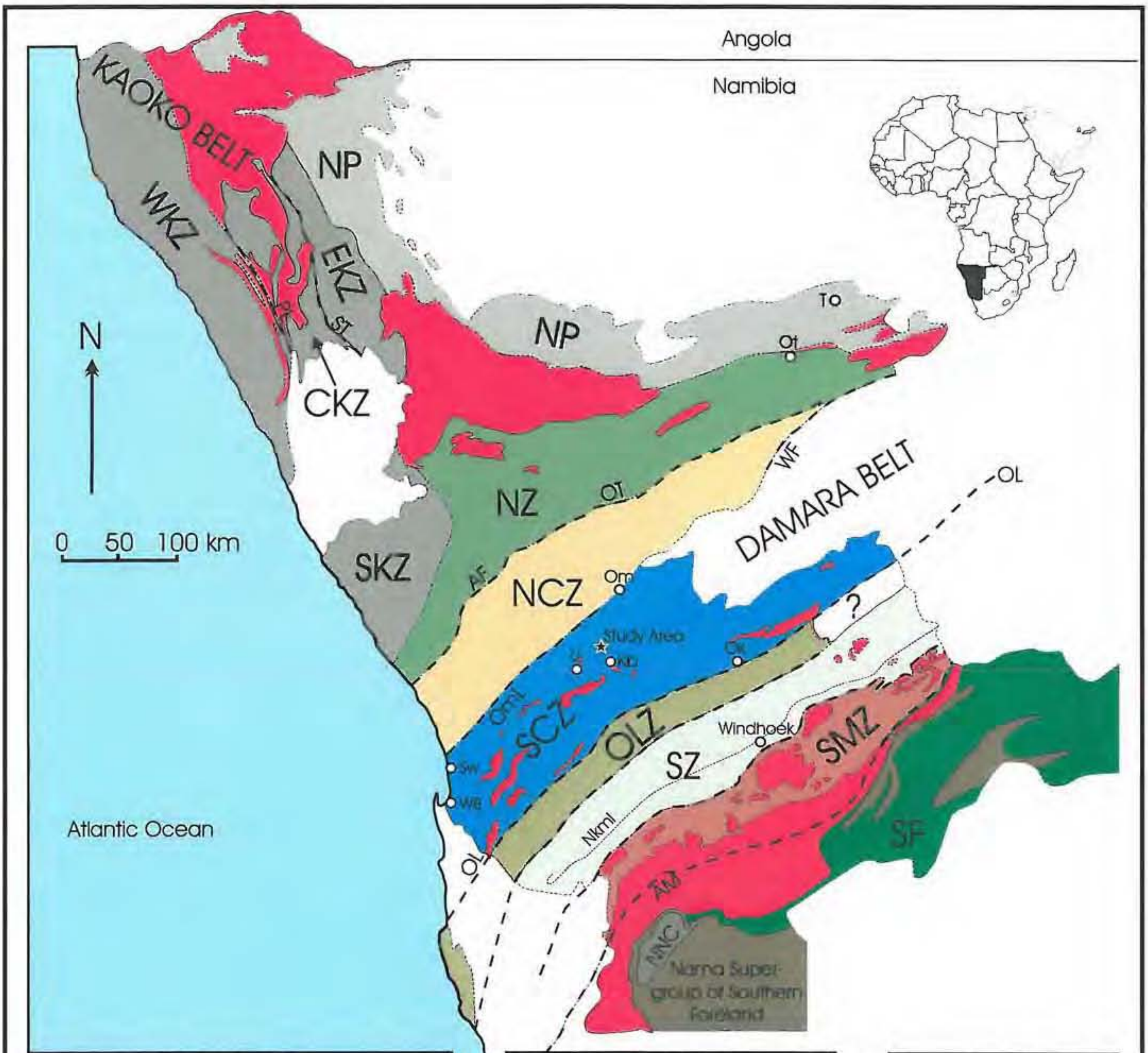

Geological Key	
⬜	Large areas of post-Damaran cover
▩	Nama Supergroup
Nkml	Matchless Amphibolite Member
🟥	Pre-Damara Basement

Zone Boundaries	
AM	Areb Mylonite
OL	Okahandja Lineament
OmL	Omaruru Lineament
WF	Waterberg Fault
AF	Autseib Fault
OT	Otjihorongo Thrust
PL	Purros Lineament
ST	Sesfontein Thrust

Towns	
Kb	Karibib
Ok	Okahandja
Om	Omaruru
Ot	Otavi
Sw	Swakopmund
T	Tsumeb
WB	Walvis Bay
U	Usakos

Tectonostratigraphic Zones		Basic Geological Charateristics
NP	Northern Platform and Foreland	Overlies Congo craton edge; consists of low-grade platform carbonates; open folding.
NZ	Northern Zone	Experienced greenschist metamorphism; deformation resulted in tight folds of variable trend.
NCZ	Northern Central Zone	High temperature, low pressure zone; higher level stratigraphy than SCZ; complex dome structures and granites.
SCZ	Southern Central Zone	High temperature, low pressure zone; lower level stratigraphy than NCZ; abundant basement inliers; complex dome structures; abundant syn- and post-tectonic granites.
OLZ	Okahandja Lineament Zone	High pressure, low-to-moderate temperature zone; occurrence of Donkerhuk granites.
SZ	Southern Zone	Consists predominantly of flysch-type mica schists; enigmatic Matchless amphibolite belt.
SMZ	Southern Margin Zone	Low temperature, high pressure belt; intense over-folding and thrusting towards the southeast.
SF	Southern Foreland and Platform	Overlies northern edge of Kalahari Craton; characteristic Nama Group, Ediacaran fauna fossils.
NNC	Naukluft Nappe Complex	Allochtonous terrane thrust onto the Nama Group sediments of the SF.

Fig. 2.3: Tectonostratigraphic zones of the Damara Belt *sensu stricto* (modified after Miller, 1983c, Fig.2, p.434). Refer to Fig. 2.2 for explanation of the Kaoko Belt symbols.

features is reflected in the abrupt change from high-pressure, low-to-moderate temperature metamorphism in the south, to high-temperature, low-pressure metamorphism to the north of the lineament (Downing and Coward, 1981). The OLZ also experienced intrusion by extensive, post-tectonic, garnetiferous, two-mica granites, known as the Donkerhuk Granite. The northern extent of the Donkerhuk Granite is generally marked by the Okahandja Lineament.

(v) The Southern Zone (SZ) has also been referred to as the Trough Zone (Barnes and Sawyer, 1980) or the Khomas Zone (Hoffmann, 1983). This zone shares the same single lithostratigraphic unit as the OLZ, a flysch-type mica schist, and as a result the two zones have often been referred to as the Khomas Trough (e.g. Martin and Porada, 1977). However there are many differences between the two zones, the most notable of which, includes the persistently south-eastward vergent structures of the SZ in comparison to the more upright OLZ structures. Furthermore, there is the enigmatic occurrence of a linear amphibolite belt, 350 km long and 1 to 3 km wide, which has a MORB-composition in the southern third of the SZ (Miller, 1983c).

(vi) The Southern Margin Zone (SMZ) is up to 70 km wide, and is characterized by intense over-folding, shearing and thrusting towards the southeast. The intensity of deformation gradually increases southwards, so eventually pre-Damara basement slices, in addition to the continental-margin facies of the Damara Sequence, are involved in the thrusting event. Alpine-type serpentinites have been syntectonically emplaced along or near many of the thrust planes. Metamorphic grade increases progressively northwards from greenschist facies in the southern part of the SMZ to amphibolite facies in the mid- to northern-parts of the SZ and into the OLZ. Together with the SZ, the northern portion of the SMZ is characterized as a low-temperature, high-pressure metamorphic belt.

(vii) The Southern Foreland (SF) overlies the northern edge of the stable Kalahari Craton, and gradually passes southwards into an undeformed Southern Platform (SP). The SF and SP share the same characteristic Nama Group sediments, which are world famous for their Ediacaran fauna fossils. Sediment supply was initially from the east and southeast (deposited as the Kuibis and Schwarzrand Subgroups), but as the Damara and Gariep Orogens rose, so sediment supply switched to derivation from the north and west respectively (deposited as the Fish River Subgroup). The Nama Group is tectonically overlain in the northwest by the Naukluft Nappe Complex (NNC).

2.3. Stratigraphy of the Damara Belt

The correlation of lithological units across the Damara Belt, as with many Precambrian orogens, has been problematic because of poor biological control and the scarcity of reliable age determinations with sufficient resolution to be useful (Porada, 1985). In many Precambrian terrains lithostratigraphic subdivisions can only be established for restricted parts of the orogen, and assumptions have to be made concerning their mutual relationships. Correlations across the Damara Belt rely on the interpretation of the Chuos Formation as a glacial deposit and therefore as a chronostratigraphic marker in every part of the belt (Gevers, 1931; Martin, 1965; Miller, 1980; Hoffmann, 1983). The major Damaran subdivisions and correlations (South African Committee for Stratigraphy, 1980) are presented in Table 2.1. Simplistically, this lithostratigraphic chart shows that the Damara Sequence consists of 4 major stratigraphic units, which are from oldest to youngest (Miller, 1983c):

(i) a basal arkosic arenite with local alkaline volcanics and evaporites (Nosib Group);
(ii) a middle carbonate sequence which includes an extensive marker mixtite (Otavi Group in the North and lower Swakop Group in the central parts of the Damara Belt);
(iii) an upper pelitic to semipelitic succession (Swakop Group) which includes the Amphibolite Matchless Member;
(iv) a northern molasse (Mulden Group) and a younger, southern molasse (Fish River Subgroup of the Nama Group).

The Damaran metasedimentary rocks generally overlie older continental basement in most parts of the Damara Belt (Marin and Porada, 1977; Martin, 1983a). Relics of the pre-Damara basement generally yield radiometric ages that suggest there were two periods of tectono-thermally-induced isotopic resetting. The ages fall into either Eburnian (~2000 Ma) or Kibaran (1400 to 900 Ma) time periods (Porada, 1979). Basement inliers in the NZ and CZ are commonly as old as 2.0 Ga (Burger & Walraven, 1976; Jacob *et al.*, 1978), whereas in the south, pre-Damara supracrustal rocks may reflect a significant magmatic event 1.1 Ga ago (Watters, 1976).

Table 2.1: Stratigraphic nomenclature and proposed correlations between the northern carbonate shelf, and the central and southern parts of the Damara Belt, as proposed by the South African Committee for Stratigraphy, 1980 (modified after Martin, 1983a, Table 1, p. 477).

NORTH

GROUP	SUBGROUP	FORMATION	LITHOLOGY (MAXIMUM THICKNESS)
MULDEN		OWAMBO	Shale, marl, siltstone, sandstone (1000 m)
		KOMBAT	Shale dolomite lenses
		TSCHUDI	Quartzite, conglomerate, arkose, argillite (3000 m)
UNCONFORMITY IN NW			
OTAVI	TSUMEB	HUTTEN-BERG	Dolomite with chert shale, limestone, stromatolites, oolites (900 m)
		ELANDS-HOEK	Dolomite with chert stromatolites (1100 m)
		MAIEBERG	Dolomite, limestone, slump breccia (950 m)
		CHUOS	Mixtite, dolomite, limestone, sandstone, itabirite, oolite chert (700 m)
	LOCAL DISCORDANCE		
	ABENAB	AUROS	Dolomite, limestone, marl, shale (450 m) stromatolites
		GAUSS	Dolomite, limestone, oolitic chert, sandstone (750 m)
		BERG AUKAS	Dolomite, limestone, stromatolites, arkose, greywacke (525 m)
LOCAL DISCORDANCE			
NOSIB		VARIANTO	Mixtite, tuff, itabirite
		ASKEVOLD + NAAUWPOORT	Rhyolite, tuff, agglomerate, andesite, epidosite, bostonite (6000 m)
		NABIS	Quartzite, arkose, conglomerate

CENTRE

GROUP	SUBGROUP	FORMATION	LITHOLOGY (MAXIMUM THICKNESS)
SWAKOP	KHOMAS	KUISEB	Quartz-biotite schist, biotite-garnet-corderite schist, amphibolite schist, quartzite, marble, calc-silicate rock (3000 m)
		KARIBIB	Marble, biotite schist, quartz schist, calc-silicate rock (700 m)
		CHUOS	Mixtite, marble, quartzite (700 m)
	LOCAL DISCORDANCE		
	UGAB	ROSSING	Marble, quartzite, conglomerate, biotite schist, biotite-hornblende schist, calc-silicate rock (700 m)
LOCAL DISCORDANCE			
NOSIB		KHAN	Calc-silicate rock, amphibole-pyroxene gneiss and quartzite (1100 m)
		ETUSIS	Quartzite, arkose, conglomerate schist, rhyolite (3500 m)

SOUTH

GROUP	SUBGROUP	FORMATION	LITHOLOGY (MAXIMUM THICKNESS)
NAMA GROUP PARTIALLY ?			
SWAKOP	KHOMAS	KUISEB	Biotite schist, biotite quartzite, graphitic schist, calc-silicate rock, amphibole (matchless member) (10 000 m)
		AUAS	Quartzite, schist, marble, amphibole, itabirite (1800 m)
		CHUOS	Pebbles, schist, mixtite, quartzite, schist, itabirite, amphibolite, calc-silicate rock (1650 m)
	KUDIS	BLAU-KRANS	Graphite schist, quartzite, quartz-mica schist, conglomerate, itabirite (1700 m)
		? HAKOS	Quartzite schist (2000 m)
		CORONA	Dolomite schist, conglomerate (400 m)
LOCAL DISCORDANCE			
NOSIB		DURU-CHAUS	Phyllite, quartzite, conglomerate, limestone (5000 m)
		KAMTSAS	Quartzite, arkose, conglomerate (6700 m)

2.4. Evolution of the Damara Belt

The Damara Orogen has been the subject of intense, multidisciplinary research for the last three decades. The aim of many of these studies has been to elucidate the geodynamic evolution of the intracontinental Damara Belt (Martin, 1983a). The purpose of this section is to review the basic sedimentary and orogenic features of the Damara Belt, with as little bias towards a particular geodynamic model as possible. It is these features which must first be recognized and understood, before a model can be proposed or evaluated, and confidently used in predicting mineral potential. The development of the Damara Belt is most simply viewed as having two stages: an initial rifting phase that created the depositories for sediment infilling; and a second, orogenic stage, that resulted in polyphase deformation and metamorphism of the Damaran Sequence. The chronological evolution of the Damara Belt spans approximately 400 Ma (see Miller, 1983c for a review of Damaran geochronology) and is summarized in Table 2.2. However, it must be pointed out that Damaran geochronology still remains poorly constrained, and until recently, relied largely on Rb-Sr whole rock ages.

2.4.1. Intracontinental Rifting

Damaran supracrustal rocks appear to have been largely deposited on continental crust, and are noteworthy because they lack voluminous volcanic rocks, being predominantly of sedimentary origin (Tankard *et al.*, 1982). The Damara Belt passed through an initial stage of continental rifting (Martin and Porada, 1977), which began 1000-900 Ma ago, and lasted until ~750 Ma ago (Miller, 1983c; Porada, 1989). The presence of extensive pre-Damara sialic crust along the orogen margins, as well as large inliers scattered throughout much of the Damara Belt (Fig. 2.4), is seen as good evidence for rifting. Furthermore, the shallow-water or terrestrial sedimentary affinities of the Damara Supergroup also point to deposition in a rift environment (Tankard *et al.*, 1982). Although poorly constrained, it is possible that rifting could have eventually progressed to an ocean-opening stage (Barnes and Sawyer, 1980; Kasch, 1983c; Miller, 1983c)

The Damaran sedimentary succession has been divided into three main sedimentary facies and these are commonly referred to as the early Nosib graben stage, the miogeoclinal Otavi platform stage and the Swakop eugeoclinal stage (Martin, 1983a; Goodwin, 1991).

Table 2.2: Simplified non-genetic chronological evolution of the Damara Orogen (modified after Kröner, 1980a, 1982; Miller, 1983c).

Ages	Events
~280 Ma	Almost complete removal of the Damara mountain belt (pre-Karoo surface coincides more or less with present land surface).
<420 Ma	Mineral fission-track cooling ages.
455-420 Ma	Biotite cooling ages in the CZ, closure of the Rb-Sr isotopic system.
495-460 Ma	Further uplift, granite generation and intrusion in CZ (high level in SCZ); deep erosion between 540 and 460 Ma.
480-460 Ma	D_3 doming in the NCZ; duration of tectonic evolution in NCZ may have been between 650-460 Ma?
495-480 Ma	Intrusion of the evaporite-derived, fluid-solid mush into the sole thrust of the NNC to form a lubricating layer; final, gravity-induced, 35 km emplacement of NNC onto folded Nama Group rocks.
~500 Ma	Emplacement of Rössing alaskite (Zircon U-Pb) [Rb-Sr date of 458 Ma too young?]
540-495 Ma	Rising isotherms due to isostatic rebound of CZ, SZ and SMZ, granite formation in CZ (at higher crustal levels in the SCZ) and locally in the NZ and SMZ. Erosion and tilting of pre-existing stratigraphic, metamorphic and structural boundaries.
510-490 Ma	Rb-Sr biotite cooling ages in NZ and SMZ.
± 510 Ma	D_2 in NCZ.
523 Ma	Post-tectonic, post-metamorphic emplacement of the Donkerhuk Granite in the OLZ and SZ.
pre-523 Ma	~10 km rebound of SZ relative to OLZ.
post-534 - pre-523 Ma	Post-D_3 peak of regional metamorphism in CZ, OLZ, SZ and SMZ; high temperature-low pressure (660 °C, 250-400 MPa) in CZ, low temperature-high pressure (570 °C, 800 MPa) in SZ and SMZ.
540 - post-534 Ma	D_2 in SZ and SMZ again culminating in intense southeasterly thrusting in the SMZ. Folding of the Nama Group on the southern edge of the Damara Belt with the formation of a penetrative slaty cleavage (534 Ma). Continental collision in the SZ; the duration of the tectonic evolution in the SZ and SMZ may have been 542-534 Ma?
~ 542 Ma	D_3 doming in the SCZ; D_1 deformation in OLZ, SZ and SMZ culminating in intense southeasterly thrusting in SMZ. Emplacement of serpentinites along D_1 thrusts in the SMZ and SZ; high pressure metamorphism (590 °C, 1000 MPa) in SZ and SMZ; uplift and erosion; possible deposition of the distal, CZ- and SZ-derived molasse Fish River Subgroup. Initial deformation of the proximal syntectonic sediments at the SMZ thrust front. Duration of tectonic evolution of SCZ is 650-540 Ma.
550 Ma	Widespread intrusion of Salem-type granites in CZ, post-D_1 - pre-D_2 in NCZ and post-D_2 in SCZ; uplift in CZ and erosion; possible deposition of southern, CZ-derived, distal molasse of Nomtsas Formation and Fish River Subgroup of Nama Group. SMZ still an undeformed passive margin.
590-570 Ma	Post-tectonic intrusion of Salem-type granites in the SKZ and NZ
600 Ma	D_2 in the NP, NZ and CZ; deformation of Mulden Group. Continental collision in the Kaoko Belt
~650-630 Ma	Reversal from extension to orogenesis in the Damara Belt; intense D_1 deformation in northern Kaoko Belt and CZ, gentle in NZ; metamorphism in CZ; post-D_1 intrusion of the first diorites, Salem-type granites, and red granites in the SCZ; uplift in the Kaoko Belt, erosion, deposition of Mulden Group in NP, NZ, EKZ and SKZ; start of deposition of lower Nama Group.
~ 650 Ma	Emplacement of pre- to early syn-tectonic (?) diorite of Palmental igneous complex in CZ
730-650 Ma	Possible evolution from rifting to spreading; deposition of the Otavi Group and most of the Swakop Group; evolution of the SZ into a deep ocean; continuous deposition in the Pan-African South Atlantic; most clastic sediments derived from the east.
840-730 Ma	Waning rifting phase; alkaline igneous activity; playa-like deposits, deep Pan-African South Atlantic ocean. Duration of rifting ± 200 Ma.
~ 1000-900 Ma	Initiation of intracontinental rifting in the Kaoko belt and northeast-trending Damara Belt. Nosib Group deposition.

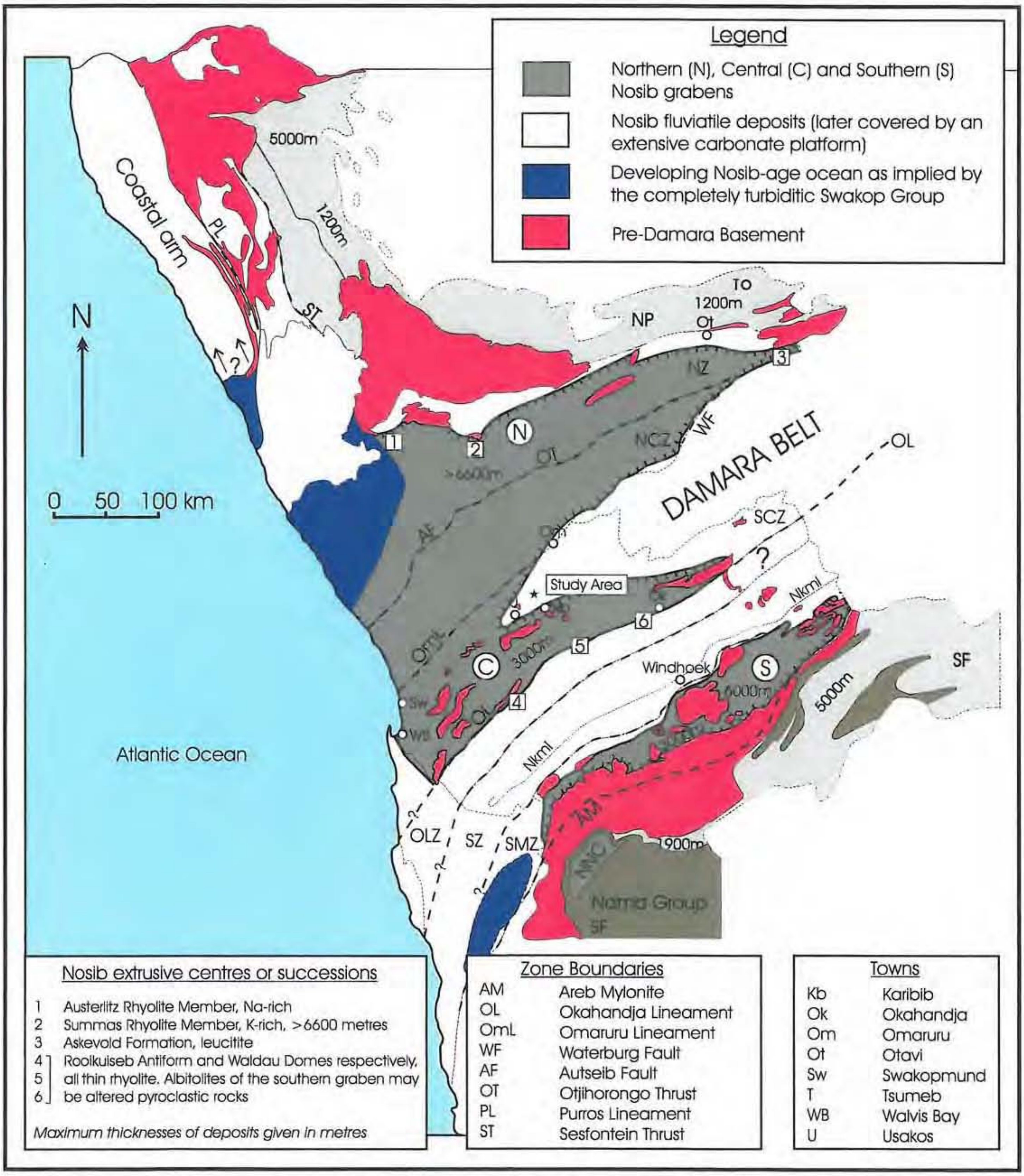

Legend

▨	Northern (N), Central (C) and Southern (S) Nosib grabens
☐	Nosib fluviatile deposits (later covered by an extensive carbonate platform)
■	Developing Nosib-age ocean as implied by the completely turbiditic Swakop Group
🟥	Pre-Damara Basement

Nosib extrusive centres or successions

1 Austerlitz Rhyolite Member, Na-rich
2 Summas Rhyolite Member, K-rich, >6600 metres
3 Askevold Formation, leucitite
4, 5, 6 Roolkuiseb Antiform and Waldau Domes respectively, all thin rhyolite. Albitolites of the southern graben may be altered pyroclastic rocks

Maximum thicknesses of deposits given in metres

Zone Boundaries

AM	Areb Mylonite
OL	Okahandja Lineament
OmL	Omaruru Lineament
WF	Waterburg Fault
AF	Autseib Fault
OT	Otjihorongo Thrust
PL	Purros Lineament
ST	Sesfontein Thrust

Towns

Kb	Karibib
Ok	Okahandja
Om	Omaruru
Ot	Otavi
Sw	Swakopmund
T	Tsumeb
WB	Walvis Bay
U	Usakos

Fig. 2.4: Location of the northern, central and southern Nosib grabens, Nosib fluviatile deposits and the developing Nosib ocean (Pan-African South Atlantic). [after Miller, 1983c, Fig.4, p.438]

(a) Nosib graben stage

It is widely accepted that the development of the Damara Belt began with a phase of continental rifting, but there is still some uncertainty about the number and location of the rift zones (Porada, 1985). Facies development and thickness changes, as well as the distribution of the basal clastic series (Nosib Group) of the Damara Sequence, and the related acid to alkaline rocks, indicate that there may have been three initial, sub-parallel rift structures in the Damara Belt (Martin and Porada, 1977; Porada, 1979; 1985; 1989). These major rift structures were probably located in the NZ, CZ and SMZ, as is shown in Fig. 2.4 (Martin and Porada, 1977). Table 2.3 summarizes the main events of this stage.

(b) Miogeoclinal Otavi platform stage

With continued extension and subsidence, following (Martin and Porada, 1977) or during Nosib times (Martin, 1983a), the three initial rift structures of the Damara Belt coalesced and the area of deposition widened dramatically (Tankard *et al.*, 1982). For the first time sediments overstepped the subsiding basement 'highs' and the miogeoclinal-eugeoclinal dichotomy developed. As a result, the Otavi Group platform succession accumulated on a gently subsiding Congo craton foreland, while flysch-type clastic sediments of the Swakop Group were deposited in a deepening trough south of the miogeocline (Tankard *et al.*, 1982). The main events of the miogeoclinal Otavi platform stage are summarized in Table 2.4.

(c) Eugeoclinal Swakop stage

Concurrently with carbonate deposition in the NP, there was continued extension in the central and southern parts of the Damara Belt. This resulted in the formation of a fourth rift commonly referred to as the Khomas Trough (Martin and Porada, 1977, Tankard *et al.*, 1982). Martin and Porada (1977) and Porada (1989) envisaged that the Khomas rift zone developed between two half-graben structures, marked by the original central and southern rifts, as can be seen in Fig. 2.4 (see geodynamic models later). Sediments of the Swakop Group filled the deepening Khomas Trough, to lie unconformably and paracomformably on the clastic sediments of the Nosib grabens (Tankard *et al.*, 1982). Table 2.5 summarizes the main events of this stage.

Table 2.3: Main events of the Nosib graben stage during intracontinental rifting in the Damara Belt.

Main Events	Details	References
1.Trough Infilling	- sedimentation commenced with infilling of discontinuous and restricted, fault-bounded troughs and basins; - extensive fluviatile deposition and possible shallow-marine infilling; - basal Nosib Group feldspathic to arkosic, locally conglomeratic sands laid down in troughs approximately 50-70 km wide and 200 km long; - Nosib Group may have attained a thickness of almost 6000 m in the deepest parts of individual basins	Martin & Porada, 1977 Kröner, 1982 Tankard *et al.*, 1982 Miller, 1983c
2. Bimodal Volcanism	- towards the end of the Nosib graben stage (~840-730 Ma) sedimentation accompanied by mantle-derived, bimodal, alkaline volcanism and plutonism; - volcanic activity was relatively minor in the 2 southern rift zones but extensive in the northern rift *(refer to numbered localities in Fig. 2.4.)* - major boundary faults may have exerted structural control on volcanism e.g. Summas fault, which marks northern edge of NZ, associated with considerable amounts of alkaline and peralkaline volcanic, volcaniclastic, and intrusive rocks (Naauwpoort Formation); - bulk of volcanic rocks are K-rich ignimbrites and may have reached 6600 m in thickness; - Na-rich ignimbrites are found in the southern parts of the northern Nosib graben, associated with subvolcanic intrusions of feldspar porphyry, syenite, nepheline syenite, carbonatite and gabbro; - in the two other Nosib grabens to the south the main volcanic rock is alkali rhyolite.	Miller & Hoffmann, 1981 Kröner, 1982 Tankard *et al.*, 1982 Hawkesworth *et al.*, 1983 Miller, 1983c Porada, 1989
3. Marine incursion and carbonate formation	- during Late Nosib times marine incursion may have resulted in deposition of impure carbonates and evaporites (subsequently metamorphosed to calc-silicate rocks during Damaran orogeny); - evidence for extensive exhalative and evaporitic activity in southernmost rift system; possible for evaporites to have formed in northern rift? - predominance of calcic and sodic minerals over locally deposited borates, all of which formed in playa environments.	Tankard *et al.*, 1982 Miller, 1983c

Table 2.4: Main events of the Miogeoclinal Otavi Platform stage during intracontinental rifting in the Damara Belt.

Main Events	Details	References
1. Rift structure coalescence	- with continued extension and subsidence the three initial rift structures coalesced (towards the end or just after the Nosib Graben stage); - sediments overlapped the basement highs and the miogeoclinal-eugeoclinal dichotomy developed; - the Otavi Group platform succession accumulated on a gently subsiding Congo craton foreland, while contemporaneously to the south, flysch-type clastic sediments of the Swakop Group were deposited in a deepening trough.	Martin & Porada, 1977 Tankard *et al.*, 1982
2. Otavi Group deposition	- stable conditions in the NP allowed the deposition of the extensive dolomitic limestone (lower Otavi Group), which in places attained 3000 m; - distinctive 'marker' stromatolites are preserved in the carbonates and can be traced for distances over 300 km; - carbonates accumulated in a largely shallow-marine environment - Otavi Group lies unconformably on the basement and clastic rocks of the Nosib Group	Miller, 1983c Goodwin, 1991
3. Deposition of basement-derived Mulden Group molasse	- platform carbonates were overlain by a basement-derived molasse (Mulden Group) in the period spanning 660 - 570 Ma; - Mulden Group is up to 2000 m thick and consists of quartzite, arkose, greywacke and shale, with minor carbonate intercalations; - NP sedimentation ended with the deposition of the Owambo Formation composed of molasse-type, fine-grained terrigeneous clastic rocks.	Kröner, 1980a Tankard *et al.*, 1982

Table 2.5: Main events of the Eugeoclinal Swakop stage during intracontinental rifting in the Damara Belt.

Main Events	Details	References
1. Half-graben amalgamation to form the Khomas Trough	- continued extension in the central and southern parts of the belt led to the development of a fourth major rift; - envisaged that Khomas rift zone developed between two half-graben structures, marked by original central and southern rifts *(see Fig. 2.4)*; - sediments of the Swakop Group filled the deepening Khomas Trough, to lie unconformably on the clastic sediments of the Nosib Grabens;	Martin & Porada, 1977 Porada, 1983 Tankard *et al*, 1982 Porada, 1989
2. Lower Swakop Group sedimentation in Khomas Trough and CZ	- Abenab (North), Ugab (Centre) and Kudis Subgroups (South) are lowermost subgroups of Swakop Group *(see Table 2.1)*, and bear testimony to an initial period of sporadic carbonate and terrigeneous, clastic sediment deposition; - sediments began to overlap basement and started to extend beyond the rift shoulders of the subsiding grabens; - within grabens Ugab and Kudis deposits attained maximum thicknesses of ~4,9 km and 3 km respectively (equivalents in the CZ only attain 200 m in thickness); - carbonates are interbedded with thick turbidites and clastic sediments, and indicates graben structures continued to subside relatively rapidly; - in CZ lensoid nature of many sedimentary layers, alternation of various rock types and occurrence of local amphibolites indicates unstable crustal conditions.	Miller & Hoffmann, 1981 Tankard *et al.*, 1982 Miller, 1983c
3. Glacial period and tectonic unrest	- the middle Swakop Group consists of the Chuos Formation mixtitic sediments, interpreted to be of glacial origin; - appears that diamictites of the Chuos Formation were deposited during a time of tectonic unrest, marked by a terrain with considerable basinal relief.	Miller & Hoffmann, 1981 Tankard *et al.*, 1982 Miller, 1983c
4. Development of shallow, continental shelf and platform	- period of relative tectonic quiescence allowed the development of shallow, continental shelf and platform; - extensive calcareous turbiditic sequences of Karibib Formation, and foetid or stromatolitic carbonates of the Tsumeb Subgroup (upper Otavi Group) were deposited on platform; - in central Swakop terrain, stratigraphic equivalents of Tsumeb carbonates comprise moderate-to-deep water carbonates of the Okawayo-Karibib Formation, and interbedded fine-grained clastics of lower Ondundu and Oberwasser Formations; - upper Karibib Formation and equivalents formed during a starved-basin evolutionary phase.	Tankard *et al.*, 1982 Miller, 1983c Hoffmann, 1990
5. Deposition of Kuiseb Formation (bulk of Khomas Subgroup)	- the Kuiseb Formation mica schists form the bulk of the Khomas Subgroup (estimated that 10 km of pelites and psammites were laid down in the centre of Khomas Trough); - consists of monotonous flysch-type succession of argillites; - appear to have been transported along Damaran trough, passing southwards through Botswana before final deposition in present position.	Tankard *et al.*, 1982 Porada, 1989 Miller, 1983c
5. Matchless Amphibolite Member	- Kuiseb mica schists include the enigmatic *(see geodynamic models, section 2.6)*, pre-tectonic Matchless amphibolites that extend as a linear belt for some 350 km northeastwards; - represents a mafic suite of volcanic rocks (pillow structures) similar to ocean-floor tholeiites.	Barnes & Sawyer, 1980 Kröner, 1981a Tankard *et al.*, 1982

2.4.2. Orogenic Stage

Rifting or possible ocean floor spreading is thought to have slowed and stalled by about 700 Ma, to leave the Congo and Kalahari cratons at their maximum separation during the entire Pan-African event (Miller, 1983c). Following this, at about 650-630 Ma, the Congo and Kalahari cratons began to converge and orogenesis in the Damara Belt was initiated. The cause of this reversal from extension to orogenesis is still debated, and both plate tectonic and ensialic geodynamic models have been suggested *(see section 2.5)*. The unusually prolonged orogenic stage may have extended from 650 Ma to 460 Ma, and involved numerous episodes of granitic intrusion, metamorphism and tectonic activity (Miller, 1983c; Jacob *et al.*, 2000b). No attempt has been made to explain the orogenic features in terms of a particular model (as with the previous section). Only a brief assessment of the main structural, metamorphic and magmatic characteristics of this stage will be presented. In this regard, Miller (1983c, p.504) provides an excellent review of Damaran orogenesis.

(a) Structure

The Damara Belt has been subdivided into tectonostratigraphic zones largely on the basis of its structure (Miller, 1983c). It is convenient for this discussion of Damara Belt structure, to assume that the Okahandja Lineament marks a major crustal change (whatever the geodynamic model chosen) and that it divides the belt into structurally distinct northern (CZ, NZ and NP) and southern parts (OLZ, SZ, SMZ and SF). This interpretation is well accepted in the literature (e.g. Martin and Porada, 1977; Barnes and Sawyer, 1980; Downing and Coward, 1981; Miller, 1983c) and is based on a multitude of evidence, including marked changes in the stratigraphy, structural style, metamorphism and geophysical responses observed across the Okahandja Lineament (Miller, 1983c). The gradation and evolution of structures either side of the Okahandja Lineament is illustrated in Fig. 2.5 and summarized in Table 2.6.

The structural evolution of the Damara Belt, including the number of phases of deformation and their timing, remains poorly constrained. The brief account that follows is based exclusively on Miller's (1983c) review of orogenesis and structure. In the northern Damara Belt, the first deformation event (D_1) is associated with early syntectonic dioritic to granitic rocks that yield ages of 650 Ma. This event produced a strong, bedding-parallel S_1 foliation in the SCZ, northern Kaoko Belt and parts of the eastern NZ. The first record of D_2 deformation north of the OL is in the Kaoko Belt where it resulted in large-scale eastward

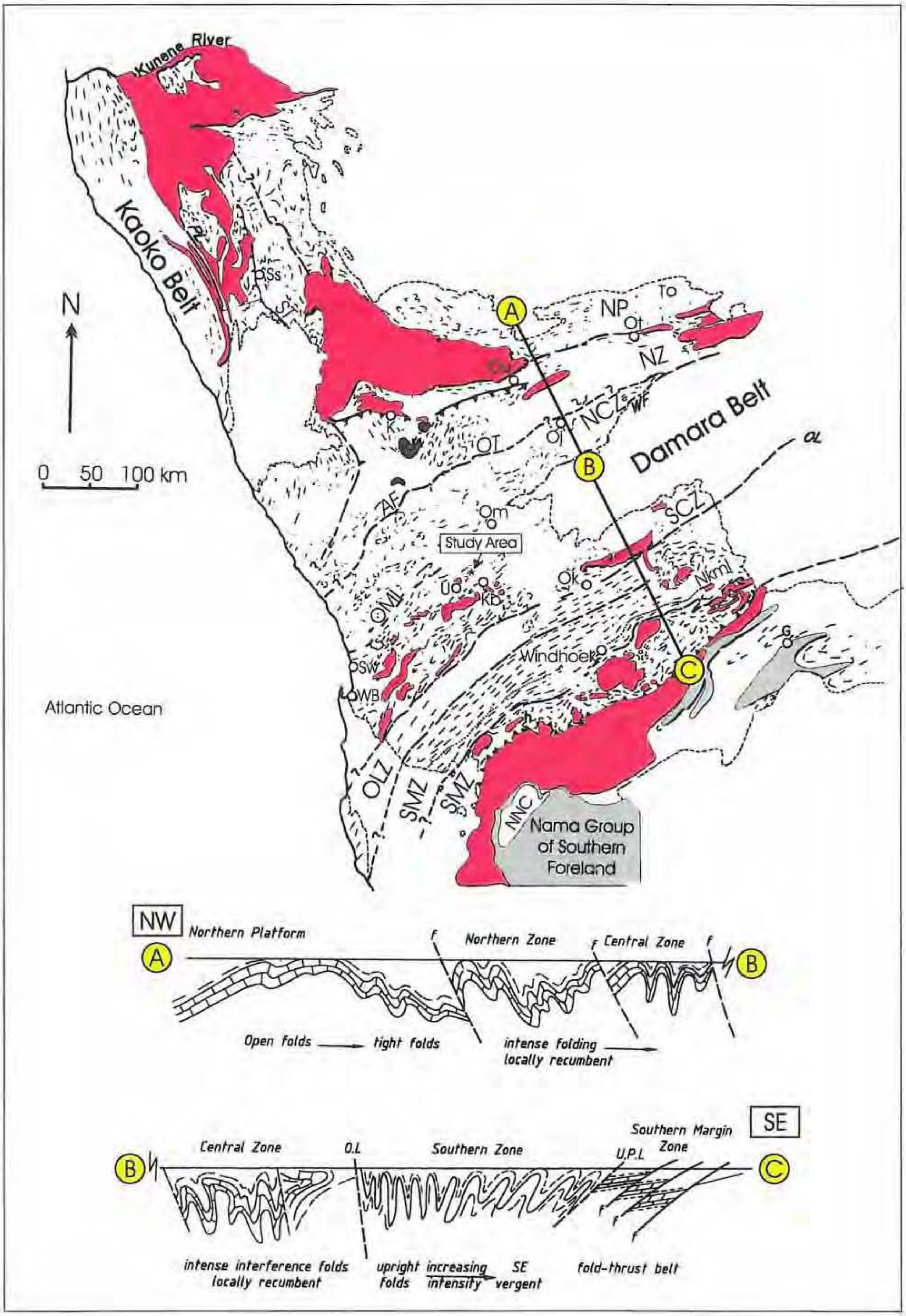

Fig. 2.5: Structural form lines across the Damara Belt illustrating the contrasting structural styles of the different zones (modified after Miller, 1983c, Fig.17, p.457). The location of the simplified cross section (A - C) is shown on the map (after Henry *et al.*, 1990, Fig. 3, p.69).

Table 2.6: Summary of the evolution and gradation of structures across the tectonostratigraphic zones of the Damara Belt (based mainly on Miller, 1983c).

Zone		Description of structures	References
Northern part of Damara Belt	**NP**	- it appears that only one phase of deformation affected the NP to produce E-W-trending structures that parallel those in the adjoining northern belt of the NZ (i.e. Transitional Zone *sensu stricto*); - structures in the NP increase in intensity southwards, so that folds change from open and upright in the NP, to more tight and slightly overturned adjacent to the NZ.	Miller, 1983c
	NZ	- only two phases of deformation occurred in NZ; the numerous basement inliers that form E-W-trending northern edge of the NZ have exerted strong control on the orientation of structures formed during Damaran orogeny; - F_1 folds are upright to northward-vergent and E-W-trending; F_2 folds are very tight with a northward vergence; - the Autseib Lineament marks a sharp structural transition from the less complicated open to tight folding of the NZ, to the elongate dome structure of the NCZ; however the southern belt of the NZ (i.e. NZ *sensu stricto*) still shares the same stratigraphy as the CZ.	Miller, 1983c Corner, 2000
	CZ	- postulated that the CZ experienced at least three main phases of deformation, or prolonged progressive deformation; - in the NCZ, D_1 and D_2 were intense and resulted in strong foliations and tight closures in the marbles, and well-developed schistosities in the Kuiseb Formation; D_3 is thought to have resulted in the formation of the CZ dome and basin structure; - SCZ and NCZ are separated by the Omaruru Lineament - Waterberg Fault, and although the structural style does not change markedly across this divide, there is a major change in the stratigraphic level; - Kuiseb Formation schists outcrop extensively in the NCZ and attest to the higher stratigraphic level of this belt compared to the SCZ; - the complex F_3 domes of the NCZ are cored by Karibib marbles, or schist and calc-silicate rocks of the Chuos and Khan Formations and enveloped by thick marble; - domes of the SCZ normally expose pre-Damara Abbabis basement or granitic rocks (*see section 3.2.2 for more detail on SCZ*).	Miller, 1983c Oliver, 1994, 1995
Okahandja Lineament (OL) - ***marks a major crustal change between the northern and southern parts of the Damara Belt (see Fig. 2.5 cross sections)***			
Southern part of Damara Belt	**OLZ**	- immediately adjacent to the Okahandja Lineament (OL) there is a belt of isoclinal folding, in which the bedding, axial planar cleavage and local, closely-spaced shear zones are all parallel, and vertical or steeply inclined; - southwards, folds gradually become more open, and like the SZ share a linear structural fabric (*see Fig. 2.5*)	Miller, 1983c
	SZ	- upright structures of OLZ progressively become more SE-vergent and more intensely deformed towards southern edge of the SZ; - S_1 schistosity interpreted to be same as found in OLZ and correlated with S_3 in CZ; implication of this is that sequence south of OL could be a younger syntectonic deposit because it lacks the older fabrics found in northern parts; - S_1 represented by metamorphic banding cleavage; S_2 expressed as reorientation of micas and S2-parallel dislocation planes;	Miller, 1983c
	SMZ	- tight to isoclinal folds of SZ eventually grade into thrusts in the SMZ as deformation becomes more and more intense southwards; - F_1 and F_2 in SMZ are characterized by development of overturned and recumbent folds; significant compency contrasts between the different lithologies result in strong strain localisation and heterogeneity; - southwards, the pre-Damara basement becomes increasing involved in main D_1 and D_2 thrusting as complex packet of thrust sheets.	Miller, 1983c
	SF	- northern edge of SF has experienced tight to open folding and local overturning towards the southeast; - further SE, open, undulating folds rapidly die out into the undeformed SP; - emplacement of the Naukluft Nappe Complex (NNC) followed folding in the SMZ, and is consequence of at least 5 deformation events.	Miller and Hoffman, 1981 Miller, 1983c

recumbent folds and nappes. The D_2 event appears to have been roughly coeval in the Kaoko Belt, NP and NZ, and may have developed during a continental collision phase in this region at around 600 Ma. F_2 structures in the CZ predate the intrusion of widespread 550 Ma-old Salem-type granites, and may have been produced by the same intense southeast-directed tectonism that resulted in F_2 (east-verging) structures in the CKZ. A final D_3 stage followed the emplacement of the 550 Ma-old granites and is characterized by large-scale, elongate doming in the SCZ. The dome and basin structure of the CZ may have resulted from upright F_3 folding of earlier F_1 and F_2 isoclinal, recumbent folds *(see Chapter 3 for more detail on SCZ structure).*

The tectonic evolution of the Damara Belt south of the Okahandja Lineament appears to have been significantly delayed and is notably shorter (~20 Ma duration). At the time of D_2 deformation and granitic intrusion in the CZ, the SMZ and SF were still undeformed. Only on collision of the Congo and Kalahari cratons was intense deformation transferred from the SCZ to the southern parts of the belt. D_1 in the OLZ and SZ occurred at about 540 Ma and can be correlated with D_3 in the SCZ. In the OLZ, F_1 folds are upright and open-to-tight but towards the SZ become more isoclinal and southeast vergent. The final stages of D_1 are associated with intense deformation and large-scale thrusting. F_2 folds share many of the same characteristics as the earlier F_1 structures, progressively becoming more isoclinal and overturned towards the SZ. Sheath folding and intense thrusting may also have occurred during this stage. D_3 caused minor crenulation folding in the SZ and produced NE- and EW-trending domes containing large thrust slices in the SMZ. Tectonic activity terminated in the southern parts of the belt before the emplacement of the approximately 523 Ma-old Donkerhuk Granite.

(b) Metamorphism

Although the grade of metamorphism can be seen to generally increase from the margins of the Damara Belt towards the CZ (see Fig. 2.6), this is a great simplification. A gross asymmetry exists between the prograde patterns of the southern (low-T, high-P) and northern (high-T, low-P) parts of the belt (Miller and Hoffmann, 1981; Sawyer, 1981; Kasch, 1983a; Miller, 1983c). In addition, the growth of Damaran metamorphic mineral phases has been attributed to either a prolonged and progressive increase in metamorphic grade during the entire tectonic event (e.g. Hartnady, 1978; Puhan, 1983a, b), or to two or three discrete metamorphic peaks separated by a significant drop in temperature (e.g. Barnes and Sawyer, 1980; Kasch, 1983a, b). Table 2.7 highlights these two main arguments.

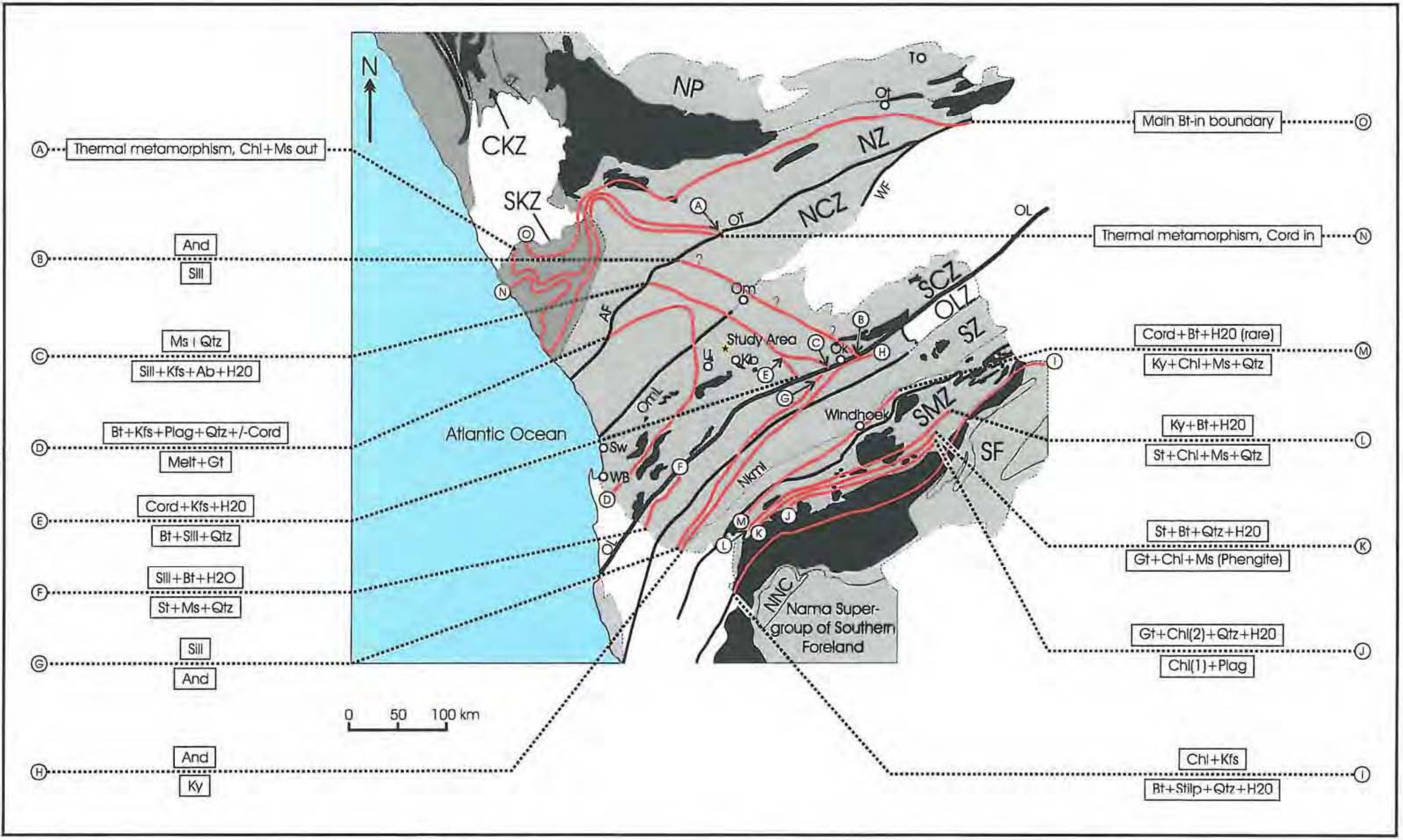

Fig. 2.6: Isoreactiongrads and phase boundaries in the pelitic rocks of the Damara Belt (modified after Miller, 1983c, Fig. 26, p.470). Ab-albite, And-andalusite, Bt-biotite, Chl-chlorite, Cord-cordierite, Gt-garnet, Kfs-potash feldspar, Ky-kyanite, Ms-muscovite, Plag-plagioclase, Qtz-quartz, Sill-sillimanite, St-staurolite, Stilp-stilpnomelane. General symbols and abbreviations as per Fig. 2.3, p.15.

Table 2.7: Summary of two main arguments for poly-metamorphism and single, diachronous prograde metamorphism (based on Hartnady, 1978; Barnes & Sawyer, 1980; Hartmann *et al.*, 1983; Kasch, 1983a, b; Miller, 1983c; Puhan, 1983a, b).

Damaran metamorphism	Main arguments	References
1. Single, diachronous prograde metamorphic event	- this entails a single, diachronous prograde event, which started syntectonically and then rose to a syn- to post-tectonic peak; - may be supported by observation of syntectonic metamorphic recrystallisation during the formation of only one dominant slaty cleavage in the low to very low grade regions of the belt; - argue that formation of syn- and post-tectonic cordierites in high-grade metapelites of CZ are result of 2 different reactions that occur at different temperatures and involve different mineral phases, as part of prograde stages of single metamorphic event; - also majority of mineral reactions are at least bivariant, and as a result can occur over a significant temperature range; - during Damaran tectonism likely that temperature changes lagged behind successive orogenic movements; - as a result it is possible that several deformation events could have been outlasted by formation of the respective metamorphic minerals.	Jacob, 1974 Puhan, 1983a, b Hartmann *et al.*, 1983 Miller, 1983c Kasch, 1987 Steven, 1993
2. Two or three discrete metamorphic events	- microtextural studies indicate that metamorphic minerals grew during 2 distinct periods of regional metamorphism; - garnets in Omitara area (SMZ) show continuous growth from D_1 to early D_3 (i.e. syntectonic), and although there are abundant post-tectonic garnets (i.e. post D_4), there is a stark absence of late-tectonic garnets; - may indicate temperature decrease below that required for garnet growth during late D_3, but followed by a late- to post-D_4 temperature increase which resulted in renewed growth; - geothermometry indicates 2 peak metamorphic temperatures of 570±50°C (~D_2) and 588±50°C (post-tectonic) separated by a post tectonic temperature of well below 500±50°C; - maximum pressures of 900-1000±120 MPa were obtained peak of M_1, but towards the end of M_1 event pressure dramatically decreased to 200 MPa; - pressure did not increase again during M_2 event; - postulated that Damara Belt underwent a post-tectonic thermal relaxation event.	Sawyer, 1981 Kasch, 1983b, c Miller, 1983c

In the Southern Damara, geothermometry supports a polymetamorphic interpretation and indicates two peak metamorphic temperatures of 570±50 °C (~D_2) and 588±50 °C (post-tectonic) separated by a late-tectonic temperature of well below 500±50 °C (Kasch, 1983b). During the peak of the first metamorphic event, a maximum pressure of about 9-10±1.2 kbars was reached, but towards the end of M_1, the pressure decreased dramatically by 2 kbars. Kasch (1983b, c) shows that the pressure did not increase again during the M_2 event (6-8 kbars), and postulates that this was due to post-tectonic, thermal relaxation in the belt.

Metamorphism in the CZ accompanied and outlasted both deformation and granite intrusion (Miller, 1983c). The emplacement of post-tectonic alaskites and pegmatites suggests high temperatures may have persisted until about 460 Ma (Miller, 1983c; Steven, 1993). The exact timing of the peak of regional metamorphism in the CZ remains contentious, with estimates ranging from 540 Ma to 520 Ma (Kröner, 1982; Haack and Martin, 1983; Steven, 1993). Metamorphic pressures in the CZ and the western parts of the OLZ, are estimated to have been about 4 kbars during the syntectonic event, but probably decreased to between 4 and 2.5 kbars during the post-tectonic M_2 peak (Miller, 1983c). The CZ largely experienced amphibolite-facies metamorphism *(see chapter 5)*, but in the western parts of the CZ, granulite-facies rocks are found and widespread anatexis has occurred (Brandt, 1985).

(c) Magmatism

Plutonic rocks related to Damaran orogenesis intrude pre-Damara basement and Damaran metasedimentary rocks over an extensive area of the belt (Miller, 1983c). There are over 300 syn- to post-tectonic plutons in the Damaran granitic province that are composed of a wide variety of rocks from gabbro to leucogranite (Miller, 1983c; Brandt, 1987). Some of the earliest intrusives, the Palmental diorites, have been dated at ~750 Ma (Kröner, 1982; Rb-Sr isochron method) but Miller (1983c) believes this to be a source age, their true age being similar to associated granodioritic veins at ~650 Ma. The vast majority of Damaran granites were emplaced significantly later in the period between 570 and 450 Ma (Miller, 1983c).

The bulk of Damaran granitic plutons are concentrated in the CZ where they generally form permissive, harmonious intrusions without obvious thermal aureoles (Miller, 1983c). Generally the early intrusives have I-type characteristics, while the majority of syntectonic intrusives are S-type, alkalic, peraluminous granitic and leucogranitic rocks with higher Rb/Sr ratios (~1), close to that of continental crust (Brandt, 1987). Miller (1983c) distinguishes 3 major syn- to post-tectonic groups of granites in the CZ as follows (these will be discussed in more detail in chapter 3):

(i) red, medium-to fine-grained granites;

(ii) coarsely porphyritic, biotite monzogranites and associated dioritic rocks types of the Salem Granitic Suite; and

(iii) fine- to coarse-grained leucogranites, pegmatitic alaskites and pegmatites.

In the lower grade NZ, the intrusions are discordant and have wide thermal aureoles (Miller, 1983c). The voluminous post-tectonic and post-metamorphic Donkerhuk Granite occurs mainly in the OLZ, and is bound to the northwest by the Okahandja Lineament (Miller, 1983c). The SMZ contains small bodies of post-tectonic, alkali granite and numerous scattered pegmatites (Miller, 1983c).

2.5. Geodynamic Models for the Damara Belt

Geodynamic models for the Damara Belt must successfully account for the key sedimentary, metamorphic and structural characteristics, and must explain the magmatic evolution and mineralization of this somewhat enigmatic Pan-African belt. Numerous models have been suggested to explain Damara Belt evolution, and fall into two main groups of thought. One camp holds that the Damara and Kaoko Belts are genetically related and that they formed as a result of ensialic geodynamic processes, involving a mantle hot spot, continental rifting with eventual aulacogen formation, followed by an orogenic cycle set in motion by continental or Ampferer subduction (Martin and Porada, 1977; Porada, 1979; Kröner, 1980a, 1981a, b, 1982; McWilliams and Kröner, 1981).

The other group maintains that plate tectonics, similar to what is observed in today's orogenic zones, were responsible for the development of the Damara Belt (Barnes and Sawyer, 1980; Kasch, 1983c; Miller, 1983c; Hoffmann, 1990; Kukla & Stanistreet, 1991). The plate tectonic camp cite evidence for either partial or wide-ocean formation followed by ocean-floor or Benioff subduction. Fundamentally, this argument centres around whether a uniformitarianism view of Earth processes is valid in explaining the very early geological history of the planet (De Wit, 1998; Hamilton, 1998). A critical review of the different geodynamic models for the Damara Belt was last undertaken by Martin (1983b), and a good summary of models is provided in Tankard *et al.* (1982). A thorough understanding of the geodynamic evolution of the Damara Belt is crucial in developing predictive exploration programmes for the region and should underlie all ore genesis models, such as those proposed for gold mineralization in the SCZ.

3. GEOLOGY AND MINERAL POTENTIAL OF THE SOUTHERN CENTRAL ZONE

3.1. Introduction

In this chapter emphasis has been placed on the distribution and types of mineralization found in the SCZ of the Damara Belt. A brief review of Damaran metallogenesis and details of significant SCZ epithermal gold discoveries are provided in section 3.2. This is followed by an overview of SCZ lithostratigraphy (section 3.3) and its potential for Cu-Au mineralization. Section 3.4 presents a brief description of SCZ crustal structure and magmatism and discusses their possible relationships to known hydrothermal mineralization. The second half of this chapter (sections 3.5 and 3.6) concentrates on the identification of lineaments and magmatic bodies (from geophysical and remote sensing imagery) that may have relevance to mineralization in the Karibib region surrounding the Onguati study area. The study successively focusses in on the Onguati area and its known Cu±Au deposits.

3.2. Damaran Metallogenesis

Reviews of the metallogenesis of the Damara Belt have been undertaken by Martin (1978) and Miller (1983b, 1983c, 1992), while Foster *et al.* (2001) have recently re-evaluated Pan-African metal potential. Early ideas on Damaran mineralization centred on ensialic geodynamic models, and distinguished mineral deposits of the geosynclinal stage and the orogenic phase (Martin, 1978). Miller (1983b, 1983c, 1992) alternatively related ore deposit distribution and mineralization potential to a plate tectonic model, and this has gained widespread acceptance in recent years (e.g. Foster *et al.*, 2001).

At least five main mineral provinces can be recognised over the Damara Belt: (i) carbonate-hosted Cu-Pb-Zn deposits in the Otavi Mountain Land of the NP; (ii) Matchless-type, massive sulphide Cu-Zn(-Ag-Au) developed along the 350 km strike length of the Matchless Amphibolite Belt within the SZ; (iii) disseminated and vein-type Au in the SCZ, but also in the NCZ and less importantly in the NZ (section 3.2.1); (iv) Sn-W pegmatite belts in the CZ and NZ; and (v) the Rössing U-province in the zone of anatexis in the southwestern part of the CZ (Miller, 1983c). Tabulated summaries of the main types of mineralization are provided overleaf (p.35-36), and differentiate between mineralization that occurred during

Table 3.1: Syngenetic mineral deposits of the Damara Belt related to the intracontinental rifting stage (based mainly on Miller, 1983b, 1983c).

Mineral Potential	**Zone**	**Group/Formation/ Lithology**	**Mineralization**	**References**
Au	**All zones (esp. CZ, NZ)**	**Nosib Group**	- palaeoplacer gold deposits in fluvial fans and deltas?	Miller, 1983b,c
Cu	**SZ, SMZ**	**Duruchaus Formation** *evaporitic and exhalative sediments*	- contain Cu mineralization; - significant potential for Sn, W, Zn and Au mineralization.	Miller, 1983b,c
	All zones	**Nosib Group** *sandstones and conglomerates*	- sediments derived by denudation of pre-Damara basement; - sediment-hosted copper in SMZ (e.g. Oamites Mine [?] may be situated in an inlier of pre-Damara basement).	Martin, 1978 Miller, 1983b,c Foster *et al.*, 2001
	All zones	Upper Nosib Group	- Cu mineralization abundant in upper Nosib sediments across the Damara Belt; - Naaupoort and Askevold Formation volcanic rocks may be source of Cu; - sub-aqueous hydrothermal discharge deposits along faults?	Miller, 1983b,c
	SCZ	Khan Formation	- bedding-parallel, Cu-bearing layers (e.g. Khan Mine); - may have had a syn-sedimentary evaporitic origin?	Miller, 1983b,c
	SMZ	*Marbles*	- syngenetic disseminated Cu frequently occurs with Pb and minor Zn.	Miller, 1983b,c
	SZ	**Matchless Amphibolite Member**	- numerous massive pyrite, copper sulphide ore bodies are found sporadically developed along the 350 km, strike-length of the Matchless Amphibolite Belt; - amphibolites show ocean-floor affinity and preserved pillow lavas; - compared to Besshi-type mineralization but lack typical carbonate and quartzite association.	Miller, 1978b,c Foster *et al.*, 2001
Pb-Zn	**CZ**	**Karibib and Okawayo Formation** *carbonates*	- Mississippi Valley-type/ evaporitic and volcano-exhalative Pb-Zn (e.g. Namib Lead Mine near Usakos); - does not appear linked with volcanic rocks or plutonic rocks; - may be result of basin-wide, saline thermal water circulation.	Miller, 1983b,c Martin, 1978
	All zones (especially CZ and NZ)	**Nosib Group** *alkaline intrusives*	- potential for sub-aqueous volcano-exhalative mineralization.	Miller, 1983b,c
BIF	**NZ (and adjoining Otavi Platform)**	**Chuos Formation**	- siliceous, haematite-magnetite iron-formation is widespread; - primary ore Fe+Mn makes up 40% of rock (Mn contents usually low 0.9-7.5%;) - iron-formations may be confined to basement highs where deposition occurred in local basins with restricted circulation; alternatively may have been deposited in high energy, estuarial-deltaic continental margin environments	Martin, 1978 Miller, 1983b,c

Table 3.2: Epigenetic mineral deposits of the Damara Belt related to the orogenic stage (based mainly on Miller, 1983b, 1983c).

Mineral Potential	Zone	Group/Formation/ Lithology	Mineralization	References
Au-Cu	CZ, NZ	**Okawayo and Karibib Formation** *marbles and calc-silicate rocks mainly, also turbidites*	- gold showings have been found associated with [1] thrust zones (e.g. Natas W-Au deposit), [2] shear zones (e.g. Abbabis basement, Sandmap deposit), and hosted by [3] turbidite sequences (e.g. Ondundu Mine, Sandamap deposit) [4] and marble and calc-silicate rocks (e.g. Navachab Mine, Onguati deposits). - newly discovered Otjikoto gold deposit may contain >1 million ounces Au; gold associated with pyrrhotite, magnetite, and pyrite, along with almandine, amphibole and free gold.	Pirajno *et al., 1991* Pirajno & Jacob, 1991 Steven, 1993, 1999, 2000 Steven *et al.*, 1994 Wilton *et al.*, 2002
	All zones where Pre-Damara basement is exposed	**Pre-Damara Basement** (e.g. Abbabis, Metamorphic Complex), *wide range of lithologies (see section 3.1.1)*	-recent discovery of high-grade, iron oxide-copper-gold mineralization (IOCG) in pre-Damara basement of Kamanjab Inlier at junction of NP, NZ and Kaoko Belt; - previously unknown mineralization type in Damara Belt. - ENE-WSW trending shear zones and associated quartz veins contain Au (~1g/t) in the Abbabis Inlier of the SCZ.	Boulder Mining Cooperation, April 2, 2003 press release Steven, 1993
U	SCZ	**Abbabis basement and Nosib Group**	- uraniferous alaskites and pegmatites; - Rössing U-Mine, located between Usakos and Swakopmund, is one of the world's largest producer of U; annual production 15-16 Mt of ore grading 0.031% U_3O_8; - late-to-post tectonic Rössing alaskites emplaced ~70 Ma main deformation phase; represent highly differentiated residual melts derived from evolved high-level crust.	Miller, 1983b,c Evans, 1993
Sn-W	CZ, NZ	**Deep stratigraphic levels, Nosib Group and lower Swakop Group**	- potential for strata-bound Sn and W mineralization in skarns or quartzite mantos associated with granitic to dioritic intrusives.	Miller, 1983c
	CZ, NZ	**Kuiseb Formation** *schists*	- tin-bearing pegmatites occur in the NCZ in upper stratigraphic levels; - only preserved in lower grade, down-faulted or down-folded blocks of the Kuiseb Fm.	Miller, 1983c
Pb-Zn (±Cu-V)	NP, NZ	**Otavi Group** *dolomites and dolomitic limestones*	- numerous, but generally widely spaced occurrences of Pb-Zn mineralization, often associated with Cu and V; -hosted by fault zones, fractured chert units, cross-cutting joint sets, solution cavities and collapse breccias; - absence of related igneous activity, low temperature of formation, shallow depth of emplacement, and consistent relationship to faults or unconformities; - likened to Mississippi Valley or Appalachian type Pb-Zn mineralization	Martin, 1978 Miller, 1983b,c Misiewicz, 1988
REE	**All zones (especially SCZ)**	**Anywhere in the stratigraphy**	- at present erosion surface, lithium-bearing and other mineralized pegmatites are common.	Miller, 1983c

intracontinental rifting and extension (Table 3.1, syngenetic mineralization) and that which took place during or after the orogenic stage (Table 3.2, epigenetic mineralization). A brief review of known gold mineralization in the Damara Belt, and more specifically in the SCZ is presented below.

3.2.1 Gold Mineralization in the SCZ and Damara Belt

A variety of hydrothermal and magmatic-hydrothermal gold showings have been discovered in many parts of the Damara Belt, but to date it is the northern parts that appear most prospective (Fig. 3.1). Pirajno &Jacob (1991, p.307) recognise four main types of orogenic gold deposits in the Damara Belt: (1) gold associated with thrust zones, mainly in the SMZ (e.g. Natas W-Au deposit); (2) gold-quartz association in shear zones (e.g. Sandamap prospect, Abbabis Inlier); (3) turbidite-hosted gold (e.g. Ondundu Mine and also Sandamap prospect); and (4) marble and calc-silicate-hosted gold (e.g. Navachab Mine and Onguati deposits).

Shear-zone hosted gold was noted by Steven (1993) in the pre-Damara Abbabis basement southwest of Karibib Town (more will be said in section 3.3.1). Recently high-grade, iron-oxide-copper-gold mineralization (IOCG) has been discovered in pre-Damara basement of the Kamanjab Inlier situated between the Kaoko Belt, and the NZ and NP of the Damara Belt (Boulder Mining Corporation, April 2, 2003 press release). Structures in the pre-Damara basement could prove to be important exploration targets in the future, and could provide alternative sources for the Cu-Au mineralization observed in the Damaran cover.

The type area of turbidite-hosted gold is the Ondundu deposit in the southern part of the NZ, but gold mineralization has also been discovered in the Kuiseb Formation sheared turbidites of the Sandamap Noord area, at the boundary between the SCZ and NCZ (Pirajno & Jacob, 1991; Steven, 1999). The defunct Ondundu Mine is adjacent to the Autseib Lineament, and is situated in the steep limb of an open, north-trending anticline with conformable quartz veins hosted by greenschist facies, turbiditic greywackes (Pirajno *et al.*, 1991). The gold is present as free gold in quartz veins, or is intimately associated with arsenopyrite or carbonate (Pirajno *et al.*, 1991). The gold carries about 3% silver, and during mining the area averaged 14 g/t Au (Hirsch & Genis, 1992).

The recently discovered Otjikoto gold deposit is also found in close proximity to the Autseib Lineament in the NZ. However unlike Ondundu, this deposit is hosted by a sheeted vein system in Karibib Formation marbles, albitites and hornfelsed biotite schists and so may

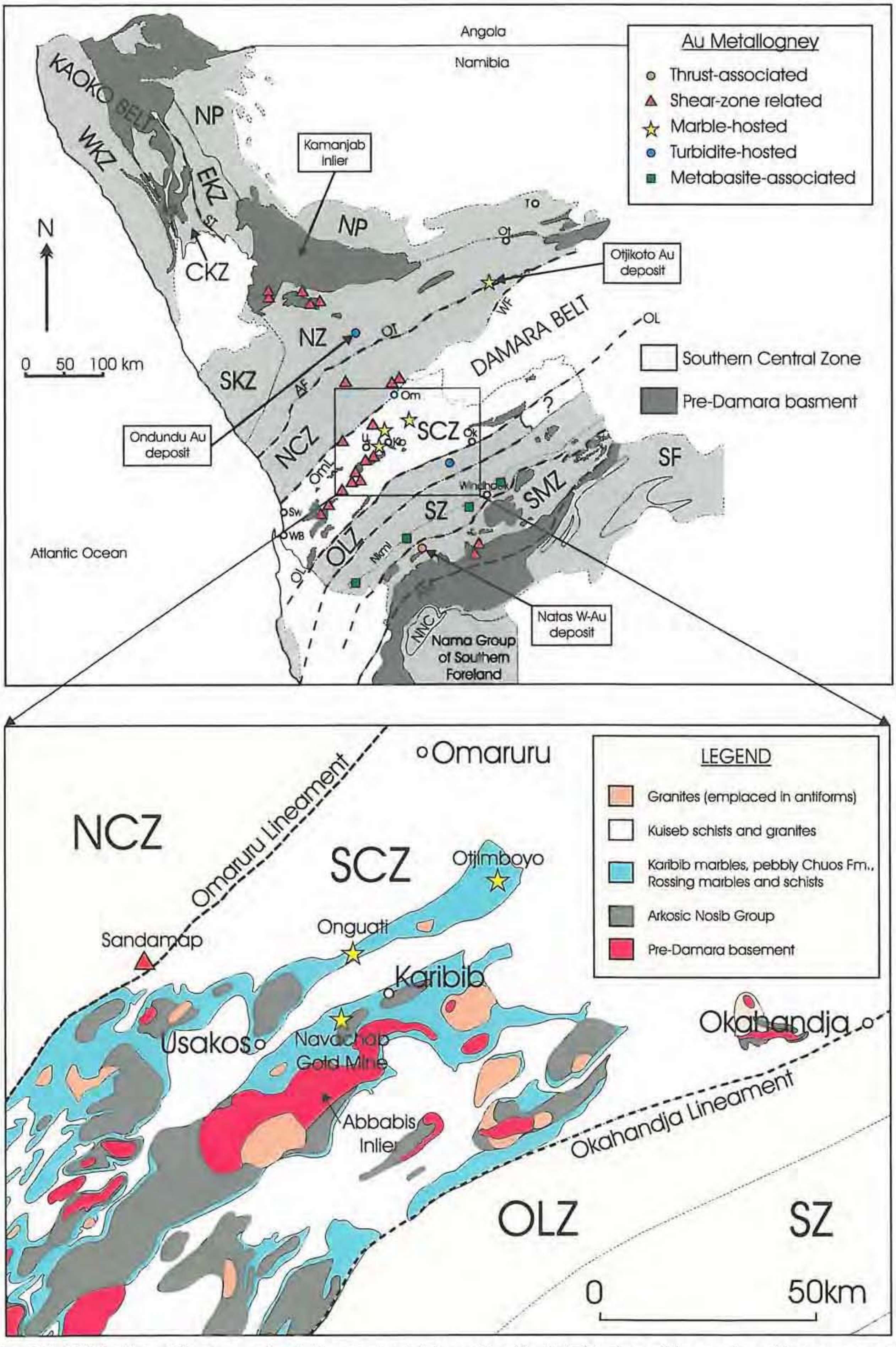

Fig. 3.1: Distribution of Damaran hydrothermal gold deposits with detail below of the main gold occurrences in the portion of the SCZ surrounding the Onguati study area (upper map modified after Pirajno & Jacob, 1991, Fig. 5, p.307; lower map modified after Miller, 1983c, Fig. 19, p.460 and 1:250 000 Geological Map series, Sheets 2114 - Omaruru, 1997 and 2214 - Walvis Bay, 1995). General symbols are the same as in Fig. 2.3.

be more akin to Navachab-style mineralization (Wilton *et al.*, 2002). The Otjikoto gold deposit may contain in excess of 1 million ounces of gold and has the potential to become Namibia's second largest gold mine (Wilton *et al.*, 2002). The gold is associated with pyrrhotite, magnetite, and pyrite, along with large rounded almandine garnets and amphibole (Wilton *et al.*, 2002).

The type example of carbonate-hosted gold is the Navachab Gold Mine in the Karibib District. Mineralization occurs in quartz-vein stockworks and in enveloping skarn (Pirajno & Jacob, 1991; Pirajno *et al.*, 1991; Steven, 1993; Steven *et al.*, 1994). In the Pan-African context, Navachab Mine is unique because it has a world-class gold reserve of 10.4 million tonnes, at a head grade of 2.4 g/t Au (Steven *et al.*, 1994). The smaller Onguati deposits studied in this project (see Fig. 3.1) can also be grouped in this class (Pirajno *et al.*, 1991).

3.3. SCZ Lithostratigraphy and Mineralization

The geology of the SCZ is characterized by several large inliers of pre-Damara basement, overlain by a thick succession of feldspathic quartzites, arkoses and marls belonging to the Nosib Group, and carbonates and pelitic to semi-pelitic rocks of the Swakop Group. Some of the earliest accounts of the geology and mineralization of the Omaruru and Karibib-Usakos areas come from Haughton *et al.* (1939) and Frommurze *et al.* (1942) respectively. The subdivision and correlation of stratigraphic units across the CZ is largely a result of work by Gevers (1931), Smith (1965), Jacob (1974), Botha (1979), Klein (1980), Watson (1982) and Brandt (1985). Together with his own mapping, Badenhorst (1987, 1992) reviewed and significantly revised the lithostratigraphy of the CZ and correlated units across the Omaruru Lineament. The latest revision of CZ stratigraphy, which is adopted in the account below, is based on field studies and LANDSAT image interpretation by Lehtonen *et al.* (1996). Table 3.3 summarizes the correlation and stratigraphic nomenclature of the lithostratigraphic units used by various workers in the CZ. Significant Cu-Au hydrothermal mineralization with reference to the lithostratigraphy is noted in the text. Table 3.4 (p.46) summarizes the main mineralization types and Au-potential of each lithostratigraphic unit in this part of the SCZ. Data on the metal contents of various CZ lithologies close to and away from mineralization are detailed in Steven (1993).

Table 3.3: Stratigraphic nomenclature and correlations of the Central Zone of the Damara Belt (modified after Badenhorst, 1992, Fig. II/2, p.9; and Lehtonen *et al.*, 1996, Table 1, p.71).

Klein 1980 (lower Omaruru River)	**Watson 1982 (Karibib area)**		**Brandt 1985 (Henties Bay - Karibib areas)**	**Miller 1983c (summary)**		**Badenhorst 1987 (Karibib area)**		**Badenhorst 1992 (Karibib area)**		**Lehtonen *et al.* 1996 (western Central Zone)**			**Lithology**
Kuiseb Formation	Kuiseb Formation		Kuiseb Formation	Kuiseb Formation		Kuiseb Formation		Kuiseb Formation		Kuiseb Formation		SWAKOP GROUP	schist; calc-silicate rock, marble, quartzite
Onguati Member	*(Onguati Member not developed)*		Karibib Formation	Onguati Member		Karibib Formation	Transitional Zone (TZ)	Onguati Formation		Karibib Formation	Onguati Member		marble, calc-silicate rock, schist
Arises River Member	Karibib Formation	Arises River Member		Arises River Member			Upper Marble Unit (UMU)	Karibib Formation	Arises River Member		Arises River Member		calcitic marble
Otjongeama Member		Otjongeama Member		Otjongeama Member					Otjongeama Member		Otjongeama Member		marble, calc-silicate rock
Harmonie Member		Harmonie Member		Harmonie Member					Harmonie Member		*(Harmonie M. not developed*		marble, calc-silicate rock, schist
Chuos Formation*	Oberwasser Formation		Oberwasser Formation	Oberwasser Formation	(a)		Upper Schist Unit (USU)	Oberwasser Formation		Arandis Formation	Oberwasser Member		schist
Rössing Formation	Rössing Formation			Rössing Formation			Lower Marble Unit (LMU)	Okawayo Formation			Okawayo Member		marble, schist, calc-silicate rock
Khan Formation	Khan Formation			Khan Formation			Lower Schist Unit (LSU)	Spes Bona Formation			Spes Bona Member		schist, calc-silicate rock
	Etusis Formation			Etusis Formation		*(Karub Member not developed)*		*(Karub Member not developed)*			Karub Member		marble, calc-silicate rock, schist
						Chuos Formation		Chuos Formation		Chuos Formation			mixtite, pebbly schist
						Rössing Formation		Rössing Formation		Rössing Formation			marble, quartzite, schist, calc-silicate rock
						Khan Formation		Khan Formation		Khan Formation		NOSIB GROUP	calc-silicate rock, biotite schist, amphibole
					(b)	Etusis Formation		Etusis Formation		Etusis Formation			arkosic quartzite, gneiss, biotite schist

--------- (a) Correlation after Botha, Klein, Watson, Brandt and Miller

——— (b) Correlation after Badenhorst and Lehtonen *et al.*

* no correlates of the Oberwasser Formation recognized

3.3.1. Abbabis Metamorphic Complex

The basal conglomerates of the Etusis Formation are separated from the underlying pre-Damara basement by an unconformity, first recognized by Gevers (1931) on the farm Abbabis 70. The Abbabis Metamorphic Complex consists of a heterogeneous assemblage of rocks that include metasediments such as quartzites, meta-arkoses and calc-silicate rocks; meta-volcanic and pyroclastic rocks; and ortho-gneisses and ortho-amphibolites (Jacob *et al.*, 1978). Grey or pink-coloured quartzofeldspathic, augen gneisses, formerly granitoids, are the most widespread and conspicuous rock type of the pre-Damara basement (Brandt, 1985).

SHRIMP U-Pb dating by Kröner *et al.* (1991) constrains the age of some of the red granite gneisses to 1038±58 Ma. Inherited zircons in the ortho-gneisses yield an age of 2093±51 Ma (Kröner *et al.*, 1991), and together with the unabraided zircon U-Pb upper intercept age of ~1925±300 Ma originally obtained for the Abbabis gneisses (Jacob *et al.*, 1978), suggest an approximately 2000 Ma protolith age. SHRIMP U-Pb dating of zircon rims from the basement gneisses gave an age of 571±64 Ma, and have been interpreted as Damaran overgrowth during regional metamorphism (Kröner *et al.*, 1991; Oliver, 1994). This age also signifies the involvement of the basement during Damaran orogeny.

The Abbabis Metamorphic Complex is of economic interest because it may contain a substantial amount of gold. ENE-WSW trending shear zones in the Abbabis Inlier, some 20 km southwest of Karibib Town, have been found to be auriferous (Steven, 1993). Quartz veins associated with these shear zones have been sampled with up to 1 g/t Au (Steven, 1993). In addition anthophyllite-chlorite magnetite rocks in the basement contain anomalous amounts of gold exceeding 300 ppb (Steven, 1993).

3.3.2. Nosib Group

The Nosib Group unconformably overlies the Abbabis Metamorphic Complex, and was first subdivided into the Etusis and Khan Formations by Smith (1965) and Nash (1971) respectively. The Etusis Formation is found over large areas of the SCZ and attains a thickness of 3300 m in the vicinity of the Abbabis Inlier (Steven, 1993). The Etusis Formation extends from the Okahandja Lineament to a line linking Walvis Bay and Usakos, across which it abruptly pinches out into the NCZ (Miller, 1983c, Brandt, 1985). The Khan Formation, initially a succession of marly sediments, is only found in the southwestern parts of the SCZ where it interfingers with the upper Etusis Formation (Smith, 1965, Jacob, 1974).

(a) Etusis Formation

The Etusis Formation consists primarily of a pink, coarse- to medium-grained, feldspathic quartzite, with minor quartzitic conglomerate and meta-pelite (Miller, 1983c). The feldspathic quartzites are poorly to moderately sorted, massive to thinly bedded, and locally grade into grits or feldspathic or lithic greywackes (Miller, 1983c). At many localities planar and cross-stratification are preserved and often contain heavy mineral laminae (Miller, 1983c). Occasionally channel deposits can be recognised with lensoid bars of conglomerate and sand (Miller, 1983c; Brandt, 1985). Geochemical and sedimentary evidence shows that these metasediments were largely derived from the underlying Abbabis basement (Miller, 1983c; Steven, 1993).

3.3.3. Swakop Group

The Nosib Group is overlain by the Swakop Group. In the SCZ the Swakop Group has been subdivided into the Rössing Formation (lies paraconformably on the Etusis Formation in the western parts of the SCZ only), Chuos Formation, Arandis Formation, Karibib Formation, and Kuiseb Formation (Lehtonen *et al.*, 1996). Some units originally defined as formations in the Karibib District by Badenhorst (1992) have now been relegated to member status in the newly defined Arandis Formation of Lehtonen *et al.* (1996). This is mainly a result of the Okawayo marble unit being absent or very thin and difficult to recognise in the western parts of the CZ, especially where the outcrop is poor (see Table 3.3). In addition, the close lithological similarity between the Spes Bona and Oberwasser units, and the absence of the Okawayo Member in the western CZ, make it difficult to trace the lithological contact between the two. The former Onguati Formation was also relegated to member status and assigned to the Karibib Formation because it is seen as transitional between the Karibib Formation marbles and the overlying Kuiseb Formation schists (Hoffmann, *pers. comm.*, 2003).

(a) Chuos Formation

The Chuos Formation is an important stratigraphic marker in the CZ (Gevers, 1931; Martin, 1965; Smith, 1965; Jacob, 1974; Henry *et al.*, 1986; Badenhorst, 1987; Badenhorst, 1988) and is well developed in the vicinity of the Abbabis Inlier. Locally the Chuos Formation lies unconformably on the Etusis Formation and commonly comprises unsorted, mixtites with angular and rounded clasts set in an abundant shaly, schistose, sandy or dolomitic matrix (Miller, 1983c). Brandt (1985) postulated that there is facies change in the Chuos Formation across a zone, roughly defined by the line Swakopmund-Usakos. To the NW of this line, the Chuos Formation consists of pebbly schist with widely scattered clasts of quartzite and vein-quartz, with subordinate meta-arkose and marbles(Brandt, 1985). On the southeastern side, the formation differs by having a wide variety of rock types, including highly packed mixtites with 80 cm wide boulders and angular fragments of quartzites, calc-silicate rocks, schists, and granitic rocks (Brandt, 1985).

(b) Arandis Formation

Arandis Formation terminology (see Table 3.3) was introduced to describe the package of undifferentiated schist and calc-silicate rock that is found between the Chuos Formation mixtites and the marbles of the Karibib Formation (Lehtonen *et al.*, 1996). The Arandis Formation consists of the lowermost Karub Member (medium-to coarse-grained marble unit of very limited extent in the western parts of the SCZ), overlain by the Spes Bona, Okawayo, Oberwasser and Daheim Members in turn (Lehtonen *et al.*, 1996). In the Karibib region the Chuos Formation is directly overlain by the Spes Bona Member (Badenhorst, 1992).

The Spes Bona Member, formerly known as the Lower Schist Unit, consists of an intercalated sequence of calc-silicate rock, schist and amphibole schist (Badenhorst, 1992). This unit has a limited distribution in the SCZ, and only reaches 30 m in thickness on the farm Spes Bona 105 but further north may attain a thickness of over 500 m (Steven, 1993).

The Okawayo Member is the first extensive carbonate sequence found below the Karibib Formation marbles and under the older stratigraphic terminology was referred to as the Lower Marble Unit (Badenhorst, 1992; Lehtonen *et al.*, 1996). On the farm Okawayo 146 in the Karibib District, the type section shows this unit to be about 50 m in thickness (Badenhorst, 1992). From an economic perspective, the Okawayo is of great importance because it hosts a significant part of the gold-bearing skarn at Navachab Gold Mine (Pirajno *et al.*, 1991; Steven, 1993).

The Oberwasser Member, formerly the Upper Schist Unit, is a consistent unit of dark grey, biotite schist directly below the Karibib Formation (Badenhorst, 1992). The Oberwasser Member occurs over large parts of the NCZ where it attains a thickness of approximately 700 m. In the Okawayo Section close to the Onguati study area it is only 50 m thick (Brandt, 1985; Steven, 1993).

The Daheim Member is a 35 to 180 m thick meta-volcanic unit which contains lava flows interbedded with tuff, coarse pyroclastic material, lava breccia, schist, marble and meta-arkose (Mullin, 1989; Badenhorst, 1992). The alkaline volcanic rocks of this member locally crop out in the antiformal closure 5 km west of the defunct Onguati Mine, and also in the northeastern part of the Navachab Dome (Badenhorst, 1992). In places the amphibolites have been relatively unaffected by deformation and volcanic structures such as pillows, lapilli and volcanic bombs are commonly still preserved (Joubert, 1989; Mullin, 1989). Layered hornblende amphibolites are also found southwest and southeast of Karibib Town as the Tsabichas and Omusema Amphibolite Members in a similar stratigraphic position to the Daheim Member meta-volcanic rocks (Miller, 1983c).

The Daheim meta-volcanic rocks do not host any known mineral deposits, but do contain minor amounts of gold. Pirajno *et al.* (1991) suggested that the Daheim Member may have been the source for the carbonate-hosted gold deposits in the overlying stratigraphy, and that hydrothermal fluids scavenged metals from the mafic rocks during prograde metamorphism.

(c) Karibib Formation

The Karibib Formation conformably overlies the Arandis Formation, and varies considerably in thickness over the CZ and NZ (Miller, 1983c). The Karibib Formation has been subdivided into the basal Harmonie Member, followed in succession by the Otjongeama and Arises River Members (Badenhorst, 1992) on the basis of abrupt changes in the upward pelitic and clastic sediment content. According to the latest stratigraphic re-organisation, the Onguati Member now forms the upper part of the Karibib Formation (Lehtonen *et al.*, 1996). In the Karibib region a further marble unit has been identified, and is known as the Navachab Member (Badenhorst, 1992). It appears that the Navachab Member is confined to this part of the SCZ, where it rests directly on the Otjongeama Member. Northwards, the Otjongeama Member is overlain by the Arises River Member (Badenhorst, 1992, Fig ii/1: Geological map, p.17-18), but the relationship between the Navachab and Arises River Members is unclear from the available literature.

The Harmonie Member is composed of abundant calc-silicate layers interbedded with calcitic and dolomitic marbles, but also has a minor schist component (Miller, 1983c; Badenhorst, 1992). Rare, deformed stromatolite structures have been found in this member, and occasionally calc-silicate units display crossbedding (Badenhorst, 1992). On the farm Okakongo 93 in the NCZ, the calc-silicate layers commonly reach thicknesses between 3 and 5 m, while individual marble beds never exceed 1.5 m in thickness (Badenhorst, 1992).

The middle Otjongeama Member is a light grey, marble-dominated unit characterized by its 1-5 cm thick, green calc-silicate interlayers (Lehtonen *et al.*, 1996). A general decrease in the amount of calc-silicate material is observed from the base of this unit upward (Badenhorst, 1992). On the farm Spes Bona 105, the Otjongeama Member reaches about 150 m in thickness, and at Okakongo it may attain a thickness of nearly 500 m (Badenhorst, 1992).

In the Okawayo Section the Navachab Member attains an apparent thickness of nearly 450 m, and at this locality and at Spes Bona, it lies conformably on the Otjongeama Member (Badenhorst, 1992). The Navachab Member contains interbedded dark and light grey calcitic marble with or without calc-silicate layers, white dolomitic marble, ribbon marble, and in places, marble breccias. Individual layers can range in thickness from cm-scale to several metres, and often contain pyrite and minor accessory sulphides (Badenhorst, 1992). The lower part of this member consists of a series of cyclical units marked by basal ribbon marble, often followed by laminated calcitic, dolomitic or laminated dolomitic marble (Badenhorst, 1992). The top part of the Navachab Member consists of thick dolomitic units with calcitic marble interbeds (Badenhorst, 1992).

The Arises River Member occurs extensively over the CZ, especially in the western parts and north of the Omaruru Lineament, and locally can reach thicknesses of up to 500 m (Lehtonen *et al.*, 1996). It comprises a pure, white to light or bluish grey, coarse-grained marble, but a graphitic, dark grey, sulphide-bearing variety also occurs in the western CZ (Badenhorst, 1992; Lehtonen *et al.*, 1996). Sedimentary breccias also occur throughout this member (Badenhorst, 1992).

Gold mineralization with associated sulphides, occurs throughout the Karibib Formation carbonate sequence. At Navachab Mine gold mineralization is largely hosted by a calc-silicate marble unit (MC unit, Navachab Mine nomenclature), but also by dolomitic (DM) and calcitic marbles (CM), all belonging to the Navachab Member (Steven, 1993). The copper-gold mineralization in the Onguati study area is also hosted by the Navachab Member, but mainly occurs in calcitic marbles with minor calc-silicate interlayers. Mineralization may extend into the overlying dolomitic marbles. Minor gold showings in Karibib Formation rocks have also been noted at the Habis Gold Prospect and in zones of massive tremolite associated with gossan on the farm Habis 71 south of Karibib Town, at Otjimboyo Oost 48, and at Hill 1166 on the farm Sandamap 64 (Pirajno *et al.*, 1991; Steven, 1993).

The Onguati Member represents a transitional zone of schist, marbles, calc-silicate rocks and quartzites that occur between the Karibib Formation carbonates and the pelitic Kuiseb Formation (Badenhorst, 1992; Lehtonen *et al.*, 1992). The intercalated sequence of rocks making up the Onguati Formation attain a thickness of 850 m at Spes Bona 105

Table 3.4: Relationship between lithostratigraphy and mineralization in the eastern part of the SCZ (based on Miller, 1983b; Pirajno & Jacob, 1991; Pirajno *et al.*, 1991; and Steven, 1993).

Lithostratigraphy of SCZ			**Mineralization**
SWAKOP GROUP	**Kuiseb Formation**		- hosts finely disseminated scheelite in vesuvianite calc-silicate lithologies (Steven, 1993); - minor tungsten skarn mineralization in carbonates; - stanniferous pegmatites are common, especially in the higher level NCZ where they form important tin belts (Miller, 1983b); - minor shear zone-hosted Au-As mineralization in NCZ schists (Steven, 1993).
	Karibib Formation	**Onguati Member**	- stratabound tourmaline-bearing rocks may be related to Damaran pegmatitic activity (Steven, 1993); - generally poorly mineralized.
		Navachab Member	- gold mineralization with associated sulphides occurs at all levels in the Karibib Formation carbonates and calc-silicate rocks (Pirajno *et al.*, 1991; Steven *et al.*, 1994); - Cu-Au mineralization in the Onguati study area is hosted mainly by calcitic marbles of the Navachab Member (Pirajno & Jacob, 1991); - at Navachab Gold Mine the best Au-grades occur in the calc-silicate marble unit (MC unit), but also in the dolomitic (DM) and calcitic (CM) marbles of the Navachab Member (Steven, 1993); - minor Au showings have been noted at the Habis Gold Prospect associated with gossan and massive tremolite skarn (Pirajno *et al.*, 1991; Steven, 1993); - minor occurrences at Otjimboyo Oost 48, and at Hill 1166 on Sandamap 64 (Pirajno *et al.*, 1991; Steven, 1993). - potential for MVT and volcano-exhalative Pb-Zn mineralization
		Otjongeama Member	
		Harmonie Member	
	Arandis Formation	**Daheim Member**	- metavolcanics contain anomalous Au contents (Petzel,1988); - suggested as a source of carbonate-hosted gold deposits in overlying stratigraphy (Pirajno *et al.*, 1991).
		Oberwasser Member	- Epako Prospect with auriferous quartz veins is the only known mineralization in this member (Steven, 1993).
		Okawayo Member	- hosts a significant part of the Au-bearing skarn at Navachab Mine (Pirajno *et al.*, 1991) - also hosts scheelite skarn deposits of Otjua W prospect in the NCZ (Steven, 1993); - potential for MVT and volcano-exhalative Pb-Zn mineralization
		Spes Bona Member	- host finely disseminated scheelite mineralization (Steven, 1993).
	Chuos Formation		- associated banded iron formation and minor sulphide showings; - devoid of significant mineralization.
NOSIB GROUP	**Etusis Formation**		- sub-economic, auriferous quartz veins have been discovered at Nordenberg Gold Prospect (Steven, 1993); - carbonates in this formation host an unusual 'skarn' deposit with magnetite-monazite mineralization; - potential for placer Au deposits in the Etusis quartzites and arenites, especially if derived from Abbabis basement. - potential for sedimentary-hosted Cu; volcano-exhalative minz.
Pre-Damara, Abbabis Metamorphic Complex			- ENE-WSW trending shear zones and associated veins and anthophyllite-chlorite rocks contain anomalous amounts of gold >300 ppb (Steven, 1993); - auriferous copper-bearing quartz veins have up to 1g/t Au (Steven, 1993); - basement could be an important source for Damaran Cu-Au deposits?

(Steven, 1993). Marble units occur in cycles of upwards decreasing carbonate, and may contain oolitic layers and trough cross-bedding in the upper parts (Badenhorst, 1992).

(d) Kuiseb Formation

The Kuiseb Formation is the youngest lithostratigraphic unit of the Damaran Sequence and covers an extensive part of the CZ, commonly preserved in synformal domains (Miller, 1983c). The Kuiseb Formation comprises a thick succession of interlayered metapelites and metagreywackes that have a minimum thickness of between 3000 m and 5000 m (Badenhorst, 1992). In the SCZ, the most common rock type of the Kuiseb Formation is quartz-biotite schist. The Kuiseb Formation has been intruded by numerous Salem-type granites and pegmatites (see section 3.4.2).

3.4. Crustal Architecture of the SCZ

In light of the apparent relationship between shear zones and gold mineralization in the northern parts of the Damara Belt (e.g. Pirajno & Jacob, 1991; Steven *et al.*, 1994), and the proposed ore genesis models which invoke 'granitic' bodies as the source of fluids and heat, or of the metals themselves (Pirajno *et al.*, 1991; Steven, 1993), it is pertinent to review the structure and intrusive evolution of the SCZ. The emphasis of this section is to characterize the major SCZ crustal lineaments, review known associations between Damaran structures and mineralization, and outline the compositions and Cu-Au prospectivity of the granitoids.

3.4.1. Crustal Structure

Several crustal-scale lineament zones have been identified in the SCZ (Fig. 3.2), and their main features and possible associations with mineralization are summarized in Table 3.5. Southwards the SCZ is bound by the NE-trending Okahandja Lineament (OL), while northwards it is separated from the NCZ by the Omaruru Lineament (OML) - Waterberg Fault (Corner, 1983). Within the SCZ there is the NNE-trending Welwitschia Lineament (WL) and the parallel Abbabis Lineament (ABL), which passes through Usakos and terminates at the intersection of the OML and Erongo Complex (Corner, 1983). Unfortunately the orientation and position of the ABL on regional geophysical maps is quite different between Fig.1 of Corner (1983, p.340) and the more recent Map 6 of Corner (2000, p.20-21), so they have

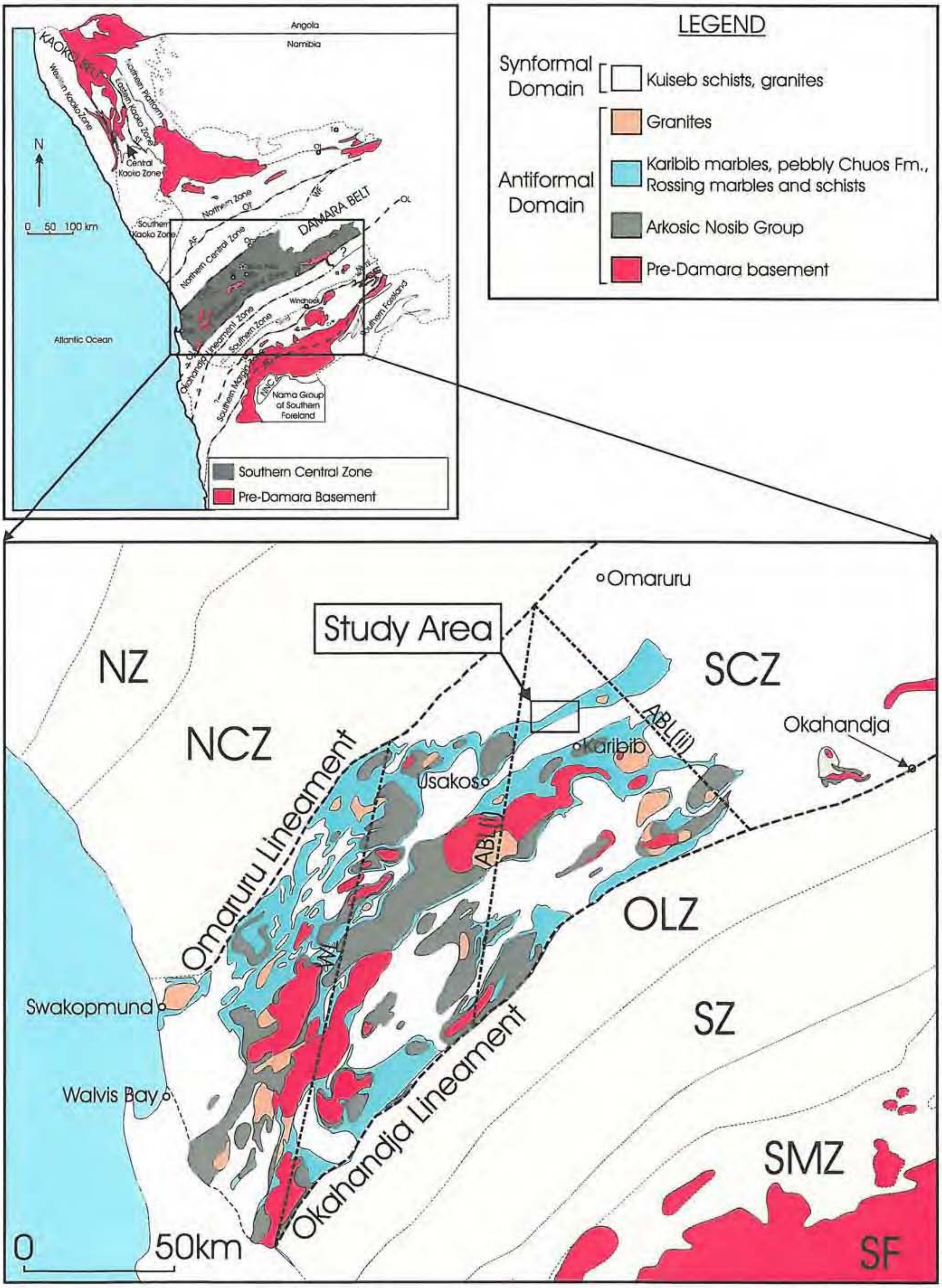

Fig 3.2: Detail of the Southern Central Zone showing the lithostratigraphic contrasts between domes and their distribution. Domes are cored by basement, Nosib arkose and Damara granite in the SCZ. The top of the Karibib Formation is taken as the upper surface of the domes (modified after Miller, 1983c, Figures 2 and 19, pages 434 and 460 respectively). WL = Welwitchia Lineament; ABL(i)=Abbabis Lineament(i) (after Corner, 1983, Fig. 1, p.340); ABL(ii)=Abbabis Lineament(ii) (after Corner, 2000, Map 6, p.20-21).

Table 3.5: Characteristics of the major crustal features in the SCZ, and relevance to magmatism and mineralization (Corner, 1983; 2000)

Lineament	Characteristics of lineament swath	Relationship to intrusives	Possible association with regional mineralization
Okahandja Lineament (OL)	- separates tectonized and magnetically disturbed CZ domain from magnetically quiet OLZ and SZ; - marks an abrupt change from the linear structural grain of the OLZ to the dome-and-basin structural patterns of the CZ; - experienced long-lived sinistral movement during transpression.	- extensive 2-mica Donkerhuk granites *(see section 3.4.2)* are bound to the north by this lineament, and it is likely that this major crustal weakness assisted intrusion.	- close proximity to alaskitic U-mineralization in western part of SCZ?; - possible association with base metal mineralization (e.g. Pot Mine; Elbe deposit).
Omaruru Lineament (OML) - Waterberg Fault (WF) line	- NE-trending terrane boundary between lower, magnetically anomalous Damaran stratigraphy of the SCZ, and more subdued and homogeneous response of the upper NCZ stratigraphy; - may have had just as large an influence on Damaran geology as better known OL (Steven, 1993); - interpreted as northern boundary of Abbabis geanticlinal ridge in coastal region, along which a line of monoclinal down-folding has occurred (similar to what has occurred along the OL); - probably underwent sinistral transpression.	- early Cretaceous Erongo Complex has utilized the intersection of OML, ABL[i] and ABL[ii] (see below).	- close spatial association between late stanniferous pegmatites and OML (e.g. Ameib Tin Mine; Sandamap Tin Mine); - Joumbira base metal deposits lies directly on Waterberg Fault; also Kranzberg Mine in close proximity; - close proximity to Klein Trekkopje U deposit.
Welwitschia Lineament (WL)	- NNE-trending crustal feature that intersects the OL and OML, and extends into the NCZ; - WL marks a discrete change in structure between eastern parts of CZ where there are only NE-trending structures, and western parts of CZ where NNE-trending fold axes are superimposed on older NE direction.	- numerous syeno- and monzo-granites occur along and in the vicinity of the WL zone, but difficult to assess whether emplacement was structurally controlled by this lineament.	- numerous Cu showings in close proximity to WL? - may be important control on the emplacement of uraniferous alaskitic granites (Corner, 1983).
Abbabis Lineament (1983) (ABL[i])	- defined by Corner (1983, Fig.1, p.340); - NNE-trending ABL[i] parallels WL, and passes through Usakos terminating at the OML; - corresponds to a broad zone of crustal lineaments.	- early Cretaceous Erongo Complex has utilized the intersection of ABL[i], ABL[ii] and OML; - numerous Karoo age (?) dolerite dykes have made use of this pre-existing Damaran weakness.	- both the Navachab Gold Mine and the Onguati Cu-Au deposits are in very close proximity to ABL[i]; - ABL[i] could link a dioritic source (Goas Magmatic Suite) to Navachab Mine and Onguati? - numerous Cu showings in close proximity to ABL[i] along its length?
Abbabis Lineament (2000) (ABL[ii])	- defined by Corner (2000, Fig.6, p.20-21); - NW-SE orientation and may extend northwards to delineate the approximate western margin of the Congo Craton.	- appears to mark the SW limit of the extensive monzogranitic batholith in the eastern parts of the SCZ *(see Fig. 3.3)*.	- both the Otjimbojo Tin Mine and Otjimbojo Cu-Au deposit may lie in the lineament swath.

been referred to in this text as ABL(i) and ABL(ii) respectively. It is quite likely that both lineament trends exist but have been called by the same name (see aeromagnetic interpretation, section 3.5.2).

Steven (1993) postulated that the Abbabis basement of the SCZ may have behaved as a relatively rigid block between the Okahandja and Omaruru Lineaments, and that it was the less competent overlying Damaran Sequence that accommodated much of the strain. The WL and ABL(i) may divide the crust into further discrete, parallelogram-shaped sub-blocks, and it is speculated that these could have dictated deformation styles in the overlying Damaran metasediments. It is also possible that these major crustal breaks could have been significant for fluid flow and a wide variety of hydrothermal mineralization at the SCZ scale (primary-order structures). Areas of low strain would have been conducive for fluid localisation and economic mineralization. Both the Navachab Mine and Onguati deposits are in close proximity to the ABL(i) zone.

SCZ structure is complex and characterized by elongate, northeast-trending dome structures and irregularly shaped synforms (Miller, 1983c). Many of the domes have steep or overturned margins, bulbous to cylindrical forms, and can have pinched out limbs (Miller, 1983c). The kilometre-scale dome structures have been interpreted to be the result of: (i) polyphase inference folding involving at least 2 or 3 phases of deformation (e.g. Smith, 1965; Coward, 1983; Jacob *et al.*, 1983; Miller, 1983c; Stanistreet *et al.*, 1991); (ii) F_2 sheath folding (Downing & Coward, 1981a); (iii) granitic diapirism (Barnes, 1981; Coward, 1981; Sawyer, 1981) or magma body ballooning (Kröner, 1984); and most recently, (iv) single-episode, progressive deformation with deep metamorphic core complex development (Oliver, 1994; Oliver, 1995; Oliver & Kinnaird, 1996; Poli & Oliver, 2001).

3.4.2. Granitic Magmatism

A large proportion of the 74 000 km^2 area underlain by orogenic plutonic rocks of the Damara Belt is found exposed in the CZ (Miller, 1983c). In the SCZ (Fig. 3.3) there are several hundred Damaran-age plutons that occupy areas ranging from less than 0.5 km^2 up to many thousands of km^2 in extent (Miller, 1983c). The majority of plutonic rocks in the SCZ are granites *senso stricto* (95% are syeno- or monzo-granites), but there are small amounts of granodiorite and tonalite (together making up to 4%), and relatively rare occurrences of quartz monzonite, quartz monzodiorites, quartz diorite, diorite, gabbro and syenite (Miller, 1983c; Brandt, 1987). Brandt (1985, 1987) divided the magmatic rocks of the SCZ into eight groups

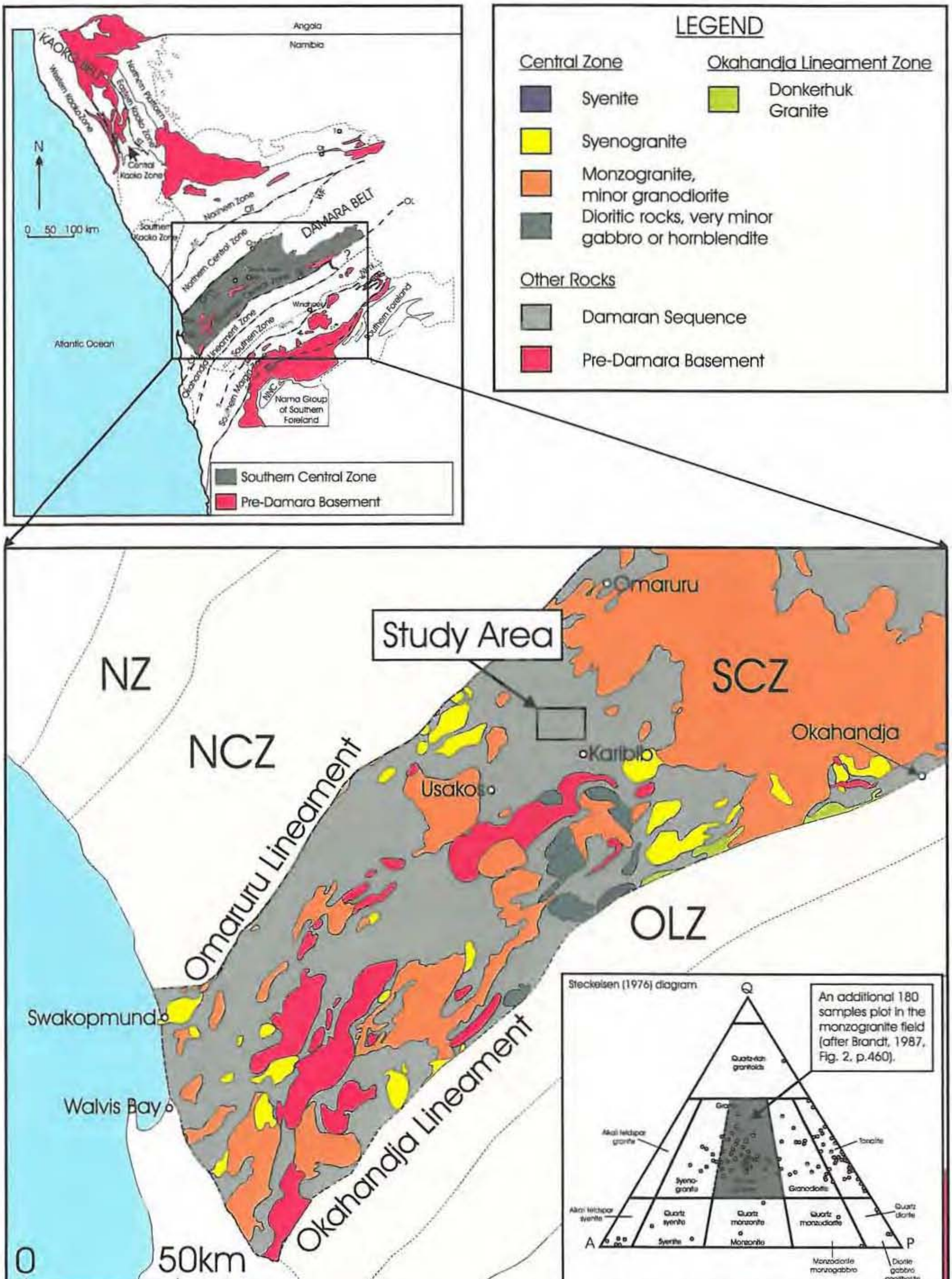

Fig. 3.3: Distribution of Damaran granites in the Southern Central Zone (SCZ) of the Damara Belt. Abbreviations are the same as in Fig. 2.3 (Modified after Miller, 1983c, Fig. 34, p.482). Inset shows the modal analyses of almost 300 plutonic rocks of Damaran age from the CZ and OLZ of the Damara Belt (after Brandt, 1987, Fig. 2, p.460).

based on their appearance, field relationships and relative ages. Table 3.6 summarizes the main features of these intrusive groupings and details the probable source areas and mineralization potential of each.

Smith (1965) noted that the main granite types appear strictly confined to specific parts of the lithostratigraphy, so that the typical porphyritic Salem-type granites are found in synclines near the base of the Kuiseb Formation, while the medium-grained red granites are found associated with Nosib group rocks in the cores of anticlinal structures. This led many investigators (e.g. Smith, 1965; Jacob, 1974, Miller, 1974) to suggest that these granites were formed by *in situ* melting of the Damaran metasediments shortly after the peak of metamorphism. While partial melting of the basement rocks and Nosib lithologies is feasible for the red granites in the higher grade western parts of the SCZ, it is highly unlikely that the widespread Salem-type granites were derived from the Kuiseb Formation or underlying Damaran metasediments. Trace element and isotopic evidence supports generation of Salem-type granites from a wide range of protoliths situated in the lower to middle crust (Haack & Martin, 1983; Miller, 1983c; Brandt, 1985, 1987). Jung et al. (2000a, b, 2001) have also shown that members of the syntectonic Salem-type leucogranites in the NCZ were derived from a heterogeneous lower crust consisting of meta-pelites (S-type source) and meta-granitoids (A-type source), and that Damaran granitic composition is additionally controlled by the temperature of melting, the availability of fluids and in some cases, country rock contamination.

The genesis of this diverse group of plutonic rocks is of economic interest because different crustal sources and melting conditions may result in magmas associated with different mineralization type and potential. The bulk of the Damaran granites have S-type affinities and some are related to Sn-W hydrothermal mineralization. However, it is the hornblende-bearing diorites and granodiorites of I-type affinity (i.e. Goas Magmatic Suite) that hold the greatest potential as the source of the Cu-Au mineralization observed in the Karibib region of the SCZ. A 'granitic' source for mineralization will be discussed in the concluding chapter of this thesis.

Table 3.6: Characteristics and mineralization potential of the eight main groups of plutonic rocks found in the SCZ (based on Miller, 1974; 1983b; 1983c; and Brandt, 1985; 1987).

Granite Group	Main Characteristics	Type/Protolith	Emplacement Relative to Deformation	Known Mineralization, and Potential as Cu±Au Source
1. Goas Magmatic Suite	- wide range of plutonic rocks including hornblende-bearing diorites, quartz diorites, tonalites, granodiorites and 2-mica leucogranites; also gabbro and hornblendite plugs and dykes (e.g. Etusis-Neikhoes pluton) - represent a small fraction of SCZ granitoids; - bulk of these rocks found to south of Karibib Town as the Goas Magmatic Suite; - initial $^{87}Sr/^{86}Sr$ ratios: 0.7050-0.7013, average Rb/Sr ratio: 0.2 (similar to primary sialic crust).	I-type granitoid Mafic lower crust	Pre-tectonic (early intrusives with emplacement before the main phase of deformation)	- composition and I-type signature may make them good candidates as magmatic source of Cu and Au; - minor sulphide mineralization associated with veins, skarn and small areas of alteration associated with Ukuib 84 porphyritic member of the Goas Magmatic Suite (just NW of the Okahandja Lineament); also defunct Cu-Au Gamikaubmund and Pot Mines in very close proximity to this plutonic body; - however these intrusives only make up a small proportion of SCZ plutonites; - found to south of Karibib away from significant Cu-Au deposits and mineralization (*see Figs. 3.1 and 3.3*).
2. Red heterogeneous granites	- comprises a very heterogeneous array of granitic rocks; - commonly contain leucocratic and biotite-rich schlieren; - occupy the same stratigraphic level as Abbabis basement or overlying Nosib Group; - frequently found in the cores of domes especially in the higher-grade part of the CZ.	S-type Partial melts of Abbabis Basement or Nosib Group ?	Pre- to Syn-tectonic	- can be anomalously enriched in U; - potential for Sn-W mineralization in associated veins, pegmatites, skarns and mantos; - favourable stratigraphic position below the Arandis and Karibib Formation if they are the source of hydrothermal fluids; - poor potential as source of Cu-Au mineralization.
3. Red and grey homogeneous granites	- not confined to any particular stratigraphic level; - in places show a well-developed biotite foliation.	S-type ?	Syn- to Post-tectonic	- S-type Sn-W mineralization potential?
4. Salem-type granites	- generally grey (weathers red), coarsely crystalline, porphyritic (K-feldspar), biotite-rich monzogranites; - both foliated and non-foliated members; - contain xenoliths of sedimentary or igneous origin; - association with coarse-grained early diorites and tonalites; - found in synclinal domains where they have intruded the base of the Kuiseb Formation schists.	S-type (diorites have I-type, mantle-derived signatures; some A-type - metagranitoid source?) Derived from a wide range of lower to middle crust protoliths, excluding Damaran sediments.	Wide range of ages Span ~190 Ma period Pre-, Syn- and Post-tectonic members.	- minor potential for Sn-W and other incompatibles in associated pegmatites; - dioritic members of this group can have more I-type affinity and therefore a small, potential source of Cu-Au; - most members of Salem granites occupy upper stratigraphic positions above the Arandis and Karibib Formations where known mineralization is hosted.
5. Alkali complexes	- include porphyritic (K-feldspar) hornblende syenites, aplites and non-porphyritic syenites; - outcrop in close proximity to the Okahandja Lineament; - most notable example is Otjimbingwe Alkali Complex; - strong planar fabrics in these rocks may be related to movement along the Okahandja Lineament.	Alkaline ?	Syn-tectonic?	- poor potential for economic mineralization in the SCZ because they are of such limited extent; - feldspar-rich veins containing magnetite cut rocks of the Otjimbingwe Complex.
6. Post-tectonic Donkerhuk Suite, Gawib, Bloedkoppie and Kubas granites	- light grey, medium-grained biotite-muscovite granites (peraluminous); - intrusives are discordant with respect to the main structural trend of the Damaran rocks; - Donkerhuk granites are found mainly in the OLZ but extend just north of the OL into the SCZ.	mainly S-type, but also late I-type granites (peraluminous). Derived from partial melting of the Kuiseb Formation schists?	Post-tectonic	- very unlikely as source of Cu-Au; - only occur along the OLZ in the southernmost parts of the CZ.
7. Alaskites	- found in the higher grade, western parts of the SCZ; - form sheet-like bodies and tend to be porphyritic; - confined to the deepest stratigraphic levels.	Resulted from prolonged differentiation of high-level, Abbabis basement/Nosib-derived magmas.	Syn- and Post-tectonic	- alaskites can host economic concentrations of U which is mined at Rössing Mine; - do not occur in eastern parts of SCZ and confined to Nosib Group.
8. Pegmatites, pegmatitic granites and leucogranites	- intruded after peak of metamorphism; - form irregular, scattered bodies not confined to any stratigraphic level or area.	Most cannot be related to any of the Damaran granites, except for the ones associated with groups (5) and (6).	Late Syn- to Post-tectonic	- south of Karibib; the Rubicon Mine pegmatite is auriferous and has a Sn-W association; - Karibib pegmatites contain gem-quality tourmaline; - higher level pegmatites host Sn mineralization.

3.5. Geophysical Interpretation of the Karibib Region

Interpretation of SCZ geology and crustal structure within an 80 km arc of the Onguati study area have been carried out through visual analysis of high-resolution geophysical images, obtained with the kind permission of the Geological Survey of Namibia (GSN). The aim of this section has been to elucidate possible regional geological controls on known hydrothermal mineralization. In this regard, the structure of the Onguati study area (inset on regional scale maps) and its surrounds has been a major focus. The types and figure numbers of all the geophysical images utilised in this study are summarized in Table 3.7 below. Coloured or textured interpretative maps have also been produced, while tracing versions have been placed over each of the images for ease of reference.

Table 3.7: Summary of high-resolution geophysical images used in sections 3.5.1, 3.5.2 and 3.5.3.

Figure	Description	Section, Page
Fig. 3.4a ***(with overlay)***	Regional ternary (RGB) radiometric image draped over the first vertical derivative of the total magnetic field *(introduction to geology of region).*	*section 3.5.1* *p.56*
Fig. 3.4b	Regional interpretative line map of Fig. 3.4a showing the main lithologies and intrusive bodies, domes and basic structure.	*section 3.5.1* *p.57*
Fig. 3.5a ***(with overlay)***	Regional total magnetic intensity (TMI) image.	*section 3.5.2(a)* *p.60*
Fig. 3.5b	Regional interpretative map of Fig. 3.5a showing broad regions of high, moderate and low magnetic susceptibility and major lineaments.	*section 3.5.2(a)* *p.61*
Fig. 3.6a ***(with overlay)***	Regional first vertical derivative (1vd) image of the total magnetic field.	*section 3.5.2(b)* *p.63*
Fig. 3.6b	Regional interpretative map of Fig. 3.6a emphasizing lineaments, domal features and intrusive bodies.	*section 3.5.2(b)* *p.64*
Fig. 3.7a ***(with overlay)***	Study-area scale, first vertical derivative (1vd) image of the total magnetic field for the Onguati-Kranzberg antiformal structure.	*section 3.5.3* *p.66*
Fig. 3.7b	Study area-scale, interpretative map of Fig. 3.7a emphasizing lithologies of high magnetic susceptibility and lineaments with inferred sense of shear.	*section 3.5.3* *p.67*

The GSN has carried out airborne geophysical surveys (magnetics and radiometrics) over much of Namibia, typically at a 1000 m line separation and a 100 m flight height (Eberle & Hutchins, 1995). In recent years, the GSN has placed emphasis on the collection of high-resolution airborne magnetic and radiometric data to improve and supplement the existing Namibian geophysical database. The surveys, flown with a line spacing of 200 m and at a height of 80-100 m above ground surface, provide better quality data for mineral exploration and complement the regional geological coverage. Sampling interval for the aeromagnetic surveys is 5-7 m (one tenth of a second), and data integration is at 70 m (1 second) for gamma-ray spectrometry. Both the airborne radiometric and magnetic surveys have ground resolution cells of 50 m (R. Wackerle, *pers. comm.*, 2000).

3.5.1. Airborne Radiometric Response at the Karibib Regional Scale (1:500 000)

A ternary radiometric (Red-Green-Blue, RGB) image was draped over the first vertical derivative of the total magnetic field in Fig. 3.4a and was used to create a basic overview of the geology around the Onguati study area. Radiometric images provide a 3-element (K, Th and U) chemical map of the ground surface, whereas magnetics (discussed later) highlight underlying structure. In the past, radiometric surveys have been used in the western parts of the SCZ to identify sites of favourable U-mineralization. More recently radiometric images have been used to map internal zoning and igneous facies change within plutonic bodies (e.g. Etusis-Neikhoes intrusion; Viljoen, 2000). Gamma-ray data have often proven complementary to magnetic data and enable more precise location, and in some instances, redefinition of geological boundaries. This is especially the case where the stratigraphy is non-magnetic (Jacques *et al.*, 1997).

A simplified interpretative map of the geology and structure of this part of the SCZ was prepared from Fig. 3.4a. Units identified on this image were compared with Sheet 2 of the 1:500 000 geological map of the Damara Orogen (1988) to ascertain the radiometric characteristics of the stratigraphy. Composite radiometric-over-magnetic images, have been found to be particularly useful for mapping lithologies in complex terrains with discontinuous outcrop. Ternary radiometric images can qualitatively and quantitatively 'fingerprint' particular rock types on the basis of their commonly unique, 3 radio-element ratios.

On the ternary radiometric image, large areas of the map are black or violet. To the east and northeast (label A on the overlay), this is a result of the extensive batholith of Salem-type granites (high K and Th, moderate U), and to the north (label B) is due to the roughly

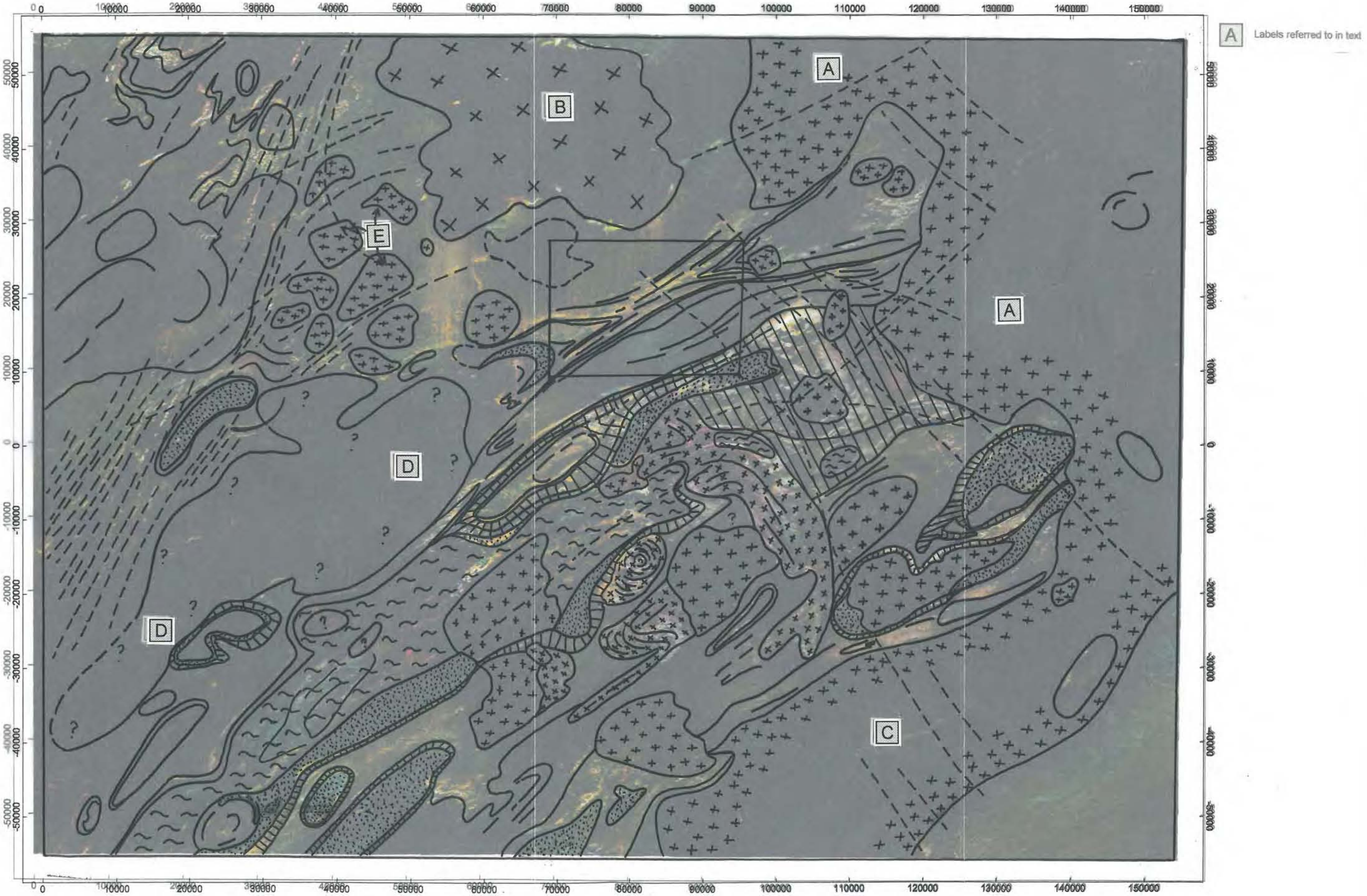

Central Meridian: E15
Latitude of Origin: S22
Central Scale Factor: 1.0
False Easting: 0.0
False Northing: 0.0

5000 0 5000 10000 15000
metres

Fig. 3.4a: Ternary (RGB) radiometric image (K = green, Th = pink, U = yellow) draped over the first vertical derivative of the total magnetic field (1vd), for the SCZ region around the Onguati study area (insert). Black areas correspond to places where rocks and surface cover have high concentrations of all three radio-elements; rocks and surface cover devoid of K, Th and U appear white. The regional scale image spans the area between approximately 0 and +150 000 on the x-axis (E015°00' to E016°30'), and from -50 000 to +50 000 on the y-axis (S21°30' to S22°30'), LO (Gauss Conformal) Projection, Bessel 1841 Spheroid (Schwarzeck Datum). Data provided by kind permission of the Geological Survey of Namibia, 2001©.

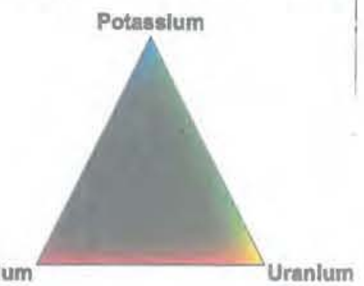

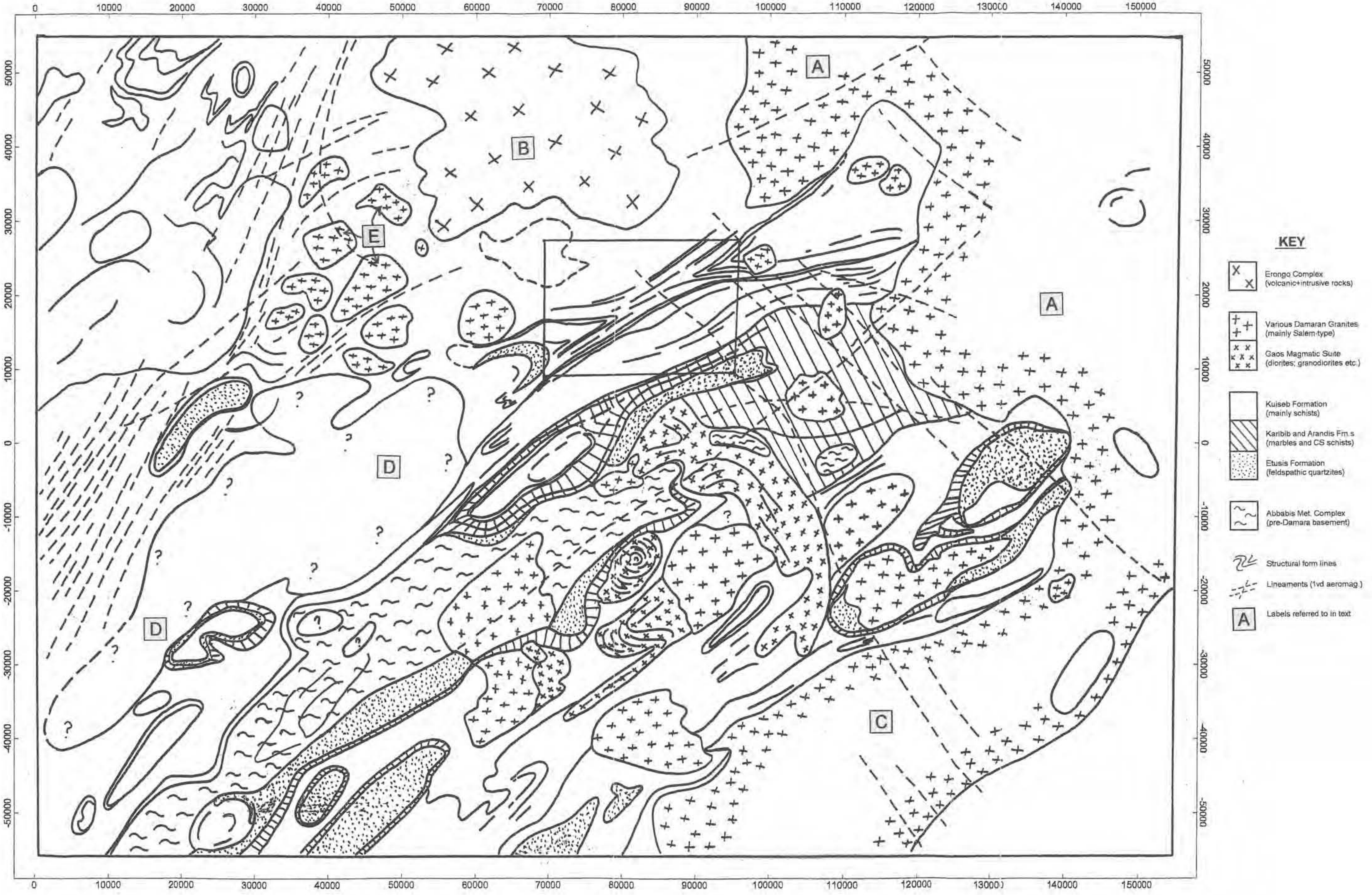

Fig. 3.4b: Interpretative map of the ternary (RGB) radiometric image draped over the first vertical derivative of the total magnetic field (1vd), Fig. 3.4a, for the SCZ region around the Onguati study area (insert). The regional scale image spans the area between approximately 0 and +150 000 on the x-axis (E015°00' to E016°30'), and from -50 000 to +50 000 on the y-axis (S21°30' to S22°30'), LO (Gauss Conformal) Projection, Bessel 1841 Spheroid (Schwarzeck Datum). Data provided by kind permission of the Geological Survey of Namibia, 2001©.

Central Meridian:	E15
Latitude of Origin:	S22
Central Scale Factor:	1.0
False Easting:	0.0
False Northing:	0.0

circular, post-Karoo Erongo Complex. The dark blue-black region to the SE (label C) corresponds to outcrop of the extensive Donkerhuk Granites, the northern edge of which is marked by the OL. Intrusive rocks in the SCZ, commonly have high proportions of all three radioactive elements. In the western part of Fig. 3.4a, a dark belt oriented NE-SW (label D) is likely to be a low-lying area of superficial cover that drains the nearby post-tectonic leucogranites (label E) and pegmatites, and possibly the Erongo granodiorites and granites to the north.

Light-coloured areas of the map correspond reliably to Damaran metasediments. The Onguati-Kranzberg anticlinorium is mainly composed of Karibib Formation marbles, (inset on Fig. 3.4a) and shows up in light shades of yellow and white. Either side of the anticlinorium pale blue-to-green colours correspond to the synformal domains of Kuiseb Formation schists and overlying sand cover. On the southwestern side of the Onguati-Kranzberg structure, the dark blue-to-black area correlates with outcrops of Etusis Formation quartzites, and to the NE, a post-tectonic leucogranite shows up as a blue, oval area.

3.5.2. Aeromagnetic Response at the Karibib Regional Scale (1:500 000)

Aeromagnetic data only comprise responses from magnetic minerals, and consequently are unaffected by non-magnetic cover, including vegetation, water and superficial cover (Jacques *et al.*, 1997). The ability to accurately map a single geological parameter in a uniform manner over very large areas makes aeromagnetic surveys highly suited to structural and lithological mapping over a wide range of scales in many different terrains. A complete magnetic interpretation requires an understanding of the geological significance of magnetic-bearing rock units, including mineralogy, chemistry and metamorphic grade (Jacques *et al.*, 1997). Very simply, the magnetic susceptibility of rocks depends on the proportion of magnetic minerals present. In this study, the exact cause of the magnetic responses is generally unknown, although many of the Damaran metasedimentary and igneous rocks can contain substantial amounts of magnetite. Pyrrhotite, which is commonly associated with Cu-Au mineralization at both the Navachab Mine and the Onguati deposits, can also impart a considerable magnetism where it is abundant.

The objective of this section is to identify and characterize regional scale structures in close vicinity to the Onguati study area which may have played a part in hydrothermal fluid flow and mineralization. Two aeromagnetic images are presented in this project, because the signal of the total magnetic field carries 2 main types of information. In its basic form, magnetic data are dominated by the lowest frequency components of the magnetic signal, and these types of data are useful to detect large and deep-seated heterogeneities. The higher frequency (or shorter wavelength) component of the magnetic signal corresponds to more superficial heterogeneities, such as shallow granitic bodies, contacts or faults. Different displays of short-wavelength (e.g. first vertical derivative, 1vd) can be employed to emphasize structural features (Jacques *et al.*, 1997). The first vertical derivative (also called the vertical gradient) indicates the rate of change of the magnetic field with elevation. The effect of this procedure is to suppress regional anomalies whilst enhancing local ones (Robinson & Çoruh, 1988).

(a) Total magnetic intensity (TMI)

The TMI image (Fig. 3.5a) for the SCZ region around the Onguati study area shows a broad, homogeneous band of lithologies and superficial cover with positive (high) magnetic responses. The zone of high magnetism sharply terminates at the boundary with the NCZ (line labelled F on the overlay) and this situation implies there may have been considerable tectonic upheaval in the northwestern parts of the SCZ, possibly generated by movement along the OML. Surrounding the Erongo Complex (label G) there is a broad negative magnetic anomaly that may be a consequence of thermal demagnetisation. To the south and southwest the magnetic response becomes more varied. It is generally Salem-type granites and magmatic rocks of the Goas Suite (label H), and in places, meta-sedimentary units within the Etusis and Chuos Formations that are responsible for positive magnetic anomalies. Damaran meta-sedimentary rocks commonly have low, negative magnetic responses (blues and greens on Fig. 3.5a). The geophysical image has been simplified in Fig. 3.5b to emphasize regional-scale magnetic anomalies. Structural form lines (continuous lines) and lineaments (dashed lines) not obscured by areas of high magnetic response, have also been highlighted.

Within the Onguati-Kranzberg structure (square inset) there are units that impart a considerable positive magnetic response. The outer, highly magnetic bands of the antiform may correspond to rocks of the Onguati Member-Kuiseb Formation transition. Calc-silicate schists of the Oberwasser Member or underlying Daheim Member amphibolites highlight the northeastern fold closure particularly well. To the southwest superficial cover, probably derived from the high-standing, magnetically anomalous Etusis fold core and Chuos mixtites, obscures the various lithologies of the antiform saddle region. Some major lineaments also cut the Onguati-Kranzberg structure in close vicinity to Onguati Mine.

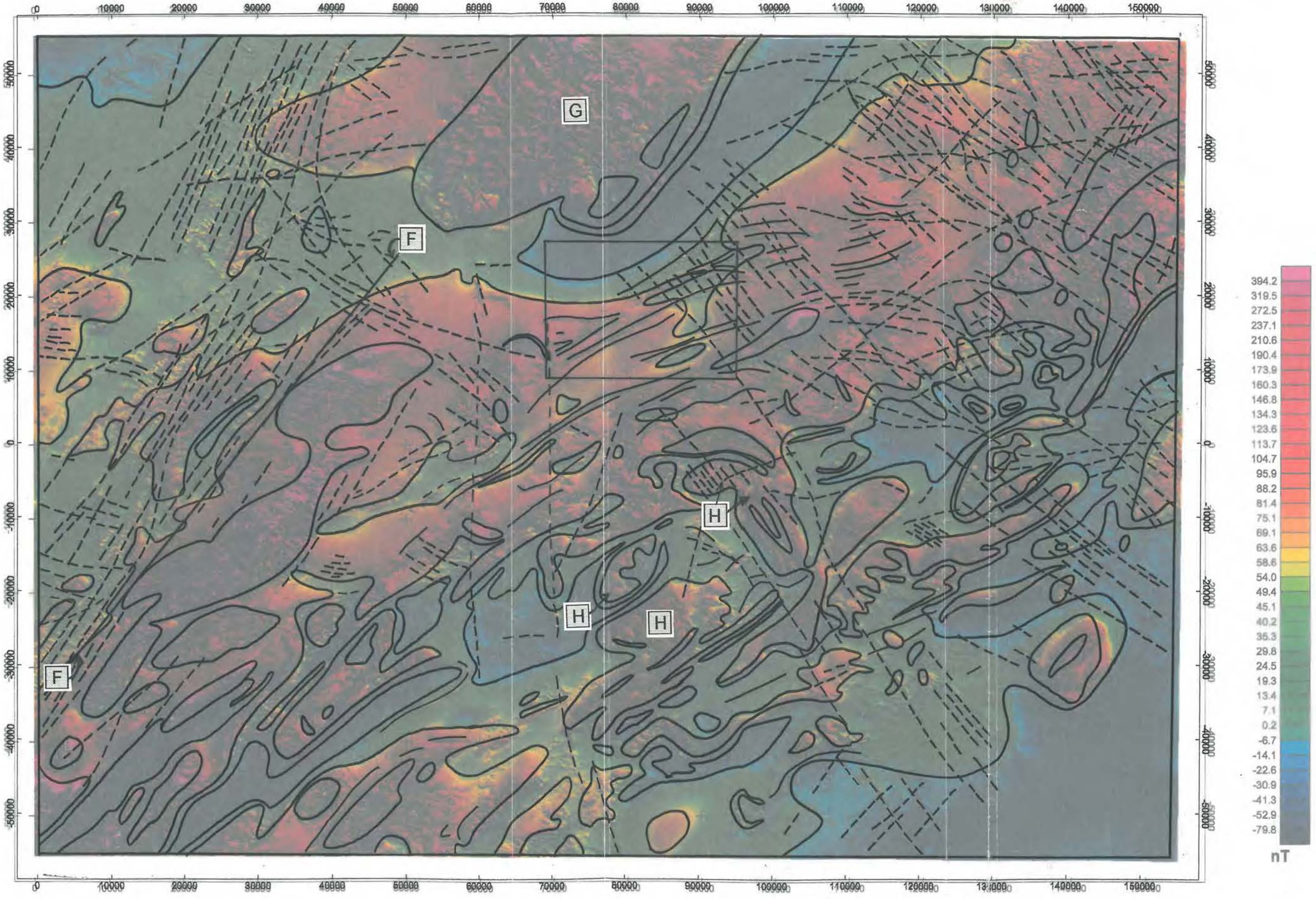

Fig. 3.5a: Total magnetic intensity (TMI) image for the SCZ region around the Onguati study area (insert). Simplistically, pinks and reds ('hotter' colours) indicate areas of high magnetic susceptibility, while areas devoid of magnetic minerals show up as shades of dark blue. The regional scale image spans the area between approximately 0 and +150 000 on the x-axis (E015°00' to E016°30'), and from -50 000 to +50 000 on the y-axis (S21°30' to S22°30'), LO (Gauss Conformal) Projection, Bessel 1841 Spheroid (Schwarzeck Datum). Data provided by kind permission of the Geological Survey of Namibia, 2001©.

Central Meridian: E15
Latitude of Origin: S22
Central Scale Factor: 1.0
False Easting: 0.0
False Northing: 0.0

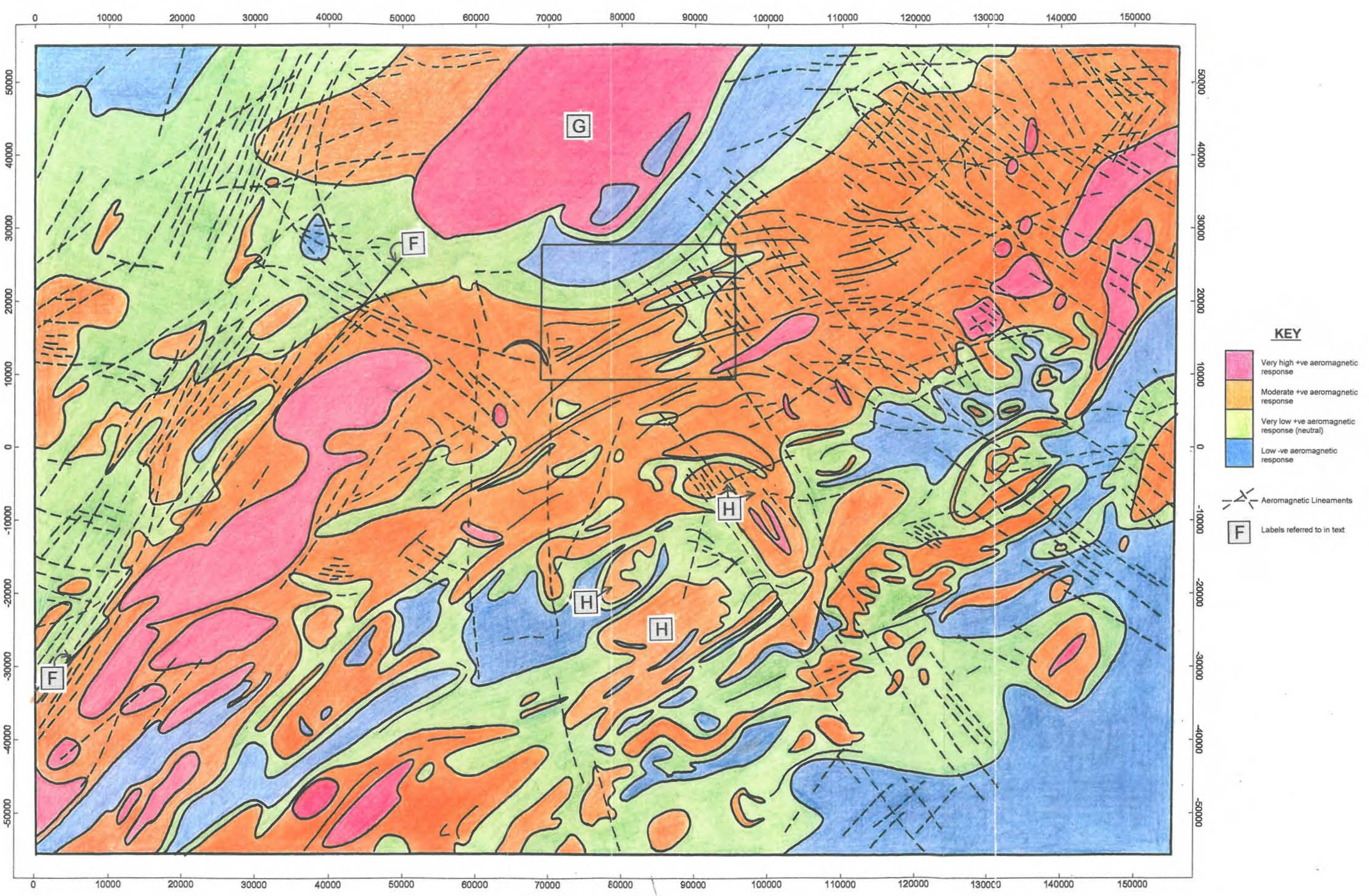

Fig. 3.5b: Interpretative map of the total magnetic intensity (TMI) image, Fig. 3.5a, for the SCZ region around the Onguati study area (insert). The regional scale image spans the area between approximately 0 and +150 000 on the x-axis (E015°00' to E016°30'), and from -50 000 to +50 000 on the y-axis (S21°30' to S22°30'), LO (Gauss Conformal) Projection, Bessel 1841 Spheroid (Schwarzeck Datum).

Central Meridian:	E15
Latitude of Origin:	S22
Central Scale Factor:	1.0
False Easting:	0.0
False Northing:	0.0

5000 0 5000 10000 15000
metres

(b) First Vertical derivative of the total magnetic signal (1vd)

The regional image of the first vertical derivative emphasizes the extents of granitic bodies and highlights internal zoning. Fig. 3.6a also shows the form of SCZ domes and structures, in particular, the many regional crustal lineaments. These lineaments can be divided into four main groups based on orientation:

(i) A prominent NNE-SSW lineament belt (label I on overlay) exists to the west of the Erongo Complex, and was identified by Corner (1983) as the WL zone. As the lineaments approach the OML they curve gently to the SW and become sub-parallel to the regional structural grain, in places overprinting Damaran domes. Numerous NW- to W-trending lineaments intersect this lineament zone at right angles, and may be dykes related to fractures radiating around the Erongo Complex (see (ii) below). The WL belt is known to extend into the SCZ and is thought to be a Damaran-age crustal feature (Corner, 1983). In the NCZ it is likely that this pre-existing structural weakness was utilized by post-Karoo dolerite dykes. In places the lineaments cross-cut and offset the western ring dyke of the Erongo Complex. These lineaments have therefore had a long-lived tectonic history, and appear to have been a major crustal weakness during Damaran times. Lineaments of this orientation, especially in close proximity to known hydrothermal mineralization, should be investigated in detail;

(ii) N-S to NW-SE oriented lineaments (labels J and K respectively) to the south of the Erongo Complex. The more northerly trending lineaments (label J) in the lower middle region of *Fig. 3.5a* may roughly correspond to ABL(i) of Corner (1983), while the SE-trending lineaments (label K) may be Corner's (2000) ABL(ii). These lineaments may be mafic dykes related to post-Karoo magmatism, and appear to radiate around the Erongo Complex in the southern and eastern parts of Figs. 3.5a and 3.6a. Some of these lineaments cross-cut the Onguati-Kranzberg structure and extend southeastwards across the post-tectonic Donkerhuk granites of the OLZ, a distance of at least 85 km. Lineaments with such a NW-SE alignment may have utilized original Damaran crustal weaknesses oriented perpendicular to the regional structural grain. However it is likely that new crustal weaknesses were created with the emplacement of the post-Karoo Erongo Complex. As a result many of these structures could post-date Pan-African mineralization.

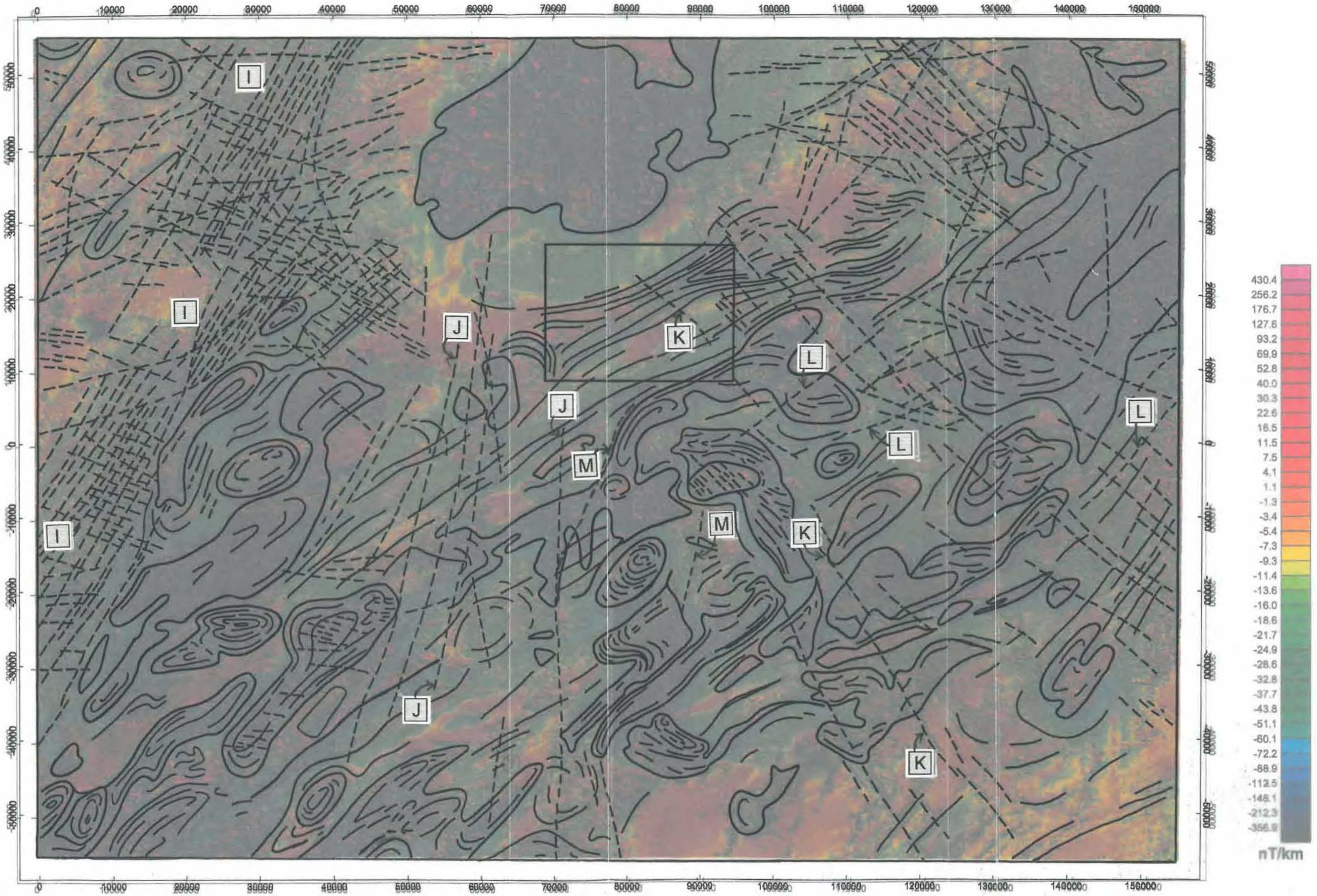

Fig. 3.6a: First vertical derivative (1vd) image of the total magnetic field for the SCZ region around the Onguati study area (insert). Simplistically, pinks and reds ('hotter' colours) indicate areas of high magnetic susceptibility, while areas devoid of magnetic minerals show up as shades of dark blue. The regional scale image spans the area between approximately 0 and +150 000 on the x-axis (E015°00' to E016°30'), and from -50 000 to +50 000 on the y-axis (S21°30' to S22°30'), LO (Gauss Conformal) Projection, Bessel 1841 Spheroid (Schwarzeck Datum). Data provided by kind permission of the Geological Survey of Namibia, 2001©.

Central Meridian: E15
Latitude of Origin: S22
Central Scale Factor: 1.0
False Easting: 0.0
False Northing: 0.0

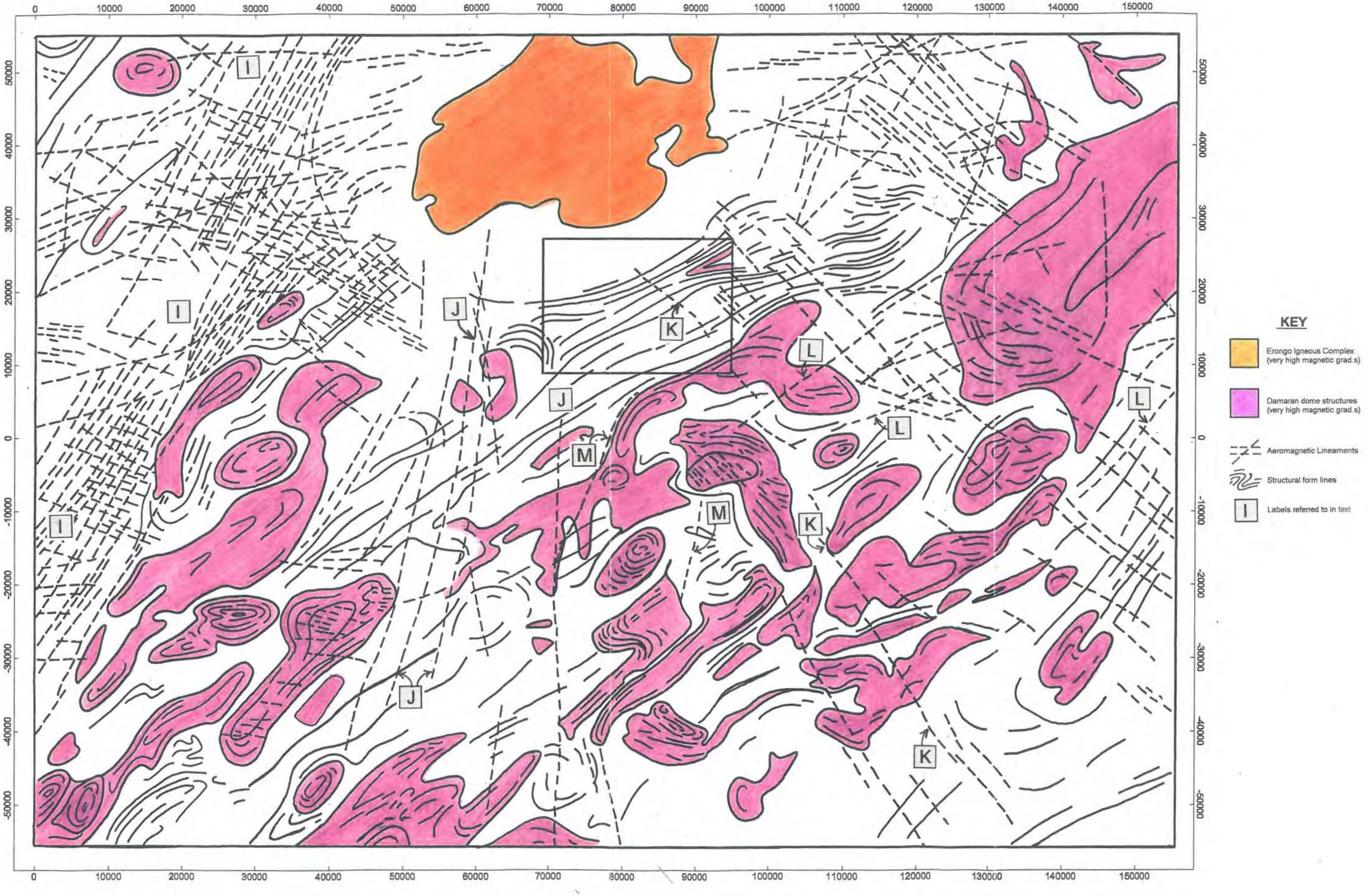

Fig. 3.6b: Interpretative map of the first vertical derivative (1vd) image of the total magnetic field, Fig. 3.5a, for the SCZ region around the Onguati study area (insert). The regional scale image spans the area between approximately 0 and +150 000 on the x-axis (E015°00' to E016°30'), and from -50 000 to +50 000 on the y-axis (S21°30' to S22°30'), LO (Gauss Conformal) Projection, Bessel 1841 Spheroid (Schwarzeck Datum). Data provided by kind permission of the Geological Survey of Namibia, 2001©.

Central Meridian:	E15
Latitude of Origin:	S22
Central Scale Factor:	1.0
False Easting.	0.0
False Northing:	0.0

(iii) Rare NE-SW lineaments (label L), lie parallel or sub-parallel to the alignment of the SCZ dome-and-basin structures. These lineaments cut Damaran-age granites and where they intersect northerly tending, post-Karoo dolerite dykes have resulted in significant dextral displacement. The NE-SW lineaments may have been inherited from the Damaran Orogeny and require field study to ascertain if they have relevance to Damaran hydrothermal mineralization;

(iv) Very rare NNE-SSW lineaments (label M). These lineaments cut the Abbabis basement, Salem-type granites and dome structures in the middle south of Fig. 3.6a, but do not appear to cross-cut plutons of the Goas Magmatic Suite. These structures may represent remnant Damaran faults or dykes and could be potential fluid pathways for hydrothermal mineralization.

The regional 1vd image clearly shows the form of the Onguati-Kranzberg structure (square inset). The Onguati study area is located in the saddle region between the two plunging fold closures. Mineralized parts of the study area do not appear to be associated with any nearby Damaran-age crustal lineaments. A major lineament does cut the anticlinorium but is probably of post-Karoo age. The Etusis Formation is exposed near the southwestern edge of the insert (alternating units of high and low magnetism) and due to its competent nature has resulted in a broad, smoothly curved isoclinal fold closure. On the northeastern end and saddle region of this structure the fold closures are tight and flattened because they are composed of more ductile marbles and schists of the Arandis and Karibib Formations.

3.5.3. Aeromagnetic Response at the Onguati-Kranzberg Antiform Scale (1:100 000)

The 1vd aeromagnetic response at the scale of the Onguati-Kranzberg anticlinorium is shown in Fig. 3.7a, and a 1:100 000 scale interpretative map is presented as Fig. 3.7b. Comparison with the Omaruru 2114 Geological Map (Fig. 4.0 is a portion of this map at the same 1:100,000 scale) shows that many of the lithologies making up the antiform could be reasonably well mapped from the 1vd image alone. For example, in the NE of the structure it is possible to identify units of high magnetic response which correspond to rocks of the Okawayo Member, and the contact region between Oberwasser and Navachab/Daheim Members. In both the SW and NE, areas underlain by Navachab Member marbles appear as distinct negative magnetic anomalies (blues and greens). Rocks of the upper parts of the

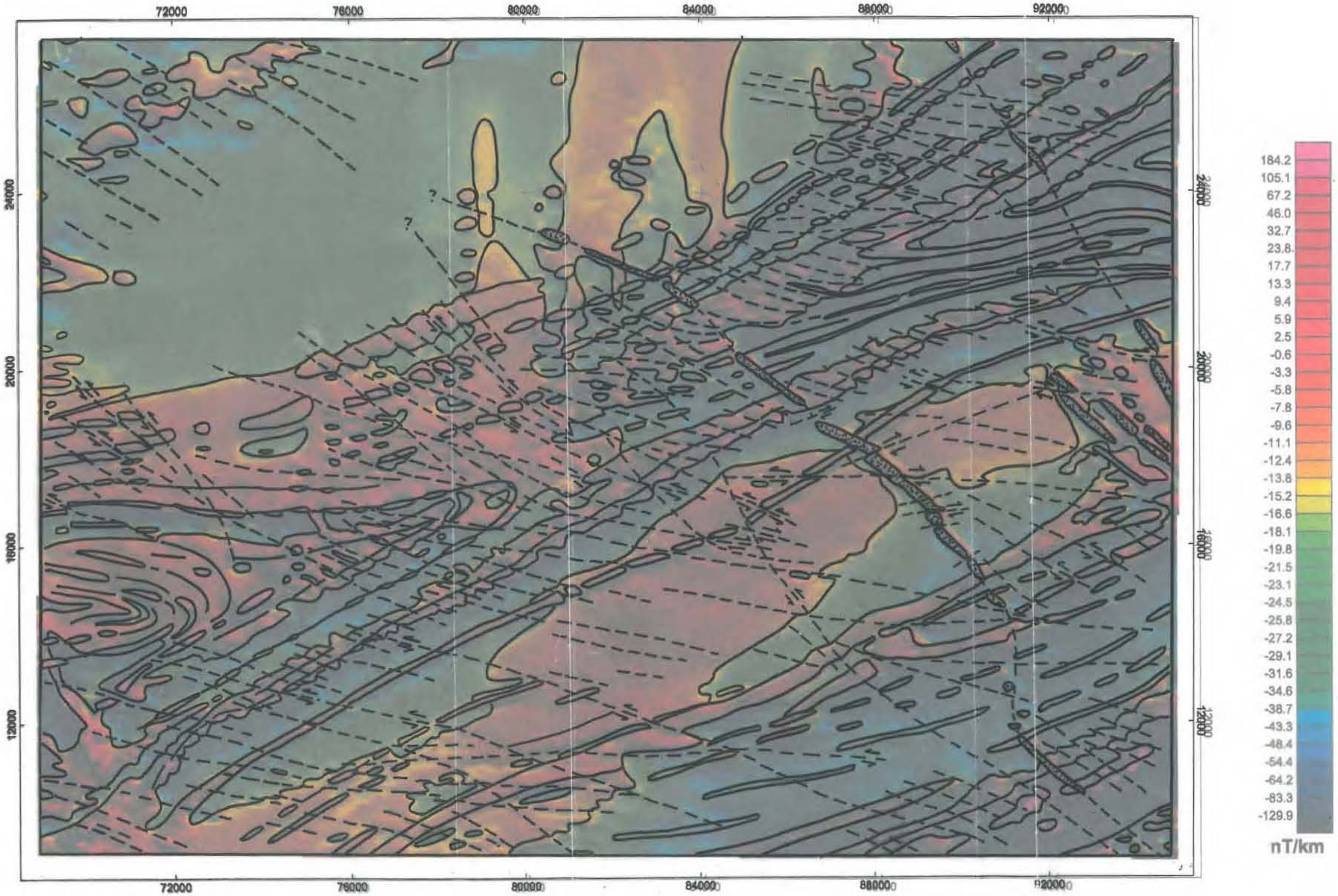

Fig. 3.7a:Detailed image of the first vertical derivative (1vd) of the total magnetic field for the Onguati-Kranzberg antiformal structure in which the study area is situated. Simplistically, pinks and reds ('hotter' colours) indicate areas of high magnetic susceptibility, while areas devoid of magnetic minerals show up as shades of dark blue. The image spans the area between approximately +69 000 and +95 000 on the x-axis, and from +9 000 to +27 000 on the y-axis, LO (Gauss Conformal) Projection, Bessel 1841 Spheroid (Schwarzeck Datum). Data provided by kind permission of the Geological Survey of Namibia, 2001©.

Central Meridian: E15
Latitude of Origin: S22
Central Scale Factor: 1.0
False Easting: 0.0
False Northing: 0.0

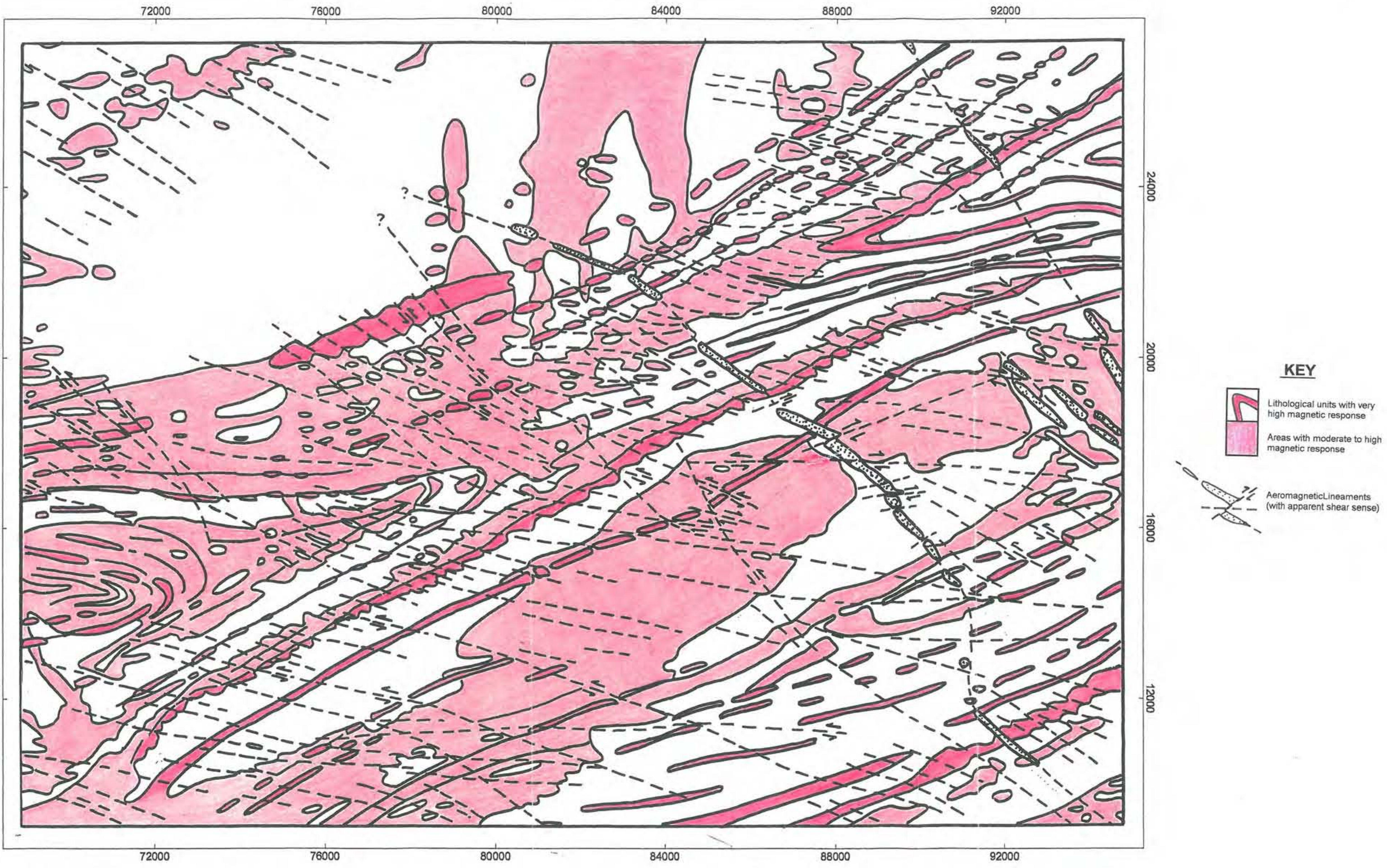

Fig. 3.7b: Interpretative map of the first vertical derivative (1vd) image of the total magnetic field, Fig. 3.5a, for the Onguati-Kranzberg antiformal structure in which the study area is situated. The image spans the area between approximately +69 000 and +95 000 on the x-axis, and from +9 000 to +27 000 on the y-axis, LO (Gauss Conformal) Projection, Bessel 1841 Spheroid (Schwarzeck Datum). Data provided by kind permission of the Geological Survey of Namibia, 2001©.

Central Meridian:	E15
Latitude of Origin:	S22
Central Scale Factor:	1.0
False Easting:	0.0
False Northing:	0.0

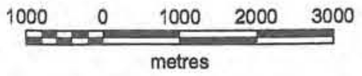

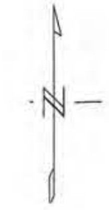

Onguati Formation yield positive magnetic responses in contrast to the overlying Kuiseb Formation schists which appear in hues of blue and green.

The 1vd image clearly displays the fold closures of the doubly-plunging Onguati-Kranzberg antiform, and indicates a number of major crustal lineaments, some of which have already been identified on the regional aeromagnetic maps. The most prominent are the approximately NW-SE aligned lineaments which curve slightly as they cross-cut the antiform. In many places along this lineament zone there is considerable evidence for dextral displacement by northeasterly-trending faults.

More subtle, but vastly more numerous NW- to NNW-trending lineaments appear on careful inspection of aeromagnetic anomaly breaks and offsets. Occasionally, these lineaments are characterized by weak positive anomalies, but in most places they have been inferred by linking apparent offsets in the more magnetic lithologies. On the northern limb in the extreme west and in the lower central regions of Fig. 3.7a the best signs of these lineaments are present. A considerable sinistral component of displacement is common along these lineaments. They do not share the indicative magnetic response of the late Karoo dolerite dykes, and this together with their apparent displacement suggests these lineaments are faults. The lineaments may curve from a northwesterly trend in the central regions of the image, to lie more NNW in orientation further south. The NW- to NNW-trending lineaments appear to be significant geological features but need to be verified by further fieldwork. It is difficult to ascertain the relative timing of these features, but nowhere in Fig. 3.7a is there strong evidence for these lineaments displacing the NW-trending post-Karoo dykes. These structures may therefore be of Damaran age and of major significance to mineralization in the Onguati Mine, Brown Mountain and Western Workings areas.

3.6. Aerial Photographic Interpretation of the Onguati-Kranzberg Antiform

A series of 1:80 000 scale black and white aerial photographs (97-1, roll NAM 9-I, strips 7:26 - 7:30 and 8:24 - 8:28) were examined for a strike distance of nearly 45 km along the Onguati-Kranzberg anticlinorium. From this analysis, Fig. 3.8 (p.70) was prepared and was reduced further in size to a scale of 1:150 000. A second interpretative map was produced from a series of 1:10 000 scale aerial photographs commissioned by AngloGold, and includes detail of the Onguati prospects and their immediate surrounds. Map 1 is included at 1:10 000 scale in a map pouch at the back of this thesis, while an A3-size, 1:50 000 scale version has been included in this section as Fig. 3.9 (p.72).

3.6.1. Onguati-Kranzberg Antiform Scale (1:80 000)

The structural form lines in Fig. 3.8 illustrate the 'hour-glass' shape of the Onguati-Kranzberg anticlinorium with its inwardly-plunging fold axes. During Damaran deformation ductile marbles of the higher level Karibib Formation appear to have been thinned-out in the antiform saddle region. The fold shape in the middle of the structure is also severely flattened and has inwardly curving limbs. The lower Damaran lithologies, such as those of the Etusis Formation and Spes Bona Member, outcrop as high elevation regions on the northeastern and southwestern ends of this complex fold. These comparatively competent rocks fold with a much larger wavelength, and give the 'ends' of the antiform a bulbous appearance. The less competent marbles of the Karibib Formation become further thinned out in the SW, where they wrap around the broad inner core of Etusis quartzites.

In the NE, an oval-shaped, apparently post-tectonic (non-foliated) leucogranite outcrops amongst calc-silicate schists of the Spes Bona Member. Heating of the Arandis and Karibib Formation marble and calc-silicate wall rocks may have allowed the rocks to flow and thin on the northwestern and southeastern sides of the pluton. This may indicate that the emplacement of the granitic body was rather late-tectonic than post-tectonic. During the final stages of deformation in the Onguati-Kranzberg fold, high strain regions may have developed to the NW and SE of the crystallising granite intrusion. If this granite was significantly rigid at this stage, then a triangular shaped strain shadow could have developed, terminating towards the Onguati study area. On the opposite end of the antiform, it is also likely that a low strain region could have formed to the NE of the hard, quartzitic, fold core.

In the central regions of the antiform, including the Onguati study area, there may be a major rheological contrast between the Navachab and Onguati Members. The contacts between the Navachab marbles and the Onguati calc silicate schists and quartzites, on either side of the Onguati-Kranzberg antiform, may therefore mark a local decollément surface along which faulting and thrusting may have occurred (NE-trending, dashed red lines on Fig. 3.8). The 1:80 000 scale aerial photographs show evidence of highly oblique truncation and this has been highlighted as a bold red line southwest of middle in the interpretative map.

The two local decollément surfaces are connected by several NNE-trending lineaments cross-cutting marbles of the Navachab Member. Fieldwork near Western Workings has confirmed that one of these lineaments is a reverse or thrust fault with at least several metres of displacement (see structural chapter later). As these faults approach the northern contact of the Navachab and Onguati Members they curve sharply northeastwards and parallel the

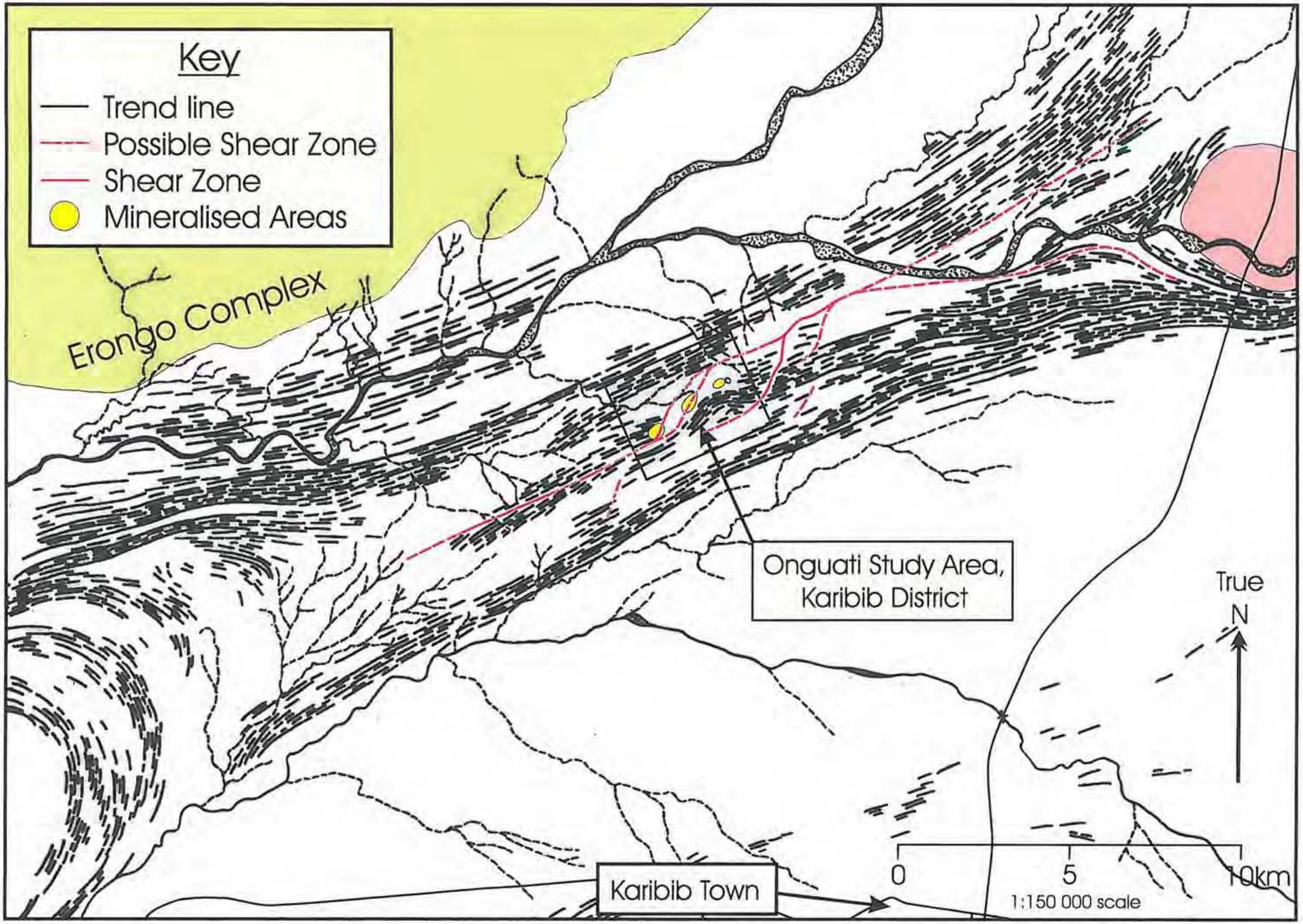

Fig. 3.8: Aerial photograph interpretation of the Onguati-Kranzberg anticlinal structure, showing the main structural trends, faults and shear zones, and areas of known Cu-Au mineralisation. Prepared from 1:80 000 scale, black and white aerial photographs (97-1, roll NAM 9-I, strips 7:26 - 7:30 and 8:24 - 8:28, 31/08/1997).

regional structure (opposite on the southern contacts). The resultant fault pattern has an apparent parallelogram shape. All three mineralized areas in the Onguati study area lie in close proximity to the junctions or extensions of these local faults. Interestingly, a similar orientation, parallelogram arrangement of structures is seen at the regional scale as the OML-ABL(i)-OL-WL system.

On the aerial photographs there is no evidence of the NNW to NW-trending lineaments identified on aeromagnetic images, nor of the apparent post-Karoo dolerite dykes that show up a short distance to the east of the study area.

3.6.2. Study Area Scale (1:10 000)

On the 1:10 000 scale aerial photo-mosaic it was possible to distinguish between the Navachab and Onguati Members of the Karibib Formation. The Navachab Member is characterized by light grey and white tones and has a smooth, banded texture (central strip of Fig. 3.9). For the most part, areas underlain by marbles of the Navachab Member form low-lying surfaces. Marbles in the mineralized areas (i.e. higher vein densities) or incised by fault zones (i.e. siliceous infilling and veining) can become hills or ridges because of their increased resistance to weathering. Rocks of the Onguati Member make up higher, sometimes more rugged topography and appear as broad expanses of alternating dark and medium grey bands on either side of the central band of Navachab marbles. In the extreme NW, exposures of Kuiseb schist form an irregular, low-lying landscape, and are characterized by their strong foliation and medium grey tones. Large regions are overlain by superficial cover (light grey, speckled appearance), and only areas of outcrop with at least 50% exposure were represented on Fig. 3.9.

Aerial photographs of the areas immediately around Onguati, Brown Mountain and Western Workings show considerable detail of local fold structures. In the calc-silicate lithologies of the southeastern region of Fig. 3.9 there are a number of tight-to-isoclinal, M-type fold closures. A possible synform is also apparent at Western Workings, in the central regions of the photograph.

Southwards between Brown Mountain and Onguati, the structural form lines deviate substantially from the regional trend and appear to trace the form of an open, buckle fold. However this apparent fold orientation is perpendicular to the regional non-cylindrical fold axes and so may be better explained as a thrust wedge. Although exposures in this part are shown as Navachab marbles, it is possible that these rocks could be of the Onguati

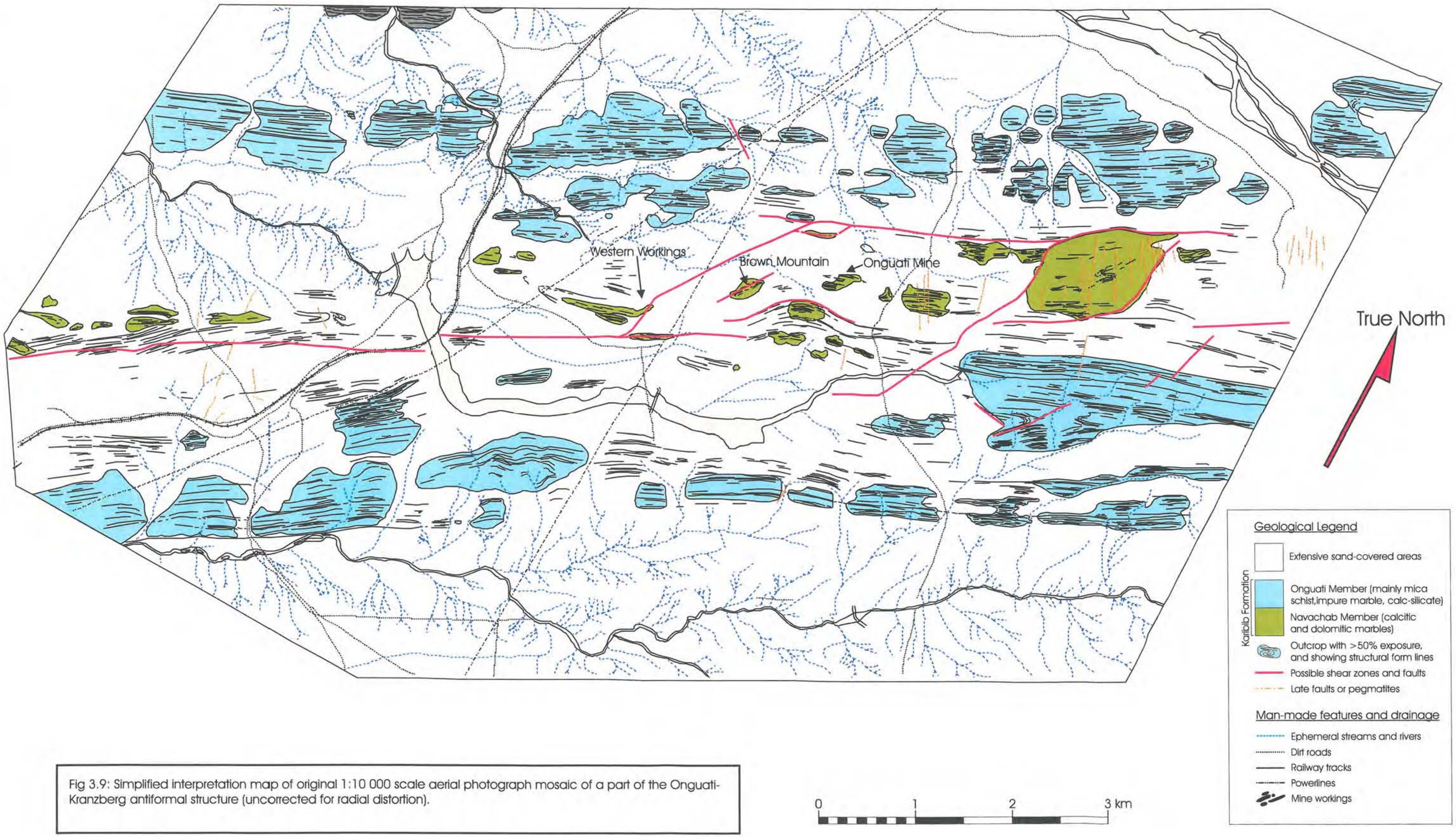

Fig 3.9: Simplified interpretation map of original 1:10 000 scale aerial photograph mosaic of a part of the Onguati-Kranzberg antiformal structure (uncorrected for radial distortion).

Formation. The thrust sheet could have been transported northwestwards to lie on top of the Navachab Member. This thrust surface could be reasonably connected southeastwards with the major faults identified there (bold red lines).

In the middle, right of Fig. 3.9 the truncated bedding (identified earlier in section 3.6.1) appears to be dragged into a fault or shear zone. The fault is most probably the extension of the Navachab-Onguati Member decollément to the NE, but it also could have formed in the axial plane zone of a large, flattened isoclinal fold. The parallelogram-shaped arrangement of faults identified from the 1:80 000 scale photographs, can be seen to be repeated in various parts of the enlarged, 1: 10 000 scale images. Interestingly, Western Workings, Brown Mountain and the Onguati Mine area are found at a regular, approximately 2 km spacing along a diagonal line that runs from one corner of the main parallelogram fault system to the other.

A number of additional NW-trending lineaments, especially to the east of Onguati Mine, were found on the detailed aerial photo-mosaic (orange dashed lines in Fig. 3.9). These are most likely late Damaran age pegmatite dykes but could also correspond to the post-Karoo lineaments identified on the regional aeromagnetic images. A rare, WNW-trending lineament was found in association with one of the more marginal NNE-SSW oriented faults. This may support the earlier lineation interpretation from the local-scale 1vd image. This orientation of lineaments could be conjugate to the NNE-trending reverse folds identified on the aerial photographs.

3.7. SCZ Hydrothermal System - Possible Source Areas and Transport Structures

A hydrothermal system typically consists of three main elements: (1) a source area of metals; (2) transport structures along which mineralizing fluids can efficiently flow and focus; and (3) trapping sites where ore deposition can occur. The first sections in this chapter focussed on the known and potential mineralization of the Damaran Belt, and presented the main characteristics and mineral potential of SCZ lithostratigraphy. Low grade syngenetic mineralization in many parts of the metasediment pile and extensive lithologies with just a few ppm Au and other metals could represent enormous metal repositories and could be feasible source areas for a SCZ hydrothermal system. The review of SCZ plutonism centred on an alternative magmatic source for mineralization. However, only a very small proportion of the granitoids present in the SCZ, mainly represented by members of the Goas Magmatic Suite, could be potential Au and Cu sources.

In the final section of this chapter numerous structures were identified from geophysical images and aerial photographs that could have had sufficient dilatancy to act as major fluid pathways during Damaran Orogeny. As such, the source area and transport structures are of significance at the large scale (i.e. several 100 km- to 10 km-scales) because they either link a regional 'metamorphic' source or suitable plutonic bodies to gold mineralization. Further work is required to assess the importance of each of the regional structures to Damaran hydrothermal mineralization.

The final component of the hydrothermal system is a suitable site for precipitation to occur, and this is governed by chemical and physical conditions at the prospect-scale (i.e. 1 km-scale). This aspect is discussed in later chapters dealing with vein connectivity and fluid flow, structure and vein mineralization. It is pertinent to note at this stage that the review of Damaran lithostratigraphy indicates broad scale lithochemical control on Au mineralization. While evidence of Au hydrothermal mineralization occurs throughout the stratigraphy, it is the carbonate and calc-silicate rocks of the Karibib Formation and Okawayo Member that host the best deposits when suitable structures cross-cut them.

At the Onguati prospect scale, there is a distinct lack of suitable composition plutonic bodies to be of relevance to the mineralization there. Meta-volcanic rocks of the Daheim Member are present near the Onguati deposits and contain anomalous metal contents, but volumetrically they make up only a small part of the stratigraphy. Aeromagnetic images and aerial photographs show that a number of lineaments could be relevant to mineralization in the Onguati study area and beyond. The main geophysical and remote sensing characteristics of the lineaments and geology of the Onguati-Kranzberg region are summarized in Table 3.8 overleaf. The most obvious structures include a pair of roughly bedding-parallel, NE-trending thrusts or shear zones, with a number of linking, NNE-trending reverse faults. A more subtle set of faults with a NW-SE orientation may form a conjugate fault set with the NNE-trending elements. The close proximity of this fault or shear zone system to areas of known mineralization suggests that these structures may have played a critical part in hydrothermal fluid movement and ore body deposition in the saddle region of the Onguati-Kranzberg antiform.

Table 3.8: Main geophysical and aerial photographic characteristics of the lithostratigraphy, intrusives and lineaments of the Onguati-Kranzberg antiform.

Features		**Ternary radiometric/1vd image**	**Aeromagnetic images (TMI and 1vd)**	**Aerial Photographs (1:80 000 and 1:10 000 scale)**
Lithologies	Kuiseb Formation	Blue-green hues K ± U enrichment.	Almost homogeneous, low negative magnetic signature (shades of green); internal structure apparent e.g. possible synform SE of Onguati.	Well developed foliation seen in places, medium grey tones; forms low-lying, uneven terrain.
	Onguati Member	White to light yellow hues; Low concentrations of all 3 radio-elements.	Upper parts have strong positive magnetic response (red to pink colours).	Alternating dark and medium grey bands; can form hilly topography with ravines.
	Navachab Member	White to light yellow hues indicating low concentrations of the 3 radio-elements; Shows significant thinning in regional fold limbs.	Generally low negative magnetic response (green hues).	Light grey to white tones; smooth texture, but speckled in areas due to vegetation; Forms low-lying regions with isolated hills.
	Daheim Member	Radiometrically indistinguishable.	May have a high positive magnetic response? (red hues?).	Indistinguishable at both scales.
	Oberwasser Member	Deep blue to purple hues; Relatively high concentrations of K and Th.	Generally high positive magnetic signature (red hues); possibly due to ferruginous schists and magnetite quartzites common to this member.	Banded; alternating units of different shades of medium grey.
	Okawayo Member	Light yellow hues; Slight U enrichment.	May have a positive magnetic response? (orange to red colours?).	Relatively soft and has been eroded to form valleys and low-lying areas to NE of Onguati.
	Spes Bona Member	Light yellow hues, difficult to distinguish from Okawayo Member; Slight U enrichment.	May have a low negative magnetic response? (green hues?).	Homogeneous, smooth dark shades of grey.
	Chuos Formation	Radiometrically indistinguishable.	May have a very high positive magnetic signature? (pink hues?).	Indistinguishable at both scales.
	Etusis Formation	Enrichment in all 3 radio-elements (blue-black hues) - may be due to detrital zircon, sphene, monazite; K due to abundant feldspar.	High positive magnetic signature (red to pink hues).	Pitted and irregular textures; light grey to white tones; Etusis quartzites form rugged highland areas due to their relative hardness.
	Abbabis Basement	Highly variable radiometric response, indicating a variety of rock types, dykes etc; Generally appears relatively Th enriched.	Variable response with areas of low (green) to very high magnetic signatures (reds and pinks).	No exposures of basement observed on either of the aerial photographs.
Intrusives	Leucogranites	Dark blue hues, oval shape; Equal enrichment in Th and K, minor U.	Strong positive magnetic anomaly (red colour); Devoid of internal structure or igneous zoning.	Oval-shaped, light grey area; devoid of foliation; Cut by N-S lineaments.
Lineaments	N-S dykes	Subtle or little radiometric response (highlighted by underlying 1vd image).	High positive magnetic signature - may indicate a magnetite-rich mafic dyke (orange-red hues).	Evident in places as ravines due to preferential erosion.
	ENE-WSW faults	White or no response; (highlighted by underlying 1vd image).	No visible magnetic anomaly; indirect evidence from persistent dextral offsets in N-S dykes.	Truncation of bedding to the SW; in places forms prominent ridges.
	NNE-SSW faults	May be highlighted in Abbabis Inlier (orange hues)?	Not visible, possibly because displacement along faults has not exposed magnetically different rocks?	Apparent from prominent ridges and alignment of linear outcrops and hillocks.
	NNW-SSE faults	Not visible.	No obvious magnetic response, indirect evidence comes from alignment of numerous anomaly breaks with apparent sinistral offset.	Little evidence on aerial photographs, possible lineaments of this orientation may be seen SE of Onguati Mine on 1:10 000 scale photographs.

4. GEOLOGY OF THE ONGUATI STUDY AREA

4.1. Introduction

The Onguati study area is located in the neck of an anticlinorium and is entirely underlain by rocks of the Navachab Member, Karibib Formation (Fig. 4.0, at a scale of 1:100000). Detailed 1:500 scale maps were produced for Onguati Mine (see Map #1 in pouch at back), Brown Mountain (Map #2) and Western Workings (Maps #3A and #3B) because these parts are relatively well exposed and display the best indications of hydrothermal vein mineralization. In this chapter, A3-size versions of these maps (~1:1800 scale) have been included for the convenience of the reader as an aid to the various lithologies discussed below. The full size, 1:500 scale maps can be found in the map pouches at the back of this thesis and clearly show vein and structure measurements.

Mapping made use of the existing Goldfields grid system, and over the better mineralized parts the grid cells are spaced at 20 x 20 m, or occasionally at 20 x 40 m. Away from areas of abundant veining the grid resolution commonly reduces to a 20 x 120 m spacing across strike. The three mapping areas are linked by the "0" North baseline which runs across the trig beacons situated on Onguati Hill and Brown Mountain, to the area of copper mining at Western Workings. Only areas of good exposure were mapped (i.e. outcrop mapping) so that uncoloured parts of the maps correspond to superficial cover. On the steeper slopes of hills this cover is mainly thick marble scree and thin soil, but in the lower lying regions this is gradually replaced by extensive calcrete plains, or minor ferricrete when near mineralized veins. Inferred contacts have been drawn where they are obscured by superficial cover but for the most part geological interpretation has been kept to a minimum. The extents of mine tailings (cross-hatched lines), workings (diagonal lines) and the entrances to inclines (small, half-filled square symbols) have also been included on the maps.

4.2. Onguati Mine Area

The Onguati Mine area (~0.18 km^2) is composed of three main rock types (Fig. 4.1): a thick, lower package of calcitic marbles which host the vein mineralization, calc-silicate rocks that occur as numerous thin layers or as thick units within the marbles, and an upper veneer of dolomitic marbles which cap Onguati Hill (see Plate 1). Fig. 4.2 illustrates the large scale

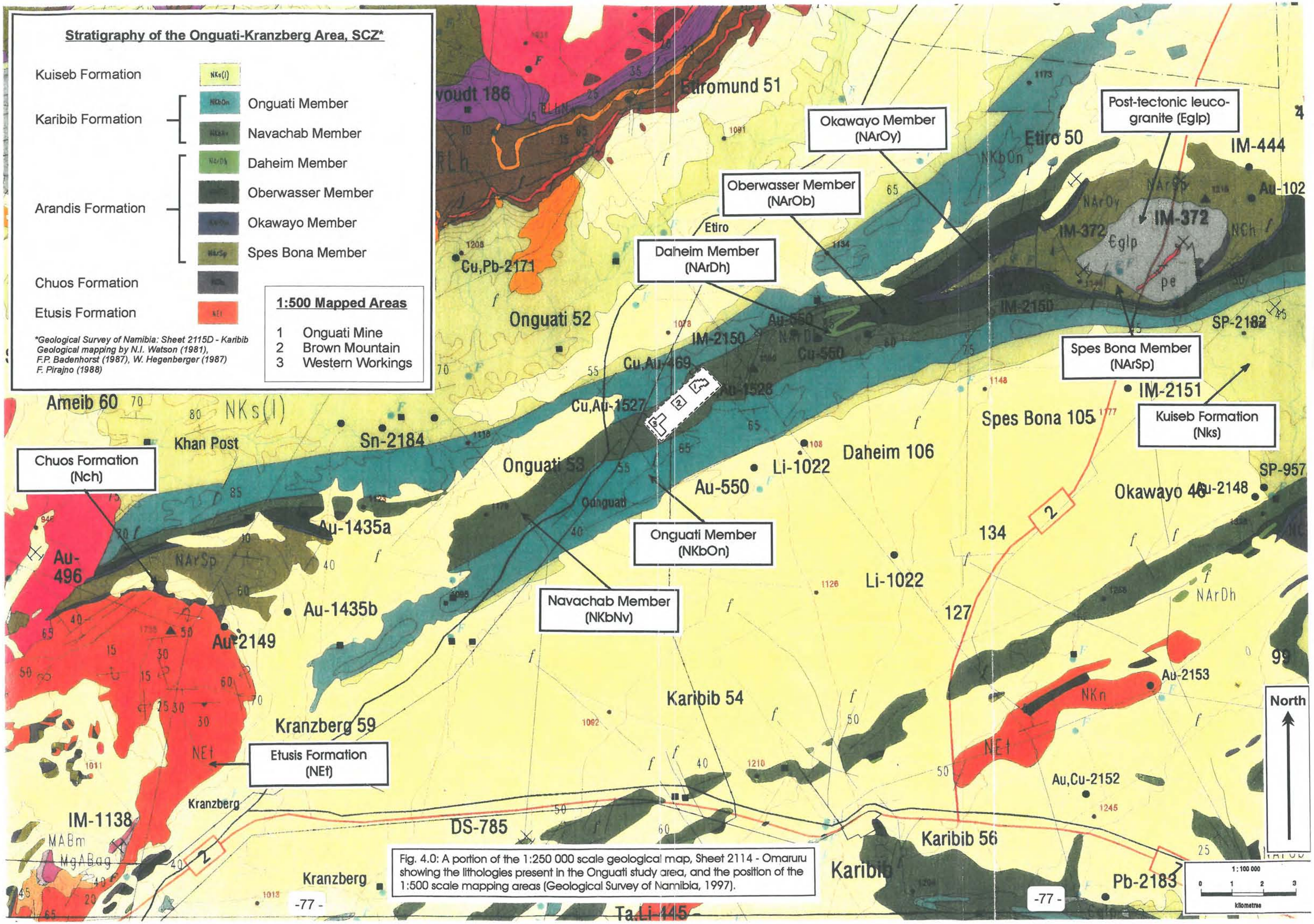

Fig. 4.0: A portion of the 1:250 000 scale geological map, Sheet 2114 - Omaruru showing the lithologies present in the Onguati study area, and the position of the 1:500 scale mapping areas (Geological Survey of Namibia, 1997).

-77-

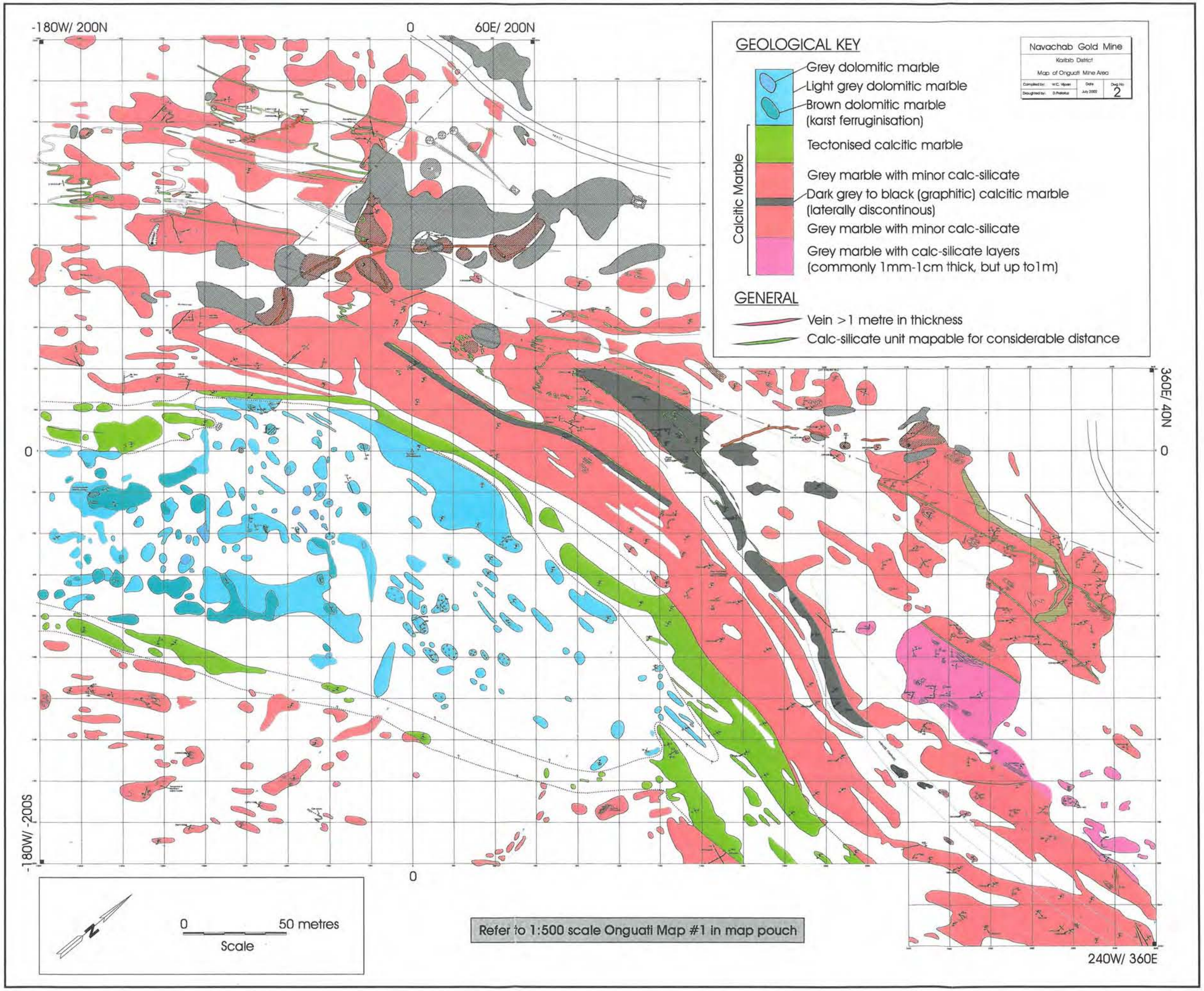

Fig. 4.1: Simplified map of the Onguati Mine area (refer to 1:500 scale map of Onguati Mine area, Map #1, for structural details).

Plate 4.1: A west-facing view of Onguati Hill. The Onguati Mine workings and tailings can be seen on the lower northern slopes (right). The prominent dark ridge in the central parts of the image corresponds to the main graphite-rich, calcitic marble unit (DGMC) in the mapping area.

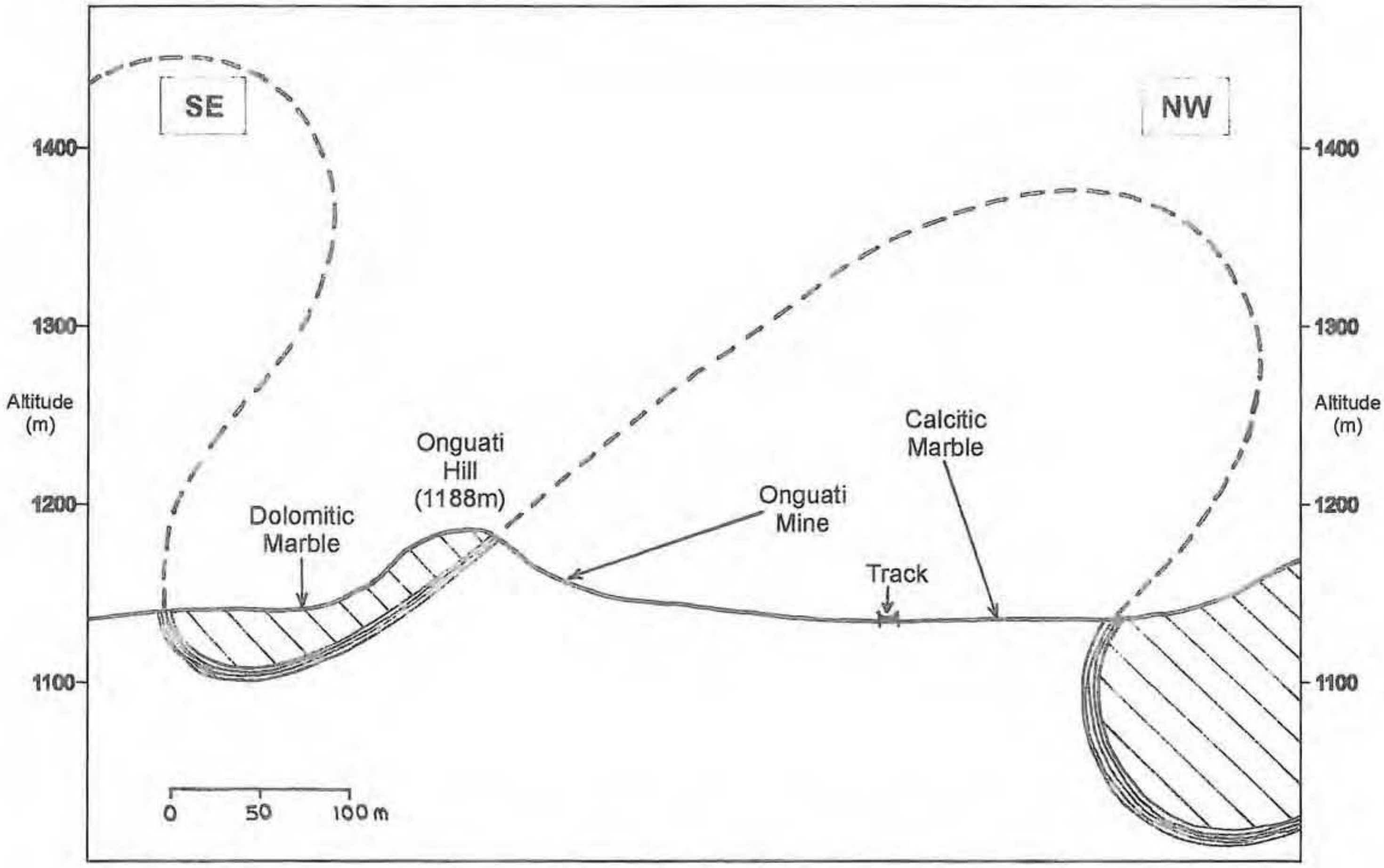

Fig. 4.2: Southeast - northwest cross section showing the basic, large scale structure of the Onguati Mine area . The fold form is highly simplified, and probably contains a multitude of S-, Z- and M-folds of multiple orders. Scale is 1:4000; vertical exaggeration is 0.

structure of the Onguati mapping area. The prospect-scale tight or isoclinal, similar folds are overturned towards the NW and most commonly plunge to the SW. The dolomitic marbles at Onguati Mine are preserved in a large shallow syncline in the southwestern corner of the map. The lower calcitic marbles make up part of the southern limb of a large overturned anticline.

4.2.1. Calc-Silicate Rocks

Calc-silicate rocks make up a significant proportion of the total volume of rocks found in the Onguati Mine area and are best developed in the lower calcitic marbles. The calc-silicate rocks are commonly found as thin layers or laminations ranging from a few millimetres to several centimetres in thickness, and are separated by marble beds of highly variable thickness (0.5 - 50 cm). In several places in the Onguati Mine area the calc-silicate layers have attained thicknesses of up to half a metre and can extend for considerable distances along strike (Plates 4.2 and 4.3). In small areas of the highly folded marbles it is possible to use these as marker units. Large units or concentrated bands of calc-silicate rocks have been marked as dark green lines on the maps. It is common to find numerous centimetre-scale calc-silicate layers alternating with marble which progressively thicken as they approach large calc-silicate units.

Many of the calc-silicate rocks contain abundant pyrrhotite which weathers to give exposed rocks a rusty brown or reddish-brown colour (Plates 4.2 and 4.3). Fresh samples have a dark grey-green colour (Plate 4.4). Calc-silicate lithologies are more resistant to weathering than carbonate rocks, and often protrude several millimetres from the marble surfaces in which they occur. Well-developed bedding can be preserved in some of the thicker units. Occasionally individual calc-silicate layers may appear to 'branch' into two thinner units (e.g. Plate 4.4, centre) but this is probably not an original sedimentary feature. It is more plausible that the marble beds separating closely spaced calc-silicate layers became thinned out by boudinage and pressure solution effects during deformation.

The calc-silicate rocks are predominantly fine-grained (0.1-0.5 mm), although coarser-grained (~1 mm) layers can be found within some of the larger units (Plate 4.3). The calc-silicate rocks consist predominantly of quartz, biotite and tremolite, with variable amounts of plagioclase and diopside. Carbonate is present as a minor constituent in all of the thin sections studied. Pyrrhotite is the most common sulphide, but arsenopyrite and pyrite (often highly fractured) can also occur within the calc-silicate rocks. Sulphides can be found along

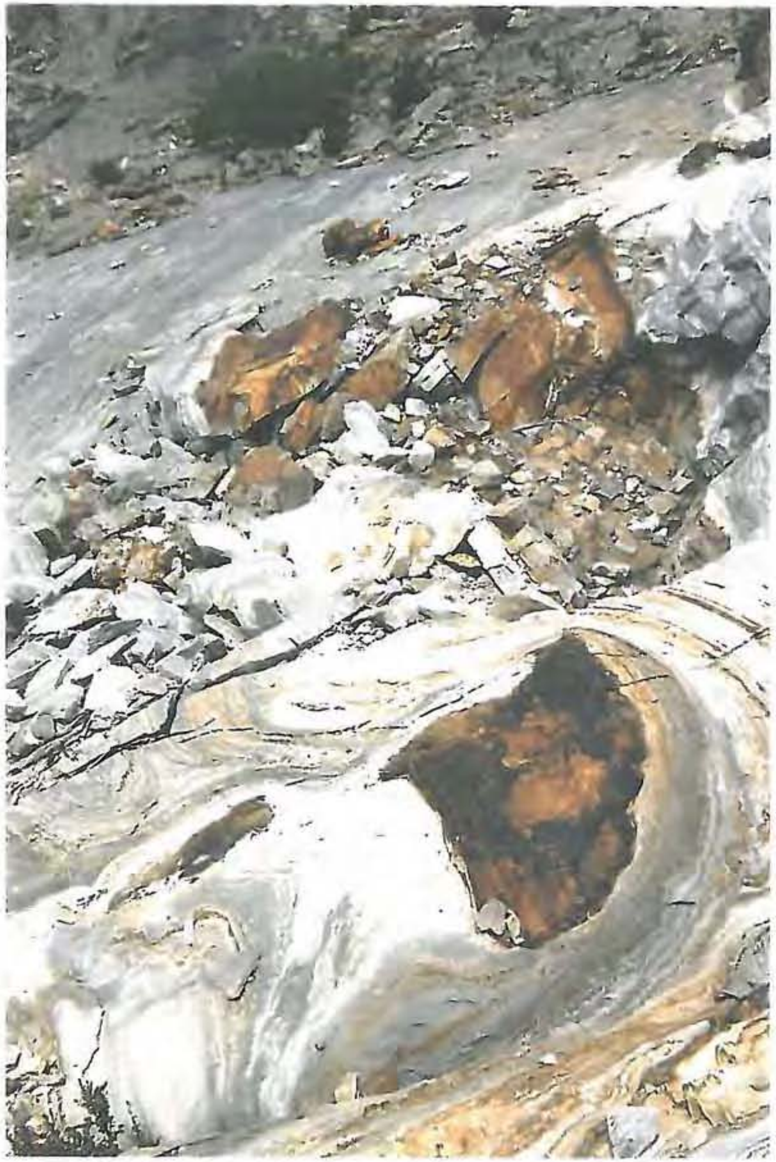

Plate 4.2: A typical thick, brown-stained calc-silicate unit from the Onguati Mine area. The calc-silicate unit has been intensely folded and severely boundinaged. Note the bleached, coarse-grained calcitic marbles adjacent to many of the calc-silicate layers. The calc-silicate fold 'nose' in the forefront is about 50 cm across.

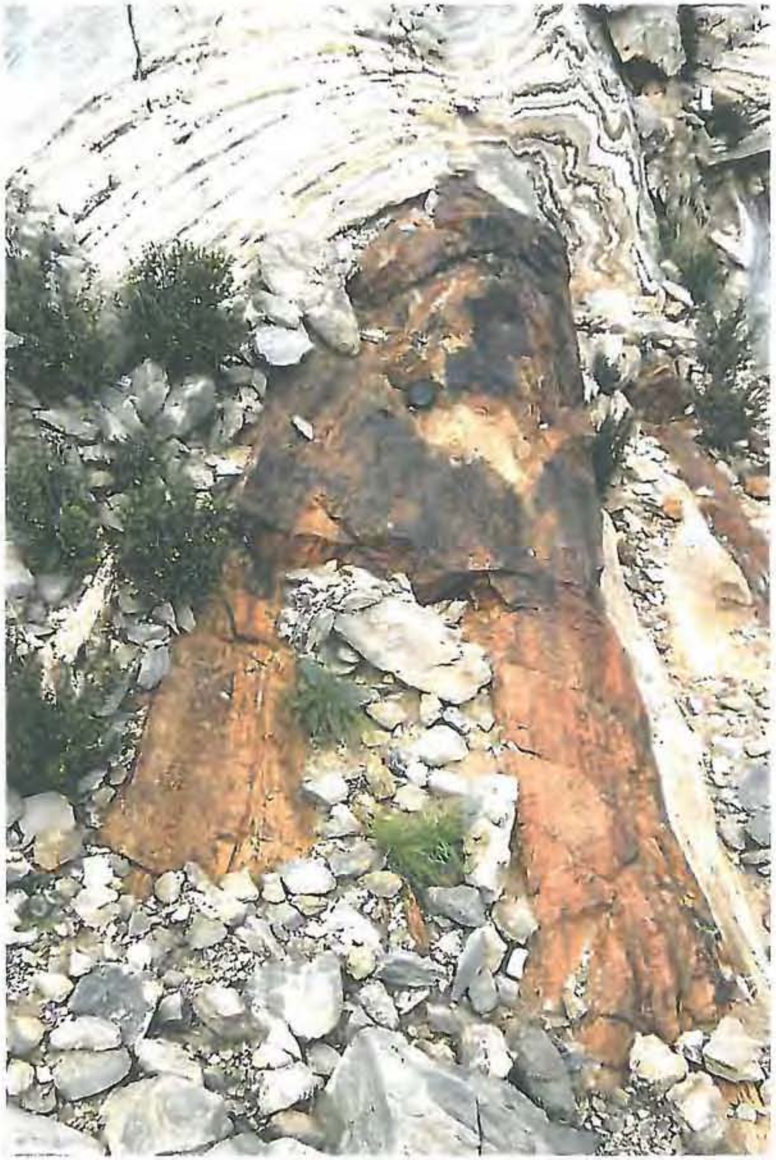

Plate 4.3: An isoclinal fold is highlighted by a thick calc-silicate unit in the Onguati Mine area. The calc-silicate rocks show a distinctive brown colouration due to weathering of contained pyrrhotite. Note the layering within the main calc-silicate unit. The calc-silicate fold limbs are between 40 and 48 cm in thickness.

ONGUATI MINE AREA


Plate 4.4

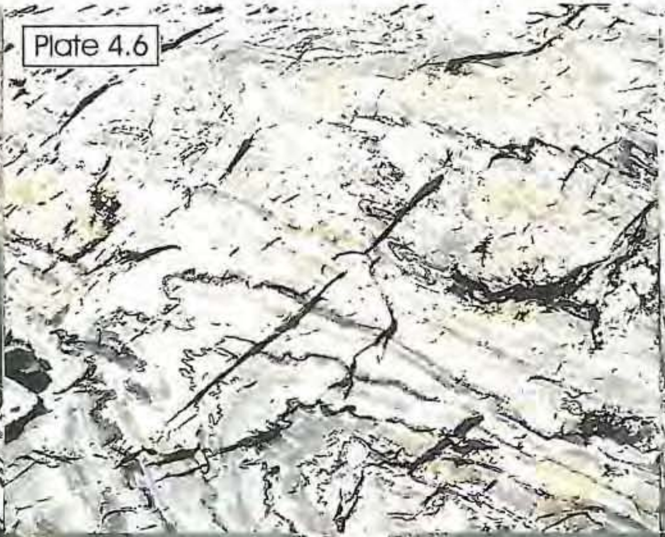
Plate 4.6


Plate 4.8


Plate 4.5


Plate 4.7


Plate 4.9

Plate 4.4: Alternating bands of calc-silicate rock and calcitic marble in the Onguati Mine area. Note the dark green-grey appearance of these more pristine calc-silicate rocks. A few small brown stains are located in the largest calc-silicate layer, and are probably centred around sulphide-rich areas. A flanking fold is developed alongside a small quartz vein in the upper half of the photograph.

Plate 4.5: Grey calcitic marble with abundant calc-silicate layers (GMC) in the northern corner of the Onguati mapping area. The calc-silicate layers are between 0.1 and 2 cm in thickness. Note the periclinal (centre) and isoclinal (right) folds developed in these marbles.

Plate 4.6: Grey calcitic marble with minor calc-silicate layers (lower GM). GM occurs over much of the Onguati Mine area and is commonly very light coloured. Small graphite-rich bands may have retained their dark colour because they are either shielded by, or sandwiched between thin calc-silicate layers devoid of sulphides. The isoclinal fold in the forefront is approximately 80 cm wide.

Plate 4.7: Dark grey, graphite-rich calcitic marble (DGMC) which separates the calc-silicate poor marbles (GM) into lower and upper parts in the Onguati Mine area. The unit is several metres thick but appears to be laterally discontinuous. The DGMC is more fine-grained than the other calcitic marbles because graphite inhibits grain growth during recrystallisation. Field of view is 0.65m x 1m.

Plate 4.8: Grey calcitic marble with minor calc-silicate layering (upper GM) near the 60N/80W beacon in Onguati Mine area. Note the 3D form of the flame-like folds, and the presence of light and medium grey banding. This unit overlies the prominent graphite-rich marble unit (DGMC).

Plate 4.9: Marble breccia in the upper GM unit of the Onguati Mine area. Marble breccias can also befound in the overlying laminated, calcitic marbles (TM). The brecciated marbles could be the result of early tectonic disturbance shortly after carbonate deposition. Alternatively they may have developed during flexural-slip folding of the well-bedded calcitic marbles.

the contacts of calc-silicate units as 'residuals' concentrated by intense pressure solution in the surrounding carbonates (i.e. syngenetic sulphides from the marbles dammed up against the calc-silicate lithologies) or dispersed throughout the calc-silicate rocks as small grains (i.e. syngenetic sulphides within the calc-silicate rocks). Sulphides may also be confined to meandering and branching veinlets (i.e. remobilized syngenetic sulphides, or hydrothermal sulphides). Titanite occurs as an accessory mineral in the calc-silicates, and in many of the biotite grains there are zircon inclusions with distinct pleochroic haloes. The whole-rock chemical composition of a fresh Onguati calc-silicate sample is detailed in Table 4.1.

4.2.2. Calcitic Marble Units

Calcitic marbles host the main vein mineralization and are the dominant rock type in the Onguati Mine area. The marbles are banded and have experienced widespread recrystallisation. Many of the marble bands are separated by thin calc-silicate rocks as detailed above. The bands range in colour from cream or light grey to very dark grey, the colour being largely dependent on the amount of graphite present. The lighter, graphite-poor layers are generally the most coarse grained (0.3 - 0.5 mm grain diameter). Darker graphitic marble bands tend to be fine grained (~0.05 mm) because graphite inhibits grain growth during recrystallisation.

In thin section the calcitic marbles consist primarily of subidioblastic calcite, with variable amounts of quartz and muscovite, sometimes concentrated in thin bands. In some calcite grains it is possible to find well formed secondary dolomite exsolution lamellae. Common accessory minerals include biotite; phlogopite; sulphides, especially pyrrhotite but also pyrite and chalcopyrite; tremolite; graphite; and titanite. Marbles from the Onguati Mine area were analysed by X-ray diffraction (XRD). The basic mineralogy is summarized in Table 4.2. Many of the calcite grains also display abundant deformation- or e-twinning (Passchier & Trouw, 1998). The full spectrum of e-twins can be found: straight simple twins (type I; T<200°C), thick twins (type II; T=150-300°C); crossing twins which may be slightly bent and which have pointed terminations (type III; T>200°C); and more rarely, twins with irregular, serrated boundaries (type IV; T>250°C).

In the Onguati Mine area there are stark differences in the quantity and spacing of calc-silicate rocks within the calcitic marbles. This allows four main units to be identified and mapped: a basal medium grey, calcitic marble with abundant calc-silicate layering; a thick middle, light grey calc-silicate–poor marble; a thick dark grey to black graphitic marble

Table 4.1: Whole rock chemical analysis of a typical calc-silicate rock, sample ONG-2.

Majors elements as oxides (wt%)	**ONG-2**
SiO_2	49.22
TiO_2	0.59
Al_2O_3	12.41
Fe_2O_3	5.59
FeO	0.00
MnO	0.38
MgO	10.13
CaO	14.87
Na_2O	0.72
K_2O	2.36
P_2O_5	1.71
LOI	3.51
H_2O-	0.37
TOTAL	**101.86**
Selected trace elements (ppm)	
Ni	27
Cu	963
Zn	61

Table 4.2: Mineralogy from XRD analyses of the Onguati Mine area calcitic and dolomitic marbles (✓=prominent mineral peaks detected; m=minor accessory mineral; ✗=mineral not detected).

Sample No.	**Calcite**	**Dolomite**	**Quartz**	**Phlog -Biot**	**Tremolite**	**Hornblende**	**Diopside**	**Olivine**	**Relative intensity *(mineral d_1 peak heights as a % of the maximum d_1 X-ray peak height)***
ONG-03-C	✓	✗	✓	✗	✗	✗	✗	✗	100%; 54%
ONG-05-C	✓	✗	✓	✗	✗	✗	✗	✗	100%; 7%
ONG-06	✓	✗	✓	✗	✗	✗	✗	✗	100%; 16%
ONG-08-C	✓	✗	✓	✗	✗	✗	✗	✗	100%; 24%
ONG-11*	✓	✗	✓	✗	✗	✗	✗	✗	100%; 9%
ONG-12[a]	✓	✓	✓	?	?	✗	✗	✗	100%; 71%; 36%
ONG-18	✓	✗	✓	✗	✗	✗	✗	✗	100%; 12%
ONG-24	✓	✓	✓	✗	✗	✗	✗	✗	100%; 28%; 14%
ONG-26[b]	✗	✓	m	✗	✗	✗	✗	✗	100%; ~4%

* *tectonised or laminated marble found between calcitic and dolomitic marbles.*

[a] *used for calcite-dolomite solvus geothermometry (see chapter 5: metamorphism).*

[b] *bleached dolomitic marble.*

(sandwiched within the previous unit); and an upper finely bedded or laminated marble with fine calc-silicate layering.

(i) Basal grey marble with abundant calc-silicate layers (GMC)

This is the lowermost calcitic marble unit found at Onguati and is well exposed as a large pavement in the eastern part of the mapping area. The calc-silicate–rich marble is located in the core of a prospect-scale anticline which plunges WSW. Alternating bands of medium grey and dark grey calcitic marble are separated by numerous calc-silicate layers normally measuring a few millimetres or centimetres in thickness (Plate 4.5). The marble units are generally fine grained and completely recrystallized. This unit has experienced intense plastic deformation and many of the calc-silicate layers are strongly lineated. Where calcitic marble bands contact calc-silicate layers they frequently appear bleached. This may be a consequence of oxidation effects from the weathering of sulphides hosted by the calc-silicate rocks. The contact between the GMC and the overlying calc-silicate–deficient marbles is relatively sharp and is marked by a noticeable decrease in the amount of calc-silicate interlayering.

(ii) Middle, light grey marble with minor calc-silicate layers (GM)

This is the most widespread of the calcitic marble units and hosts the largest, frequently best mineralized veins (Plates 4.6 and 4.8). The GM unit consists of 5 to 50 cm thick marble bands in light shades of grey or white. The marble bands are commonly in direct contact and as a result of deformation and pressure solution effects, have diffuse, 'feathery' margins. Very thin (<1 mm), often boudinaged calc-silicate layers can also be found separating marble layers. The lightest marble bands are medium-grained (~1 mm grain diameter) and have experienced the most intense recrystallization. The widths of the marble bands are probably not reasonable estimates of the original sedimentary thicknesses because the package is intensely folded, and in the limbs of isoclinal folds highly thinned. The GM unit is subdivided into upper and lower parts by a thick graphitic marble unit (see [iii] next). There is little difference in the appearance of the two subunits, except that the upper part of the GM hosts smaller and less frequent quartz+calcite veining, and contains small zones of marble breccia (Plate 4.9).

(iii) Discontinuous, dark grey to black, graphitic marble (DGMC)

Although many small, graphite-rich marble interlayers occur within the GM, there are a few well developed graphitic marble units that outcrop for considerable distance and which deserve to be differentiated. The largest of these is 5 to 10 metres in thickness and defines the form of a tight-to-isoclinal fold closure in the central parts of the mapping area (Fig. 4.1). The graphitic marble unit contains a few thin, pure white, coarse-grained bands of calcitic marble and many thin interlayers of calc-silicate rocks (Plate 4.7). The upper contact of the DGMC is defined by an approximately 50 cm thick, intensely folded and boudinaged calc-silicate unit. A second thick calc-silicate unit is found within the DGMC fold closure and helps define the extension of the fold limbs. The southern limb of this large-scale fold can be traced approximately 100 metres eastwards before the dark, graphitic marble unit fades into light grey marbles of the GM unit. The northern limb is more difficult to follow because it is largely obscured by calcrete and soil. A zone of closely-spaced calc-silicate rocks to the NE may correlate with the upper calc-silicate rocks found at the fold closure and could define a less graphitic limb extension of this unit. The graphitic marble unit may be laterally discontinuous because deposition was of limited extent, or may be a result of folding, so that this less competent unit became pinched out. A further graphite-rich marble unit was identified in the upper parts of the GM and is 1 to 2 metres wide. It extends for about 100 metres before becoming difficult to delineate.

(iv) Laminated and tectonized calcitic marble (TM)

The TM unit ranges in thickness from 5 to 10 metres and is characterized by very fine, calcitic marble layers (1-10 mm width). The marble layers may alternate with thin calc-silicate laminations (Plate 4.10). Towards the contact with the overlying dolomitic marbles it is common to encounter centimetre-scale layers of dolomitic marble with small tremolite blebs. The laminated marbles appear to have experienced intense deformation especially towards their upper margins. The original finely layered or laminated nature of these calcitic marbles may have been utilized and enhanced during deformation to produce a well developed foliation.

4.2.3. Dolomitic Marble Unit (DM)

The uppermost rock type in the Onguati Mine area is a thin dolomitic marble unit. The dolomitic marbles exhibit a pitted and irregular weathering surface (Plate 4.11) quite distinct from the lower calcitic marbles. The original bedding is preserved in a few places, normally near the lower contacts with the laminated calcitic marbles. For the most part the dolomitic

Plate 4.10: Typical laminated marble (TM) in the upper parts of the calcitic marble package at Onguati Mine. Note the thin, medium grey dolomitic marble layers which contain small tremolite + quartz masses in the lower half of the image. The frequency of these layers increases towards the contact with the massive, dolomitic marble (DM) unit.

Plate 4.11: Light grey dolomitic marble (DM) found on the upper southern slopes of Onguati Hill. Two thin, planar sets of veins cut the dolomitic marble and consist of quartz and tremolite with minor amounts of carbonate. Note the distinctive dolomitic marble weathering surface.

marbles appear massive and can be extremely fine grained (<0.05 mm grain diameter). During mapping the dolomitic marbles were subdivided into three main types: a light grey dolomitic marble (dominant type); a medium grey dolomitic marble, and a brown dolomitic marble. The colour variations are thought to have resulted from karstic activity, probably during more humid times. It is likely that the broad zones of light grey dolomitic marble represent 'bleached' forms of the medium grey dolomitic marble (pristine dolomitic marble). The brown dolomitic marbles could have been stained by Fe-rich ground waters circulating through veined or sulphide-bearing rocks in the surrounding karst system. Near the claim beacon in the extreme southwest of the mapping area, there is a metre-wide zone of dark brown to black wad in the brown dolomitic marbles. The wad is mainly composed of iron and manganese oxides and hydroxides, and contains large flakes of phlogopite (1 - 2 mm).

The dolomitic marbles are heavily fractured and in places, two thin vein sets were found with a quartz+tremolite fill (Plate 4.11). These veins were most likely formed during the same hydrothermal event/s that resulted in mineralization of the lower calcitic marbles. Towards the hinge zone of the large-scale syncline in the Onguati Mine area there are pockets of intensely brecciated dolomitic marble (areas with small triangles in Fig. 4.1.). Angular and semi-rounded fragments are surrounded by a tremolite ± quartz matrix. While the brecciated layers in the upper parts of the calcitic marbles have an uncertain origin, it is very likely that these breccias were formed by tectonism because of the size of the fragments and the irregular, wide extents of these zones.

In thin section some of the dolomitic marble samples show a distinctive banding with alternating fine grained (0.05 - 0.08 mm grain dimensions) and coarse grained, equigranular layers (0.3 - 0.7 mm grain dimensions). Subidiomorphic dolomite makes up more than 90% of the marbles, and both the fine- and coarse-grained bands have granoblastic textures. Intergrowths of tremolite + quartz ± diopside ± feldspar occur as blebs or centimetre-scale nodules throughout the dolomitic marble package. Small amounts of quartz and calcite can also be found in the dolomitic marbles. Minor accessories include phlogopite, muscovite, diopside, feldspar and titanite.

In all the areas mapped in this study, the dolomitic marble unit appears to be of primary origin, although at Western Workings, there are small pockets of dolomitic marble which were probably formed by the secondary action of Mg-rich fluids related to hydrothermal vein mineralization (see section 4.4.2). Evidence for the primary origin of the extensive DM unit comes from a number of sources. Firstly the contact between the calcitic and dolomitic marbles appears to occur at a similar stratigraphic position throughout the study area, even though the marble sequence is heavily folded into large-scale synclines and anticlines. In addition thin, conformable layers of alternating calcitic and dolomitic marble can be found below the base of the DM unit and this points against hydrothermal replacement. Perhaps most convincingly, dolomitization must have occurred at an early stage (i.e. soon after deposition or during diagenesis, but before commencement of Damaran orogeny) because the DM unit is characterized by a completely different style of deformation (see Chapter 6 for detail) which is related to its competent nature compared to the calcitic marbles.

4.3. Brown Mountain

The mapping area over Brown Mountain is about 0.16 km^2 in size. It is underlain mostly by calcitic marbles which host the bulk of the quartz-sulphide veining. Dolomitic marbles are best exposed along the northwestern edge of the mapping area, near their contacts with the underlying calcitic marbles (Fig. 4.3). The mineral assemblages and microtextures of both the calcitic and dolomitic marbles are almost identical to the Onguati Mine area and are not repeated here. The low-lying plains surrounding Brown Mountain are mostly covered by thick calcrete (10 - 30 cm), which is in turn, often blanketed by thin sandy soils. Brown Mountain has relatively steep NW-facing, scree-covered slopes and small cliffs (Plate 4.12). The southeastern slopes have more moderate gradients but often have patchy exposure due to thicker scree and soil accumulations. Brown Mountain is located in the core of a large-scale anticline as shown in Fig. 4.4.

4.3.1. Calcitic Marble Units

The calcitic marbles at Brown Mountain have been divided into a thick, lower package of marbles with minor calc-silicate interlayering (GM equivalent at Brown Mountain), and an upper laminated and tectonized calcitic marble (TM equivalent at Brown Mountain). It is not possible to further differentiate the exposed calcitic marbles (eg. GMC, DGMC) because the rocks are mostly stained dark brown by the weathering of abundant vein sulphides. The mineralogy of the Brown Mountain calcitic marbles is summarized in Table 4.3.

(i) Grey calcitic marble with minor calc-silicate layering (GM)

Much of the Brown Mountain mapping area appears to be underlain by calcitic marbles that contain only minor calc-silicate layering. At Brown Mountain the spacing of the calc-silicate

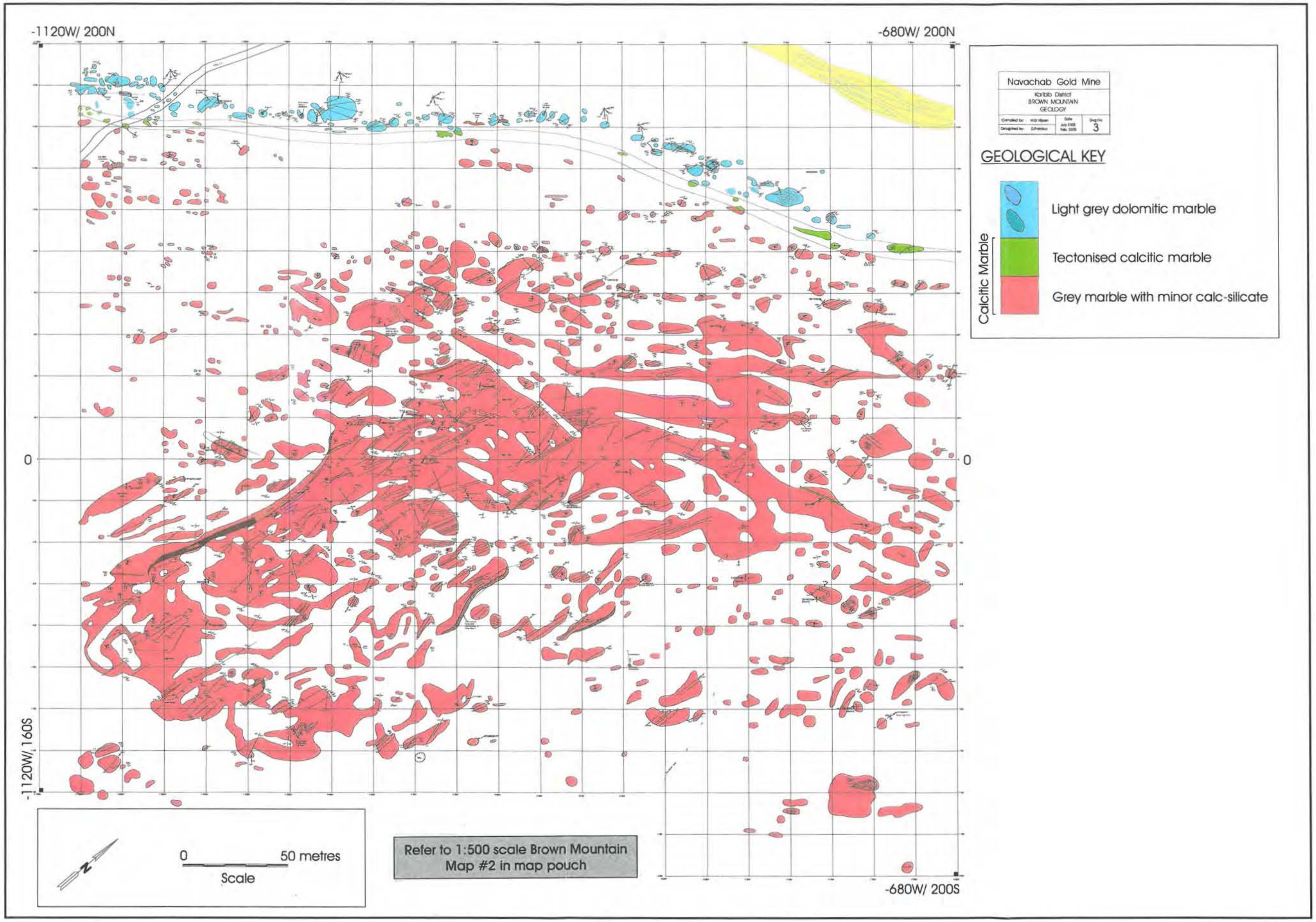

Fig. 4.3: Simplified map of the Brown Mountain area (refer to 1:500 scale map of Brown Mountain, Map #2, for structural details)

Plate 4.12: An east-facing view of Brown Mountain (forefront). The hill is entirely underlain by calcitic marbles. Dolomitic marble outcrops on the low-lying plains to the north of Brown Mountain. Note the dark brown staining of the rock surfaces and scree.

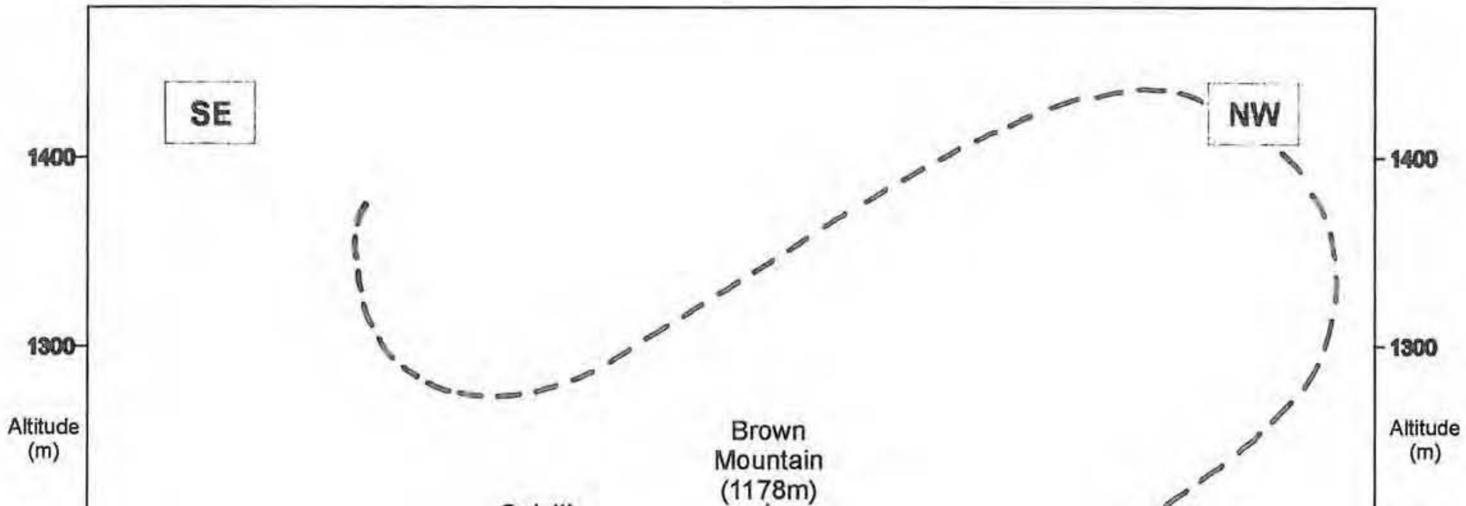

Fig. 4.4: Southeast - northwest cross section showing the basic, large scale structure of the Brown Mountain area. The fold form is highly simplified, and probably contains a multitude of S-, Z- and M-folds of multiple orders. Scale is 1:4000; vertical exaggeration is 0.

Table 4.3: Mineralogy from XRD analyses of Brown Mountain area calcitic marbles and quartzites/meta-cherts. (✓=prominent mineral peaks detected; m=minor accessory mineral; ✗=mineral not detected).

Sample No.	**Calcite**	**Dolomite**	**Quartz**	**Phlog - Biot**	**Tremolite**	**Hornblende**	**Diopside**	**Olivine**	**Relative intensity *(mineral d_1 peak heights as a % of the maximum d_1 X-ray peak height)***
BMT-01A	✓	✓	✓	✗	✗	✗	✗	✗	14%; 100%; 8%
BMT-02A-C	✓	✗	✓	✗	✗	✗	✗	✗	100%; 13%
BMT-03A[*]	m	✓	✓	✗	✗	✗	✗	✗	~1%; 7%; 100%
BMT-04-C1	✓	✗	✗	✗	✗	✗	✗	✗	100%
BMT-05-C	✓	✗	✓	✗	✗	✗	✗	✗	100%; 50%
BMT-06-C	✓	✗	✓	✗	✗	✗	✗	✗	100%; 40%
BMT-08[a]	✓	✗	✓	✗	✗	✗	✗	✗	100%; 5%
BMT-13A[+]	✓	✓	✓	✗	✗	✗	✗	✗	26%; 100%; 83%
BMT-15-C[b]	m	m	✓	✗	✗	✗	✗	✗	~2%; 100%
BMT-16-C	✗	✓	✗	✗	✗	✗	✗	✗	100%

[*] *thick pisolith-bearing, chert boudins in dolomitic marbles.*
[a] *travertine found in surface joints.*
[+] *thick pisolith-bearing, chert boudins in dolomitic marbles.*
[b] *vein sample hosted by dolomitic marble.*

interlayers does not seem as close, or the units as large and well developed as at the Onguati Mine area. During fieldwork only three thick calc-silicate units (all <30 cm) were encountered. These were not useful for mapping because they were largely obscured by superficial cover. Where calc-silicate interlayers occur between marble bands, they normally measure from a few millimetres to several centimetres in thickness. Calc-silicate layers are often stained darker brown than their adjacent marble bands (Plate 4.13).

(ii) Laminated and tectonized calcitic marble (TM)

Near the top of the calcitic marble package the carbonates become more finely bedded and laminated and are mapped as a distinct unit. Although the TM lower contact is not always easy to delineate because of poor exposure, the unit appears to be thinner (<5 m) than in the Onguati Mine area. This could be either an original sedimentary feature or it may indicate that the upper parts of the calcitic marble package underwent thinning during folding and deformation. As with the Onguati TM unit, thin dolomitic layers are present in the upper parts of the laminated calcitic marbles at Brown Mountain, and become more abundant as the contact with the dolomitic marbles is approached.

4.3.2. Dolomitic Marble Unit (DM)

A strip of small, dolomitic marble exposures occur in the far northwest of the Brown Mountain mapping area, and are mineralogically identical to the DM unit of the Onguati Mine area. The dolomitic marbles are very fine grained and massive, and host numerous centimetre-scale quartz veins, especially near the contacts with the underlying TM unit. The dolomitic marbles contain many joints and can be filled by dark brown iron hydroxides derived from pyrrhotite-rich veins on Brown Mountain (Plate 4.17). Unlike the Onguati Mine area, the dolomitic marbles at Brown Mountain do not contain tremolite nodules and have an almost uniform tan brown colour.

The dolomitic marbles at Brown Mountain also host a number of large quartzitic or meta-chert units. The fine-grained quartzitic bodies may exceed 50 cm in thickness but are all laterally discontinuous, seldom reaching more than a metre in length before pinching out. Some of the quartzitic units contain small (2-3 mm diameter) spherical bodies which may be pisoliths, or possibly even silicified ooliths (Plate 4.18). In thin section most of the pisoliths have experienced widespread static recrystallisation, but in some, faint rings and internal structure are preserved. The quartzitic layers have been interpreted as small, shallow,

BROWN MOUNTAIN AREA


Plate 4.13

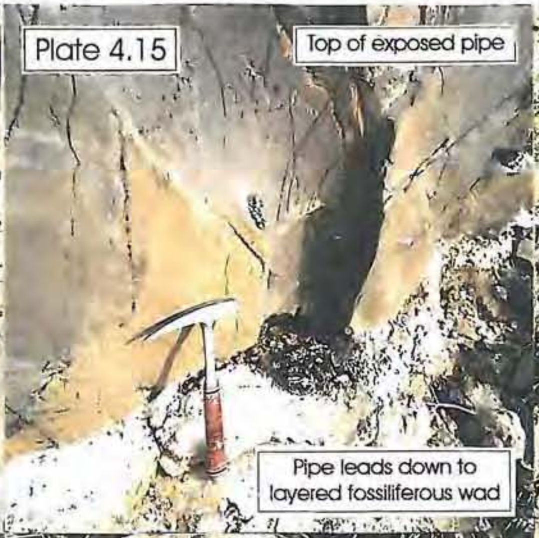
Plate 4.15


Plate 4.17


Plate 4.14

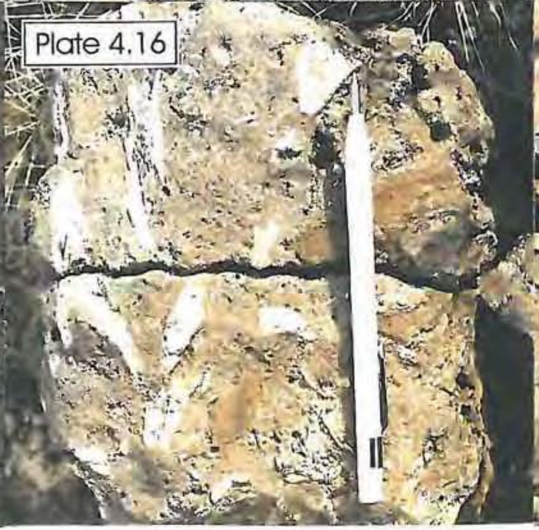
Plate 4.16


Plate 4.18

Plate 4.13: An outcrop showing the original grey colour of the Brown Mountain calcitic marbles (GM). The marbles are bleached a cream colour near the contacts with thin calc-silicate layers. Strong staining has occurred along the two sulphide-bearing quartz veins. Note the typical dark brown marble scree in the bottom, left-hand corner of the image.

Plate 4.14: Wad breccia deposit with fossil bone fragments. The majority of the large bone material belongs to *Equus Capensis*, a species of large horse that roamed parts of Southern Africa during the Pleistocene. Note the hollow form of many of the bones and the porous, spongy bone tissue that is still preserved. The pen measures 15 cm in length.

Plate 4.15: Exposed half of a karst solution pipe in the calcitic marbles of Brown Mountain (close to 810W/30N). The pipe leads down to a layered fossiliferous wad deposit. A close up of some of the bone material is shown in Plate 4.14 above.

Plate 4.16: Sample of Brown Mountain wad containing Pleistocene fossil bone fragments. These may belong to *Equus Capensis*, a species of large African horse, or to an antelope (*Antidorcas sp.*). The pen measures 15 cm in length.

Plate 4.17: Dolomitic marble joint planes and intersections filled by ferruginous material in the northern parts of the Brown Mountain mapping area. Note the light tan brown colour of the dolomitic marbles.

Plate 4.18: Quartzitic boudin with abundant pisoliths hosted by dolomitic marbles (DM) of the Brown Mountain mapping area (near 200N/1080W). The quartzitic layers may represent small channel fill deposits which have been further modified by deformation. Pisoliths may have been washed into the channels from subaerially exposed areas. The pen measures 15 cm in length.

channel fill deposits, while the spherical bodies could represent pisoliths washed into the system with siliceous sediments.

4.3.3. Shallow Karst Infillings and Epikarst Wad Deposits

Fossiliferous wad and breccia (purple/mauve areas in central parts of Fig. 4.3) were discovered on the northwestern slopes of Brown Mountain during mapping. At one locality in calcitic marble (near 30N/810W) part of a small karst pipe is exposed and well preserved (Plate 4.15). The pipe leads down to a thick (50 - 90 cm), layered pile of calcareous sediments with abundant bone material. The infilling is generally brown in colour, but white and tan layers are also found. The wad is coarse grained and poorly sorted, and formed by successive in-washing of surface material into the upper parts of an epikarst system. The majority of bone material was discovered in the vicinity of the 20N/800W grid beacon. In other areas thin (<10 cm) horizontal joints have been filled by more iron-rich sediments or travertine normally devoid of fossil bone.

Palaeontologists (Pickford & Senut, 2001) visited the site during the course of fieldwork for this project, and studied the karst infillings and bone material. Pickford & Senut (2001) identified a number of large vertebrate bone fragments (Plates 4.14 and 4.16) belonging to species of antelope (*Antidorcus sp.*) and a large African horse (*Equus Capensis*). Smaller bone material was also recognised from two species of rodents (*Petromus and Aethomys*). Several blocks of wad contained small gastropod shells (*Xerocerastus*). From the fossil assemblage, Pickford & Senut (2001) concluded that the sites are Pleistocene in age. The wide variety of large and small animal life, and the well developed karst system in the higher levels of Brown Mountain, suggest the climate was more humid than present.

4.4. Western Workings

Two adjoining areas were mapped at Western Workings. The first area (Fig. 4.5[a]) is situated over the best exposed parts of a large, several kilometre-long fault zone, in close proximity to mineralization at Western Workings. Mapping was centred either side of the "0" North baseline from 1580W to 1920W, and covered an area of approximately 0.08 km^2. The second mapping strip (Fig. 4.5[b]) is nearly twice the size of the first (~0.16 km^2) and was positioned across strike to include areas of major vein mineralization and all the main rock types at Western Workings.

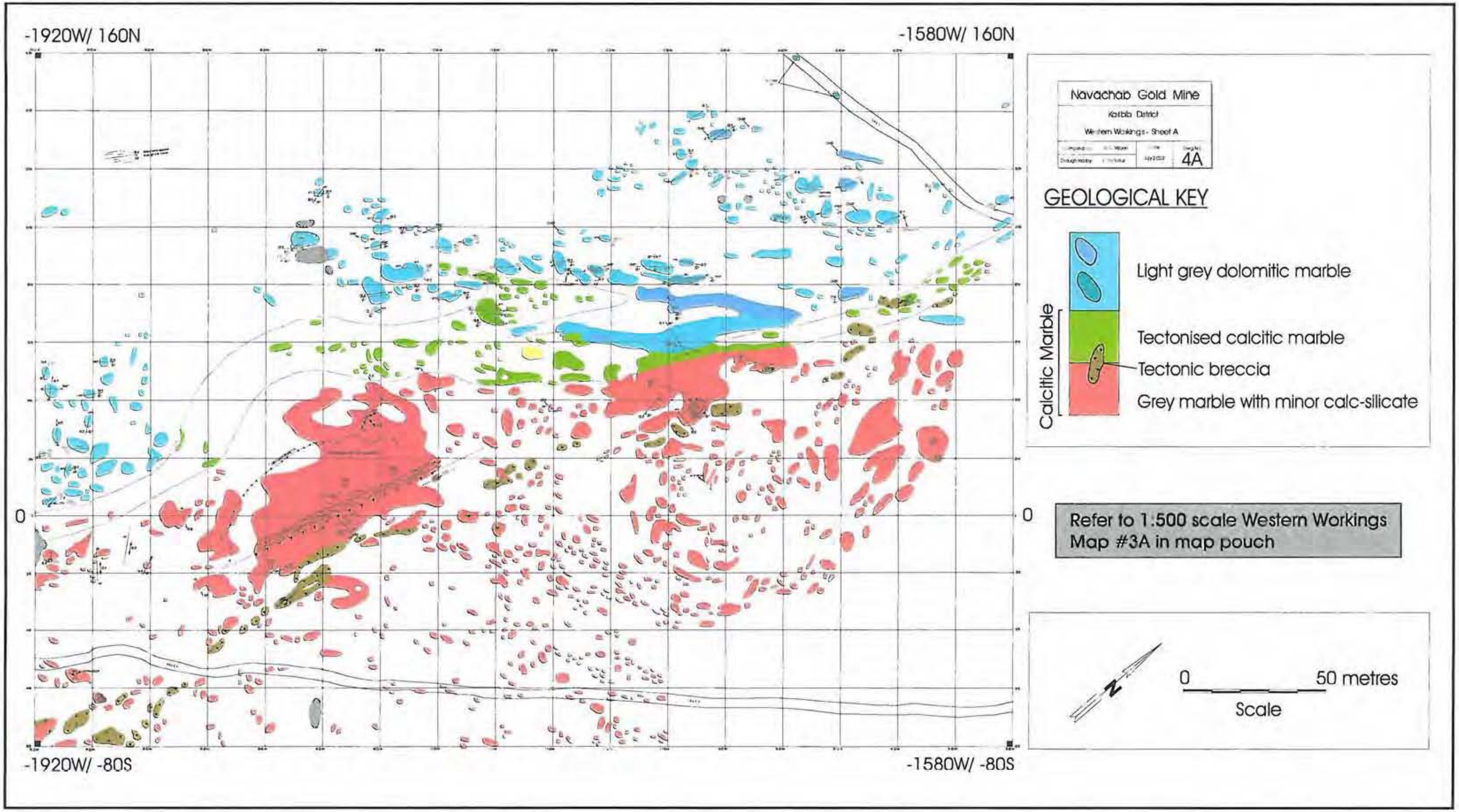

Refer to 1:500 scale Western Workings Map #3A in map pouch

Fig. 4.5a: Simplified map of the Western Workings area - part A (refer to 1:500 scale map of Western Wokings, Map #3A, for structural details).

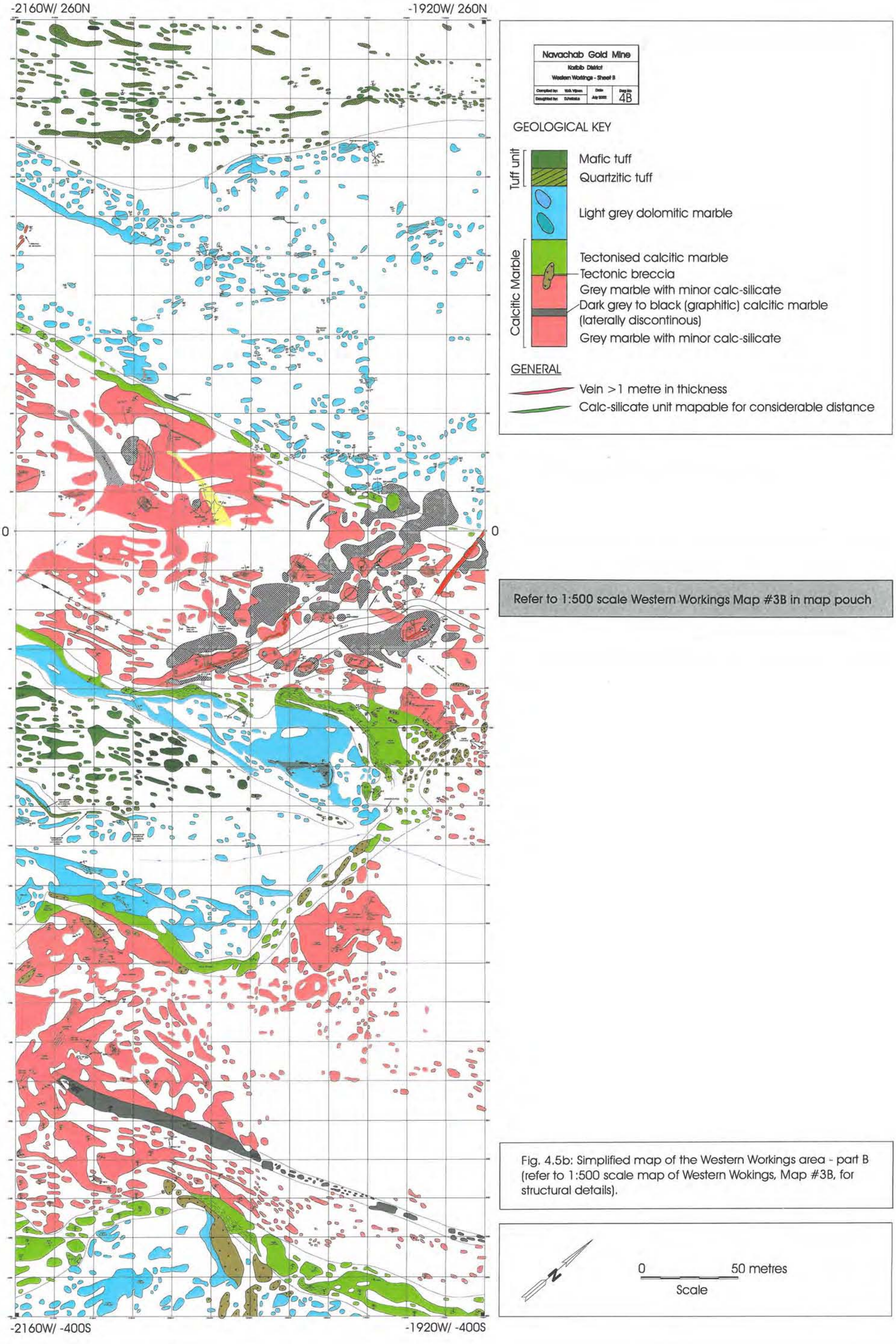

Refer to 1:500 scale Western Workings Map #3B in map pouch

Fig. 4.5b: Simplified map of the Western Workings area - part B (refer to 1:500 scale map of Western Wokings, Map #3B, for structural details).

Western Workings shares the same calcitic (i.e. GM, DGMC, TM) and dolomitic marble units (i.e. DM) as the Onguati Mine area and Brown Mountain, but differs by having higher stratigraphic level, mafic meta-tuffs and quartzites. Western Workings is situated on the northeastern side of an extensive highland area of rolling hills and ridges (Plate 4.19). The prospect-scale structure of the Western Workings area includes a series of large anticlines and synclines as shown in Fig. 4.6. Generally speaking the lowermost calcitic marbles form the cores of anticlines, whereas complete sections of dolomitic marble and remnants of mafic tuffs and quartzites are preserved in synclinal closures.

4.4.1. Calcitic Marble Units

The calcitic marbles at Western Workings have been divided into three units which include: a thick lower package of light grey calcitic marbles with minor calc-silicate interlayering (GM); a thin discontinuous dark grey, graphitic marble unit (DGMC); and a laminated upper calcitic marble (TM). The mineralogy of the marbles and calc-silicate rocks is similar to those at Onguati (Table 4.4).

(i) Grey calcitic marble with minor calc-silicate layering (GM)

The GM unit is composed of light to dark grey bands, and generally only contains millimetre-thick calc-silicate interlayers. This thick calcitic marble package can be correlated with the GM units of Brown Mountain and Onguati Mine further to the northeast. At Western Workings there are a few localities where thick (10 - 30 cm), closely spaced calc-silicate units (marked in dark green on maps) are exposed, but these cannot be traced for any distance. Some of the better developed calc-silicate rocks host tremolite nodules up to 0.5 cm in diameter, and may have abundant pyrrhotite. The whole rock chemical composition of a typical Western Workings calc-silicate rock is provided in Table 4.5.

In the middle to upper parts of the GM unit there are thin (1-2 mm), discontinuous quartzitic layers that alternate with calcitic marble bands. Where the siliceous layers are folded they are frequently boudinaged. Some of the quartzitic layers contain silicified ooliths or pisoliths a few millimetres in length, but in thin section no internal structure is preserved. The pisoliths are frequently deformed into ellipsoidal forms and can be aligned parallel to local fold axes. Calcitic marbles at Western Workings appear to have had more siliceous input than the Onguati Mine or Brown Mountain areas.

At two localities in the Western Workings mapping area, near the upper GM –

Plate 4.19: A southwest-facing view of the Western Workings area. The abandoned mine workings are located in the valley the NW of the hills

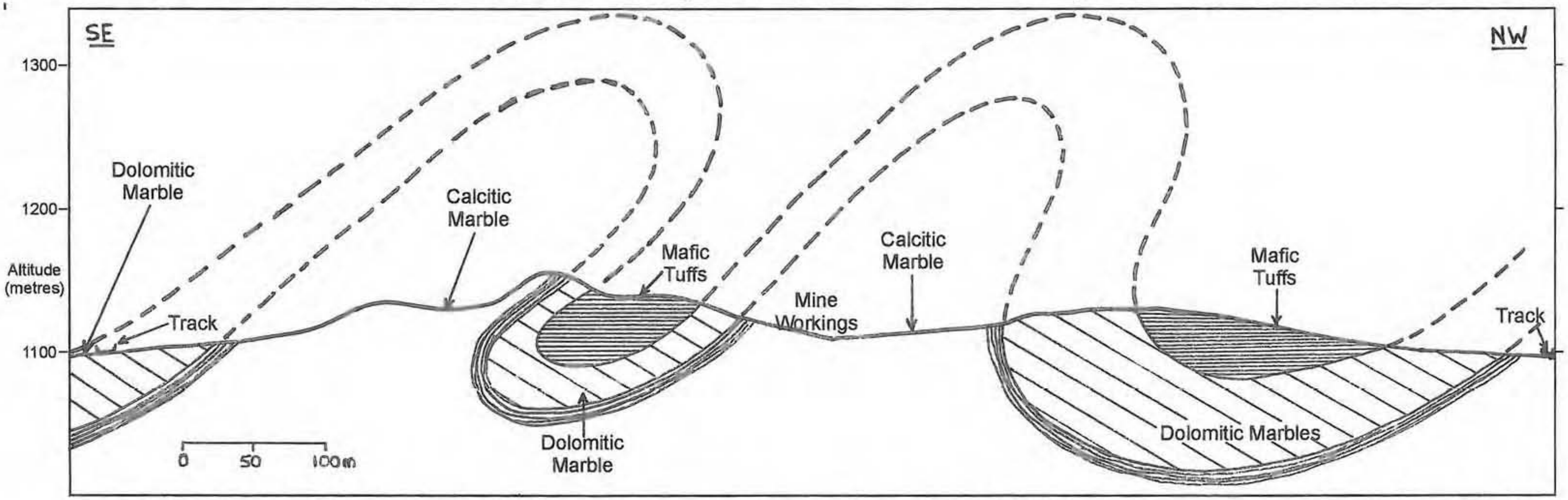

Fig. 4.6: Southeast - northwest cross section showing the basic, large scale structure of the Western Workings area. The fold form is highly simplified, and probably contains a multitude of S-, Z- and M-folds of multiple orders. Scale is 1:4000; vertical exaggeration is 0.

Table 4.4: Mineralogy from XRD analyses of Western Working area calcitic marbles, dolomitic marbles, quartzitic and mafic meta-tuffs (✓=prominent mineral peaks detected; m=minor accessory mineral; ✗=mineral not detected).

Sample No.	Calcite	Dolomite	Quartz	Phlog - Biot	Tremolite	Hornblende	Diopside	Olivine	**Relative intensity *(mineral d_1 peak heights as a % of the maximum d_1 X-ray peak height)***
WW-5A*	✓	✓	✓	✓	✓	✗	✗	✗	33%; 11%; 100%; 10%; 18%
WW-06-C	✗	✓	✗	✗	✗	✗	✗	✗	100%
WW-07[a]	✓	✓	✓	✗	✗	✗	✗	✗	7%; 100%; 5%
WW-07-C2(a)[b]	✓	✗	m	✗	✗	✗	✗	✗	100%; ~3%
WW-07-C2(b)[b]	✓	✗	✓	✗	✗	✗	✗	✗	41%; 100%
WW-09	✓	✗	✓	✗	✗	✗	✗	✗	100%; 49%
WW-09-C1	✓	✓	✗	✗	✗	✗	✗	✗	24%; 100%
WW-10[c]	✗	✓	✓	✗	✓	✗	✗	✗	100%; 10%
WW-15A1[d]	✓	✗	✓	✓	✗	?	?	✗	~6%; 100%; 25%
WW-15A2[d]	m	✗	✓	✓	✗	?	?	✗	~4%; 100%; 22%
WW-15B[d]	?	✗	✓	✓	✗	?	?	✗	100%; 27%
WW-15C[d]	m	✗	✓	m	✗	✗	✗	✗	~3%; 100%; ~3%
WW-15D[d]	m	✗	✓	✓	✗	✗	✗	✗	~3%; 100%; 8%
WW-15E[d]	✗	✗	✓	✗	✗	✗	✗	✗	100%
WW-15F[d]	✓	m	✓	✗	✓	✗	✗	✗	35%; ~5%; 100%; 44%
WW-22	✓	✗	✓	✗	✗	✗	✗	✗	100%; 63%
WW-24[e]	✓	✓	✓	✓	✓	✗	✗	✗	54%; 16%; 100%; 24%; 54%
WW-25A[f]	✓	✓	m	✗	✗	✗	✗	✗	100%; 8%;~4%

* *calc-silicate unit with nodules of tremolite.*

[a] *brecciated dolomitic marble stained brick red.*

[b] *late carbonate vein with quartz margins.*

[c] *dolomitic marble with few large tremolite laths.*

[d] *quartzites, pquartzitic meta-tuffs and mafic meta-tuffs.*

[e] *dark green calc-silicate sample.*

[f] *fault breccia.*

Table 4.5: Whole rock chemical analyses of a typical calc-silicate rock (WW-24), and a red-stained dolomitic marble (WW-07) from the Western Workings region. The dolomitic marble has undergone intense brecciation, silicification and staining (WW-7).

Majors elements as oxides (wt%)	WW-24 (Calc-Sil)		WW-07 (Dol. M.)
SiO_2	44.11		30.57
TiO_2	0.60		0.03
Al_2O_3	10.88		0.46
Fe_2O_3	4.31		0.93
FeO	0.00		0.00
MnO	0.22		0.07
MgO	7.96		11.69
CaO	15.23		23.07
Na_2O	0.17		0.00
K_2O	4.08		0.04
P_2O_5	0.19		0.09
LOI	10.90		31.54
H_20-	0.54		0.54
TOTAL	**99.19**		**99.03**
Selected trace elements (ppm)			
Ni	17		7
Cu	791		27
Zn	58		23

laminated marble contact, large oval-shaped structures of unknown origin are found (Plates 4.21, 4.22 and 4.23). The elliptical structures appear confined to a 50 cm thick unit in well bedded calcitic marbles near the fault zone at 0N/1840W (Fig. 4.5[a]). At another locality close to the 60N/2100W grid beacon and at a similar stratigraphic level (Fig. 4.5[b]), oval-shaped structures are found within two closely spaced fine-grained quartzitic layers (5 - 8 cm thick). Near the fault zone, the oval-shaped structures are exposed on the bedding planes of the calcitic marbles, but at the second site, the structures are hosted by the entire thickness of the quartzitic layers, occasionally extending into the marble bands on either side. These observations may suggest the structures have an ellipsoid shape, but a structure found on a loose marble slab appears disc-like in form (1 - 2 cm thickness?). It is difficult to verify the shape because intact 3D exposures of the elliptical structures have not been found.

The oval-shaped structures are commonly around 10 cm long and 8 cm wide, but large examples can measure 30 x 20 cm in size (Plate 4.22). Some of the elliptical structures appear to have been flattened and deformed (Plate 4.20). The best preserved elliptical structures show complex internal structures. The core areas of the elliptical structures can consists of lighter grey, more siliceous material (Plate 4.20), or may be composed of carbonate material (Plates 4.21 and 4.22). Where the core is well defined it is often surrounded by faint rings of fine light and dark calcitic marble. The rings may reach a total thickness of about a centimetre before they are sharply replaced by radiating calcitic and graphitic growths which can extend for several to tens of centimetres in length. In thin section the grains in this region have a long, blade-like appearance. The outer few centimetres of the elliptical structures are surrounded by alternating dark and light grey calcitic marble rings which sharply contact with the host rocks.

Similar oval-shaped structures with radiating textures were observed by Badenhorst (1992) at the top of the Karibib Formation in the Spes Bona area. Badenhorst (1992, p.117) named these "colloform structures" and suggested a possible stromatolitic origin. However a stromatolite interpretation is difficult for the Western Workings structures because they do not appear columnar, but are rather more disc-like or ellipsoid in form. Although oncolites can attain diameters of 5 to 10 cm (e.g. Ore Lake, Michigan; Scholle *et al.*, 1998) and pisoliths can grow to 20 cm in diameter (e.g. spring fed, supersaturated pans in the Andean Altiplano, Pastos Grandes, Bolivia; Scholle *et al.*, 1998), these are exceptional cases and not likely interpretations for the marble-hosted structures at Western Workings.

An alternative interpretation is that the Western Workings structures represent diagenetic concretions or nodules that formed around decaying, organic material (e.g. algal

WESTERN WORKINGS AREA


Plate 4.20


Plate 4.21


Plate 4.22

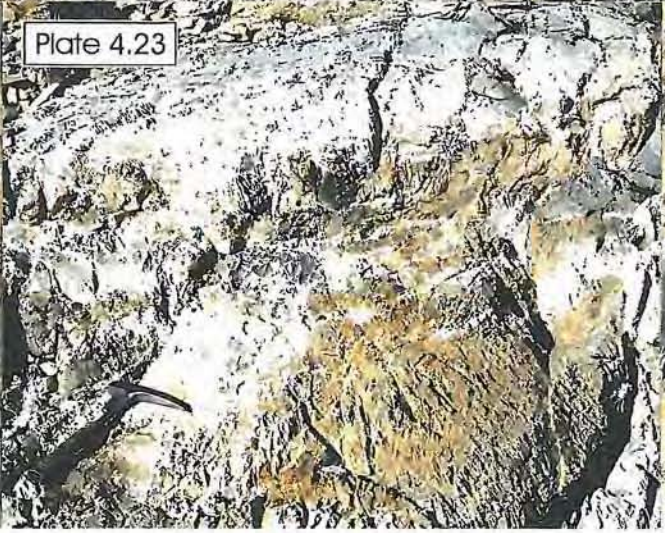
Plate 4.23


Plate 4.24


Plate 4.25

Plate 4.20: Oval-shaped structures hosted by a fine-grained quartzitic layer, in the upper parts of the GM unit at Western Workings (near 60N/2100W). Some of these display strong internal structure. The oval-shaped structures on the right-hand side of the image appear to be deformed and flattened. Pencil measures 14 cm in length.

Plate 4.21: This oval-shaped nodule shows well developed internal structure. A light grey carbonate core is surrounded by thin rings of calcitic marble, followed by thin, radiating 'fibres' of light and dark marble, and then by outer marble rings. This structure was found on the well bedded marble (GM) pavement near 0N/1840W. The pen measures 15 cm in lenght.

Plate 4.22: This is the largest oval-shaped structure found at Western Workings (near 0N/1840W). The large size of the object suggests that it may be a diagenetic concretion or nodule that formed around decaying organic matter. The nodule is exposed on the bedding surface of calcitic marbles.

Plate 4.23: Areas of grey-brown, secondary dolomitic marble in the upper GM unit of Western Workings. The dolomitic marble patches are associated with quartz + tremolite veining and have discoloured the adjacent calcitic marbles. These dolomitic marbles were probably formed by the action of Mg-rich hydrothermal fluids, and do not share the same origin as the overlying DM unit. Note the contrasting weathering surface of the calcitic and dolomitic marbles.

Plate 4.24: A typical lapilli meta-tuff showing well developed layering at Western Workings (near 100S/2100W). In the forefront note the 'ribbed' weathering surface that is often developed on the steeply dipping meta-tuff units.

Plate 4.25: Dark, fine-grained mafic tuff near 100S/2100W at Western Workings. The mafic tuffs are typically well layered and break with a conchoidal fracture (e.g. lower, right-hand corner).

remains). The nodules may have formed when semi-lithified calcareous sediments were sub-aerially exposed. A local reducing environment would have developed and constituents may have migrated and precipitated around the organic nuclei. The larger the amount of organic material, the steeper the chemical gradients and ultimately, the greater size of the nodule. Such processes could explain the growth of nodules within or across layering, and perhaps even the confinement of disc-like concretions to individual marble beds. It is also possible that disc-like forms represent highly flattened nodules (i.e. finite strain ellipsoid is oblate). The concentric textures found in the Western Workings structures may represent original concretions in the nodules, while the radial textures could be a result of later recrystallisation.

(ii) Discontinuous, dark grey to black, graphitic marble (DGMC)

A 5 to 10 metre thick unit of very fine grained, graphite-rich calcitic marble occurs as a prominent ridge in the southeastern parts of the Western Workings mapping area (Fig. 4.5[b]). Although laterally discontinuous, the dark marble unit may highlight the southern limb of a large-scale fold structure. It is difficult to ascertain whether the graphite-rich calcitic marbles at Western Workings are the stratigraphic equivalent of the main Onguati DGMC unit, but both occur in the middle to upper regions of the lighter grey, calc-silicate–deficient marbles (GM) which host them. The DGMC unit at Western Workings is devoid of calc-silicate rocks but there are a few siliceous interlayers which can host well formed pisoliths measuring a few millimetres across.

(ii) Laminated and tectonized calcitic marble (TM)

This unit is about 5 metres in true thickness and consists of well bedded and laminated calcitic marble. The laminated marbles are generally fine grained, and can contain thin layers (<1 mm) of fine grained quartz and muscovite. A characteristic of the TM unit is that it lacks any significant folding (i.e. no metre-size isoclinal or periclinal folds) such as seen in the lower calcitic marbles. As with the other mapping areas, the TM unit marks the upper limit of the calcitic marbles, above which there is a rapid transition to dolomitic marble.

4.4.2. Dolomitic Marble Unit (DM)

The dolomitic marbles at Western Workings are very fine grained and mainly light grey or tan brown in colour, but near the fault zone can be stained darker brown. Joints, openings or solution breccia pipes can be filled by ferruginous wad, but are devoid of obvious bone material. In the southeastern parts, the DM unit is heavily fractured and jointed, and elongate zones of tectonic breccia are common. Brecciated dolomitic marbles can often appear a brick red colour due to the weathering of an iron-rich, siliceous cement which bonds the marble fragments together (see Table 4.5. for whole rock chemical composition). It is likely that the siliceous cement is related to faulting and regional hydrothermal activity but no sulphides or oxide boxworks after sulphide have been found.

The mineralogy of typical Western Workings dolomitic marble is summarized in Table 4.4, and is similar to the other mapped areas. Towards the upper parts of the DM unit, about 2 to 3 metres from the contact with the overlying mafic tuffs and quartzites, numerous tremolite nodules and laths (1 - 2 cm long) are found concentrated along a 50 to 100 cm wide dolomitic marble band. It is very likely that quartz in an originally siliceous marble bed reacted with dolomite during regional metamorphism to form the large tremolite masses.

At Western Workings there are small, irregular areas of secondary dolomitic marble which occur in the upper parts of the calcitic marble package (Plate 4.23). This dolomitic marble does not share the same origin as the DM unit and was probably formed by the migration of Mg-rich hydrothermal fluids through permeable parts of the calcitic marbles. In many parts the dolomitic marble 'islands' contain abundant hydrothermal quartz veining. The DM unit in all three mapping areas appears to be primary in origin, probably having formed during carbonate deposition or diagenesis as detailed earlier (section 4.3.2).

4.4.3. Volcanic Meta-tuff Units

Volcanic meta-tuffs were found in the far northwestern and central parts of Western Workings (Fig. 4.5[b]). In previous work, similar rocks have also been descriptively referred to as hornfelses (R. Jacob, 2004, *pers. comm.*). During mapping these rocks were divided into two main units: a thin, lower quartzite or quartzitic meta-tuff unit; and an extensive mafic meta-tuff unit, in a manner similar to Petzel (1988a). The mineralogy and whole rock compositions of a range of meta-tuff samples have been provided in Tables 4.4 and. 4.6 respectively. The meta-tuff units are largely obscured by flat soil- and calcrete-covered plains which have accumulated in the hinge zones of two prospect-scale synclines.

(i) Quartzitic Meta-tuffite (QMT)

The quartzitic units are found at the base of the meta-tuff package and are estimated to be only a few metres thick. They are commonly fine grained, light grey to pink in colour and can

Table 4.6: Whole-rock chemical analyses of the quartzites, quartzitic meta-tuffs and mafic meta-tuffs found in the upper lithostratigraphy of the Western Workings area.

Majors elements as oxides (wt%)	**WW -15A**	**WW -15B**	**WW -15C**	**WW -15D**	**WW -15E**	**WW -15F**
SiO_2	54.71	57.59	76.45	66.10	70.86	43.70
TiO_2	0.61	0.73	0.72	0.50	0.58	0.68
Al_2O_3	16.33	17.35	9.13	10.86	12.00	14.96
Fe_2O_3	6.94	8.54	3.75	4.55	4.17	7.84
FeO	0.00	0.00	0.00	0.00	0.00	0.00
MnO	0.37	0.15	0.06	0.17	0.05	0.75
MgO	5.36	3.90	2.08	3.71	3.35	3.94
CaO	5.57	1.67	0.72	4.83	0.89	17.66
Na_2O	0.99	0.97	2.33	0.85	1.34	0.33
K_2O	5.48	6.43	2.02	3.47	5.12	0.85
P_2O_5	0.16	0.12	0.20	0.11	0.09	0.16
LOI	2.93	2.29	2.08	4.28	1.92	7.72
H20-	0.42	0.39	0.48	0.38	0.41	0.37
TOTAL	**99.87**	**100.13**	**100.02**	**99.81**	**100.78**	**98.96**
Selected trace elements (ppm)						
Ni	70	78	23	47	34	59
Cu	9	13	90	791	7	62
Zn (ppm)	58	62	69	62	93	116

be finely laminated. The quartzitic units consist predominantly of poorly sorted layers which contain xenoblastic quartz grains (0.5 - 0.02 mm length) and quartzitic lithoclasts (0.1 - 0.4 mm length), with minor amounts of muscovite and chlorite. Quartzitic rocks also occur within the overlying mafic meta-tuffs and from mapping appear either as discrete beds or discontinuous lenses. It is often difficult to trace the lateral extents of these units or find contacts with the overlying mafic meta-tuffs because of the extensive superficial cover.

The quartzitic units could have a variety of origins. Petzel (1988a) suggested that these rocks are altered versions of the overlying mafic volcanic tuff because the two units share similar textures and because the quartzitic units host patches of disseminated pyrrhotite and pyrite mineralization. Alteration could have arisen during the hydrothermal event/s that gave rise to the vein mineralization in the lower carbonate rocks. However, disseminated mineralization has been found in both the "altered" quartzitic rocks and in the 'parent' mafic tuffs in this study. In addition the quartzitic units are poorly sorted and preserve xenoblastic quartz grains and lithoclasts which suggest a primary, sedimentary origin. An alternative interpretation could be that the quartzitic units were derived from nearby quartz-rich sediments or volcanic rocks and that they were contaminated to varying degrees by pyroclastic material at the start of volcanic activity in the Western Workings area. If the quartzitic unit is a consolidated mixture of pyroclastic and sedimentary detritus then it may be more appropriate to call this rock a quartzitic meta-tuffite.

(ii) Mafic Meta-tuffs (MMT)

Mafic meta-tuffs are found directly above the main quartzitic meta-tuff unit, and were probably in excess of 10 metres thick. The mafic meta-tuffs are typically a grey to black or dark green colour and have well developed, finely spaced layering (Plate 4.25). The meta-tuff layers are mostly very fine grained (0.01 - 0.06 mm grain diameters) but there are also more coarse-grained layers with grains up to 0.1 mm in length. In places the mafic meta-tuffs outcrop as small ridges, and more resistant layers yield a 'ribbed' weathering surface. Lapilli (1 - 5 mm across) are commonly found in these rocks and may be more abundant within some of the layers. Where the lapilli make up a sizeable (>10%) proportion of the rock they have been termed lapilli tuffs (Plate 4.24). It is thought that the lapilli meta-tuffs occur interspersed throughout the mafic meta-tuff package, and no attempt was made to map out individual units. Patchy exposure would also have hindered the distinction of such units in the field.

The mafic meta-tuffs commonly consist of a fine-grained aggregate of subidioblastic, pale green to tan brown biotite and xenoblastic quartz, with variable amounts of green subidioblastic hornblende or actinolite. Minor amounts of tremolite and calcite can also be found in some of the samples studied. In many of the sections there are millimetre-size cubic areas filled by granoblastic quartz or carbonate aggregates, commonly surrounded by large, subidioblastic biotite laths. It is likely that these represent pseudomorphs after pyrite which may be of syngenetic origin.

5. CALCITE–DOLOMITE SOLVUS GEOTHERMOMETRY

5.1. Introduction

Early investigation of subsolidus phase relationships in the binary system $CaCO_3$ - $CaMg(CO_3)_2$ by Harker & Tuttle (1955) and Graf & Goldsmith (1955), led to the realisation that the magnesian content of calcite in equilibrium with dolomite is strongly temperature dependent. Subsequently, extensive experimental work was carried out by Goldsmith and coworkers (e.g. Goldsmith & Heard, 1961; Goldsmith *et al.*, 1961; Goldsmith & Newton, 1969) to calibrate the calcite-dolomite solvus for use as a potential geothermometer. More recently Anovitz & Essene (1987) have re-evaluated the available experimental reversals to ensure an internally consistent calcite-dolomite solvus, and along with work by Bickle & Powell (1977) and Rice (1977), have assessed the effect of small amounts of $FeCO_3$ in metamorphic temperature determination. Detailed reviews of calcite-dolomite solvus geothermometry, and comparisons to other techniques, have also been provided by Essene (1982, 1983, 1989).

Calcite-dolomite solvus geothermometry is an appealing technique in metamorphic studies because of the common occurrence of calcite and dolomite in many marbles, and because of the advent of routine electron microprobe analysis of carbonate rocks. Essene (1983, p.88) notes additional advantages of using this system to evaluate metamorphic conditions which include the insensitivity of the calcite-dolomite immiscibility gap to pressure, independence from fluid compositional effects, and the closeness of calcite and dolomite to the $CaCO_3$ - $CaMg(CO_3)_2$ binary in metamorphic terrains. Furthermore, the solvus is experimentally well constrained (±10°C) between 500°C and 800°C (Anovitz & Essene, 1987).

In practice, the calcite-dolomite geothermometer can only be applied to rocks between 400°C and 650°C because at high temperatures $MgCO_3$ loss through retrograde exsolution and recrystallisation becomes very severe. Below 400°C the solvus curve becomes very steep (i.e. insensitive to temperature) so that small errors in analyses result in considerable error in temperature estimation. For these reasons, the calcite-dolomite geothermometer has been applied most successfully to metamorphic terrains that have undergone greenschist to lower amphibolite facies metamorphism (e.g. application to marbles in the Tauern Window of Austria by Bickle & Powell, 1977), or to contact metamorphic rocks where intrusive bodies have experienced rapid cooling, limiting the affects of retrograde resetting (e.g. Rice, 1977; Wada & Suzuki, 1983). Application of the technique to amphibolite and granulite facies rocks by Perkins *et al.* (1982) yielded metamorphic temperatures that were significantly lower than results from oxide and feldspar geothermometry, while estimates by Puhan (1976) for the upper amphibolite facies, western parts of the Damaran CZ were also at least 100°C lower than expected. The ease with which $MgCO_3$ can diffuse out of calcite and the resulting rapid re-equilibrium of carbonate systems are a major drawback of this technique (Essene, 1983). For the most part, calcite-dolomite geothermometry can only make *minimum* estimates of the peak metamorphic temperature, and the reliability of these estimates varies quite considerably, being largely dependent on the cooling histories of the metamorphic rocks studied.

Calcite-dolomite solvus geothermometry was attempted on several samples collected near Onguati Mine because of the predominance of calcitic and dolomitic marbles in the Onguati study area and the paucity of other suitable equilibrium mineral pairs. Application of calcite-dolomite geothermometry to Onguati marbles was thought favourable because this part of the SCZ has not undergone extensive partial melting and does not exceed lower amphibolite facies metamorphism (Miller, 1983c). Inferred temperature estimates should therefore be below the upper working limit of the geothermometer (i.e. 650°C).

5.2. Determination of Magnesian Contents of Onguati Calcites

The success of calcite-dolomite geothermometry relies on the coexistence of calcite and dolomite at equilibrium so that the $MgCO_3$ dissolved in calcite is a direct function of the temperature at or near peak metamorphism. There must also be sufficient quantities of primary dolomite in the samples chosen so that calcites share at least part of their boundaries with dolomite grains. This ensures abundant $MgCO_3$ was readily available in the system, and that the magnesian content of the calcites reliably reflects the equilibration temperature over as wide a part of the section as possible (i.e repeatable results).

The majority of samples from the Onguati study area show granuloblastic textures throughout and this is a good indication that widespread metamorphic equilibrium was achieved some time during Damaran metamorphism. From microstructures alone it is difficult to assess whether any retrograde resetting occurred in the Onguati samples, although there is much evidence for recrystallisation. Re-equilibration is most commonly implicated by anomalously low temperature estimates from the calcite-dolomite geothermometer. Due to the inherent difficulties in optically distinguishing dolomite from calcite, confirmation of carbonate mineralogy and the relative amounts of each carbonate mineral relied on X-ray powder diffraction (XRD) analyses. The XRD operating conditions are described in *Appendix B*. From this combined investigation, only ONG12a and ONG24 contained sufficient amounts of calcite and primary dolomite (see Table 4.1) to be suitable candidates for calcite-dolomite geothermometry. Many of the calcite grains in ONG12a showed extensive dolomite exsolution lamellae when viewed under low magnification in PPL, but little evidence of exsolution could be found in ONG24 calcites.

The average magnesian content of calcites in powdered samples of ONG12a and ONG24 were also derived by the XRD method first employed by investigators in the study of the calcite-dolomite solvus (e.g. Graf & Goldsmith, 1955; Goldsmith *et al.*, 1961). The magnesian content of calcites is simply determined by the shift in the *d*-value of the $[104]_H$ site in calcite as more $MgCO_3$ is accommodated. Quartz was used as an internal standard to ensure that the cell parameter sensitive to compositional change was unaffected by instrument error. The mole fractions of $MgCO_3$ (X_{MgCO3}) in calcites were calculated on the basis of the calibration curve presented by Anovitz & Essene (1987, Fig. 2, p.393), and first approximations of the metamorphic temperature were gained using the refined solvus equation of Anovitz & Essene (1987, p.401):

$$T = A(X_{MgCO3}) + B/(X_{MgCO3})^2 + C(X_{MgCO3})^2 + D(X_{MgCO3})^{0.5} + E - 273.15\ (°C)^* \qquad [5.1]$$

where: $A = -2360.0$
$B = -0.01345$
$C = 2620.0$
$D = 2608.0$
$E = 334.0$

$^*(R^2 = 0.99893$; S.E. of the estimate for CaCO3 - MgCO3 compositions = 7.1254)

ONG12a produced the most promising crude estimate of 518°C, while ONG24 gave a very low temperature of 472°C. These temperatures are much lower than the regional estimates but this is thought largely to reflect the inadequacies of the XRD analytical method used to estimate calcite composition. Problems arise when calcite grains contain more than 1-2 mol% Mg because they exsolve dolomite as blebs and lamellae upon cooling from peak metamorphic temperatures (Perkins *et al.* 1982). The secondary dolomite lamellae can result in increased intracrystalline coherency strain which may shift the *d*-value and lead to inaccurate calcite compositions and underestimates of the X_{MgCO3} (Essene, 1983). The quality of XRD analyses can also suffer when calcites show compositional zoning because the method gives a bulk composition for all the calcites in a sample, whether they are in equilibrium or not. The XRD method of estimating calcite $MgCO_3$ content was used in this study as a preliminary test of calcite-dolomite geothermometry on the Onguati marbles, but was not used as the primary analytical tool because of the problems detailed above.

Electron microprobe analyses were carried out on individual calcite grains in ONG12a and ONG24 in a manner similar to Puhan (1976, 1983a). A full description of the microprobe operating conditions and the standards used is given in Appendix C, and is based largely on recommendations by Puhan (1976), Essene (1983) and Wada & Suzuki (1983). From initial backscatter imaging and spot analyses it is apparent that many of the calcite grains are zoned in addition to having significant submicroscopic dolomite exsolution. In a few grains the zoning is regular so that magnesian-rich cores grade to calcian rims (Fig. 5.1). During re-equilibration, the margins of calcites would have experienced the most severe $MgCO_3$ loss. The effectiveness of diffusion processes would rapidly decrease away from the margins, perhaps leaving the cores of larger calcite grains intact. It is also feasible that dolomite exsolution further regulated Ca/Mg diffusion in calcites and that it enhanced such zoning (Essene, 1983). Secondary dolomite mobilised from calcite margins often appears concentrated along grain boundaries or within intergranular areas (Fig. 5.2, grains #3 and #4), but it is also possible that some may have precipitated on nearby primary dolomite grains. However, for many calcites the distribution of $MgCO_3$ is more erratic and difficult to predict. In some calcite grains dolomite exsolution lamellae terminate sharply against magnesian-deficient areas (see Fig. 5.2, grain #3). It is difficult to know the exact cause of this abrupt or irregular zoning but in some grains there appears to have been preferential diffusion along calcite deformation twins (e-twins) which has resulted in the disruption of exsolution lamellae and the formation of bands of low magnesian content (see Fig. 5.3).

Grains with obvious e-twins, irregular zoning or surrounded by grain boundaries with secondary dolomite (i.e. $MgCO_3$ lost from the calcite grain and impossible to reintegrate) were avoided, and only the cores of large calcite grains with significant dolomite exsolution lamellae were selected for electron microprobe analysis (Fig. 5.4). The calcite compositions used to make estimates of peak metamorphic temperature were obtained from multiple spot analyses arranged in a grid over each grain, as shown in Fig. 5.5. Analyses with good stoichiometry and totals (i.e. 98.5 wt% < T < 101.5 wt%) were averaged to reintegrate at least part of the exsolved dolomite back into the original calcite composition. Over 30 calcite grains were

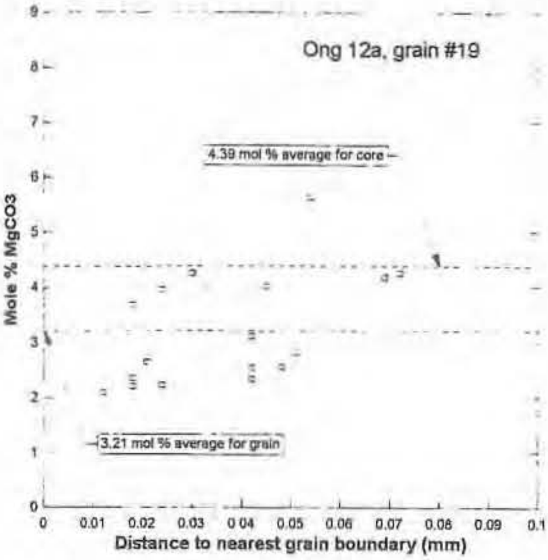

Fig. 5.1: Distribution of the magnesian content of calcite grain ONG12a #19 with increasing distance from the nearest apparent grain boundary. There is almost a 1 mol% difference between the average $MgCO_3$ content of the whole grain and that of the calcite core which was least affected by retrograde resetting.

Fig. 5.2: Backscatter electron microphotographs of grains that have experienced significant out-diffusion of $MgCO_3$ from their crystal lattices. In ONG12a #3 there are patches where the dolomite exsolution lamellae have been completely destroyed. ONG 12a #4 is almost devoid of any exsolved $MgCO_3$. In both images the $MgCO_3$ has migrated to the grain boundaries of the magnesian calcites (white rings around and between grains).

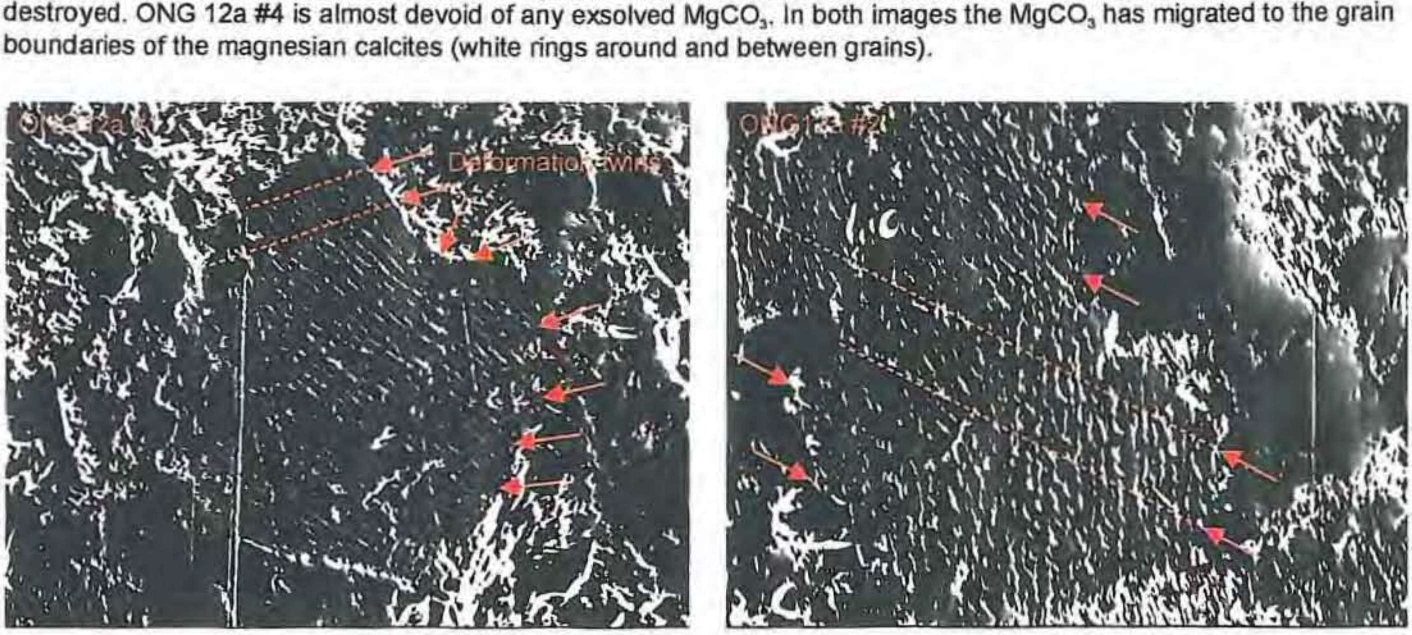

Fig. 5.3: Backscatter electron microphotographs of calcite grains showing well developed deformation twins (e-twins). ONG12a #1twins have disrupted the dolomite exsolution lamellae and have resulted in strips with low $MgCO_3$ content (enhanced diffusion along the e-twin planes). Twinning in ONG12a #2 has not affected the exsolution lamellae as severely.

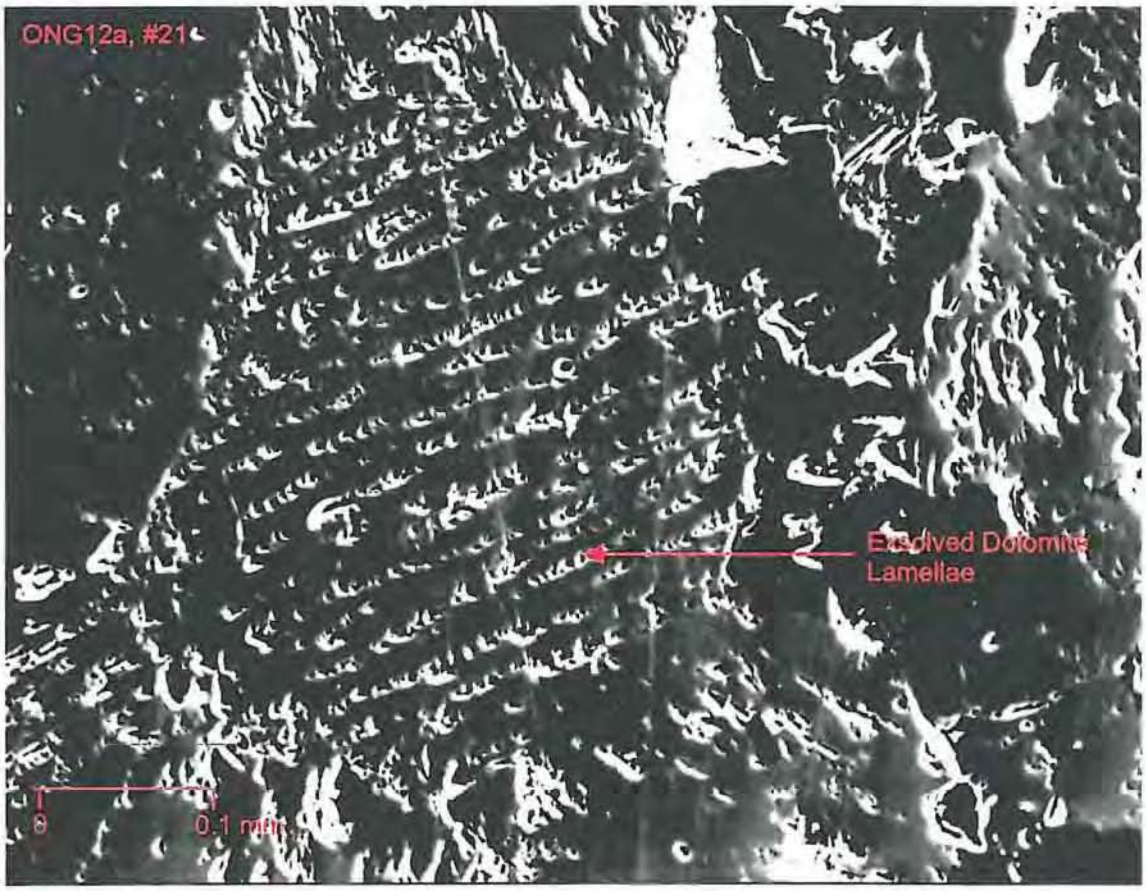

Fig. 5.4: Backscatter electron microphotograph of calcite grain #21 (see table 5.2), sample ONG12a, showing exsolution lamellae of dolomite (white).

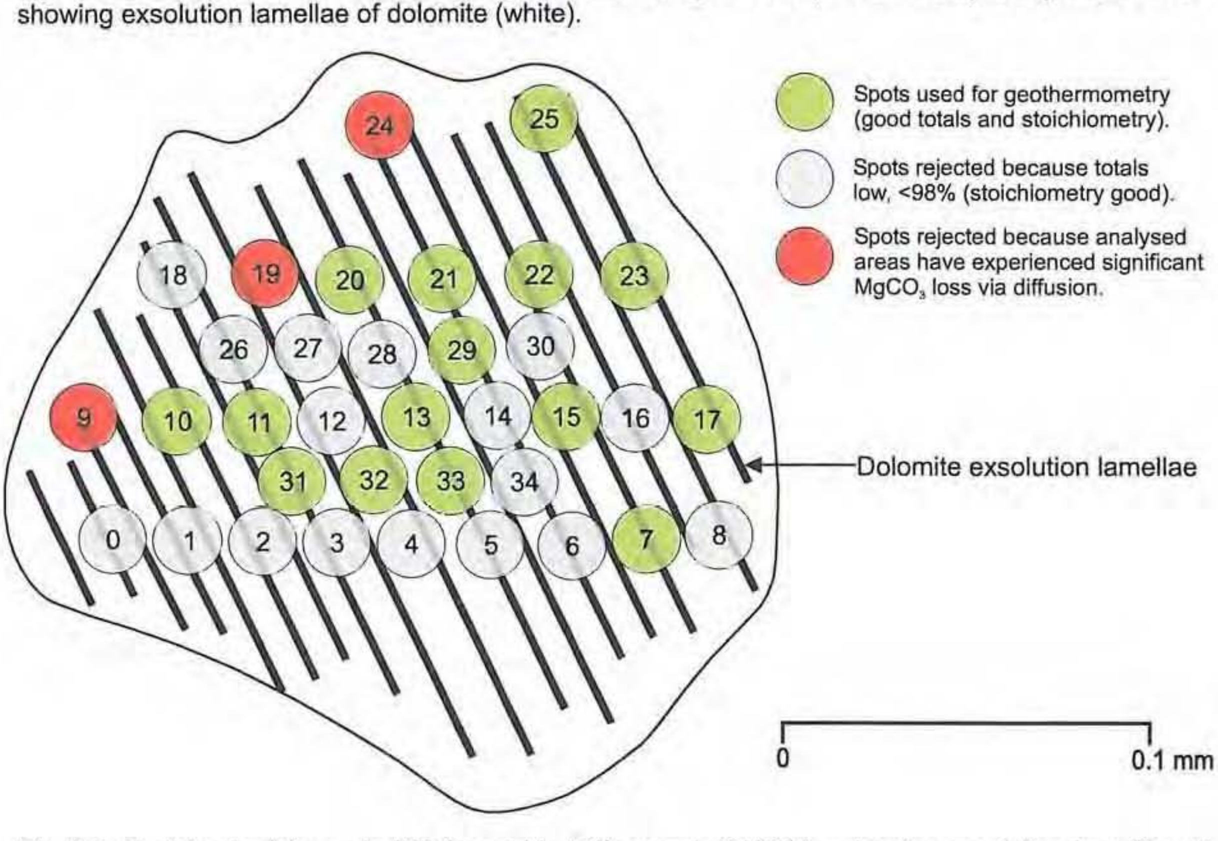

Fig. 5.5: Sketch of calcite grain #20 (see table 5.1), sample ONG12a, showing exsolution lamellae of dolomite (black diagonal lines), spots analysed and analyses used in geothermometry. When the spots with low totals, but good stoichiometry, are included in geothermometry calculations the result is similar to that obtained with just the spots that have good totals and stoichiometry.

analysed in this manner but calcites in both samples showed a wide variation in magnesian contents ranging from 2.26 to 4.86 wt% $MgCO_3$ in ONG12a, and from 3.71 to 3.91 wt% $MgCO_3$ in ONG24a. The average magnesian contents of calcites are illustrated in the histograms of Fig. 5.6. The scatter of compositions to low $MgCO_3$ contents is probably due to varying degrees of re-equilibration in the calcites. The generally lower magnesian contents of ONG24 calcites may reflect more widespread retrograde resetting than in ONG12a, or could indicate that there were insufficient amounts of $MgCO_3$ (70:30 ratio of calcite to dolomite in ONG24) during peak metamorphism to allow true equilibration between calcite and primary dolomite. The iron and manganese contents of the Onguati Mine area carbonates are extremely low and will not affect the calcite-dolomite solvus (e.g. Ong12a, grain #20 had a few spot analyses with <0.21 mol% $FeCO_3$ and <0.20 mol% $MnCO_3$)

Results of analyses for grains ONG12a-#20 and ONG12a-#21 that yield the highest $MgCO_3$ contents are shown in Tables 5.1 and 5.2 respectively. It is necessary to accept the maximum calculated temperatures rather than the average of results when re-integrating exsolved dolomite, because they commonly provide the best constraints on peak metamorphic temperatures (Essene, 1983). Grains #20 and #21 yield temperatures of 556°C and 537°C respectively using equation 5.1. Some of the spot analyses for grain #20 suffered from low totals of between 97 and 98% (but acceptable stoichiometry) and were ignored from temperature calculation as is shown in Fig. 5.2. When these low total results were included in the average they gave a similar inferred temperature of 550°C.

5.3. Discussion

The two highest temperatures inferred from application of calcite-dolomite geothermometry are most likely only minimum estimates of the peak metamorphic temperature. It is generally accepted that the northeastern part of the SCZ underwent lower amphibolite facies conditions and that the grade of metamorphism increases towards Swakopmund, so that partial melting is encountered before the confluence of the Khan and Swakop Rivers (Kasch, 1983a; Miller, 1983c). The metamorphic conditions at the Onguati study area should therefore lie somewhere between the lower and upper amphibolite facies, and not possibly as close to the greenschist - amphibolite facies boundary as determined in this study. Low temperature estimates of peak metamorphism are common for calcite-dolomite geothermometry, and at Onguati could be the result of a prolonged cooling history during Damaran metamorphism. Indications of retrograde resetting between coexisting calcite and dolomite come from the

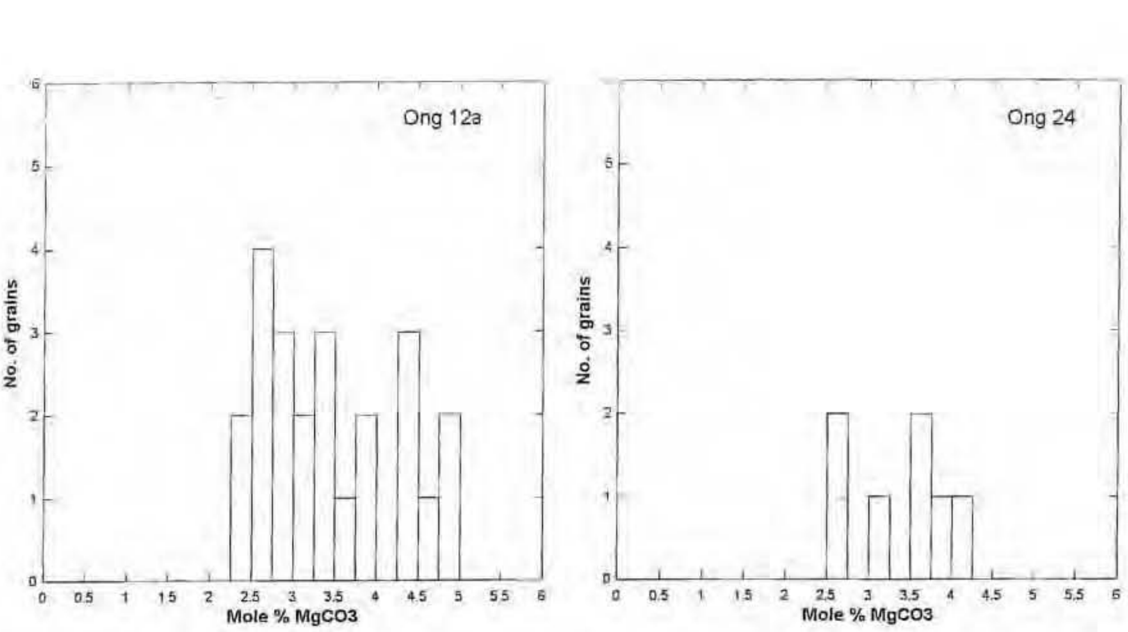

Fig. 5.6: Histograms of the $MgCO_3$ contents of calcites for samples ONG12a and ONG24. All of the values plotted are the re-integrated amounts of $MgCO_3$ in each calcite core analysed. 23 grains were analysed in sample ONG12a, 7 were analysed in sample ONG24. All analyses were carried out on a single probe section for each sample.

Table 5.1: Results of calcite-dolomite solvus geothermometry on sample ONG12a, calcite grain #20 from the Onguati study area, Karibib region. BDL = Below Detection Limit (see Appendix D for electron probe operating conditions, standards and average lower levels of detection).

Sample Name	**20.07**	**20.10**	**20.11**	**20.13**	**20.15**	**20.17**	**20.22**	**20.23**	**20.25**	**20.29**	**20.31**	**20.32**	**20.33**	**Mean**
CaO	52.51	53.00	52.84	52.62	52.28	52.29	52.13	52.68	50.63	52.59	52.90	52.03	52.45	**52.38**
MgO	2.34	1.58	1.96	2.26	2.32	2.39	2.31	2.27	3.69	2.19	2.08	2.36	2.27	**2.31**
SrO	BDL	BDL	BDL	BDL	BDL	BDL	BDL	BDL	BDL	BDL	BDL	BDL	BDL	**BDL**
FeO	0.11	BDL	0.11	BDL	0.10	BDL	0.13	BDL	BDL	BDL	BDL	BDL	BDL	**BDL**
MnO	BDL	0.10	BDL	BDL	BDL	BDL	BDL	BDL	BDL	0.08	BDL	0.13	BDL	**BDL**
CO_2*	43.83	43.37	43.60	43.68	43.56	43.55	43.52	43.77	43.59	43.69	43.71	43.46	43.62	**43.61**
Total	98.79	98.05	98.51	98.56	98.26	98.23	98.09	98.72	97.91	98.55	98.69	97.98	98.34	**98.30**
Number of ions on the basis of 6 O														
Ca	1.88	1.92	1.90	1.89	1.88	1.88	1.88	1.89	1.82	1.89	1.90	1.88	1.89	**1.88**
Mg	0.12	0.08	0.10	0.11	0.12	0.12	0.11	0.11	0.18	0.11	0.10	0.12	0.11	**0.11**
Sr	0.00	0.00	0.00	0.00	0.00	0.00	0.00	0.00	0.00	0.00	0.00	0.00	0.00	**0.00**
Fe	trace	0.00	trace	0.00	trace	0.00	trace	0.00	0.00	0.00	0.00	0.00	0.00	**trace**
Mn	0.00	trace	0.00	0.00	0.00	0.00	0.00	0.00	0.00	trace	0.00	0.00	0.00	**trace**
Total	2.00	2.00	2.00	2.00	2.00	2.00	2.00	2.00	2.00	2.00	2.00	2.00	2.00	**1.99**
X_{CaCO_3}	0.940	0.959	0.949	0.944	0.941	0.940	0.940	0.944	0.908	0.944	0.948	0.939	0.943	**0.941**
X_{MgCO_3}	0.058	0.040	0.049	0.056	0.058	0.060	0.058	0.056	0.092	0.055	0.052	0.059	0.057	**0.058**
X_{SrCO_3}	0.000	0.000	0.000	0.000	0.000	0.000	0.000	0.000	0.000	0.000	0.000	0.000	0.000	**0.000**
X_{FeCO_3}	trace	0.000	trace	0.000	trace	0.000	trace	0.000	0.000	0.000	0.000	0.000	0.000	**trace**
X_{MnCO_3}	0.000	trace	0.000	0.000	0.000	0.000	0.000	0.000	0.000	0.001	0.000	0.000	0.000	**trace**
Average metamorphic temperature gained for ONG12a grain[a]														**556 °C**

** calculated stoichiometrically.*

[a] based on the $MgCO_3$ content of calcite in equilibrium with dolomite, using the equation of Anovitz & Essene (1987, p.406-407).

Table 5.2: Results of calcite-dolomite solvus geothermometry on sample ONG12a, calcite grain #21, from the Onguati study area, Karibib region. BDL = Below Detection Limit (see Appendix D for electron probe operating conditions, standards and average lower levels of detection).

Sample Name	**21.00**	**21.01**	**21.02**	**21.03**	**21.05**	**21.06**	**21.07**	**21.08**	**21.09**	**21.10**	**21.11**	**21.12**	**21.13**	**Mean**
CaO	52.84	53.91	53.88	53.88	53.24	53.29	53.18	53.05	52.57	52.93	52.69	52.90	52.66	**53.16**
MgO	2.33	2.04	1.65	1.34	2.25	2.42	2.20	2.31	2.36	2.32	2.32	2.11	1.96	**2.12**
SrO	BDL	BDL	BDL	BDL	BDL	BDL	BDL	BDL	BDL	BDL	BDL	BDL	BDL	**BDL**
FeO	BDL	BDL	BDL	0.10	BDL	BDL	BDL	BDL	BDL	0.13	BDL	BDL	BDL	**BDL**
MnO	BDL	BDL	BDL	BDL	BDL	BDL	BDL	BDL	BDL	BDL	BDL	BDL	BDL	**BDL**
CO_2*	43.95	44.49	44.01	43.75	44.15	44.38	44.09	44.14	43.74	44.15	43.75	43.75	43.34	**43.98**
Total	99.12	100.44	99.54	99.07	99.64	100.09	99.47	99.50	98.67	99.53	98.76	98.76	97.96	**99.26**
Number of ions on the basis of 6 O														
Ca	1.88	1.90	1.92	1.93	1.89	1.88	1.89	1.89	1.88	1.88	1.88	1.89	1.90	**1.89**
Mg	0.12	0.10	0.08	0.07	0.11	0.12	0.11	0.11	0.12	0.11	0.12	0.11	0.10	**0.11**
Sr	0.00	0.00	0.00	0.00	0.00	0.00	0.00	0.00	0.00	0.00	0.00	0.00	0.00	**0.00**
Fe	0.00	0.00	0.00	trace	0.00	0.00	0.00	0.00	0.00	trace	0.00	0.00	0.00	**trace**
Mn	0.00	0.00	0.00	0.00	0.00	0.00	0.00	0.00	0.00	0.00	0.00	0.00	0.00	**trace**
Total	2.00	2.00	2.00	2.00	2.00	2.00	2.00	2.00	2.00	1.99	2.00	2.00	2.00	**2.00**
X_{CaCO3}	0.942	0.950	0.959	0.965	0.945	0.941	0.946	0.943	0.941	0.941	0.942	0.947	0.951	**0.947**
X_{MgCO3}	0.058	0.050	0.041	0.033	0.055	0.059	0.054	0.057	0.059	0.057	0.058	0.053	0.049	**0.053**
X_{SrCO3}	0.000	0.000	0.000	0.000	0.000	0.000	0.000	0.000	0.000	0.000	0.000	0.000	0.000	**0.000**
X_{FeCO3}	0.000	0.000	0.000	trace	0.000	0.000	0.000	0.000	0.000	trace	0.000	0.000	0.000	**trace**
X_{MnCO3}	0.000	0.000	0.000	0.000	0.000	0.000	0.000	0.000	0.000	0.000	0.000	0.000	0.000	**trace**
Average metamorphic temperature gained for ONG12a grain[a]														**537 °C**

* *calculated stoichiometrically.*

[a] *based on the $MgCO_3$ content of calcite in equilibrium with dolomite, using the equation of Anovitz & Essene (1987, p.406-407).*

heterogeneous distribution of $MgCO_3$ within many of the calcites analysed. The highly variable magnesian contents of calcite cores also suggests that grains have suffered differing degrees of retrograde re-equilibration within the Onguati marbles. These observations highlight the importance of selecting calcite cores which contain the highest amounts of $MgCO_3$, and is strong evidence against combining grain analyses to obtain a sample average for determining temperature. It is also possible that even the most magnesian-rich calcite cores from the Onguati Mine area have not been completely preserved and that their compositions do not reflect calcite-dolomite equilibration close to peak temperatures during the Damaran Orogeny. If it were possible to successfully re-integrate all the secondary dolomite observed, back into the composition of the calcite core it may still record low temperatures.

Comparison of Onguati calcite-dolomite geothermometry to other temperature estimates in the Karibib region is good. Puhan (1983a) used the XRD method of Goldsmith & Heard (1961) to estimate the magnesian contents of calcites taken from marbles 20 km SSW of Karibib Town, and calculated a calcite-dolomite solvus temperature of 555°C. This temperature estimate of peak conditions may be unreliable because the XRD method is susceptible to error when there is dolomite exsolution (as discussed above). With the use of calcite-graphite isotope geothermometry, Valley & O'Neil (1981) obtained a maximum temperature of 598°C from several marbles in the Karibib area, while Steven (1993) calculated a maximum temperature of 626°C (586°C average) for an area in the NCZ, about 80 km NNE of Onguati 52. Almost 85 km to the SW of the Onguati study area, Puhan (1983a, b) estimated temperatures of 580°C and 615°C by calcite-dolomite geothermometry for marbles on Marmor 111 and Bloemhof 109 respectively. When the average magnesian values of the calcites analysed by Puhan (1983a) were used in equation 5.1 to recalculate metamorphic temperatures the results were significantly different. Sample C126 from Marmor 111 gave an inferred temperature of 620°C (40°C higher), while the Bloemhof sample, C135 yielded an estimate of 657°C (42°C higher). Although these results may give a more reasonable estimate of peak metamorphic temperature because they rely on a more comprehensive calcite-dolomite solvus dataset and are close to conditions of the upper amphibolite facies, it is still possible that they are underestimates of temperature. In this higher grade region of the SCZ there are already indications of migmatite development (R. Jacob, 1974).

Basic metamorphic data for the CZ were plotted on a petrogenetic grid (Fig. 5.7) to aid comparison with the Onguati temperature results, as well as to obtain possible pressure constraints at peak temperatures. This study has made use of the pelitic reaction isograds

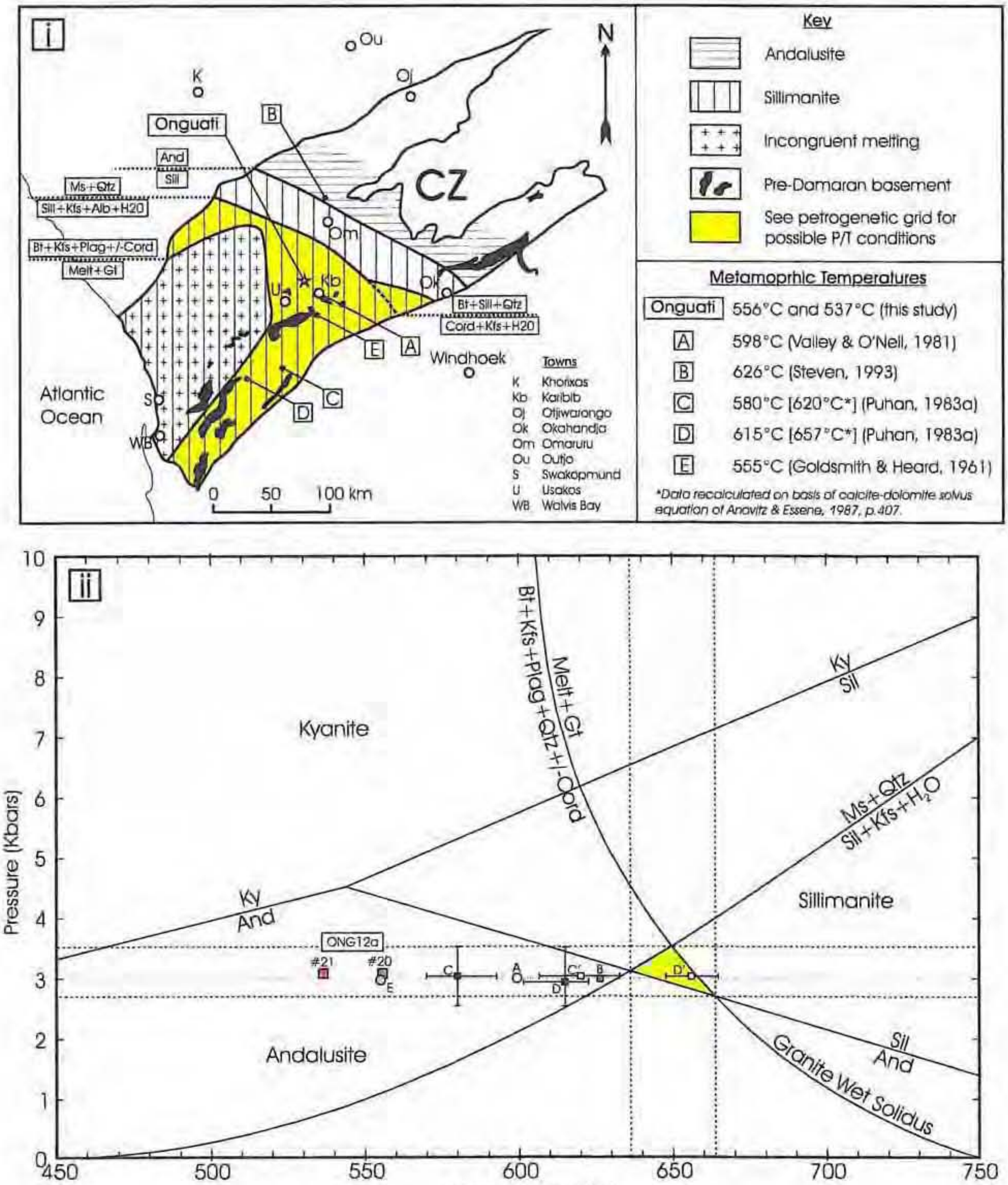

Fig. 5.7: Petrogenetic grid for metapelitic rocks of the SCZ. Reaction curves and Al_2SiO_5 triple point based on Fig. 28-2 of Winter (2001) for the KFMASH system at $p_{H2O} = P_{total}$. The yellow triangular area may bracket the prograde metamorphic conditions experienced in the Onguati area during orogeny, and is based on the Damaran isoreationgrads and phase boundaries mapped and compiled by Miller (1983c, Fig.26, p.470), as shown in the upper inset [i]. Results of calcite-dolomite geothermometry in the Onguati study area (this study) are shown in petrogenetic grid [ii] for calcite #20 and #21, sample ONG12a, and yield temperatures of 556EC and 537°C respectively.

A = 598°C, calcite-graphite isotope geothermometry (Karibib area), Valley & O'Neil (1981);
B = 626°C, maximum calcite-graphite isotope temperature (Omaruru area), Steven (1993);
C = 580°C, calcite-dolomite geothermometry (sample C126, Farm Marmor 111), Puhan (1983a);
D = 615°C, calcite-dolomite geothermometry (sample C135, Farm Bloemhof 109), Puhan (1983a);
C' = 620°C, C126 data of Puhan (1983a) recalculated using solvus equation of Anovitz & Essene (1987);
D' = 657°C, C135 data of Puhan (1983a) recalculated using solvus equation of Anovitz & Essene (1987);
E = 555°C, calcite-dolomite geothermometry [XRD method], (marbles 20km SSW of Karibib), Puhan (1983a).
**Pressure estimates included on C and D are from Puhan (1983a) and are based on stability of five-mineral assemblage forsterite+diopside+tremolite+dolomite+calcite for area west of Usakos.*

mapped and compiled by Miller (1983c, Fig. 26, p.470) for the Damara Belt. A simplified map version showing the CZ isoreactiongrads is presented in Fig. 5.7[i]. Several significant metamorphic isograds and an Al_2SiO_5 phase boundary occur within the CZ. To the northeast and outermost from the Onguati study area it is possible to trace the andalusite-sillimanite phase boundary, which is succeeded to the southeast by the metamorphic isograd along which the reaction: muscovite + quartz $\rightleftharpoons$ sillimanite + K-feldspar + albite +H_2O is thought to have occurred. The Onguati field area lies approximately half way between this second or upper sillimanite reaction isograd and a metamorphic isograd to the southeast, along which partial melting occurs by the suggested reaction: biotite + K-feldspar + plagioclase + quartz ± cordierite $\rightleftharpoons$ melt + garnet.

From the position and intersection of reaction isograds with the Al_2SiO_5 phase boundaries (Fig. 5.7[ii]) it is apparent that the Onguati study area may have experienced a relatively small window of P-T conditions. The minimum pressure estimate for this triangular region is set at ~2.7 kbars, but in order for the P-T-t path to first cross the andalusite-sillimanite phase boundary and then the muscovite + quartz break down curve, pressures must have been in excess of 3 kbars during peak metamorphism. The upper limit of pressure at peak metamorphic temperature is fixed by the intersection of the K-feldspar + sillimanite (or second sillimanite) reaction isograd and the granite wet solidus at ~3.5 kbars, along which biotite + K-feldspar + plagioclase + quartz breakdown to form a melt. These pressure estimates are in good agreement with the pressure range determined by Puhan (1983a), which is based on the stability of the five-mineral assemblage forsterite + diopside + tremolite + dolomite + calcite.

Comparison of temperatures determined in the Onguati Mine area with those proposed by the petrogenetic grid show that the calcite-dolomite geothermometry may have underestimated peak metamorphic conditions by as much as 100°C. Peak metamorphic temperatures may have exceeded 636°C, and may have approached temperatures as high as 650°C to 660°C. Although the choice of fluid pressure (i.e. in this study $\rho_{H2O} = P_{total}$ is assumed) will affect the position of the reaction curves and hence the P-T window, it is reasonable to conclude that peak temperatures must have been below ~650°C because there is no evidence of migmatization in the area. Temperatures in the Onguati area were probably closer to the lower end of the bracketed metamorphic conditions, in the region of 630°C to 640°C, at a pressure of approximately 3 kbars.

6. STRUCTURE AT THE DEPOSIT SCALE

6.1. Introduction

In the early 1990's there was a growing awareness of the importance of structure to hydrothermal mineralization in the Karibib region, and a shift away from the 'Anglo American' stratabound skarn-type models which relied on a geochemical approach to exploration (Steven, 2000). Pirajno & Jacob (1991, p.307) recognized that orogenic gold mineralization in the CZ was intimately related to structure, and partially classified Damaran gold deposits into "shear-zone hosted" or "thrust-zone associated" types. During exploration in the Kranzberg and Onguati areas, Genmin utilized aeromagnetic data to identify potentially pyrrhotite-rich areas in the vicinity of NW-trending lineaments (Webb, 1992). Badenhorst (1993), Steven *et al.* (1994) and Steven (2000) have all highlighted the need for a more detailed understanding of the structural geology at both the regional- and prospect-scale to facilitate more effective gold exploration in the SCZ.

Despite these recommendations, limited structural work has been carried out in the Onguati study area. Gray (1988) mapped the Onguati Mine and Brown Mountain areas and showed the position and general trends of veins, but few strike or dip measurements are indicated. Genmin produced a 1:16,500 scale geological map of the Onguati 52 and 53 areas, and a 1:2,500 scale composite map centred over the Onguati Mine-Brown Mountain-Western Workings region, but these provide little vein orientation data and only indicate bedding and deposit-scale folds and faults (Webb, 1992). More recently, AngloGold commissioned a short study to assess the structural controls on epigenetic gold mineralization in the Karibib district (Dirks & Mikhailov, 2000). Although Dirks & Mikhailov (2000) provide an excellent overview of structure and establish potential structural relationships to mineralization at the Onguati prospects, their structural data base is still relatively small. Structural mapping at the deposit-scale was beyond the scope of their work.

One of the main aims of this project was to therefore produce detailed structural maps of the areas that host significant vein mineralization. 1:500 scale maps of Onguati Mine (Map 1), Brown Mountain (Map 2) and Western Workings (Maps 3A and 3B) are included in the map pouches at the back of this thesis. Observations and measurements were collected from a wide range of structures, including folds, faults, veins and joints, with the aim of creating a robust data set that could be used to constrain the structural evolution of this region.

Emphasis was placed on recording vein orientation data, vein morphology and vein cross-cutting relationships in both the calcitic and dolomitic marbles of the Onguati study area. The resulting structural data set created for these veins may help address a major information gap in the area and may be of benefit to future exploration or drilling programmes. In the final part of this chapter an effort has been made to integrate earlier observations made from regional geophysical imagery and aerial photographs with structural observations made at the deposit- and outcrop-scale in the Onguati study area. The examination of a diverse spectrum of structures at a variety of scales presents independent means of estimating the state of strain and the direction of greatest principal subregional or local stress at the time of formation of each of the structures. This helps ensure "structural compatibility" (Davis & Reynolds, 1996, p.95).

6.2. Foliations, Folds and Associated Lineations

Many of the rocks found in the Onguati study area possess a compositional foliation that is marked by layers or laminations of different mineralogical composition. The calcitic marble package possesses an especially strong compositional foliation marked by light and dark (more graphitic) calcitic marble layers and calc-silicate laminae (Plate 4.4). The upper TM unit can contain thin, delicate interlayers of calcitic and dolomitic marble (Plate 4.10). The mafic meta-tuffs and quartzitic meta-tuffites also possess a distinct layering, and layers or bands of layers can be saturated or completely devoid of lapilli (Plates 4.24 and 4.25). Where the compositional layering is marked by continuous layers or laminae of different mineralogical composition, they represent an original lithological layering (S_0).

However, caution should be exercised in calling the compositional foliation in the calcitic marble package "bedding" because there is extensive evidence of transposition. Generally speaking only in very small areas, often only at the scale of the outcrop, where the calcitic layers are sharply defined and appear laterally continuous, can the layering be referred to as bedding (S_0). Thin, continuous calc-silicate interlayers in calcitic marble (e.g. Plates 4.4 and 4.5) or thick, well-developed units of calc-silicate rock (e.g. Plate 4.2) are also good evidence of an original S_0 lithological layering. It is generally more appropriate to refer to the marble compositional layering as a composite foliation ($S_{0,1}$) formed by superposition of a bedding-plane transposition on an earlier bedding (Plate 6.1).

Within the calcitic marbles there are numerous examples of small-scale, tight-to-isoclinal, intrafolial F_1 folds. Intense transposition is normally limited to metre-wide series of

Plate 6.1: In the lower, lefthand corner of the image, light and dark calcitic marble layers and calc-silicate laminations define a clear, largely undisturbed compositional layering. In the middle of the image, the marble layering has been heavily disrupted by transposition so that lenses of 'feathery', white calcitic marble are dispersed in a graphite-rich, calcitic marble. The compositional foliation is thus a composite ($S_{0,1}$) of an original sedimentary bedding (S_0) and a bedding-parallel, transposition foliation (S_1).

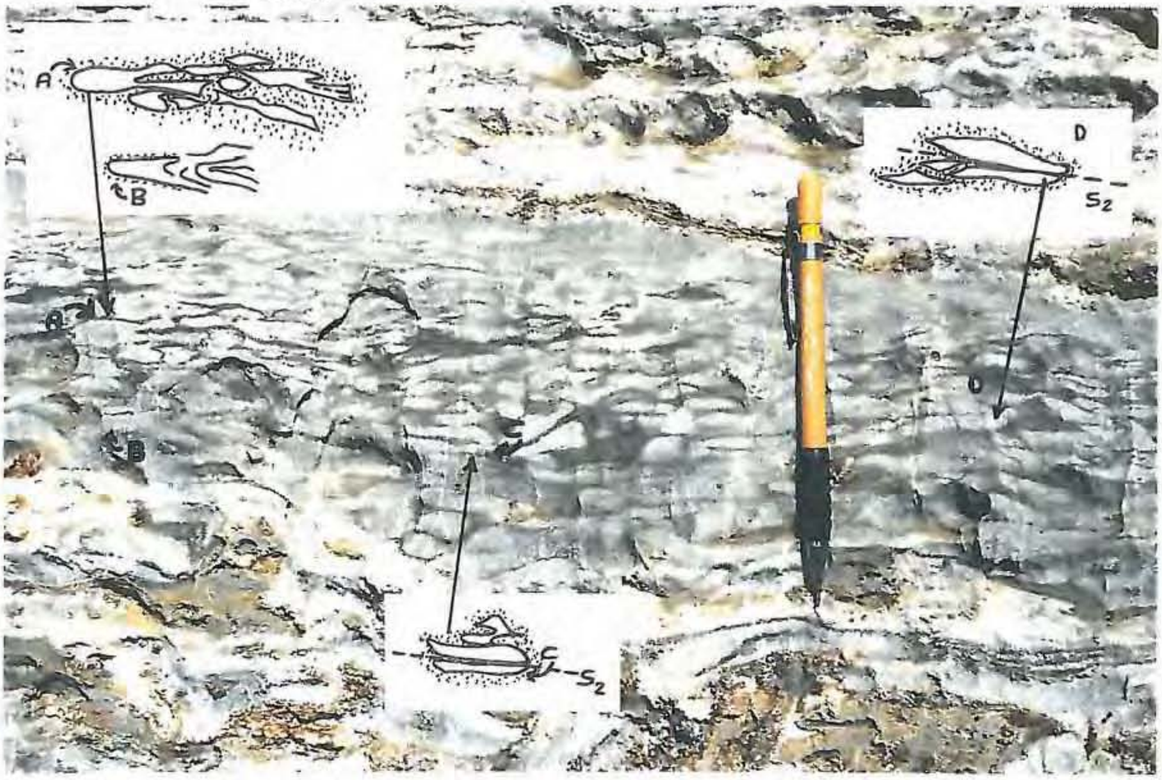

Plate 6.2: This marble breccia does not have a sedimentary origin like many other breccias in the Karibib Formation. Instead, light grey calcitic marble layers were tightly folded, and then transposed to lie sub-parallel or parallel to the compositional foliation. The layers were broken-up in a more ductile, graphite-rich marble (matrix) and the fragments rotated and deformed. In places it is possible to recognize intrafolial hinges, often cut by an axial planar cleavage (S_2).

units so that more-or-less undisturbed S_0 layering can be found adjacent to transposed zones (e.g. Plate 6.1). The development of asymmetric tight-to-isoclinal, drag folds and strain localization into receptive calcitic marble layers caused the compositional layering to become dismembered (Plate 6.2) with "slip parallel to the axial planes of the developing flexures" (Davis & Reynolds, 1996, p.455). When the intrafolial lenses are calc-silicate remnants, they often resist flattening and it may be possible to recognise relatively undeformed fold hinges and reconstruct fold form (e.g. Fig. 6.11a). In the less competent calcitic marble layers, both intrafolial hinges and limbs are streaked-out so that 'feathery' lenses of closely packed, light and dark calcitic marble are commonly seen (Plate 6.1). While many marble breccias in the Karibib Formation have a proven sedimentary origin (e.g. Badenhorst, 1992), some apparent 'marble breccias' may have formed from the fragments of intrafolial limbs and hinges (e.g. Plate 6.2). These tectonic breccias often contain plastically deformed fragments (very angular limb fragments can also be found as in Fig. 4.9) and an axial planar cleavage (S_2), parallel to the $S_{0,1}$ foliation, may be recognized in preserved intrafolial hinges and lenses.

The $S_{0,1}$ composite foliation is refolded in the Onguati study area by F_2 folds. F_1 and F_2 structures share similar fold hinge and axial plane orientations (i.e. similar attitude) and appear to have formed during progressive deformation in the highly ductile calcitic marbles. The F_2 folds vary in wavelength from a few centimetres (e.g. corrugation folds) to deposit-scale size. A wide range of F_2 fold forms are possible in the calcitic marbles and include open-to-isoclinal folds with broad-to-tall aspect ratios and subrounded-to-angular fold closures (see Table 6.1 for summary of fold characteristics). F_2 folds generally display more gently inclined axial planes the smaller the interlimb angle. NW-directed overthrusting resulted in tightening of the fold limbs and overturning of F_1 and F_2 folds so that they developed SE-dipping axial planes. In some of the larger F_2 tight folds a convergent fanning cleavage (S_3) can be defined by concentrations of graphite (Fig. 6.8, a). Within the individual limbs of these folds, it is common to find the S_3 cleavage modified into sigmoidal shapes (Fig. 6.8, b and c). A flexural flow mechanism of folding in the ductile calcitic marble layers could have resulted in shearing in the limbs and consequent deformation of the S_3 cleavage.

In Figs. 6.1a to 6.3a it can be seen that the axial planes of isoclinal F_1 and F_2 folds parallel the $S_{0,1}$ foliation. Minor fold axes (MFA), mullions and corrugation fold axes in the folded calc-silicate rocks and calcitic marbles define an L_1 lineation (see Figs. 6.1b to 6.3b). The average L_1 orientation at Onguati Mine is 231°-21° (trend-plunge) and is similar to that at Western Workings (239°-20°). L_1 at Brown Mountain can be oriented either at 235°-22° or 062°-18° (trend-plunge) and suggests that Brown Mountain is situated in the core of an

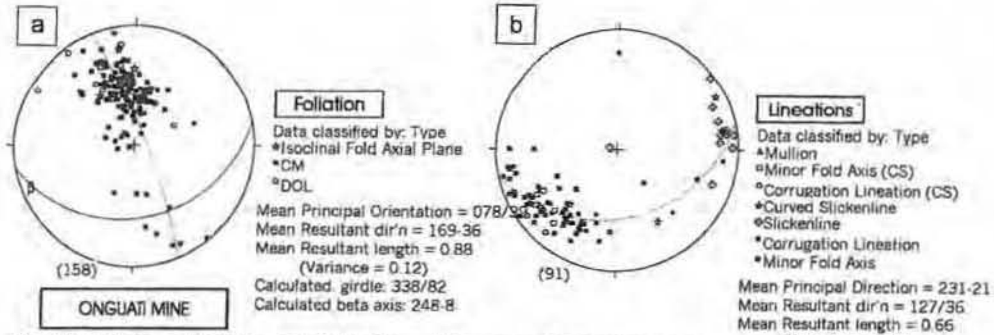

Fig. 6.1: Foliation and lineation data for the Onguati Mine area. (a) Equal area plot of poles to S_{a1} and isoclinal fold axial planes. (b) Classified lineation data - mainly minor fold axes and corrugation fold lineations. CM = calcitic marble; DOL = dolomitic marble; CS = calc-silicate rocks. (lower hemisphere, equal area projections).

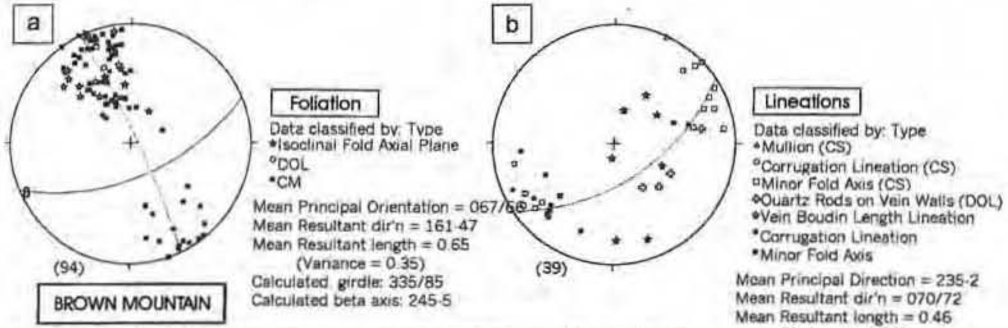

Fig. 6.2: Foliation and lineation data for the Brown Mountain area. (a) Equal area plot of poles to S_{a1} and isoclinal fold axial planes. (b) Classified lineation data - mainly minor fold axes and corrugation fold lineations. CM = calcitic marble; DOL = dolomitic marble; CS = calc-silicate rocks. (lower hemisphere, equal area projections).

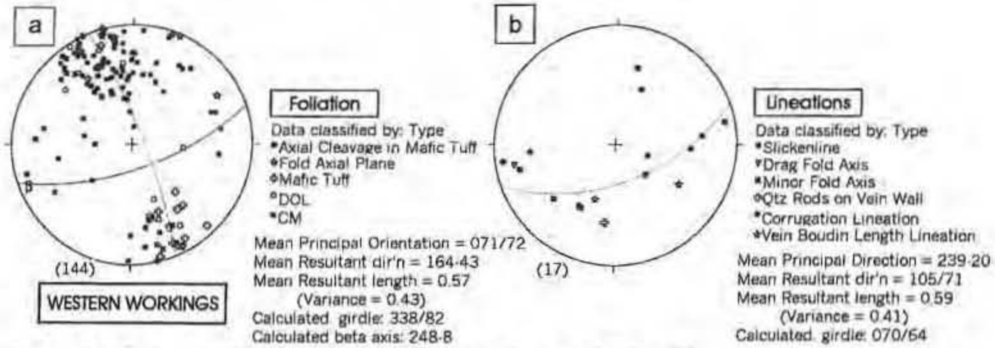

Fig. 6.3: Foliation and lineation data for the Western Workings area. (a) Equal area plot of poles to S_{a1} and isoclinal fold axial planes. (b) Classified lineation data - mainly minor fold axes and corrugation fold lineations. CM = calcitic marble; DOL = dolomitic marble; CS = calc-silicate rocks. (lower hemisphere, equal area projections).

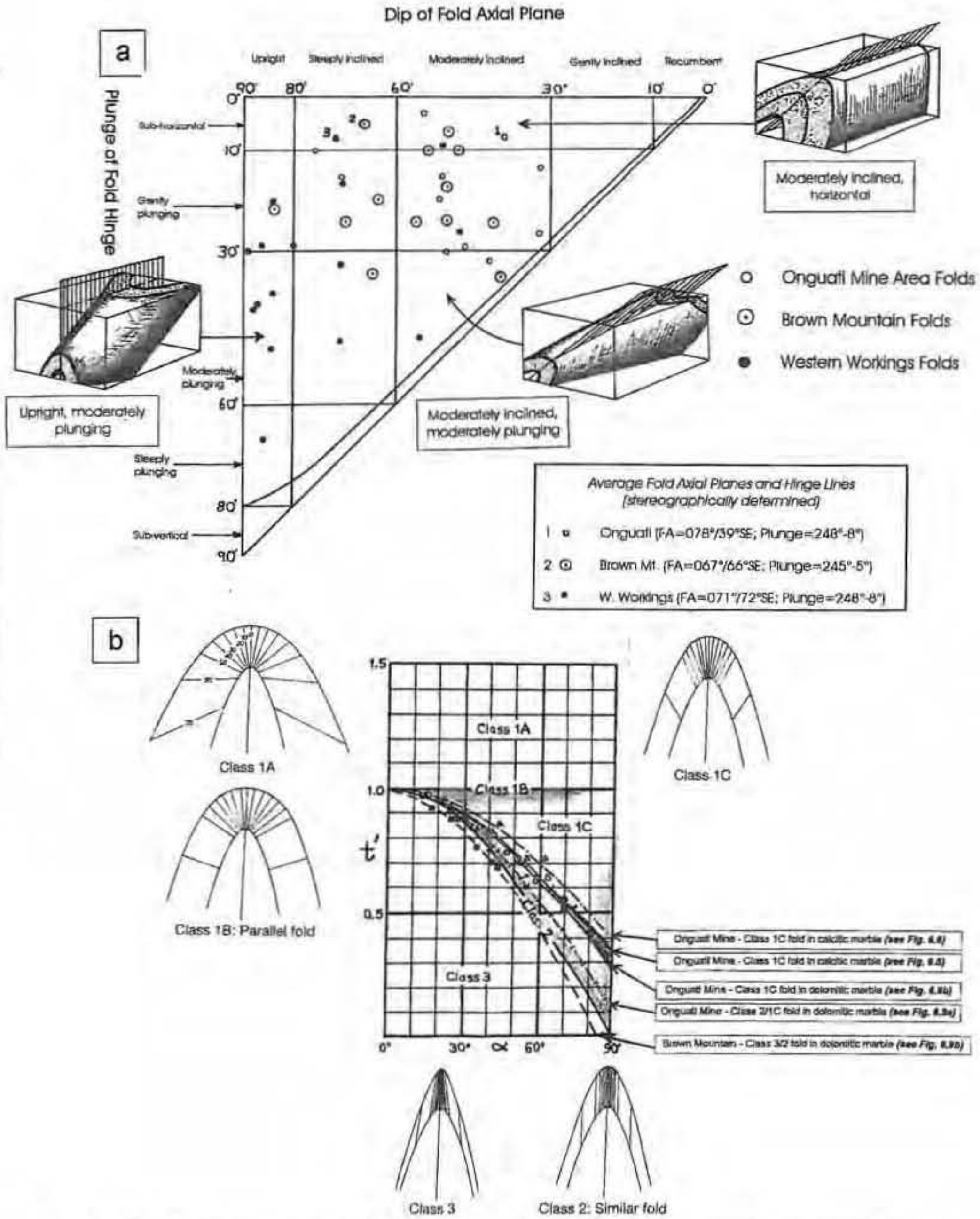

Fig. 6.4: Classification of folds found at the Onguati Mine, Brown Mountain and Western Workings localities based on fold attitude and on folded layer shape. (a) The dip of the axial plane and plunge of the hinge line of folds in the Onguati study area were plotted on the Fleuty diagram. Note that the bulk of the folds are moderately inclined and gently plunging, but that differences exist between folds of the three areas. (b) Thickness variation of folded layers with increasing α (from hinge to limb) for folds in the Onguati study area shows that most are class 1C to class 2 (similar) folds according to Ramsay's classification.

elongate, deposit-scale periclinal or domal fold structure. There are numerous metre-scale examples of periclinal or domal folds in the calcitic marbles of the Onguati Mine area.

Table 6.1: Summary of dominant fold characteristics in the calcitic and dolomitic marbles of the Onguati Mine, Brown Mountain and Western Workings localities. CM = calcitic marble; DM = dolomitic marble.

		Interlimb angle (α)	Aspect ratio (P)	Closure shape (b)	Ramsay's classification	Notes
Onguati Mine	CM	Close-to-isoclinal	Short to equant	Subrounded to subangular	Class 1C	Periclinal and elliptical folds common
	DM	Close	Broad to equant	Subrounded	Class 1C/2	Folds only found at base of DM unit
Brown Mountain	CM	Open-to-tight; small isoclinal	Broad to equant	Subrounded	Class 2/3	Small intrafolial folds common
Western Workings	CM	Tight-to-isoclinal	Short to tall	Subrounded to angular	Class 1C	Elliptical folds common

It should be noted that there are significant differences in fold attitude and orientation between the three mineralized areas in the Onguati study area. In Fig. 6.4a it can be seen that F_2 folds in the Onguati Mine area tend to have gently-to-subhorizontally plunging fold hinges with moderately inclined axial planes. Brown Mountain F_2 fold hinges have similar plunges to Onguati Mine but have moderate-to-steeply inclined axial planes. F_2 folds at Western Workings possesses upright-to-steeply inclined fold axial planes and fold hinges with gentle-to-moderate plunges. Figs. 6.5 to 6.13 illustrate the variety of fold forms possible in the calcitic and dolomitic marbles at the three sites in the Onguati study area.

When F_2 folds are classified according to their layer shape (see Fig. 6.4b and various fold diagrams), the vast majority of folds can be seen to be Class 1C. In the lowermost dolomitic marbles of Onguati Mine it is possible to find 'similar' or Class 2 folds (Fig. 6.9a), and in the Brown Mountain calcitic marbles, folds may be borderline Class 3 types (Fig. 6.10). The method of Lisle (1992) was used to calculate the post-buckle flattening strain of folds, assuming that the folds had 'parallel' Class 1B shapes before flattening. Strain ellipses were visually fitted to graphs in polar coordinates where each of the points represents $1/t_\alpha$ plotted as a function of the layer tangent orientation. The orientation of the strain ellipses created in this manner confirm field observations that the direction of greatest principal subregional

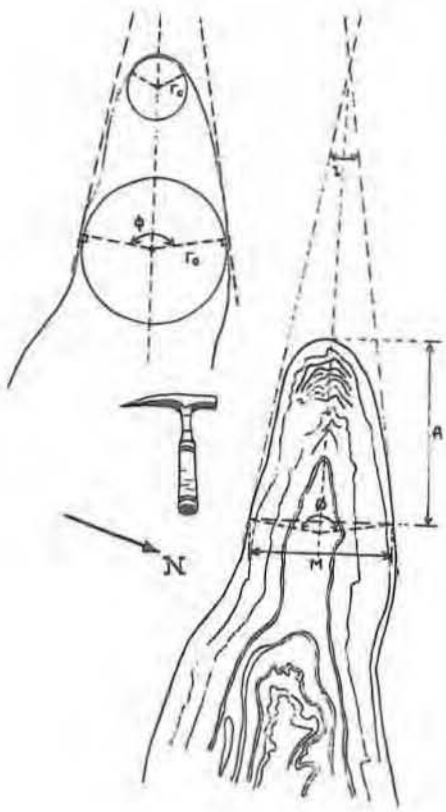

Summary of Fold Characteristics		
i	16°	Tight fold (30 ≥ i > 0)
φ	165°	
A	55 units	
M	28 units	
P	1.96	Short aspect ratio (1.58 ≤ P < 4)
r_c	12 units	
r_o	28 units	
b	0.67	Subrounded (0.4 ≤ b < 0.8)
Ramsay's Classification	Type: Class 1C	

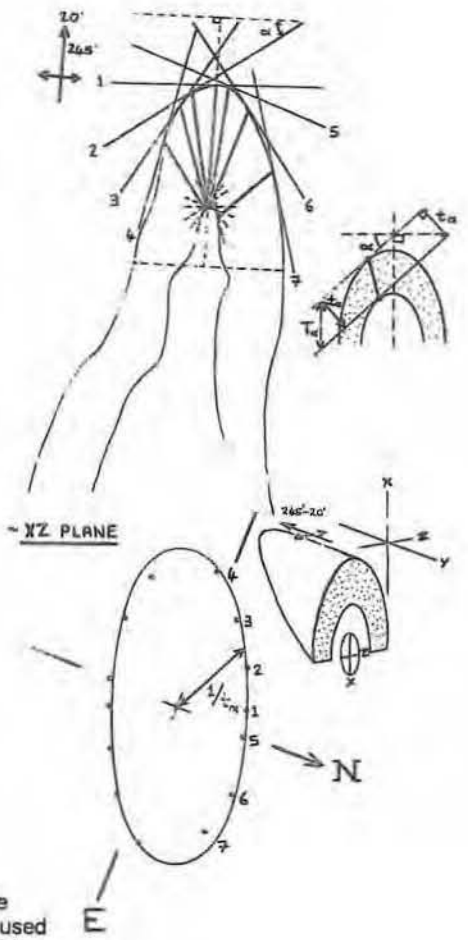

Fig. 6.5: A tight fold exposed on the calcitic marble pavement to the east of Onguati Mine. The diagrams and table summarize the main fold characteristics. The method of Lisle (1992) was used to delineate the strain ellipse above (~XZ plane) and estimate strain in this flattened buckle fold. The fold hinge may be approximately parallel to the Y-axis as shown above.

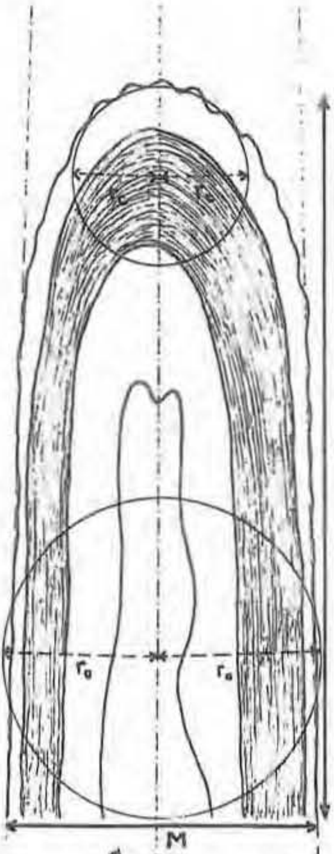

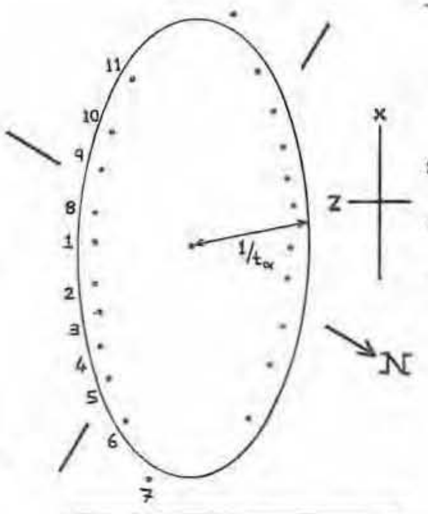

Summary of Fold Characteristics		
i	0°	Isoclinal fold (i = 0 , φ = 180°)
φ	180°	
A	140 units	
M	60 units	
P	2,3	Short aspect ratio (1.58 ≤ P < 4)
r_c	33 units	
r_o	60 units	
b	0,55	Subrounded (0.4 < b < 0.8)
Ramsay's Classification	Type: Class 1C	

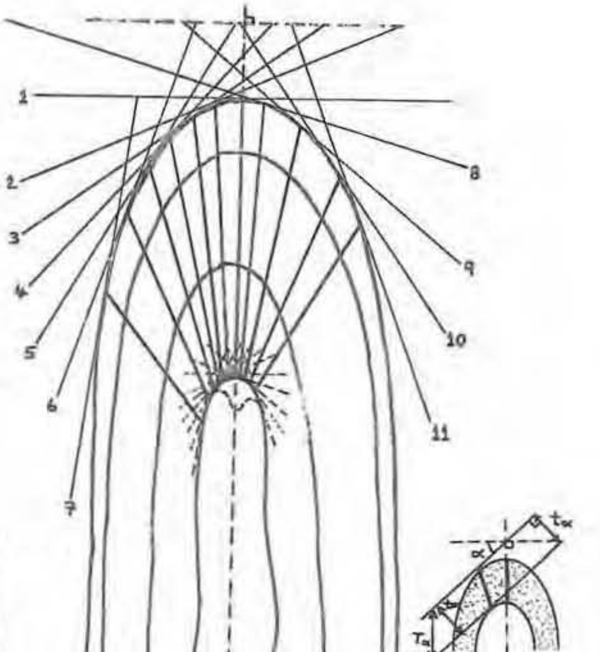

Fig. 6.6: A thick, calc-silicate unit in the calcitic marbles of the Onguati Mine area was folded isoclinally and flattened to have a Class 1C layer shape. The method of Lisle (1992) was used to estimate strain in this flattened buckle fold as shown above.

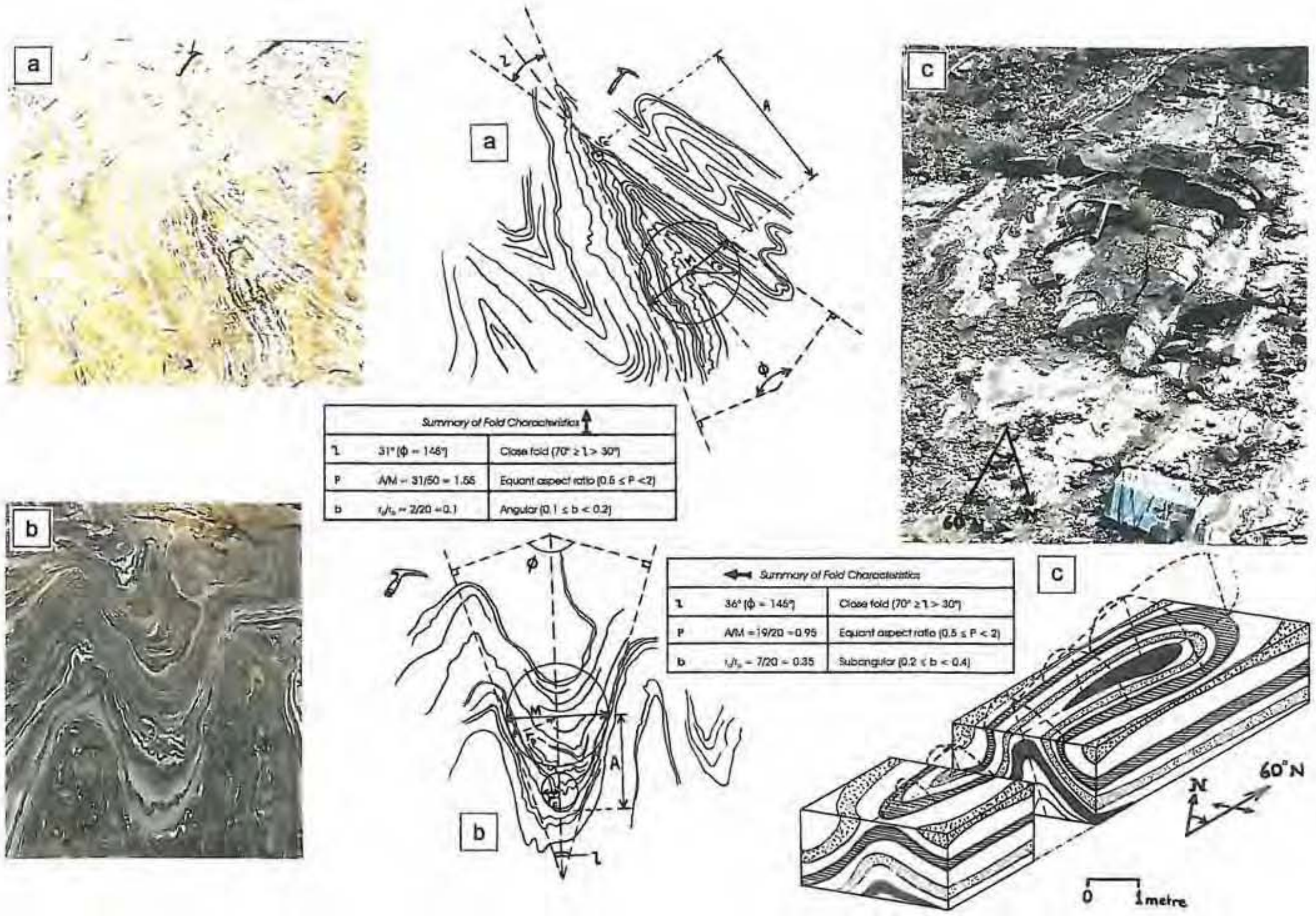

Summary of Fold Characteristics		
ι	31° (ϕ = 148°)	Close fold (70° ≥ ι > 30°)
P	A/M = 31/50 = 1.55	Equant aspect ratio (0.5 ≤ P <2)
b	r_0/r_s = 2/20 = 0.1	Angular (0.1 ≤ b < 0.2)

Summary of Fold Characteristics		
ι	36° (ϕ = 145°)	Close fold (70° ≥ ι > 30°)
P	A/M = 19/20 = 0.95	Equant aspect ratio (0.5 ≤ P < 2)
b	r_0/r_s = 7/20 = 0.35	Subangular (0.2 ≤ b < 0.4)

Fig. 6.7: Various folds found in the calcitic marbles of the Onguati Mine area. (a) Tight-to-close, angular folds are well exposed on the marble pavement to the east of Onguati Mine; (b) close, subangular folds are common in the marbles of the Onguati Mine area, and many have curved hinged lines and axial planes because the marbles have had to plastically deform and flow as space problems have arisen during folding; (c) an elongate, periclinal or domal fold in the calcitic marbles to the west of Onguati Mine.

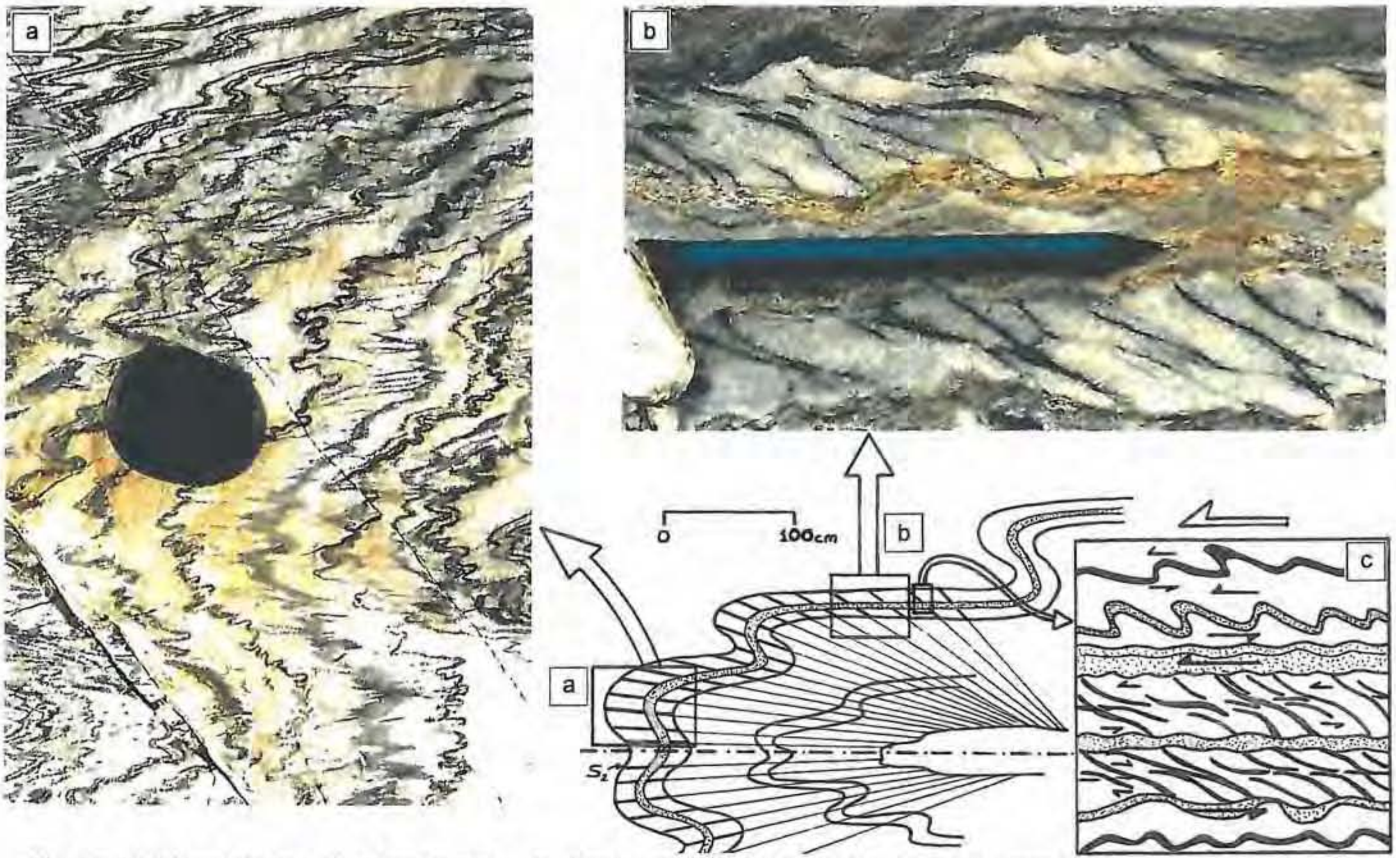

Fig. 6.8: Sketch and photographs of a convergent, fanning cleavage (S_3) that is preserved in some close-to-tight folds in the calcitic marbles of the Onguati Mine area. Graphite along the cleavage surfaces may have been concentrated as a residual by pressure solution, or may have been mobilized from nearby graphite-rich marble layers. In the hinge zone of the fold (a) the cleavage is axial planar. The cleavage is only developed in calcitic marble layers, and in the limbs (b and c) appears to have been modified into sigmoidal trajectories by flexural flow folding - strain would have been highest in the middle of each layer.

Plate 6.3: A periclinal fold developed in the calcitic marbles of the Onguati Mine area. A small, elongate periclinal fold is found just to the left of the larger fold structure. The calc-silicate unit of the bigger periclinal fold links with an isoclinal fold in the background. The limb of this isoclinal fold can be seen to return in the top, left hand part of the image, 'duplicating' the stratigraphy.

Plate 6.4: An isoclinal 'hairpin' fold highlighted by a thick calc-silicate unit in the Onguati Mine area. Note the highly boudinaged limbs and barrel-shaped boudins (lower, left-hand limb). Calcitic marble has flowed and 'folded' into the boudin necks. Marbles on the right-hand side of the fold display the diffuse and lenticular, transposition foliation clearly.

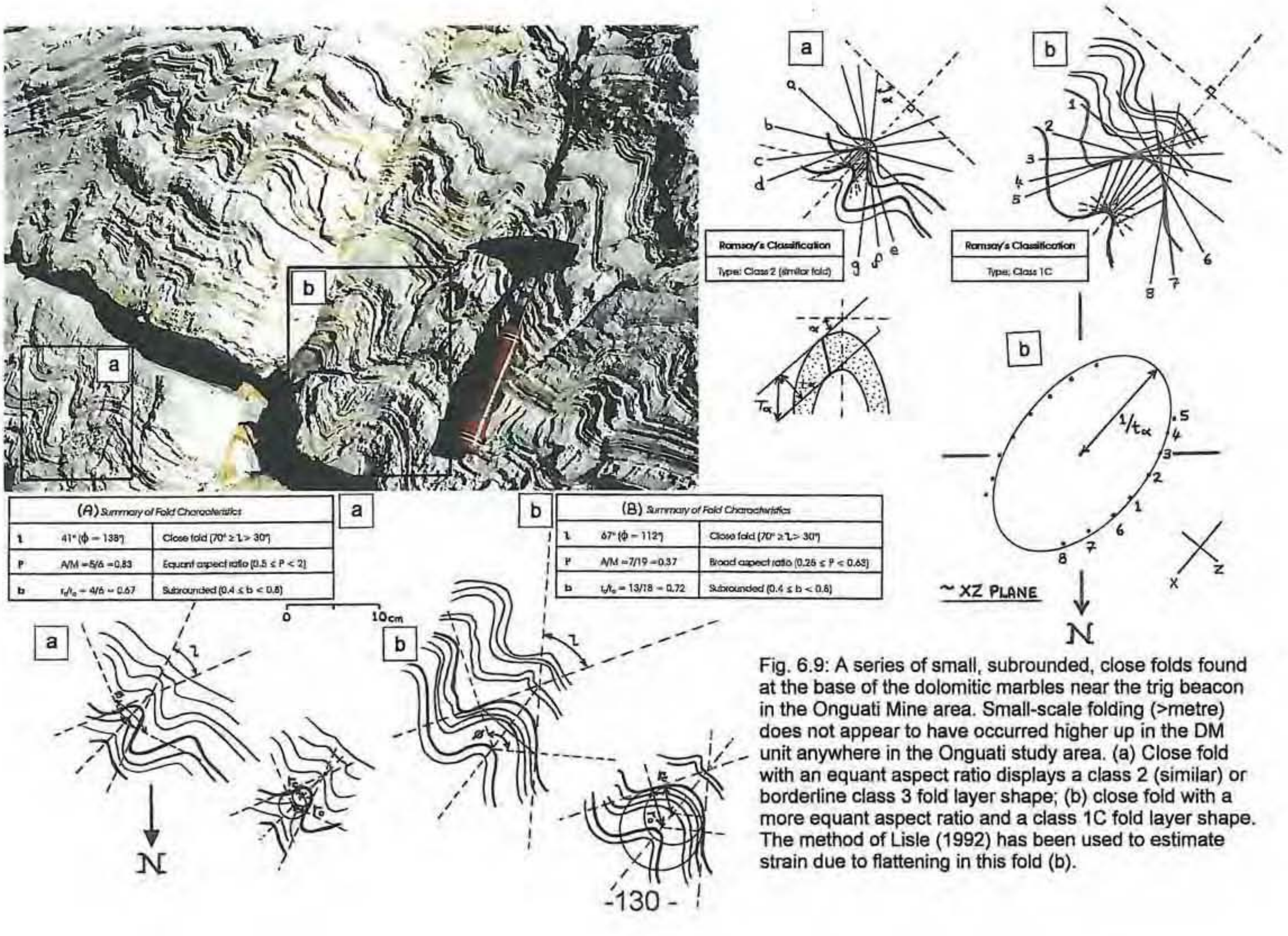

(A) Summary of Fold Characteristics		
i	41° (φ = 138°)	Close fold (70° ≥ i > 30°)
P	A/M = 5/6 = 0.83	Equant aspect ratio (0.5 ≤ P < 2)
b	r_c/r_o = 4/6 = 0.67	Subrounded (0.4 ≤ b < 0.8)

(B) Summary of Fold Characteristics		
i	67° (φ = 112°)	Close fold (70° ≥ i > 30°)
P	A/M = 7/19 = 0.37	Broad aspect ratio (0.25 ≤ P < 0.63)
b	r_c/r_o = 13/18 = 0.72	Subrounded (0.4 ≤ b < 0.8)

Fig. 6.9: A series of small, subrounded, close folds found at the base of the dolomitic marbles near the trig beacon in the Onguati Mine area. Small-scale folding (>metre) does not appear to have occurred higher up in the DM unit anywhere in the Onguati study area. (a) Close fold with an equant aspect ratio displays a class 2 (similar) or borderline class 3 fold layer shape; (b) close fold with a more equant aspect ratio and a class 1C fold layer shape. The method of Lisle (1992) has been used to estimate strain due to flattening in this fold (b).

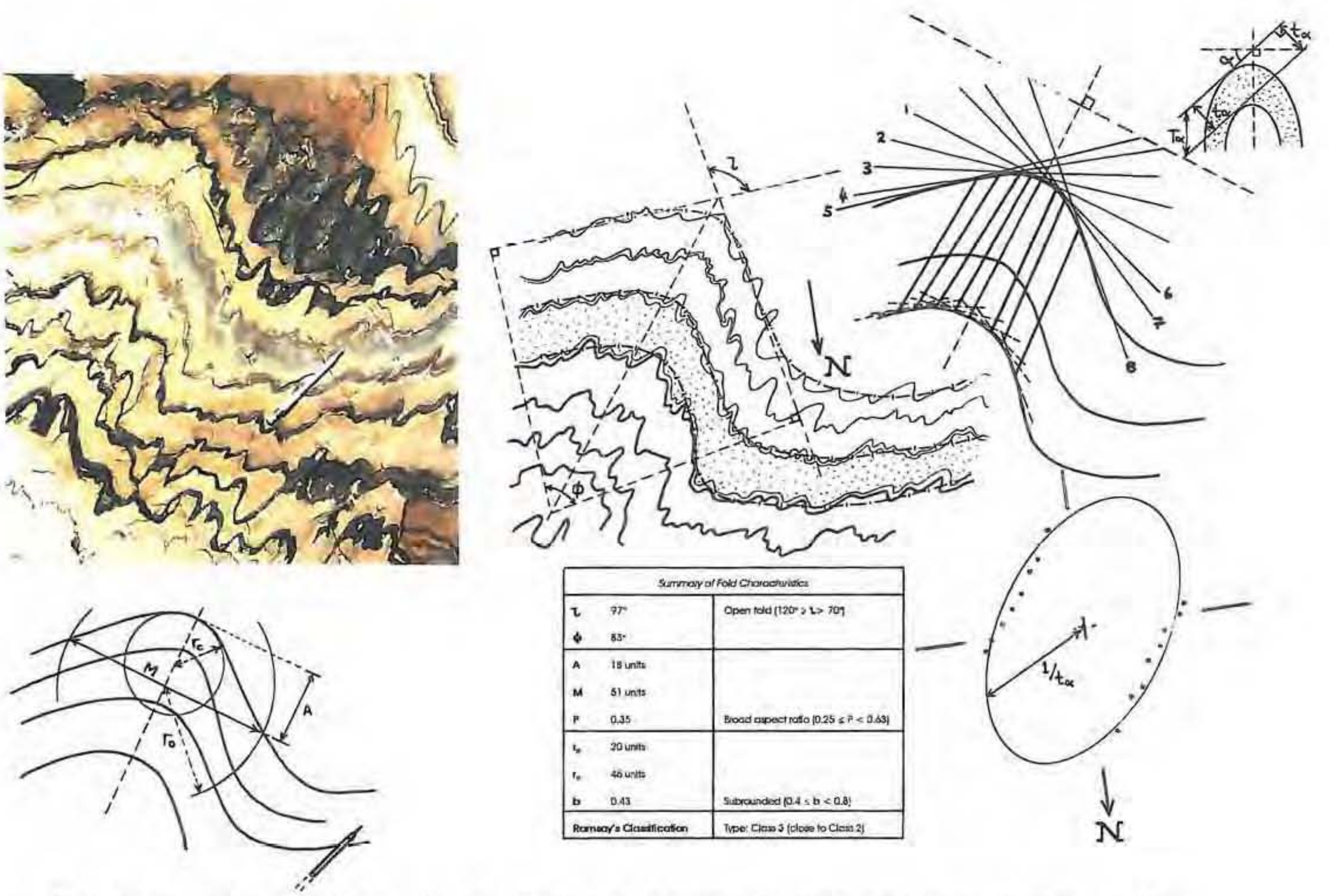

Summary of Fold Characteristics		
ι	97°	Open fold (120° > ι > 70°)
ϕ	83°	
A	18 units	
M	51 units	
P	0.35	Broad aspect ratio (0.25 ≤ P < 0.63)
r_c	20 units	
r_o	46 units	
b	0.43	Subrounded (0.4 ≤ b < 0.8)
Ramsay's Classification		Type: Class 3 (close to Class 2)

Fig. 6.10: An open, Z-fold in the calcitic marbles of the Brown Mountain area. The diagrams and table summarize the main fold characteristics. This fold possesses a borderline Class 2 (similar) or Class 3 (see Fig. 6.4b) layer shape according to Ramsay's classification. The method of Lisle (1992) was used to construct the strain ellispse above (not XZ plane in this case; closer to YZ plane) and estimate strain due to flattenning of this buckle fold. The fold hinge of this structure has a subhorizontal plunge as can be seen in the top righthand corner of the photograph where a folded calc-silicate layer is partially exposed.

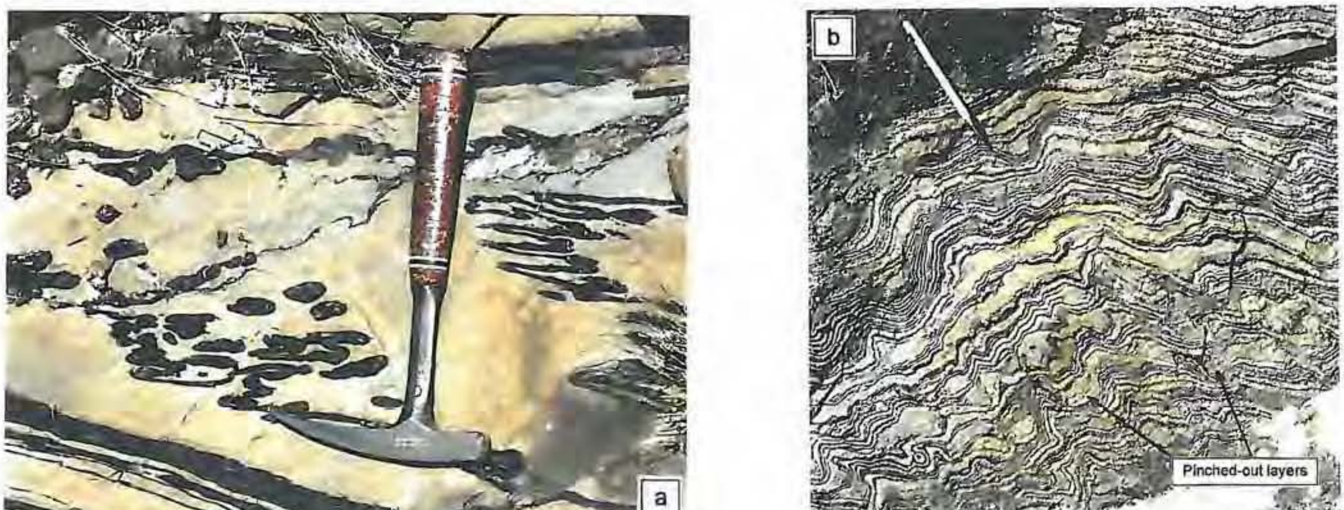

Fig. 6.11: Examples of folds in the calcitic marbles of the Brown Mountain area. (a) Intrafolial folding and transposition of isoclinal fold hinges and limbs into the composite $S_{0,1}$ foliation; (b) Disharmonic folding (common in the calcitic marbles of the Onguati study area)

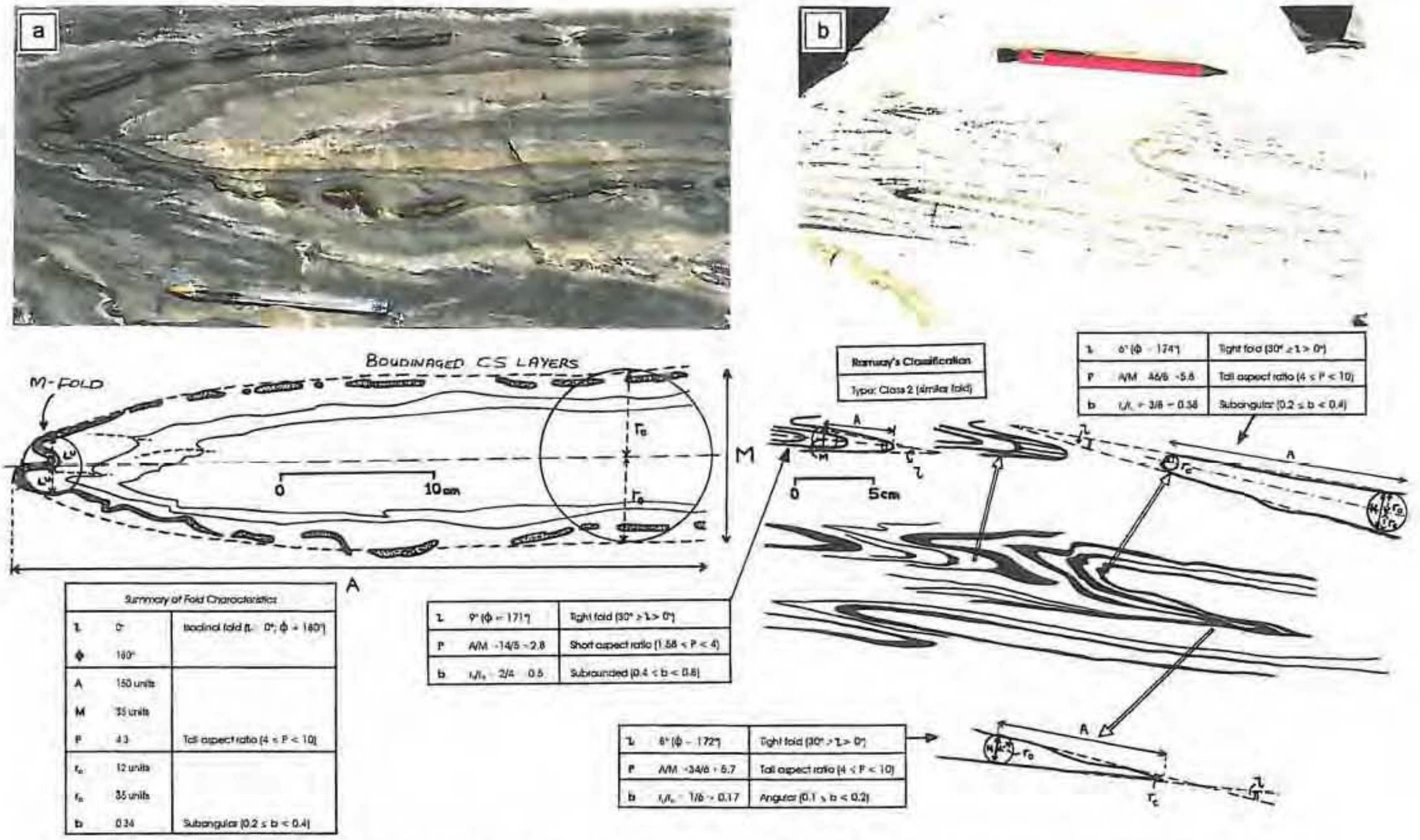

Summary of Fold Characteristics		
ι	0°	Isoclinal fold (ι = 0°; φ = 180°)
φ	180°	
A	150 units	
M	35 units	
P	4.3	Tall aspect ratio (4 ≤ P < 10)
r_c	12 units	
r_o	35 units	
b	0.34	Subangular (0.2 ≤ b < 0.4)

ι	9° (φ = 171°)	Tight fold (30° ≥ ι > 0°)
P	A/M = 14/5 = 2.8	Short aspect ratio (1.58 ≤ P < 4)
b	r_c/r_o = 2/4 = 0.5	Subrounded (0.4 ≤ b < 0.8)

Ramsay's Classification
Type: Class 2 (similar fold)

ι	6° (φ = 174°)	Tight fold (30° ≥ ι > 0°)
P	A/M = 46/8 = 5.8	Tall aspect ratio (4 ≤ P < 10)
b	r_c/r_o = 3/8 = 0.38	Subangular (0.2 ≤ b < 0.4)

ι	8° (φ = 172°)	Tight fold (30° ≥ ι > 0°)
P	A/M = 34/6 = 5.7	Tall aspect ratio (4 ≤ P < 10)
b	r_c/r_o = 1/6 = 0.17	Angular (0.1 ≤ b < 0.2)

Fig. 6.12: Folds found in the calcitic marbles of the Western Workings area. (a) Small, isoclinal fold defined by a thin, calc-silicate layer. Note the M-fold developed in the closure and the boudinaged calc-silicate layer in the limbs. Just above the pen there are lenses of light calcitic marble in a more graphite-rich calcitic marble that have developed by transposition. (b) Tight, angular, subangular and subrounded folds attest to the high degree of flattening in the marbles. A 30cm long lense of white marble in the lower half of the image is probably a result of transposition folding.

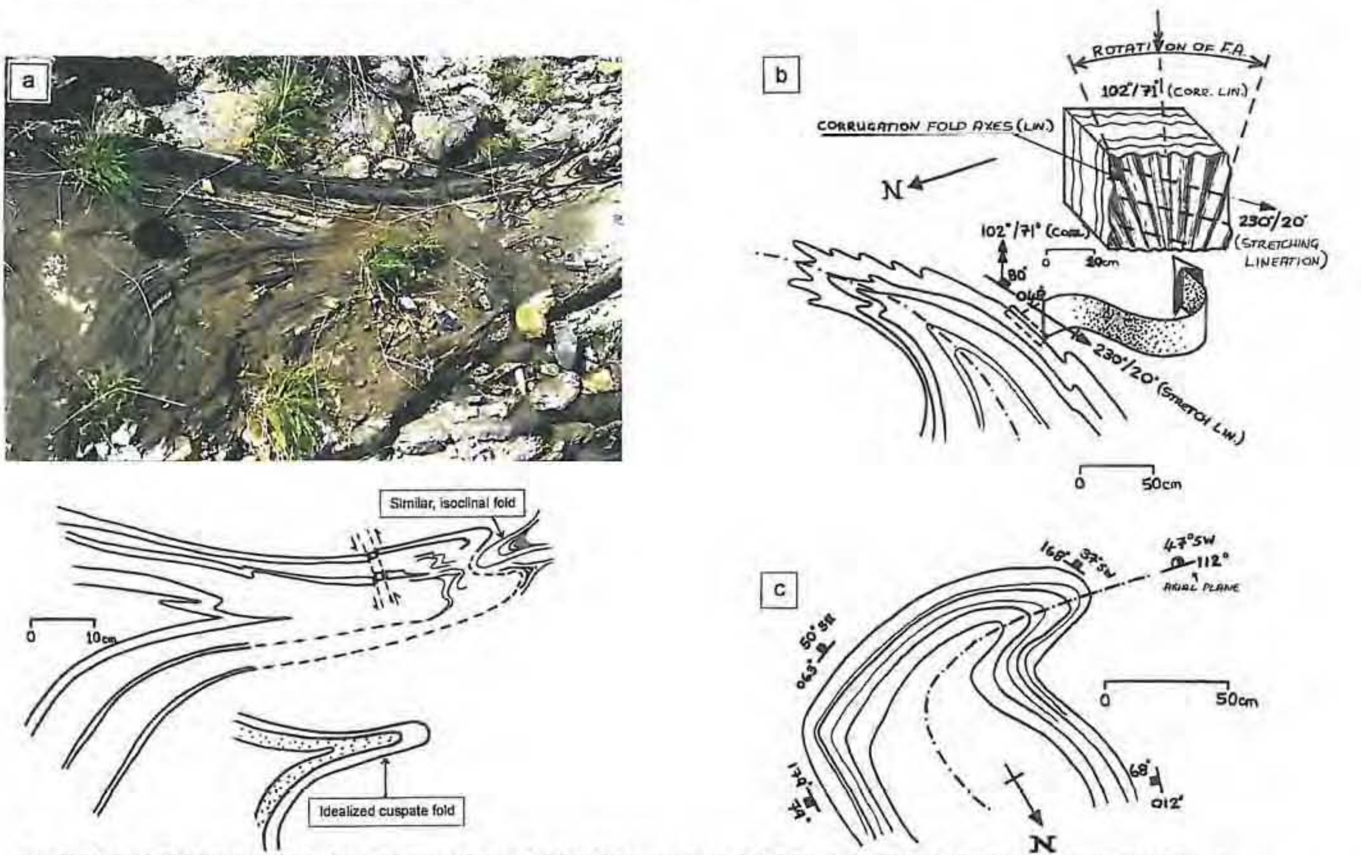

Fig. 6.13: Modified folds in the calcitic marbles of the Western Workings area. (a) Tight, cuspate fold developed as a result of space problems during folding - the ductile marble layers simply flowed and deformed in the available space; (b and c) these folds have curved axial planes (only one limb is cuspate) and were probably modified during a single episode of progressive deformation or may have been dragged into nearby marble shear zones.

stress (SRσ_1) during folding was approximately NNW-SSE to NW-SE (Figs. 6.5, 6.6, 6.9 and 6.10). Such a direction is perpendicular to the hinge line of the Onguati-Kranzberg anticlinorium.

6.3. Faults and Shear Zones

A number of approximately NW-, NNE- and ENE-trending lineaments were identified on the high-resolution aeromagnetic images and aerial photographs studied in this project (see Figs. 3.7 - 3.9). These structures may belong to a system of faults that represent the brittle expression of an earlier shear zone system that developed in the overturned Onguati-Kranzberg anticlinorium (Fig. 6.14). The Onguati study area is bound to the NW and SE by a parallel set of ENE-trending thrust or reverse faults, that extend largely along the lithological contact between the Navachab Member and Onguati Member. About 2.5 km east of Onguati Mine a prominent NNE-trending fault cuts across the foliation of the anticlinorium, and links in a sigmoidal fashion with the two ENE-trending thrusts. Part of the NNE-trending fault found in close proximity to Western Workings has been mapped and studied in detail (section 6.3.1). The Onguati Mine, Brown Mountain and Western Workings vein networks are all situated on a line close to the longest diagonal of this parallelogram-shaped system of faults (Fig. 6.14).

6.3.1. NNE-trending Thrust Fault at Western Workings

It is difficult to classify the NNE-trending fault in the Western Workings vicinity because nowhere do the marbles preserve a clear fault scarp. However, a range of evidence points to a top-to-the ~NW tectonic transport, and indicates that this structure is either a reverse fault or thrust. Near 1820W/0N (see Map 3A in map pouch) the footwall of the thrust fault is associated with an elongate zone of upwarped strata. It is likely that the ends of truncated layers were dragged into a syncline by an over-riding block that has since been eroded. The fold axis of these sharply upturned layers parallels the fault and has an approximate trend of 040° – this indicates thrusting was directed at ~310°. Within the footwall of this site, thin, near-horizontal calcitic marble layers may show top-to-the NW offsets and some may be transposed, dismembered and rotated in a more ductile, graphitic matrix. Centimetre-scale, gently inclined or recumbent, tight, asymmetric drag folds can also be found in the calcitic

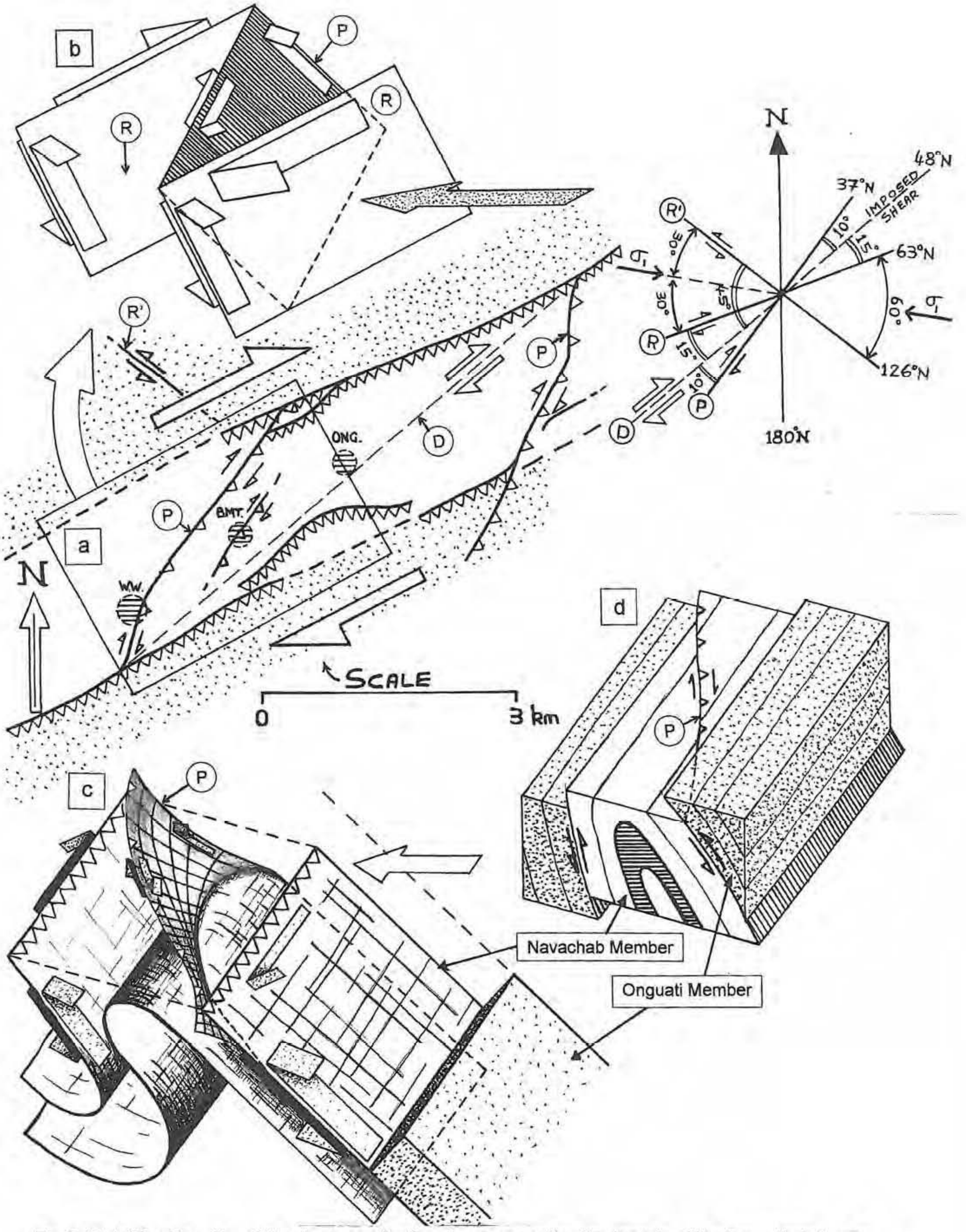

Fig. 6.14: (a) Configuration of the shear zone/fault system surrounding the deposits of the Onguati study area. Onguati Mine lies along the longest diagonal of the parallelogram-shaped arrangement of faults, possibly along the imposed shear direction or D shear of a deposit-scale, Reidel shear system. Western Workings and Brown Mountain appear to be located in or close to P shears/thrusts. (b) Simplified block diagram showing the two main thrust planes (R shears) linked by a diagonal P shear, all with a component of dextral movement. (c and d) Diagrams illustrating the location of the main thrusts along lithological contacts between the Navachab and Onguati Members on either limb of the Onguati-Kranzberg anticlinorium. The sigmoidal P shear/thrust may link with underlying thrust faults developed where there are other major lithological contrasts (e.g. contact/s between Etusis/Chuos Fm. and Spes Bona Member).

marbles along parts of the thrust and display a Z-shape when viewed down-plunge. This supports a top-to-the NW or dextral shear sense. In fact, tight to isoclinal folds throughout the Onguati study area are persistently overturned towards the NW.

Numerous bands and pockets of tectonic breccia are found along the length of the thrust fault in the Western Workings area (Plate 6.5). In places heavily fractured marble can be seen to grade into broad breccia packages that appear to dip gently towards the southeast. The marble clasts vary from a few millimetres in size to a maximum of 20 cm in length. Brecciated pockets of marble have been sites of preferential solution and often resemble breccia-filled karst pipes. The breccia is commonly cemented by a pure white, calcitic cement but in some parts, the matrix can be more ferruginous and wad-like. In the dolomitic marbles to the southeast of Western Workings, the breccia contains smaller cataclastic particles (<1 cm) that are cemented by fine, red-coloured siliceous material. Pockets of coarse breccia have also been found in the dolomitic marbles of Onguati Mine which contain a tremolite±quartz cement, but these are not related to an obvious fault and may be a consequence of space problems in the hinge zone of a large syncline (Plate 6.6).

6.3.2 NNE-trending Shear Zone in the Calcitic Marbles of Brown Mountain

Brown Mountain forms an elongate highland area that is aligned with the nearby NNE-trending thrust fault of the Western Workings surrounds (see Fig. 3.9). There are indications that parts of the calcitic marbles experienced intense ductile shearing before veining and hydrothermal mineralization. Webb (1992, p.21) identified thin zones of "mylonite" exposed on the slopes of Brown Mountain which he related to F_2 tight, recumbent folding with southeast-dipping axial planes. During this study, an extensive zone of highly sheared rocks was identified (~85S/950W) where the calcitic marble layering had been completely obliterated. This effect is quite different to bedding transposition where the intrafolial lenses parallel and accentuate the compositional foliation. This ductile shearing occurred at an earlier stage than the thrusting near Western Workings. The veins in the calcitic marbles of Brown Mountain may have developed during the brittle-ductile stage of a progressive or long-lived NW-directed, shearing event.

Plate 6.5: Large zone of brecciated calcitic marble adjacent to the NNE-trending thrust fault that cuts across the Western Workings area. The calcitic marble clasts measure a few millimetres to 20 cm in length, and are commonly cemented by a combination of wad (brown-grey patches) and white or grey calcitic fill.

Plate 6.6: Breccia pocket in the dolomitic marbles of the Onguati Mine area. In this image the clasts are largely sub-angular, but in many parts of the dolomitic marble the clasts are sub-rounded and can measure up to 40 cm in diameter. The brown-coloured matrix is composed mainly of tremolite with small amounts of quartz.

6.4. Veins

Veins are of prime structural interest in the Onguati study area because they can host significant hydrothermal Cu-Fe±Au mineralization. Many of the veins found in the Onguati study area are boudinaged or show pinch-and-swell morphologies, and are predominantly ESE- to SE-dipping planar structures. The veins may be classified as "shear-related" (Hodgson, 1989, p.231) or "fault-fill" (Robert & Poulsen, 2001, p.124) veins because of their intimate association with shear zones at the outcrop- and deposit-scale, and because of their close proximity to the Riedel arrangement of faults/shear zones at the scale of the Onguati-Kranzberg anticlinorium. The veins in the Onguati study area are not typically laminated with foliated wall-rock slivers as is characteristic for many shear-related veins (Hodgson, 1989).

In this section, the vein systems are discussed according to the areas and the host rocks in which they occur. Stereonets have been constructed for the veins found in the calcitic marbles of the Onguati Mine area, and for the distinct vein systems developed in the calcitic and dolomitic marbles of the Brown Mountain and Western Workings localities. The veins have been classified according to their morphology (e.g. boudinaged, folded etc.) and are plotted in relationship to the $S_{0,1}$ foliation, isoclinal fold axial planes and to various lineations to test for structural relationships.

The orientations and shapes of the minimum strain ellipsoids for each of the vein arrays in the Onguati study area were estimated using deformed quartz veins as strain markers, as per the method of Talbot (1970). For each vein array the orientations of a large number of veins were recorded, and on the basis of their structure, the veins were classified into those that experienced extension (i.e. boudinage, pinch-and-swell structures) or shortening (i.e. buckle folding, inter-stacking). The strike and dip of folded veins, or thick veins with pronounced pinch-and-swell structures or boudinage, were measured in the plane of the vein (i.e. measurement of a 'best-fit' planar surface in the direction of the vein).The vein data was plotted on stereographic plots as classified poles-to-planar elements of the veins, and fields of extension and shortening were delineated. The line separating the extensional field from the shortening field represents the invariant surface along which veins are equal to their original length (Talbot, 1970). The shape of the overall extension field on the stereographic projection is directly related to the shape of the strain ellipsoid (Talbot, 1970). A small, elliptical overall extension field is characteristic of oblate ellipsoids that describe homogeneous flattening. The 2 apical angles, $\psi_{XZ}°$ and $\psi_{YZ}°$ in the case of an oblate ellipsoid, are measured from Z to the intersection of the invariant surface with the XZ and YZ principal planes in the stereographic projection. The measured apical angles can then be plotted in Fig. 6.20 and the axial ratios a=X/Y and b=Y/Z of the minimum strain ellipsoid can be read off the graph (alternatively the formulae relating apical angles to axial ratios can be used; see Talbot, 1970, p.60). The approximated apical angles of each of the vein arrays were plotted on Fig. 6.20 as recommended by Talbot (1970) and Nicolas (1987) and were used to define a field showing the possible range of shapes of the oblate strain ellipsoid in the Onguati study area.

6.4.1. Onguati Mine Area

The well-mineralized Onguati Mine vein array is concentrated in the calcitic marbles on the lower, northern slopes of Onguati Hill. The vein system is characterized by the presence of several very large quartz-sulphide veins (Fig. 6.15) in addition to numerous cm- and mm-thick quartz±carbonate veins and veinlets (the vein thickness distribution of this vein array and the others at Brown Mountain and Western Workings forms the basis of Chapter 8). The largest veins typically measure 1 to 3 metres in thickness and have exposed lengths up to about 100 metres. Many of the thicker veins display pinch-and-swell structures and some possess thick vein branches. Smaller veins tend to be intensely boudinaged so that individual boudins may be separated by up to several tens of cm (Plates 6.7-6.10). In cross-section, the quartz vein boudins have small aspect ratios and are typically well-rounded, sometimes terminating in short, pointed ends (Plate 6.8). There are a few small 3D exposures of thin quartz veins in the Onguati Mine area that indicate that the boudinage is of the "chocolate tablet" variety (Price & Cosgrove, 1990, p.406). There are also a small number of thin, isolated veins with NW-SE strikes (see vein orientation-morphology diagram, Fig. 6.21, A) that are buckled (Plate 6.11) or fragmented and inter-stacked (Plate 6.12). In the DGMC unit there are a number of mm-thick ptygmatic quartz+carbonate veins.

The vast majority of veins are SE-dipping and cross-cut the $S_{0,1}$ marble foliation at acute angles of 20° to 35°. While veins of all sizes and orientations truncate the F_1 and F_2 folds, there are a number of veins that have formed sub-parallel or parallel to the fold axial planes of F_2 folds (Fig. 6.16, iv). The generally low vein densities and the NE-SW strikes of most veins in the array minimizes the number of vein cross-cutting relationships. The few cross-cutting relationships observed show that folded and boudinage veins can develop at any stage (Fig. 6.22). It is possible that some of the folded quartz-carbonate veins formed during the final stages of F_2 folding and thinning and were therefore buckled. Late

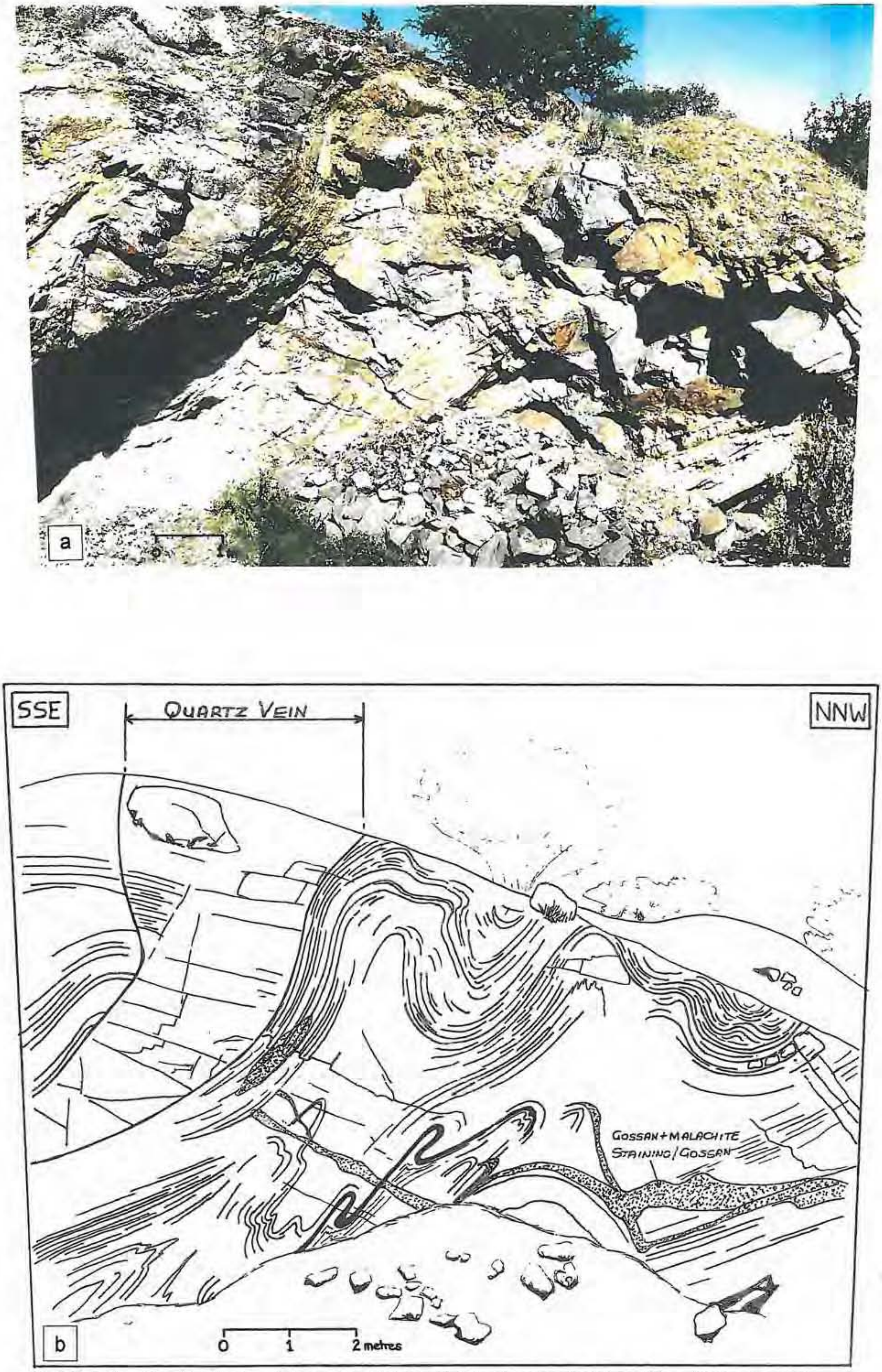

Fig. 6.15: (a) A southwest-looking view of a large, mineralized sigmoidal-shaped quartz vein at Onguati Mine, with an accompanying sketch (b) highlighting the main structural features. This vein, like most in the marbles of the Onguati study area, is associated with a S-type flanking fold with a small component of dextral shear. Note the isoclinal, Z-shaped drag folds that have developed in the ductile calcitic marbles below the vein, in the lower middle part of the image. In the upper, middle region of the plate, a series of metre-scale anticlines and synclines with near horizontal fold hinges can also be seen. Note the elliptical form of the tight fold in the righthand corner of image (a). Joints and fractured zones leading away from the veins contain abundant malachite staining and gossanous material.

ONGUATI MINE AREA

Plate 6.7

Plate 6.8

Plate 6.9

Plate 6.10

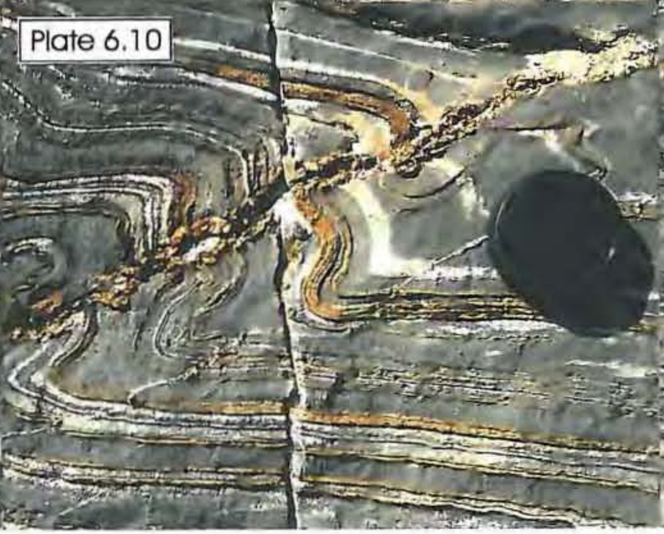

Plate 6.11

Plate 6.12

Plate 6.7: A series of thin, parallel, mineralized and intensely boudinaged veins in the Onguati Mine area. Note the n-type (no displacement) flanking fold developed about the left-most vein with a dextral sense of shear, and the large quartz vein boudin that has been rotated through ~90°. The breakdown of vein sulphides and hydrothermal sulphides found along calc-silicate–calcitic marble layer interfaces has resulted in oxidation of graphite, and the bleaching of the host marbles.

Plate 6.8: Boudinaged quartz veins with minor pyrrhotite mineralization. The well-developed vein boudin-related, s-type (synthetic displacement) flanking folds show a small component of dextral displacement most clearly in the top righthand corner of the plate. Individual calcitic marbles layers sandwiched between calc-silicate laminations are bleached up to a metre away from the vein.

Plate 6.9: Large-scale view of Plate 6.8 showing the planar arrangement of 'barrel-shaped' vein boudins. Note the prominent s-type flanking folds near the lense cap with a dextral shear sense.

Plate 6.10: Synthetic or s-type flanking fold with significant (~7cm) dextral displacement along a boudinaged quartz-carbonate vein. Shearing along the vein must have been relatively long-lived because the quartz vein boudins have fractured in a brittle manner and are filled by later carbonate.

Plate 6.11: Contorted quartz vein in the calcitic marbles of the Onguati Mine area formed by buckling of the much stiffer quartz vein in the plastically deforming calcitic marbles. Note the boudinaged limbs of the folded vein. The white carbonate material between quartz vein boudins, helping define the form of the vein, has probably been bleached by oxidation of sulphides deposited in the boudin neck zones.

Plate 6.12: A thin, interstacked quartz vein in the calcitic marbles near Onguati Mine. The rigid quartz vein had to break into boudin-like fragments when the calcitic marbles were undergoing plastic deformation, probably associated with significant pressure solution. Note the orientation of this vein (~NW-SE strike) compared to the boudinaged veins (~NE-SW strike) relative to the $S_{0,1}$ foliation.

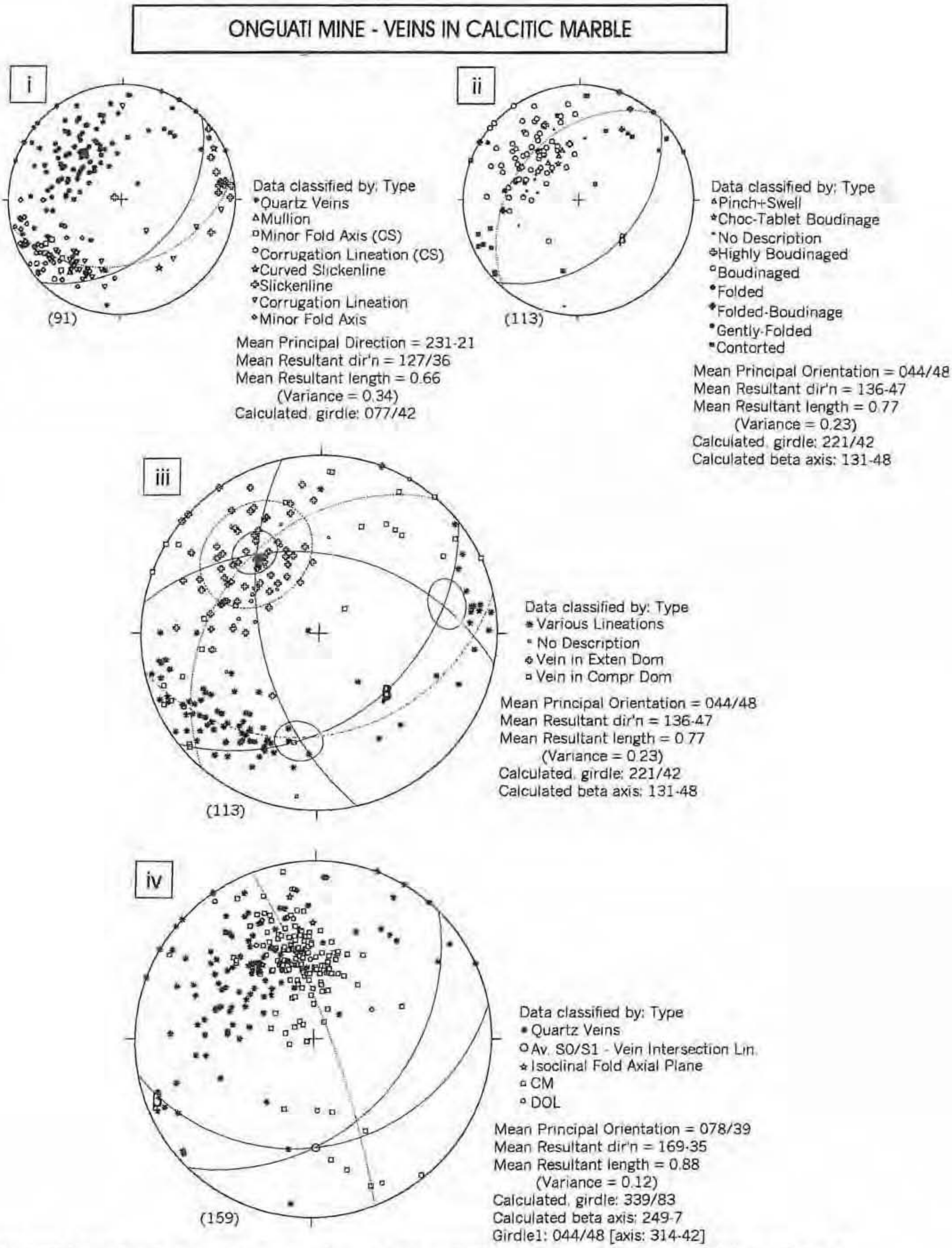

Fig. 6.16: Lower hemisphere, equal area stereographic projections of a variety of structural data in relation to the quartz veins found in the calcitic marbles of the Onguati Mine area. (i) Plot showing classified lineation data and unclassified poles-to-vein data. (ii) Plot showing a detailed morphological classification of veins (poles-to-planar elements). Open symbols correspond to poles-to-extended planar elements of veins; closed symbols correspond to poles-to-folded planar elements of veins. (iii) Poles-to-veins classified according to whether the veins are found in extensional or compressional domains. Minor fold and corrugation fold axes (see plot i) are largely parallel or sub-parallel to the Y-axis. Method of Talbot (1970) used to determine orientation and shape of strain ellipsoid: $\psi_{xz} \approx 25°$, $\psi_{yz} \approx 25°$; $a \approx 1.00$, $b \approx 2.22$; X = 077°-27°, Y = 190°-38°, Z = 321°-41° (trend-plunge of axes). (iv) Poles-to-veins and poles-to-$S_{0,1}$ foliation defining an average intersection lineation of 178°-39° (trend-plunge).

carbonate±quartz veins with 'cockscomb' textures are found in a few places but are not related to the hydrothermal event that resulted in Cu±Au vein mineralization in the area.

The marble host rock $S_{0,1}$ foliation is often severely deflected in narrow zones either side of the veins in the Onguati Mine area, and form structures known as "flanking-folds" (Passchier, 2001, p.951). Throughout the area flanking-folds share the same general orientation and their axial planes parallel the dominant NE-SW strike of the veins in the array. Two geometric types of boudin-related flanking-folds have been recognized in the Onguati study area based on the categories of Passchier (2001, p.952 and Fig. 7):

(i) "n-type" flanking-folds where the marble layers are not displaced along the vein (e.g. Plate 6.7); and

(ii) "s-type" or synthetic flanking-folds where the layers are displaced along the vein in the same direction as the hypothetical dextral rotation indicated by the flanking-fold asymmetric form (e.g. Plates 6.8-6.10).

The flanking-folds in the Onguati Mine area may have originally formed as drag-fold trains during non-coaxial flow in the calcitic marbles (Passchier's mode I mechanism). Fractures cut across the inflection points of the folded marble layers so that the flanking-folds are divided into convex-up and concave-up parts. Flanking-folds formed in this manner may provide reliable shear sense indicators (Passchier, 2001). The Onguati flanking-folds indicate a persistent dextral sense of shear.

Talbot's (1970) method for estimating the shape and orientation of the minimum strain ellipse, indicates that the Onguati Mine area experienced flattening as described by an oblate ellipsoid. The wide scatter of poles-to-extended planar elements of veins in Fig. 6.16 [iii] implies that the vein data was collected from a rock that underwent inhomogeneous deformation (Talbot, 1970, p.56). While the orientation of the Z-axis of the strain ellipsoid is relatively well constrained (i.e. 321°-41°; trend-plunge), the distinction of the principal axes in the XY plane is difficult using the geometry of the overall extension field. However the southwesterly trends of minor fold axes and corrugation lineations may be parallel/sub-parallel to the Y-axis of the strain ellipsoid. If the apical angles $\psi_{XZ}°$ and $\psi_{YZ}°$ are estimated at ~25° each, then the minimum strain ellipsoid would be uniaxial oblate (i.e. X=Y). The strain ellipse in Fig 6.21 [B], determined from the magnitude of elongation of the quartz veins embedded in the calcitic marbles of the Onguati Mine area, also supports a ~NW-SE direction for the Z-axis.

6.4.2. Brown Mountain

The veins in the Brown Mountain area can be divided into veins that are hosted by calcitic marble and those in the overlying dolomitic marble unit. Although both vein arrays formed during the same hydrothermal event, such a distinction is necessary because the veins in the calcitic and dolomitic marbles differ considerably in structural style and mineralization.

(a) Vein array hosted by calcitic marble

The vein swarm in the Brown Mountain area is predominantly composed of NNE-striking (Figs. 6.17[A] and 6.21) quartz+gossan veins, and is quite distinct from the vein systems developed in the calcitic marbles of the Onguati Mine and Western Workings areas. The veins are generally thin, only measuring 1-2 cm wide (maximum vein thicknesses ≈ 35 cm), but are very numerous in the calcitic marbles of Brown Mountain. The majority of the veins are boudinaged or display pinch-and-swell structures. Exposed 3D surfaces of quartz veins show that at least some of the vein boudinage is of the 'chocolate tablet' variety (Plate 6.15). In many places it is possible to recognize thin quartz veins arranged in the position of metre-wide Riedel shear systems (Plates 6.13, 6.14 and 6.16). The arrangement of veins in the R, P and T shear positions implies a dextral shear sense along the Riedel shear zones. Composite, laminar vein sets are also commonly developed at Brown Mountain as shown in Plate 6.17.

In Fig. 6.17[A], the Z-axis was positioned with an orientation of 295°-24° (trend-plunge) to lie in the centre of the overall extensional field (delineated with an ellipse). The positioning of the X- and Y-axes on the XY plane (perpendicular to Z) was difficult because of the wide scatter of pole-to-extended veins. The apical angles ψ_{XZ}° and ψ_{YZ}° were approximated as 28° and 25° respectively. The axial ratios a=X/Y and b=Y/Z were thus calculated at ~1.07 and 1.87 respectively.

(b) Vein array hosted by dolomitic marble

A weak vein array is developed in the dolomitic marbles in the northwestern part of the Brown Mountain mapping area. The most intense veining occurs close to the DM unit - TM unit contact and veins may measure up to ~3 cm in thickness. The veins are generally dominated by quartz and have tremolite margins, but show few signs of sulphide mineralization. The veins are planar and display pinch-and-swell structures. There is a distinct lack of folded veins in the dolomitic marbles as is illustrated in the stereographic plot (Fig. 6.17[B]) and the

BROWN MOUNTAIN AREA


Plate 6.13


Plate 6.15


Plate 6.17


Plate 6.14


Plate 6.16

Plate 6.13: Riedel arrangement of veins in the calcitic marbles of the Brown Mountain area. The upright veins may have formed in R shear fractures, while the diagonal veins may correspond with P shear fractures (acute angle between P and R shear veins is ~30°). Note that flanking folds are not well developed around these folds compared to those at Onguati Mine. Strain may have been accommodated by the various shear fractures (veins) and would not have required the development of flanking folds.

Plate 6.14: Three distinct vein sets have developed in a brittle-ductile shear zone in the calcitic marbles of Brown Mountain. The horizontal veins in this plate appear to be in the position of R shears. The two, thin diagonal sets of veins are ~conjugate (acute angle of ~53°); the veins oriented bottom lefthand corner to top righthand corner in the photo may be P shears; the other set is in the position of extensional T fractures. This arrangement of veins is compatible with a dextral sense of shear.

Plate 6.15: An exposed quartz vein surface showing strong chocolate tablet boudinage. Such deformation suggests that the strain state was of a flattening type (oblate finite strain ellipse). Note the black staining of the walls caused by karstic activity and weathering of sulphides.

Plate 6.16: Similar vein arrangement to plate 6.14, but here the T extensional veins are characteristically sigmoidal in shape. The T shear veins cut boudinaged P shear veins and are bound by a set of thin R shear veins. Note the Fe-staining of the marbles in the shear zone.

Plate 6.17: A composite, laminar vein set developed in the calcitic marbles on the slopes of Brown Mountain. As shear fractures (R shears?) were filled by quartz and solidified, so strain was transferred to the marble wall rocks and new fractures were nucleated on either side of the thick vein.

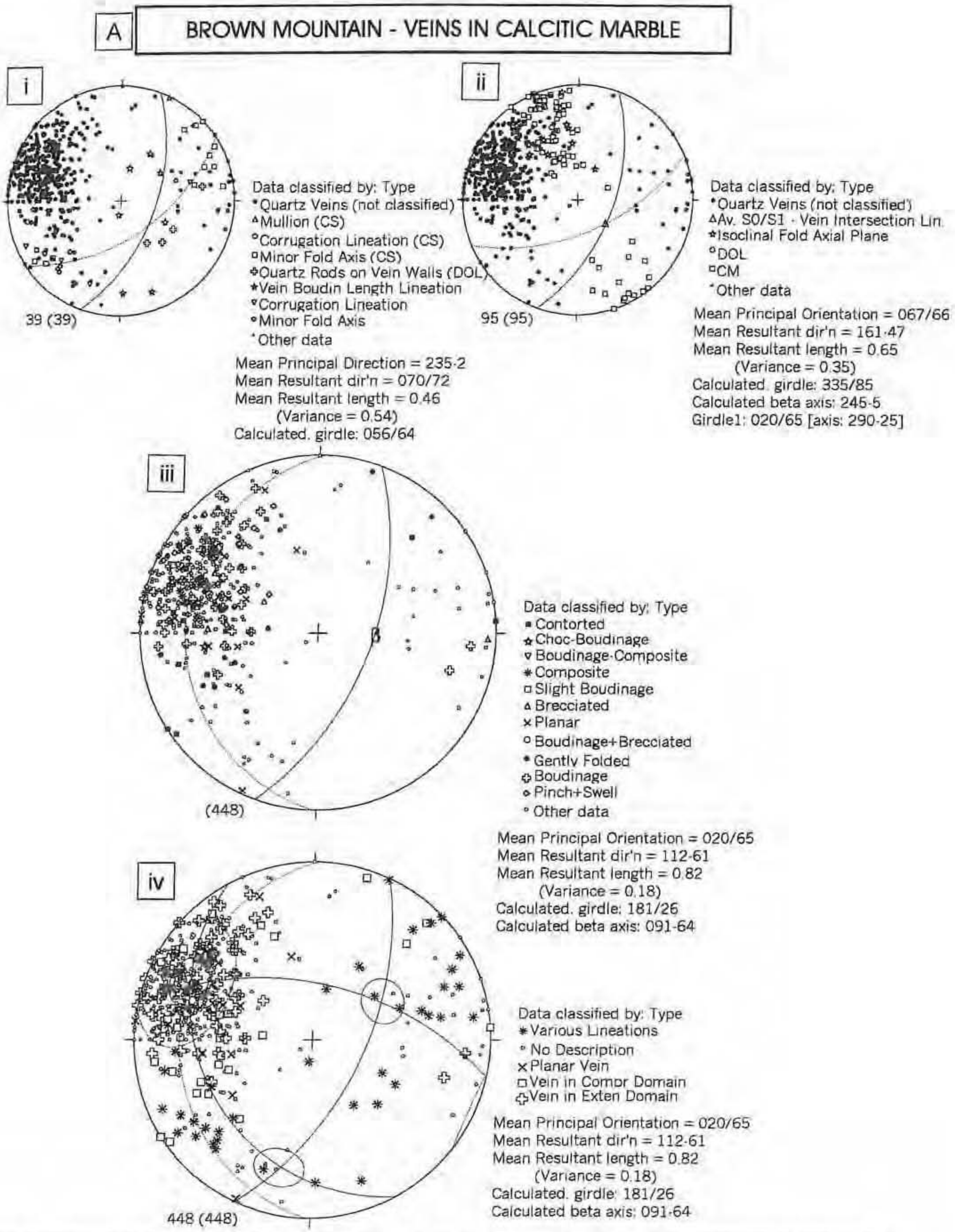

Fig. 6.17[A]: Lower hemisphere, equal area stereographic projections of a variety of structural data in relation to the quartz veins found in the calcitic marbles of the Brown Mountain area. (i) Plot showing classified lineation data and unclassified poles-to-vein data. (ii) Poles-to-veins and poles-to-$S_{0,1}$ foliation defining an average intersection lineation of 130°-64° (trend-plunge). (iii) Plot showing a detailed morphological classification of veins (poles-to-planar elements). Open symbols correspond to poles-to-extended planar elements of veins; closed symbols correspond to poles-to-folded planar elements of veins. (iv) Poles-to-veins classified according to whether the veins are found in extensional or compressional domains. Minor fold and corrugation fold axes (see plot i) are largely parallel or sub-parallel to the Y-axis. Method of Talbot (1970) used to determine orientation and shape of strain ellipsoid: $\psi_{XZ} = 28°$, $\psi_{YZ} = 25°$; a = 1.07, b = 1.87; X = 061°-53°, Y = 194°-27°, Z = 295°-24° (trend-plunge of axes).

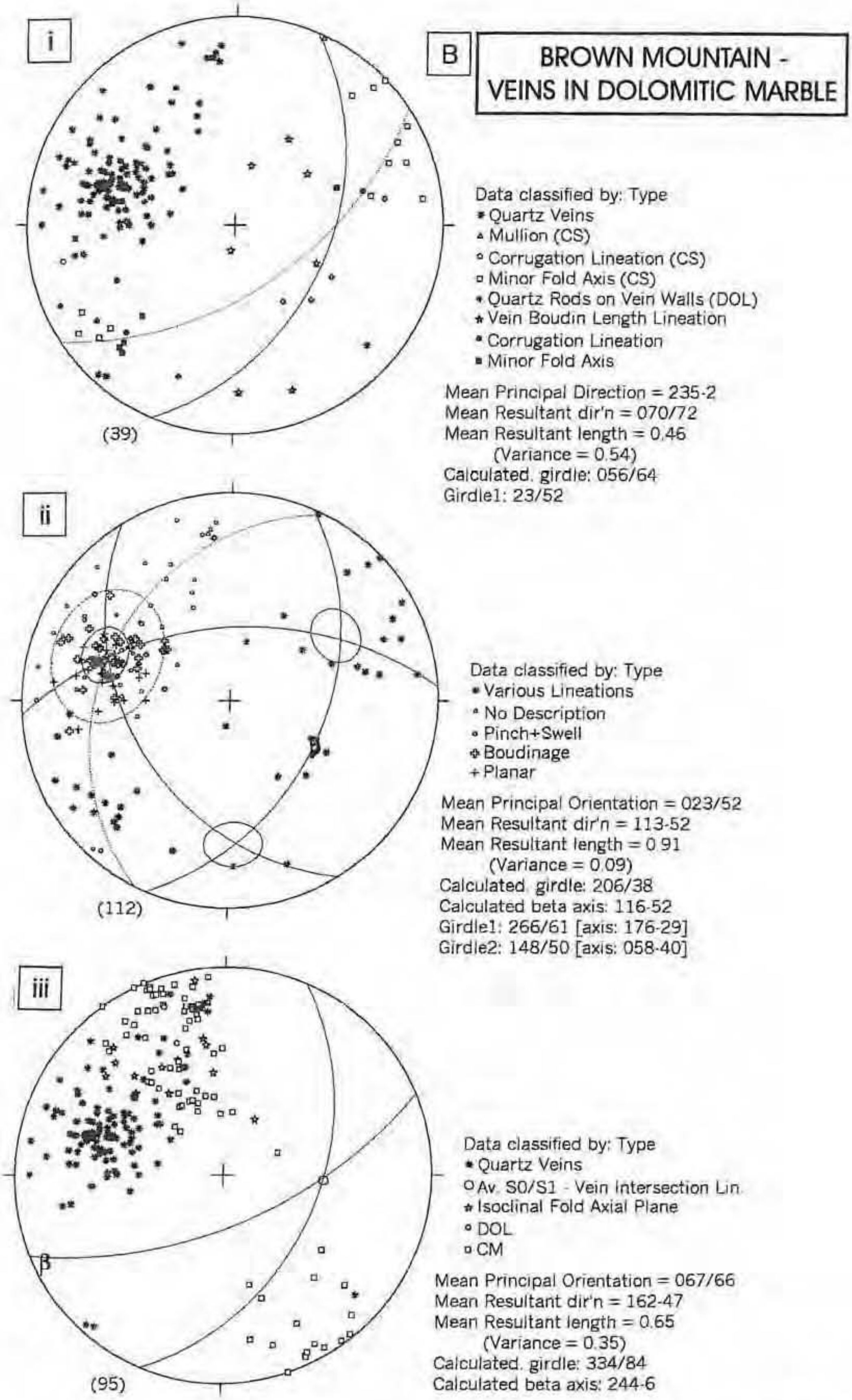

Fig. 6.17[B]: Lower hemisphere, equal area stereographic projections of a variety of structural data in relation to the quartz veins found in the dolomitic marbles of the Brown Mountain area. (i) Plot showing classified lineation data and unclassified poles-to-vein data. (ii) Poles-to-veins classified according to whether the veins are found in extensional or compressional domains. Minor fold and corrugation fold axes (see plot i) are largely parallel or sub-parallel to the X- or Y-axes. Method of Talbot (1970) used to determine orientation and shape of strain ellipsoid: $\psi_{XZ} \approx 25°$, $\psi_{YZ} \approx 20°$; $a \approx 1.24$, $b \approx 2.38$; X = 058°-40°, Y = 178°-31°, Z = 290°-36° (trend-plunge of axes). (iii) Poles-to-veins and poles-to-$S_{0,1}$ foliation defining an average intersection lineation of 093°-50° (trend-plunge).

vein orientation-morphology diagram (Fig. 6.21, D).

The overall field of extension is fairly well constrained in the dolomitic marbles. The position of the Z-axis at the centre of the extensional field is 290°-36° (trend-plunge) using the method of Talbot (1970). The apical angles $\psi_{XZ}°$ and $\psi_{YZ}°$ have been estimated at 25° and 20° respectively and imply a triaxial oblate ellipsoid where the X and Y axes have similar dimensions.

6.4.3. Western Workings

Veins are found in both the calcitic and dolomitic marbles of the Western Workings area, and as with the Brown Mountain section, are discussed according to their host rock.

(a) Vein array hosted by calcitic marble

The veins in the calcitic marbles of the Western Workings area are very similar in style to those found in the Onguati Mine area (Plates 6.18-6.21). The vein array contains very thick (1 - 3 metres), often branched quartz veins with significant sulphide mineralization. The veins have an average orientation of 012°/59° (strike/dip; righthand rule notation) and cut the $S_{0,1}$ foliation at high angle (Fig. 6.18[A]). Fig. 6.21 [E] shows the orientation and morphology of a selected number of veins from the Western Workings area, and Fig. 6.22 illustrates the cross-cutting relationships and relative timing of veins. Unlike the Onguati Mine area, it is common to find thick, quartz±sulphide mantos branching from the larger, mineralized veins at Western Workings. There are also numerous examples of sulphide-rich mantos with diffuse margins that extend along and replace the marble and calc-silicate layering. The average intersection lineation between the mean vein orientation and mean $S_{0,1}$ layering is 104°-59° (trend-plunge), similar to that in the adjacent dolomitic marbles (see Figs. 6.18[A] and [B]).

The wide spread of extended veins in Fig. 6.18[A] implies that the area experienced inhomogeneous strain. The position of Z is centred over this broad field and may be oriented at 299°-29° (trend-plunge). As with the other areas it is difficult to ascertain the relative position of the X and Y principal axes on the XY plane (perpendicular to Z), and to determine accurate apical angles to calculate the axial ratios of the minimum strain ellipsoid.

(b) Vein array hosted by dolomitic marble

Quartz+tremolite±sulphide veins hosted by dolomitic marble in the Western Workings area

WESTERN WORKINGS AREA


Plate 6.18


Plate 6.20


Plate 6.22


Plate 6.19


Plate 6.21

Plate 6.18: Typical Cu-Fe mineralized veins situated above the entrance to an incline shaft in the calcitic marbles of Western Workings. The two sub-parallel veins are slightly folded and are linked by a gently folded diagonal vein. These veins may be in the position of R and P shear fractures respectively. At their thickest, the quartz-sulphide veins are about 30 cm in width.

Plate 6.19: A southeast-looking view of a trench wall in the calcitic marbles showing a thick, mineralized quartz vein. The vein is intensely boudinaged and is displaced by a series of small, parallel carbonate±quartz-filled faults. The vein is SE-dipping and was probably displaced by dextral strike-slip movement along these small faults (slickenlines plunge sub-horizontally).

Plate 6.20: Poorly mineralized, branching quartz veins in the calcitic marbles of the Western Workings area. A weakly formed n-type (no displacement) flanking fold can be seen around the vein that branches off to the right, in the upper half of the image. This vein is also faulted and overlaps in the top righthand corner. Note the small quartz manto branching off the faulted vein.

Plate 6.21: An approximately E-W striking quartz vein (initially folded) adjacent to the large, NNE-trending thrust fault that cuts through the marbles of the Western Workings area. The vein has been heavily cut by small faults with cm-scale dextral displacement. Note the n-type flanking fold about the vein in the lower half of the image which shows an apparent sinistral motion (vein in R' shear position?).

Plate 6.22: Mineralized quartz-tremolite veins in the dolomitic marbles of the Western Workings area. The veins have a weak Riedel shear arrangement, where the two bounding veins may be in the position of P shear fractures. The very thin, tremolite-dominated veins may correspond to R shears and extensional T fractures. This Reidel vein arrangement supports a dextral sense of shear.

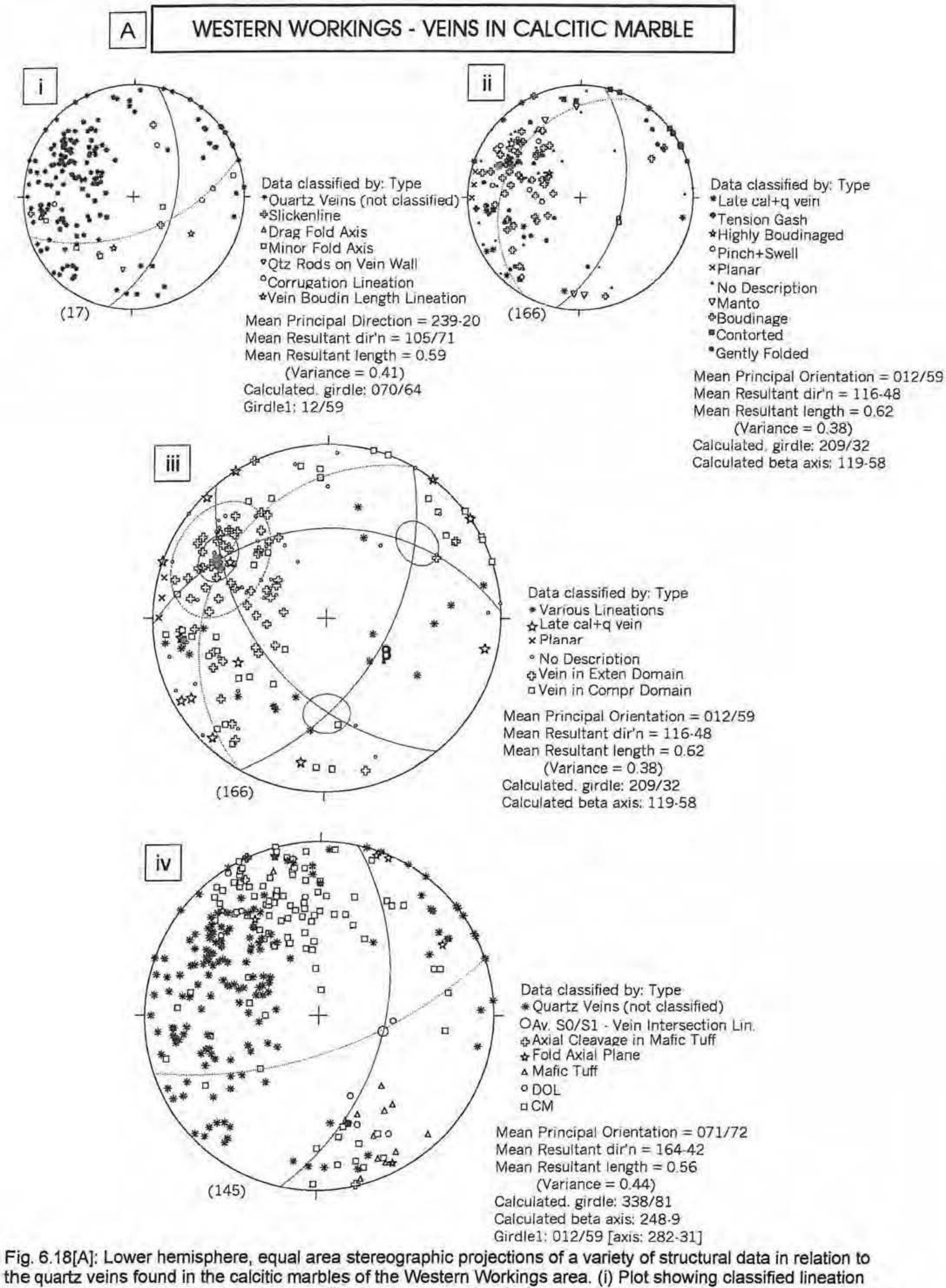

Fig. 6.18[A]: Lower hemisphere, equal area stereographic projections of a variety of structural data in relation to the quartz veins found in the calcitic marbles of the Western Workings area. (i) Plot showing classified lineation data and unclassified poles-to-vein data. (ii) Plot showing a detailed morphological classification of veins (poles-to-planar elements). Open symbols correspond to poles-to-extended planar elements of veins; closed symbols correspond to poles-to-folded planar elements of veins. (iii) Poles-to-veins classified according to whether the veins are found in extensional or compressional domains. Minor fold and corrugation fold axes (see plot i) are largely parallel or sub-parallel to the Y-axis. Method of Talbot (1970) used to determine orientation and shape of strain ellipsoid: $\psi_{xz} \approx 28°$, $\psi_{yz} \approx 28°$; a ≈ 1.00, b ≈ 1.74; X = 050°-33°, Y = 179°-44°, Z = 299°-29° (trend-plunge of axes). (iv) Poles-to-veins and poles-to-$S_{0,1}$ foliation defining an average intersection lineation of 104°-59° (trend-plunge).

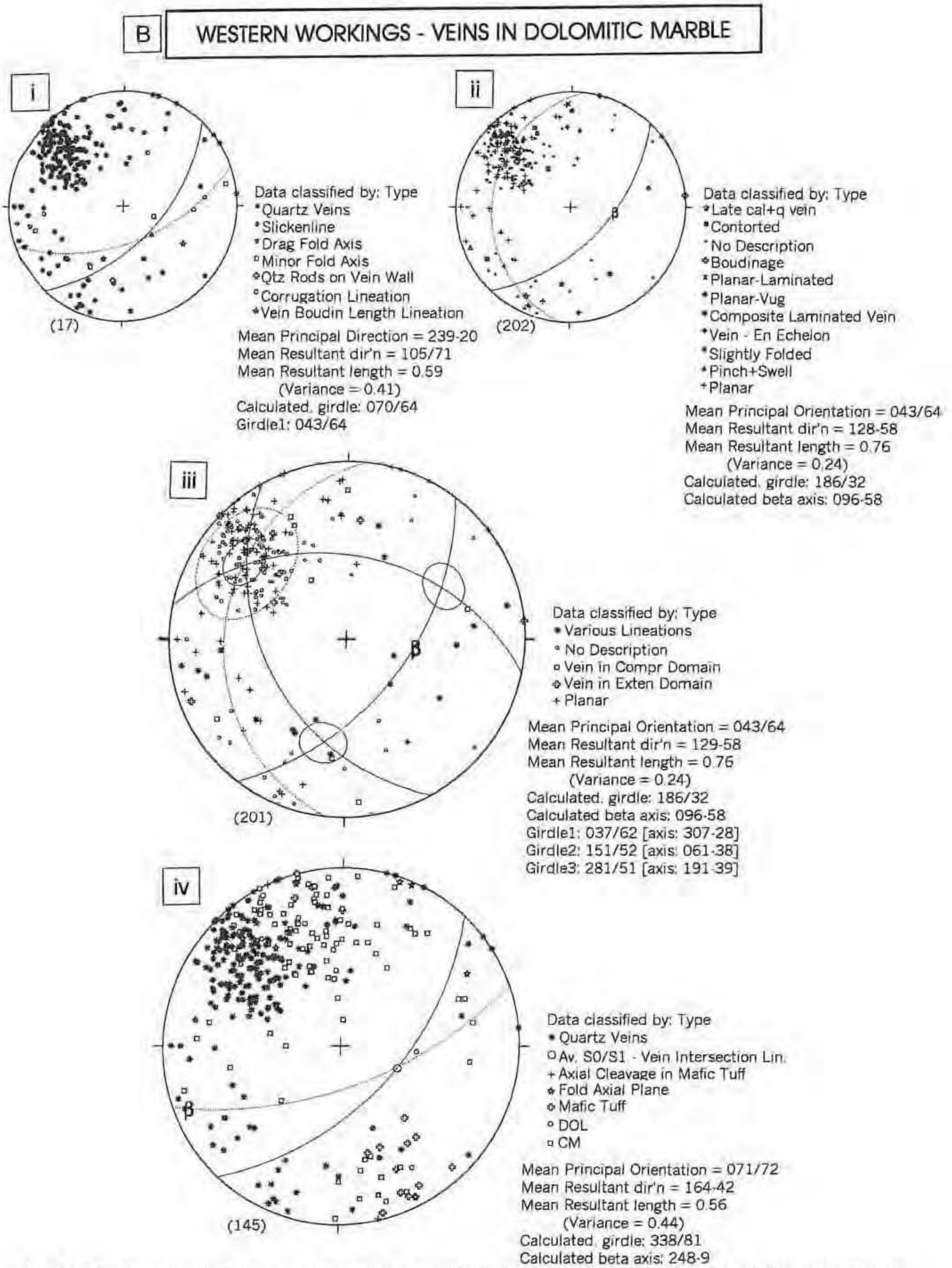

Fig. 6.18[B]: Lower hemisphere, equal area stereographic projections of a variety of structural data in relation to the quartz veins found in the dolomitic marbles of the Western Workings area. (i) Plot showing classified lineation data and unclassified poles-to-vein data. (ii) Plot showing a detailed morphological classification of veins (poles-to-planar elements). Open symbols correspond to poles-to-extended planar elements of veins; closed symbols correspond to poles-to-folded planar elements of veins. (iii) Poles-to-veins classified according to whether the veins are found in extensional or compressional domains. Minor fold and corrugation fold axes (see plot i) are largely parallel or sub-parallel to the Y-axis. Method of Talbot (1970) used to determine orientation and shape of strain ellipsoid: $\psi_{xz} = 23°$, $\psi_{yz} = 23°$; a ≈ 1.00, b ≈ 2.64; X = 061°-38°, Y = 192°-40°, Z = 307°-28° (trend-plunge of axes). (iv) Poles-to-veins and poles-to-$S_{0,1}$ foliation defining an average intersection lineation of 108°-62° (trend-plunge).

are best developed in the northwestern parts of the mapping area. The veins are generally thin (<5 cm) but can extend for several 10's of metres in length. Most of the veins hosted by dolomitic marble are relatively planar, often displaying pinch-and-swell structures. There are a few places in the lower parts of the dolomitic marble unit where poorly developed Riedel shear-related veins are found (Plate 6.22). The arrangement of veins in the P, R and T shear positions is compatible with a dextral shear sense. Near the contact between the DM unit and the TM unit, a thick composite vein is developed with significant malachite staining.

Fig. 6.18[B] shows the orientation and morphology of veins in the dolomitic marbles. The average intersection lineation between the mean vein orientation in the dolomitic marbles and the $S_{0,1}$ layering is 108°-62° (trend-plunge). The poles-to-extended planar elements of veins define a much tighter overall field of extension because of the competent nature of the dolomitic marbles. This allows the position of Z to be defined, but the differentiation of the X and Y axes remains difficult. If the apical angles, ψ_{xz}° and ψ_{YZ}° are in the region of 23° each, then this would imply a uniaxial oblate ellipsoid (Figs. 6.19-20).

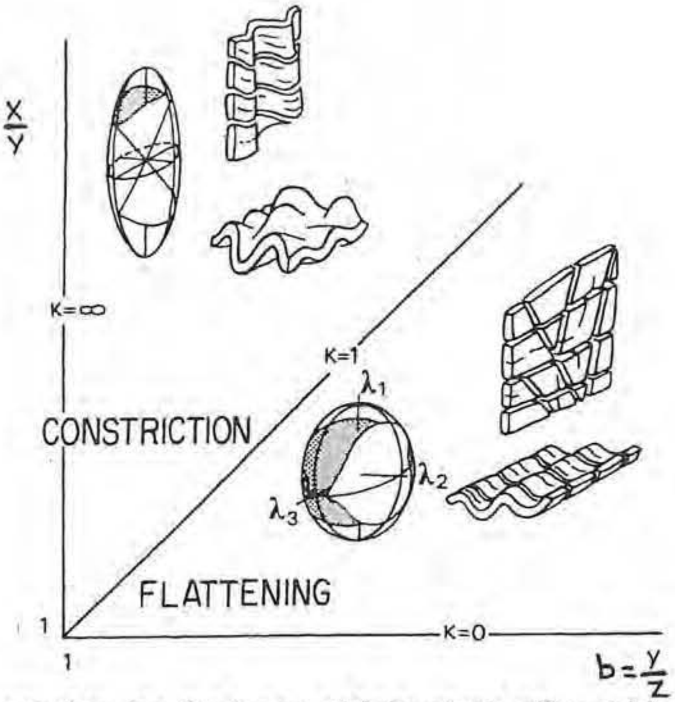

Fig. 6.19: Flinn diagram showing the types of finite strain ellipsoid found by means of invariant surfaces. a = X/Y; b = Y/Z; k = (a-1)/(b-1) and X > Y > Z. Tectonites formed through pure flattening plot along the x-axis (uniaxial oblate ellipsoid: X = Y > Z); tectonites formed by pure constriction result plot along the y-axis (uniaxial prolate ellipsoid: X > Y = Z); tectonites formed by plane strain plot along a 45°-sloping line that intersects the origin of the plot (Nicolas, 1987, Fig. II.14, p.185).

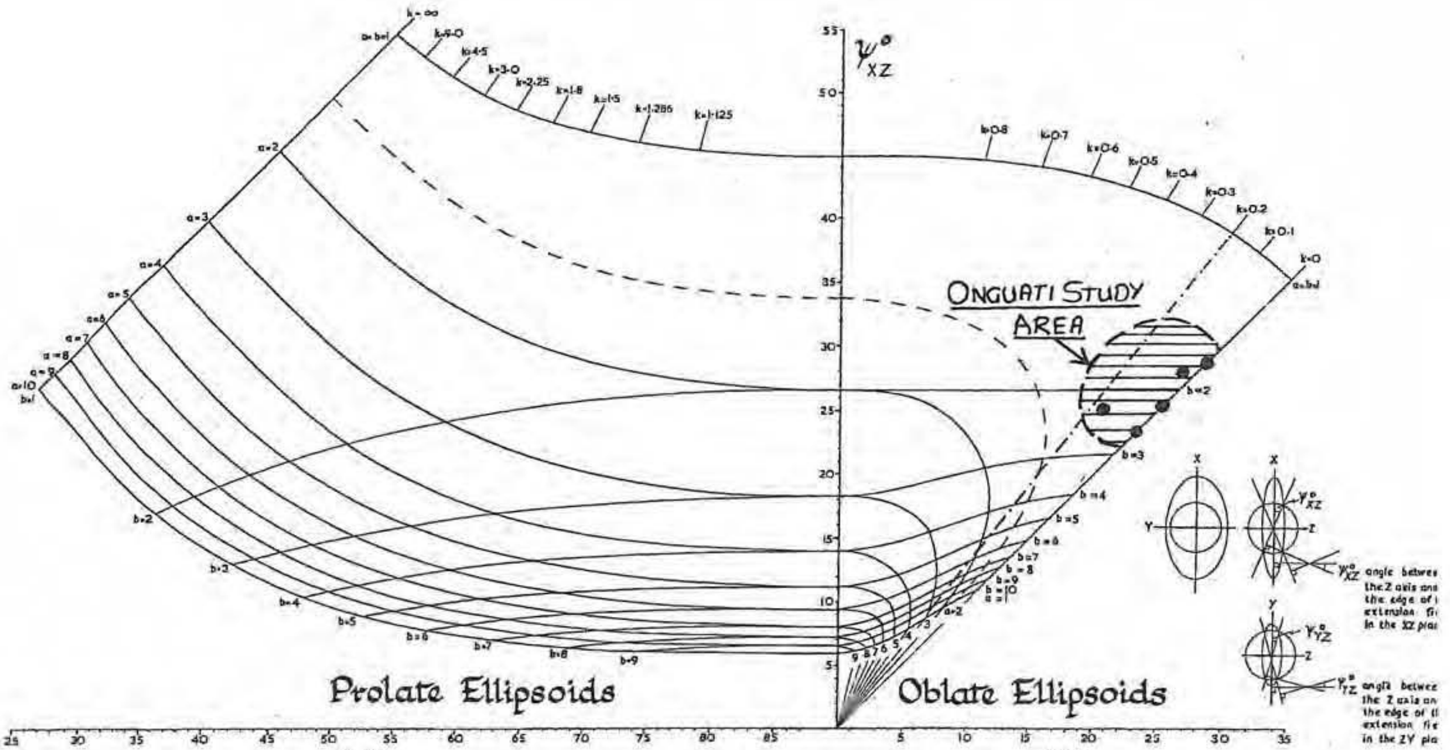

Fig. 6.20: Axial ratios (a = X/Y and b = Y/Z) of strain ellipsoids in relation to the apical angles (ψ°_{XY}, $\psi^\circ_{XZ}\psi^\circ_{YZ}$) of the surface of no finite longitudional strain in their principal planes (Talbot, 1970, Fig. 5, p.62-63). Vein data from veins in the calcitic and dolomitic marbles of the Onguati Mine, Brown Mountain and Western Working areas are plotted in the diagram, and indicate that the veins developed during a flattening strain state (X ≈ Y > Z).

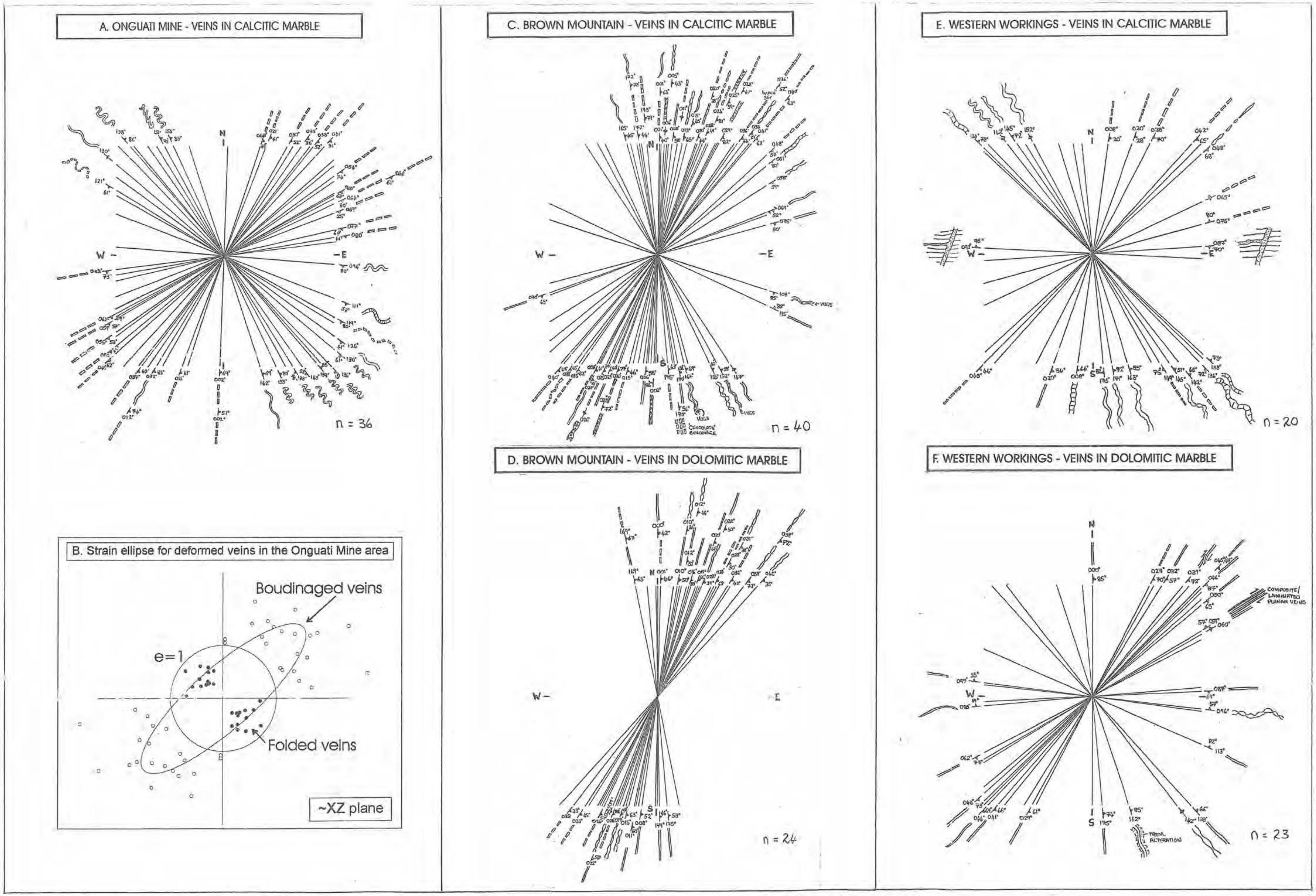

Fig. 6.21: Orientation diagrams illustrating the main vein morphologies that have developed in response to local strain in the Onguati study area. (A) At Onguati Mine, ~NE-SW striking veins are most intensely extended, whereas ~NW-SE striking veins are highly folded. (B) Strain ellipse determined from the magnitude of extension 'e' of boudinaged veins (+ve number) and compressed veins (-ve number) recorded in the Onguati Mine area. The magnitude of extension for each vein is plotted along a radius parallel to vein strike to produce each data point in the plot (n=35). (C and D) Intensely boudinaged veins in the calcitic and dolimitic marbles of Brown Mountain are generally aligned with a more NNE-SSW strike. (E and F) Intensely boudinaged veins in the calcitic and dolomitic marbles of the Western Workings area have NE-SW to NNE-SSW strikes.

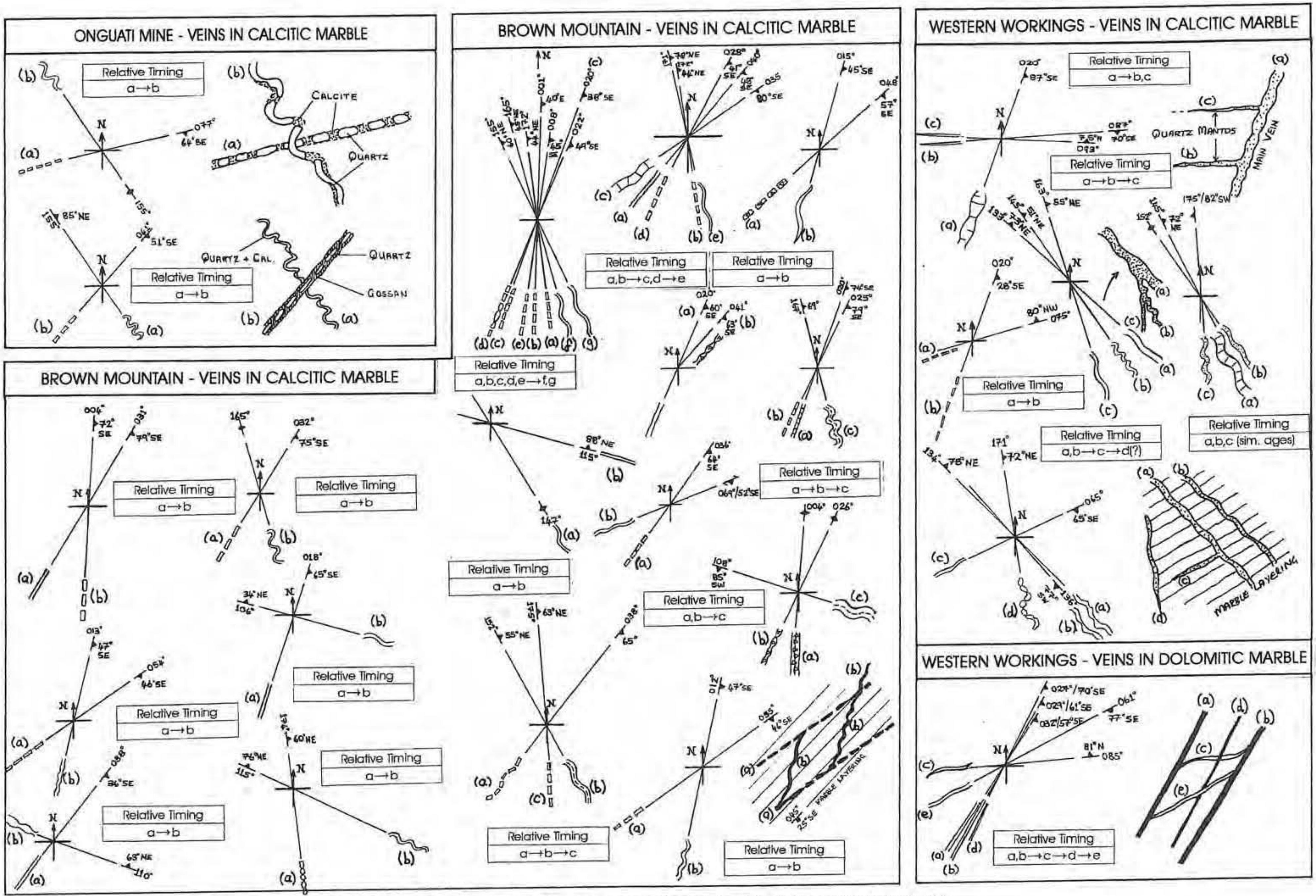

Fig. 6.22: Orientation diagrams illustrating vein cross-cutting relationships in the calcitic and dolomitic marbles of the Onguati Mine, Brown Mountain and Western Workings areas. Sketches of vein morphology and configuration have also been included.

6.5. Joints

A brief study of the joints in the Onguati study area was undertaken because these structures are such ubiquitous features of the marbles, and because in some cases, systems of joints and shear fractures may provide an additional and independent means of interpreting the orientation of the local stress field at the time of their development. Sites were chosen in the calcitic and dolomitic marbles, with preference being given to outcrops where the 3D expression of a large number of joint traces could be easily ascertained. This allowed the strike and dip of some of the systematic joints to be measured. Where it was difficult or impossible to measure the 3D orientation of joints, only the trend was recorded. In this study the "circle inventory method" of collecting joint and shear fracture orientations was employed, as recommended by Davis & Reynolds (1996, p.725). The method involves marking a circle on the jointed outcrop using chalk attached to string of a given radius (commonly a 65 cm radius was chosen), and then measuring the orientations and lengths of all the contained joints and shear fractures. One of the main advantages of this technique is that it is possible to plot joint length-azimuth rose diagrams where the length of each sector in the rose is proportional to the sum of the lengths of joints whose orientations lie in that sector. In addition, the circle inventory method allows the fracture density to be easily calculated for each station as follows (Davis & Reynolds, 1996, p.726):

$$\rho_f = \frac{L}{\pi r^2} \qquad [6.1]$$

where: ρ_f = fracture density

L = cumulative length of all fractures

r = radius of inventory circle

Joint rosettes (frequency-azimuth), joint length-azimuth rose diagrams and strike histograms are presented for joints at selected sites in the calcitic and dolomitic marbles, and for all the joint data collected (including measurements made during mapping) in the Onguati Mine (Figs. 6.23 and 6.24), Brown Mountain (Fig. 6.25) and Western Workings areas (Fig. 6.26 and Fig. 6.27). At Brown Mountain and Western Workings the joint length data was normalized to a circle radius of 65 cm before plotting in the length-azimuth rose diagrams.

From the various plots it is possible to classify the joints into four main sets (Table 6.4)

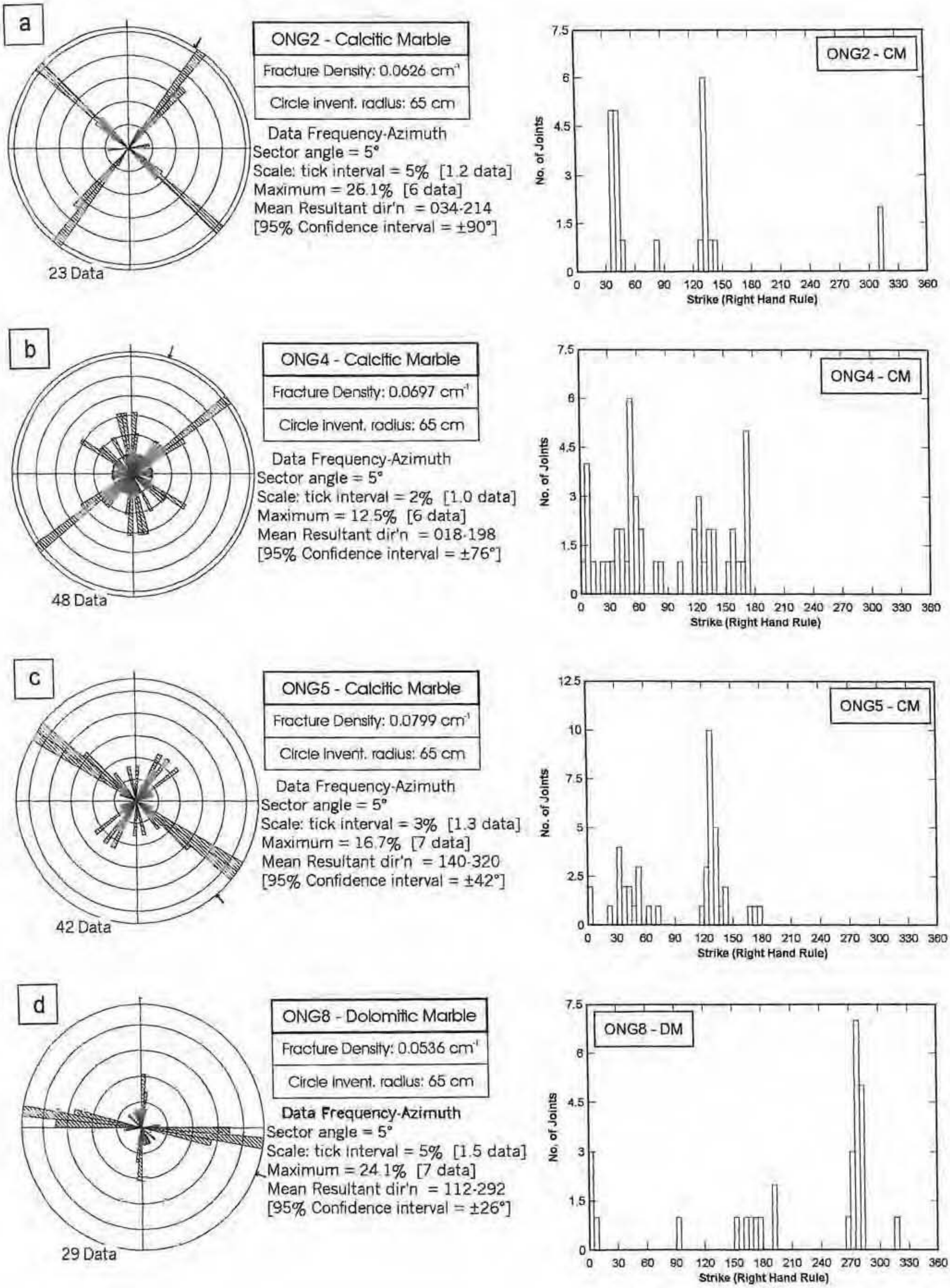

Fig. 6.23: Joint rosette diagrams (frequency-azimuth) and strike histograms for joint orientation data collected (circle-inventory method) in the calcitic (a-c) and dolomitic marbles (d) of the Onguati Mine area [joint strike recorded on histograms is related to dip direction (i.e. righthand rule); when dip could not be measured strike was simply recorded between 0° and 180°]. Locations of (a) ONG2: 120S/260E; (b) ONG4: 130S/210E; (c) ONG5: 10N/70E; and (d) ONG8: 40S/40E.

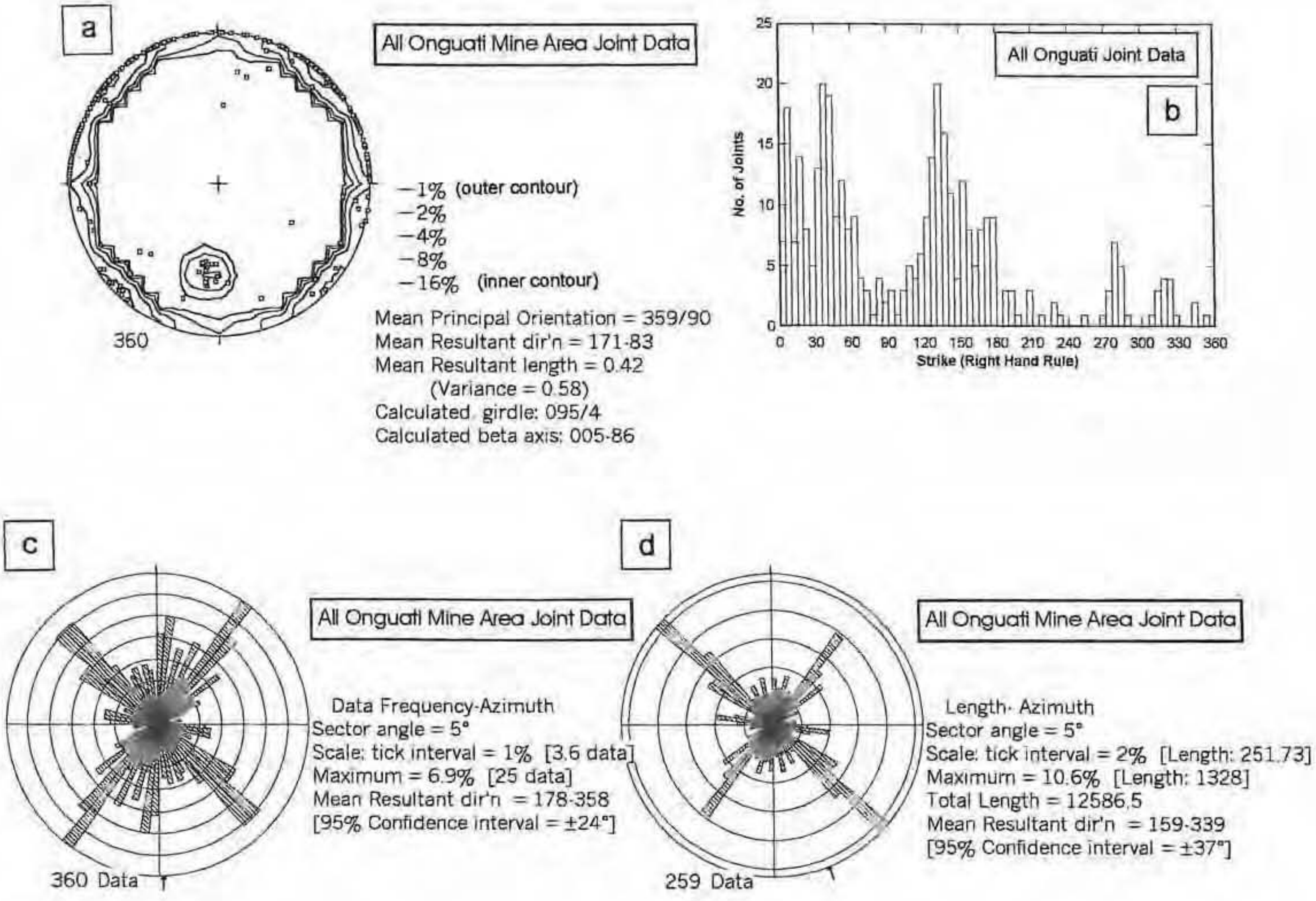

Fig. 6.24: (a) Equal area contour plot with poles-to-joints, (b) joint histogram, (c) joint rosette (frequency-azimuth) and (d) joint length-azimuth rose diagram (length in cm) for all joint data collected in the Onguati Mine area. Note that the length of each sector in the length-azimuth rose diagram (plot d) is proportional to the sum of lengths of joints measured by the circle invenotry method whose orientations lie within that sector.

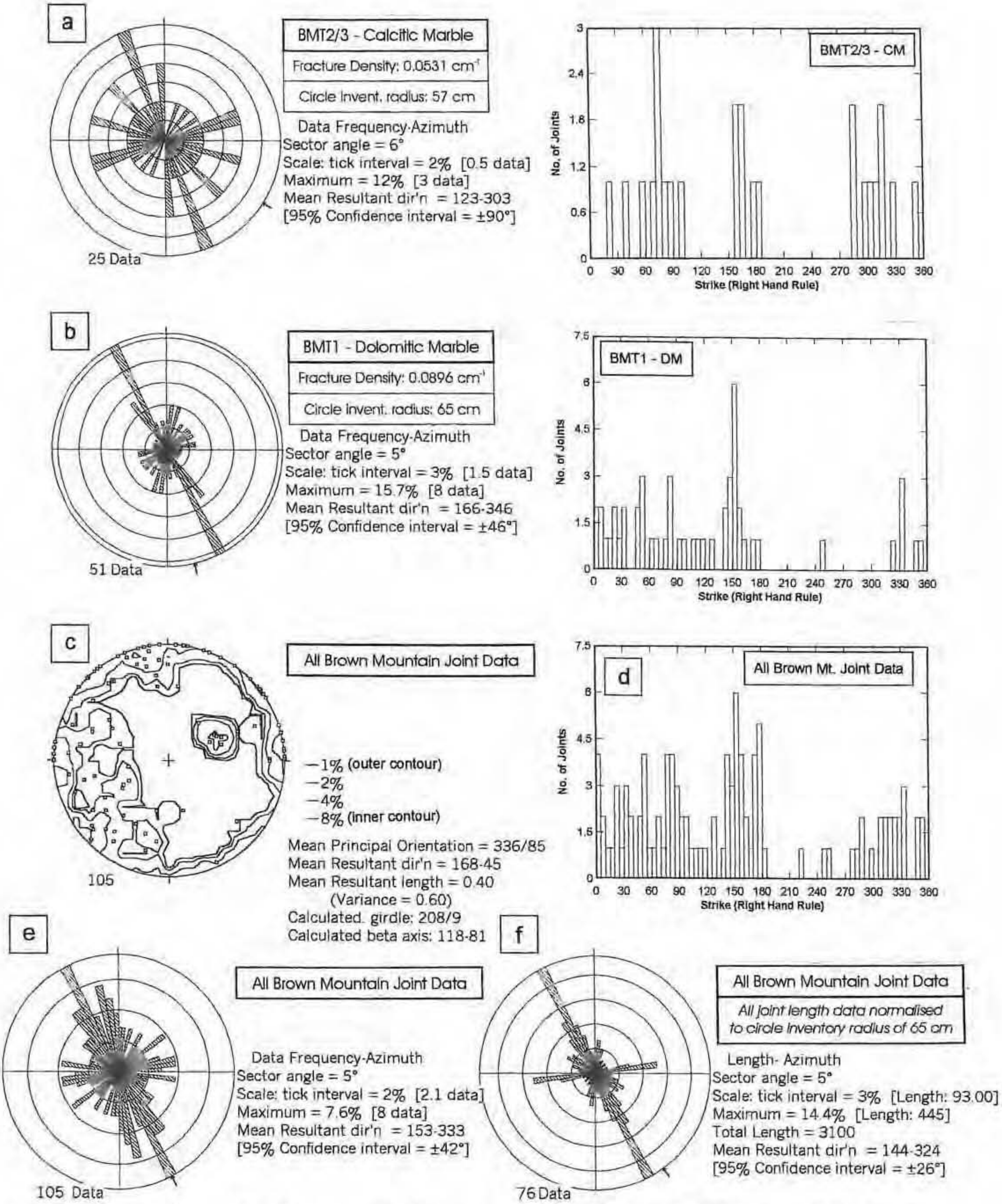

Fig. 6.25: Joint rosette diagrams, strike histograms and contour plots for joint orientation data collected (circle-inventory method) in the calcitic (a) and dolomitic marbles (b) of the Brown Mountain area [joint strike recorded on histograms is related to dip direction (i.e. righthand rule); when dip could not be measured strike was simply recorded between 0° and 180°]. (c) Equal area contour plot with poles-to-joints, (d) strike histogram, (e) joint rosette (frequency-azimuth) and (f) joint length-azimuth rose diagram (length in cm) for all joint data collected in the Brown Mountain area. Locations of (a) BMT2: 10S/840W and BMT3: 10S/980W; (b) BMT1: 180N/1080W.

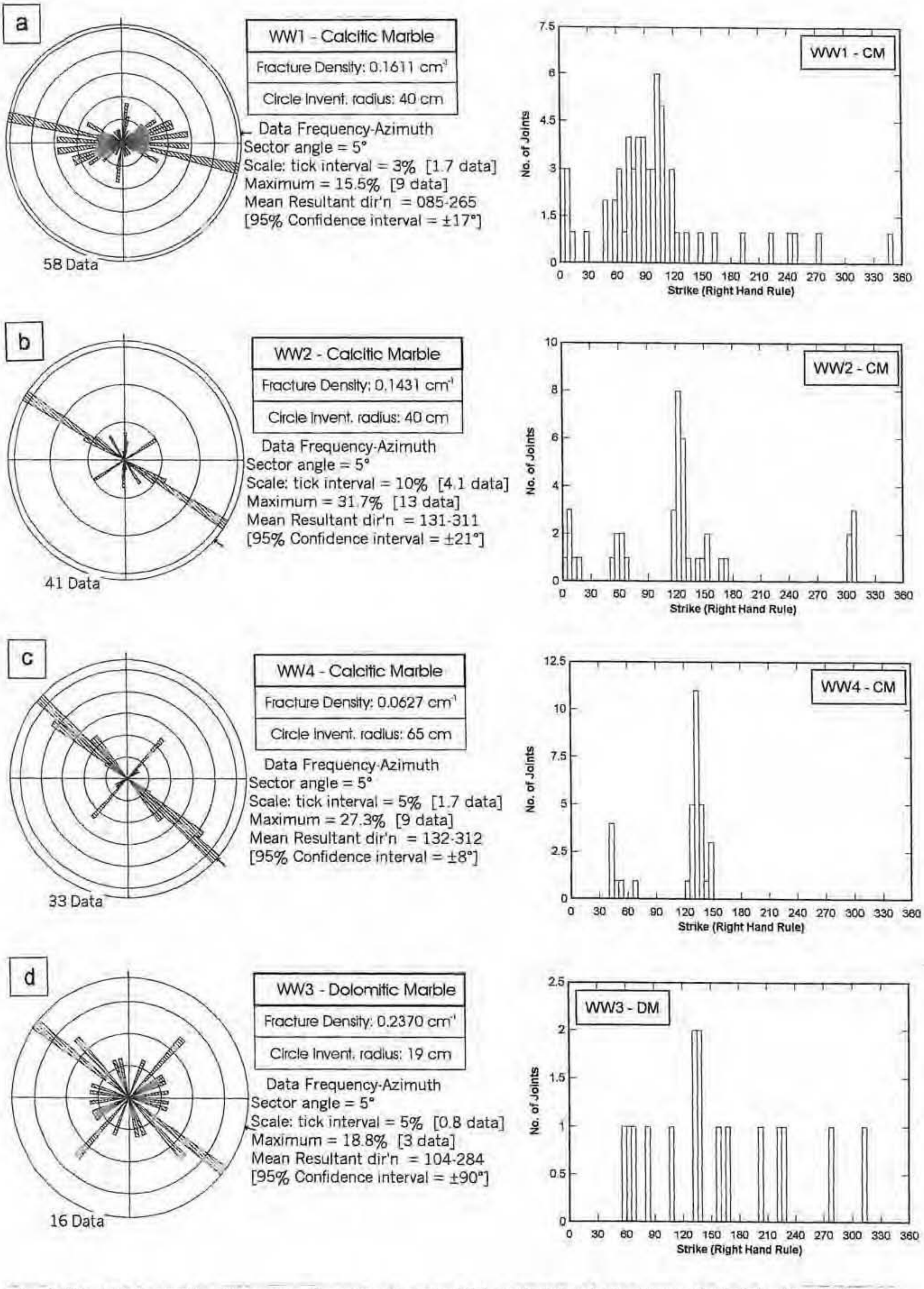

Fig. 6.26: Joint rosette diagrams (frequency-azimuth) and strike histograms for joint orientation data collected (circle-inventory method) in the calcitic (a-c) and dolomitic marbles (d) of the Western Workings area [joint strike recorded on histograms is related to dip direction (i.e. righthand rule); when dip could not be measured strike was simply recorded between 0° and 180°]. Locations of (a) WW1: 20S/1840W; (b) WW2: 20N/1800W; (c) WW4: 10N/2070W ; (d) WW3: 190N/2020W.

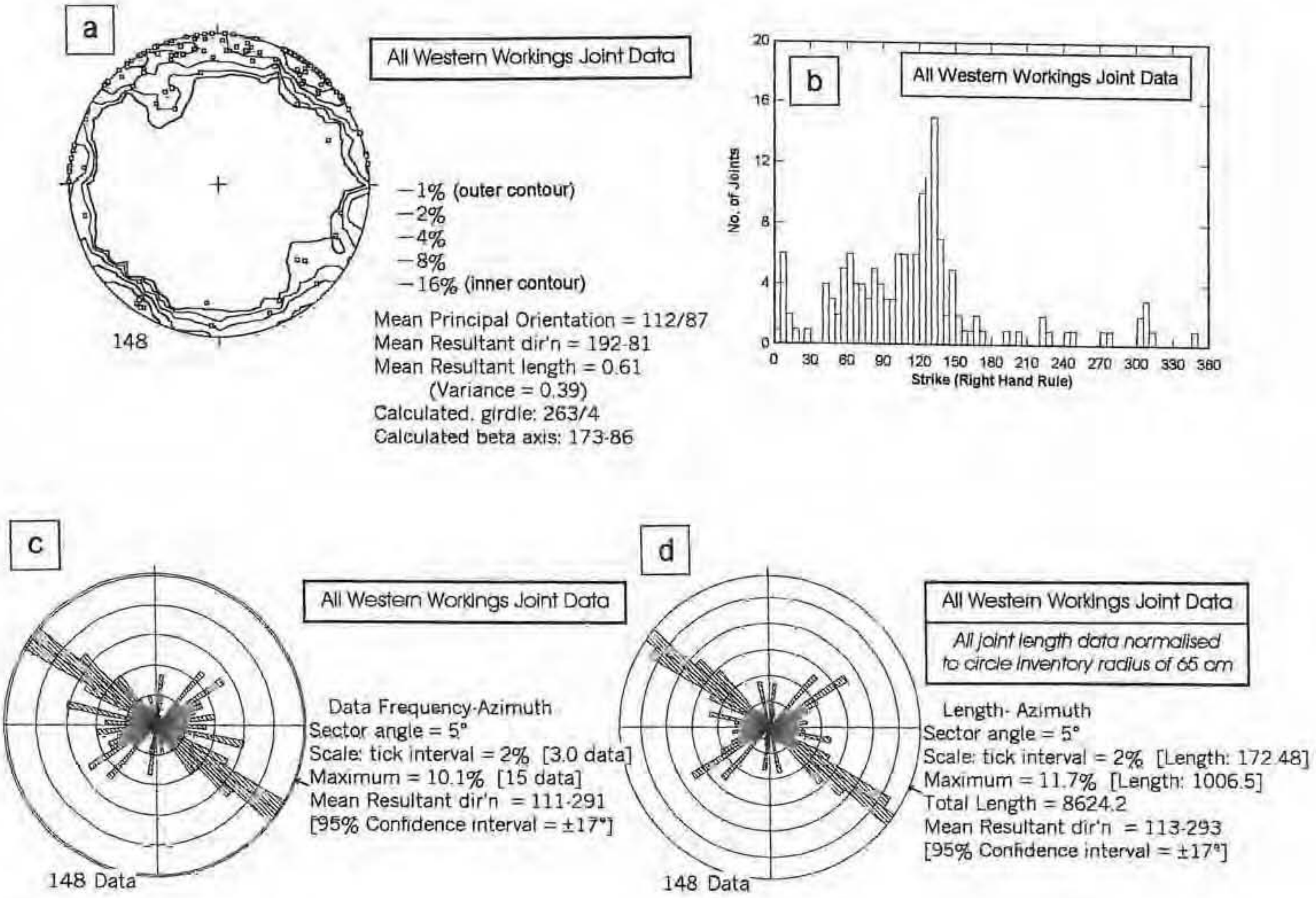

Fig. 6.27: (a) Equal area contour plot with poles-to-joints, (b) joint histogram, (c) joint rosette (frequency-azimuth) and (d) joint length-azimuth rose diagram (length in cm; all joint length data normalized to circle inventory radius of 65cm) for all joint data collected in the Western Workings area. Note that the length of each sector in the length-azimuth rose diagram (plot d) is proportional to the sum of lengths of joints measured by the circle inventory method whose orientations lie within that sector.

based on their strikes or trends (no 3D control on joint attitude). The joints have been labelled clockwise from north. In all the areas, the J1 and J3 joint sets are commonly well developed and are oriented at approximately 90° to one another. The J3 joints in the Onguati study area are the dominant joint set. J3 joints are seldom associated with displacement and may have developed by mode I 'opening' fracture processes. Joints belonging to the J2 set can display millimetre-scale, dextral displacement, while the J4 joints are often associated with sinistral offset. The J2 and J4 sets may be more appropriately termed shear fractures. It is common at individual sites in the marbles to find the J2 and J4 sets either developed perpendicular to one another, or separated by an angle of ~60°. In the latter case they are conjugate sets with complementary senses of shear.

Table 6.2: Trends of main joint sets in the calcitic and dolomitic marbles of the Onguati Mine, Brown Mountain and Western Workings areas. CM = calcitic marble; DM = dolomitic marble; ***d*** = dominant joint set; *pr* = prominent joint set; *m* = minor joint set.

Joint Set	**Onguati Mine**				**Brown Mountain**				**Western Workings**			
	CM		DM		CM		DM		CM		DM	
J1	35-50°	*pr*	-	-	~50°	*pr*	50-60°	*m*	40-60°	*pr*	40-45	*pr*
J2	85-95°	*m*	90-105°	***d***	75-90°	*m*	75-85°	*m*	90-105°	*m*	80-100°	*m*
J3	120-135°	***d***	-	-	140-155°	***d***	140-150°	***d***	120-135°	***d***	125-140°	***d***
J4	165-185°	*pr*	180-190°	*pr*	170-200°	*pr*	185-200°	*pr*	165-190°	*m*	155-170°	*m*

6.6. Structural Relationships Across Scale

In this section, an attempt has been made to relate the various structures detected on regional geophysical images and aerial photographs with structures observed in the Onguati study area. The proposed relationships are in some cases tentative, but provide a starting point for further study.

6.6.1. Development of the Onguati-Kranzberg Anticlinorium

The Onguati-Kranzberg anticlinorium is thought to have developed during a single episode of NNW-directed tectonic transport as illustrated in Fig. 6.28 (i.e. the direction of greatest principal subregional stress, $SR\sigma_1$, is aligned NNW-SSE, perpendicular to the anticlinorium fold axis). In the initial stages of anticlinorium formation, the structure may have been fairly upright, but as the fold became further tightened it was forced to overturn towards the NNW (i.e. the anticlinorium developed a moderately inclined, ~SE-dipping axial plane). At the same time, the central regions of the fold structure experienced severe thinning. The Etusis Formation quartzitic rocks that core the anticlinorium may have behaved in a more competent manner than the surrounding rocks of the Arandis, Karibib and Kuiseb Formations, and could have 'necked' during regional deformation. The overlying, less competent marbles, calc-silicate rocks and schists would have flowed into the 'neck' region to form a type of mega-scale pinch-and-swell structure with an 'hourglass' form. The escape of the Etusis Formation rocks may have helped develop the bulbous ends and crestline depression of the Onguati-Kranzberg anticlinorium.

The leucogranite body in the northeastern part of the Onguati-Kranzberg anticlinorium is classed as part of the post-tectonic Ꞓglp group of intrusives (1:250 000 Omaruru Geological Sheet 2114). However, structural relationships, such as the slightly elongated form of the intrusive body parallel to the fold axis and the severely thinned layers in the southeastern limb, suggest that it may have been syntectonic. If this was the case then this intrusive body could have acted as a rigid body in the northeastern part of the structure. Strain shadows could have developed in a triangular area SW of the granitic body, and also around the quartzitic core in the SW (Fig. 6.28). These areas warrant further exploration because they may have experienced enhanced fluid flow (i.e. sites of low mean stress) during the same event that resulted in Cu±Au vein mineralization in the Onguati study area.

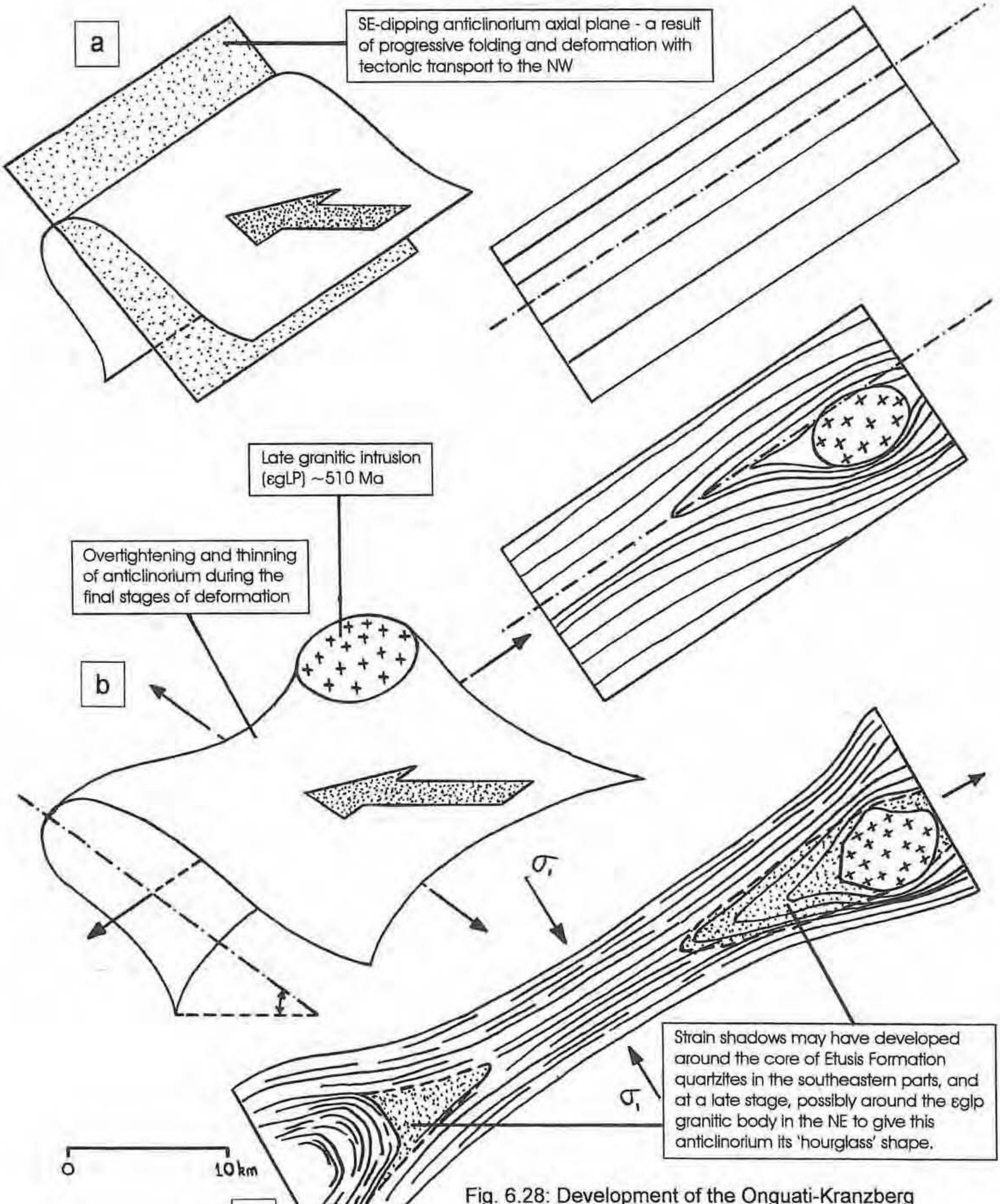

SE-dipping anticlinorium axial plane - a result of progressive folding and deformation with tectonic transport to the NW

Late granitic intrusion (εgLP) ~510 Ma

Overtightening and thinning of anticlinorium during the final stages of deformation

Strain shadows may have developed around the core of Etusis Formation quartzites in the southeastern parts, and at a late stage, possibly around the εglp granitic body in the NE to give this anticlinorium its 'hourglass' shape.

Fig. 6.28: Development of the Onguati-Kranzberg anticlinorium. (a) Anticlinorium is formed and as it becomes tightened, it becomes more overturned toward the NW; (b and c) anticlinorium develops a crestline depression (Onguati study area situated in this region) and strain shadows develop.

Fig. 6.29 illustrates how the various structures observed in the Onguati study area could be related to the development of the Onguati-Kranzberg anticlinorium. The diagram is highly simplified and does not show the final 'hourglass' shape or the overturned attitude of this regional structure. Many of the structures found in the Onguati study area can be explained in terms of the major competency contrast that exists between the calcitic and dolomitic marbles, and the potentially different mechanisms of folding that occurred in each during anticlinorium formation. It is envisaged that the ductile calcitic marble package underwent flexural flow folding which induced the formation of a series of lower-order drag folds. The occurrence of numerous S-, Z- and M-folds at the outcrop-scale in the Onguati study area represent parasitic features on higher-order, deposit-scale drag folds (Fig. 6.29, c and f). The ~SE-dipping axial planes of F_1 and F_2 folds, the post-buckle flattening and intense boudinage of the calc-silicate rocks in the limbs of folds (Fig. 6.29, d and e) are all compatible with a NNW-SSE direction of the SRσ_1. The plastic nature of the calcitic marbles can explain the curved fold hinges, the opposing ~SW- and NE-plunge directions of minor fold axes (e.g. Brown Mountain folds), and the development of periclinal or domal folds without invoking polyphase deformation.

The well-layered TM unit, separating the less competent calcitic marbles from the overlying dolomitic marbles, may have accommodated much strain by flexural slip folding, and this could have led to the creation of slickenlines oriented perpendicular to the regional fold axes. The existing layering could have been further enhanced during slip. The absence of metre-scale folding in the dolomitic marbles is a testament to their more competent nature and lack of layering, and suggests that these rocks did not experience significant flexural flow folding. Instead the dolomitic marble unit may have experienced flexural slip so that shearing was concentrated in the underlying TM unit and possibly along major lithological boundaries within the dolomitic marble unit (Fig. 6.29, j).

The four joint sets developed in the calcitic and dolomitic marbles could also be related to the formation of the Onguati-Kranzberg anticlinorium (Fig. 6.29, m). The J3 joint set is arranged perpendicular to the fold axis of the Onguati-Kranzberg anticlinorium. These cross joints parallel the proposed SRσ_1 direction and may have been formed by mode I 'opening' fracture processes (e.g. Engelder & Peacock, 2001). The J2 and J4 joints intersect at angles of between ~60° and 90°and are commonly associated with small dextral and sinistral displacements respectively. The J2 and J4 joint sets may represent diagonal or oblique joints that developed on the anticlinorium by mode II or III fracture processes. This aspect requires further study.

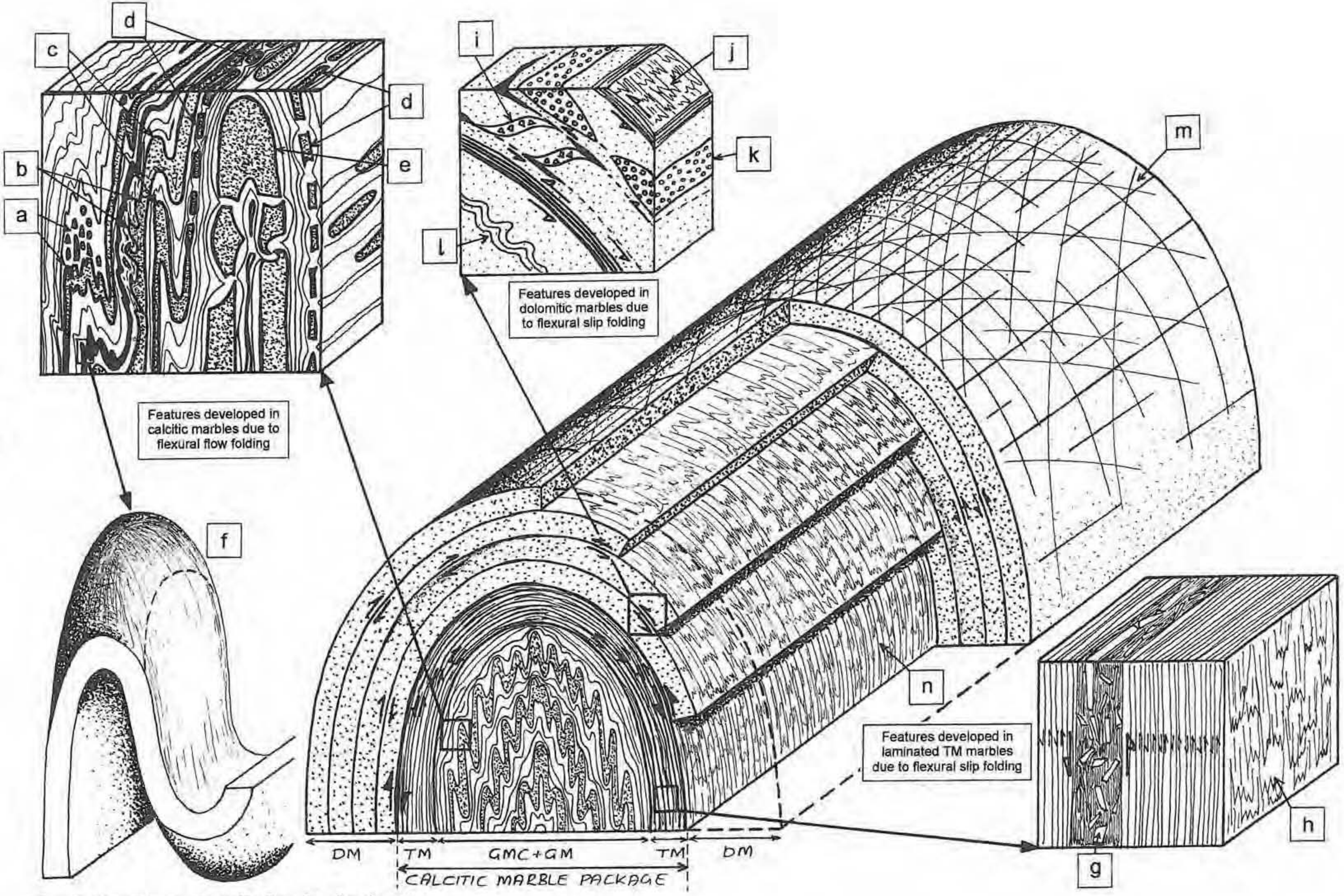

Fig. 6.29: *see overleaf for key to structures.*

Fig. 6.29: Diagram illustrating folds, joints and other structures at the deposit- or outcrop-scale and their relationship to the development of the anticlinorium in the Karibib Formation marbles of the Onguati area.

Structures related to flexural flow folding in the calcitic marbles:

(a) Transposition of isoclinal folds into intrafolial hinges and lenses to form a composite $S_{0,1}$ foliation.

(b) Drag- or asymmetric cuspate-lobate folds are formed due to the marked competency contrast between the calc-silicate unit and the surrounding ductile calcitic marbles. The calc-silicate 'tongues' are stretched out and transposed into the composite $S_{0,1}$ foliation as highly flattened lenses.

(c) Isoclinal Z-fold, parasitic to the larger anticlinal structure.

(d) Folded calc-silicate unit with boudinaged limbs – in 3D the calc-silicate layers may have experienced chocolate tablet boudinage (see top side of sketch).

(e) Isoclinal fold of calc-silicate rocks with intensely boudinage limbs.

(f) Non-cylindrical folding is common in the calcitic marbles and it is common to find periclinal or domal folds measuring many metres in length.

Structures related to flexural slip folding in the TM unit:

(g) Possible tectonic breccia due to intense flexural-slip in laminated calcitic marbles. It is also possible that isoclinal, drag folds were fragmented, rotated and transposed into the $S_{0,1}$ foliation as is the case in the lower calcitic marble units.

(h) Slickenlines may be developed on thin, calcitic marble layers.

Structures related to flexural slip folding in the dolomitic marbles:

(i) En echelon breccia pods bound by quartz+carbonate veins and fractures.

(j) Carbonate slickenlines are preserved on some layer surfaces and may be related to flexural-slip folding.

(k) Boudinaged and pinched-out quartzitic bodies containing deformed pisoliths.

(l) Near the base of the dolomitic marbles and in the upper TM unit, small open-to-tight folds can be formed.

General structures related to anticlinorium formation:

(m) Four prominent joint/shear fracture sets are developed in the Onguati study area and are most likely related to folding. The joint sets are either perpendicular or parallel to the regional fold axis of the anticlinorium, or form conjugate shear fracture sets (associated with very small displacements) oblique to the fold axis.

(n) Slickenlines developed due to flexural slip folding in the lithologies of the Onguati-Kranzberg anticlinorium.

6.6.2. Development of the Shear Zone System in the Onguati-Kranzberg Anticlinorium

A major competency contrast is thought to exist between the marbles of the Navachab Member and the overlying calc-silicate rocks, marbles and schists of the Onguati Member (Fig. 6.14). During early folding (upright axial planes), the Navachab-Onguati Member contacts on either limb of the anticlinorium may have accommodated considerable flexural-slip shearing. These surfaces could have been the precursors to major shear zones and thrusts that developed in the later stages of anticlinorium development. As the Onguati-Kranzberg anticlinorium became more overturned towards the NW and the central regions tightened, so the former flexural-slip surface on the SSE-facing limb would have experienced increased NNW-overthrusting. The major flexural-slip surface on the NNW-facing limb could also have been re-activated as a reverse fault (dip-slip shear sense would have reversed)

During the late stages of folding and at the start of NNW-directed shearing/faulting, it appears that the direction of greatest principal subregional stress (SRσ_1) was oriented obliquely to the anticlinorium fold axis. The identification of NW- to NNW-trending lineaments that offset regional layering with a dextral shear sense on the aeromagnetic images and aerial photographs, the configuration of R and R' conjugate shear zones/faults, and the NNE- to NE-strikes of boudinaged quartz veins, all suggest the SRσ_1 direction may have rotated anticlockwise from a NNW-SSE to a WNW-ESE orientation. This satisfies the small component of dextral strike-slip movement observed on the thrust fault at Western Workings, and is compatible with the formation of s- and n-type flanking-fold structures that record a dextral sense of shear along boudinaged veins. The change in SRσ_1 direction may have happened quite rapidly (possibly due to changes in tectonic configuration?) and must have occurred at the onset of brittle-ductile conditions because there is no evidence of folds with different vastly attitudes in the Onguati study area. Further study is required to constrain the structural evolution of the shear zone/fault system in the Onguati-Kranzberg anticlinorium.

6.6.3. Relationship between the Shear Zone System and Onguati Study Area Veining

In the lower half of Fig. 6.30, the positions of the Onguati Mine, Brown Mountain and Western Workings vein systems have been marked in relationship to the shear zone/fault system (elements classified as possible P, R and R' shears in a Riedel shear system) found in this part of the Onguati-Kranzberg anticlinorium. The average vein orientation of the vein arrays

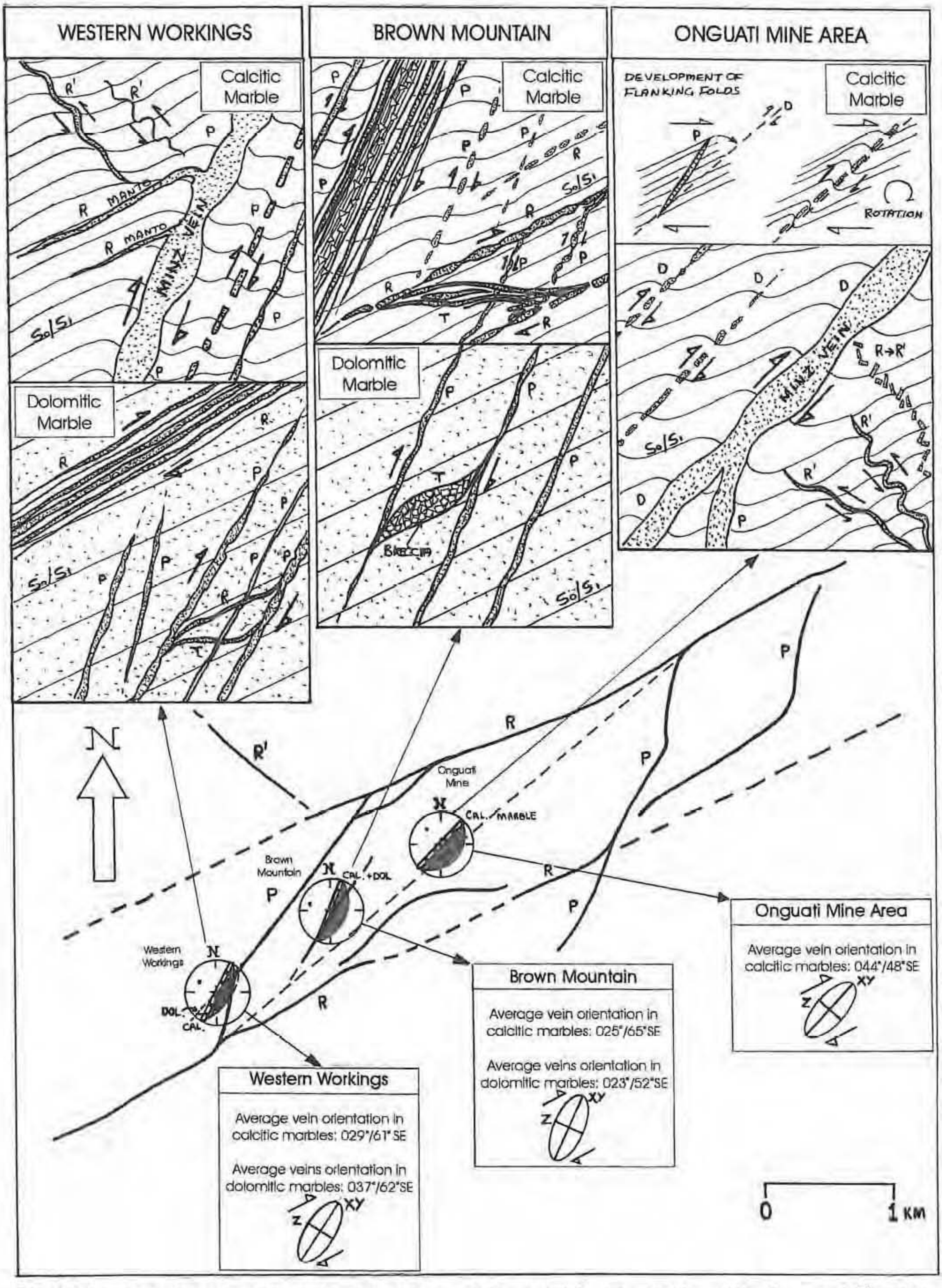

Fig. 6.30: Vein orientation and configuration in the calcitic and dolomitic marbles of the Onguati Mine, Brown Mountain and Western Workings areas. Veins at Onguati Mine are aligned with the longest diagonal of the parallelogram shaped-fault system (possible D shear, or imposed shear direction). Brown Mountain and Western Workings veins are aligned with the P shears/faults that they are closely associated with. Sketches show the geometry and style of the veins found in the different areas, and the development of flanking folds.

hosted by both calcitic marble and dolomitic marble have been shown in simple stereonet plots. It is apparent from this diagram that subtle differences exist between the average vein orientations of the 3 areas. Veins in the Onguati Mine area have a mean strike of ~NE-SW (veins with this orientation are 'necked') and align with the longest diagonal of the parallelogram-shaped arrangement of faults developed around the Onguati study area. If the shear zones/faults are correctly classified as a Riedel system then these veins parallel the direction of imposed shear (i.e. this is the direction of a possible D shear which is aligned ~45° to the SRσ_1 direction at the time of shearing/faulting). This could explain why s-type flanking-folds are so well developed around the boudinaged veins of the Onguati Mine area (e.g. Plates 6.7-6.10). Intense shearing in the calcitic marbles could have resulted in numerous drag-fold trains (dextral sense of rotation) in which veins were developed at an early stage (synthetic dextral shear displacements occurred along many of the boudinaged veins). The veins and their flanking-folds may also have undergone passive rotation as the ductile marbles flowed during deformation (Fig 6.30, top right inset).

In contrast, the veins in the calcitic and dolomitic marbles of the Brown Mountain and Western Workings areas have strikes of ~30° (NNE-SSW) and are not associated with well-formed flanking-folds. The deformed veins in these areas are largely sub-parallel to the proposed P shear directions of the shear zone developed at Brown Mountain and the thrust/reverse fault at Western Workings. Intense ductile shearing in the calcitic marbles of at Brown Mountain resulted in high density veining, local Riedel-shear vein sets (P, R, D and T shear positions), and large composite and/or brecciated vein sets (top middle inset of Fig. 6.30). At Western Workings some of the veins in the dolomitic marbles developed Riedel shear-vein arrangements, but in the calcitic marbles the style of veining is similar to that at Onguati Mine (top left hand corner of Fig. 6.30).

7. HYDROTHERMAL VEIN MINERALIZATION

7.1. Introduction

Ore mineralization is best developed in the vein arrays hosted by calcitic marble in the Onguati Mine, Brown Mountain and Western Workings areas. Veins hosted by the overlying dolomitic marbles are generally weakly developed and appear sulphide-poor. Minor disseminated, replacement-type sulphide mineralization is also encountered along marble–calc-silicate layer interfaces for considerable distances (<10 metres) either side of well-mineralized veins. The quartz veins commonly consist of pyrrhotite, chalcopyrite, sphalerite and pyrite with rare occurrences of arsenopyrite. At Onguati Mine and Western Workings, the largest veins were mined for their rich copper mineralization and are reported to have produced good Au and Ag credits (Petzel, 1988a, p.34). Descriptions of the mineralization in the Onguati study area have been provided by Gray (1988) and Petzel (1988a), and Steven (1993) has detailed the ore petrography and exsolution phenomena found at Onguati Mine. New observations of the field characteristics and ore petrography of the vein arrays are presented in this study, together with representative analyses of some of the more important or unusual sulphide phases (Tables 7.1 - 7.7).

7.2. Mineralization in Veins Hosted by Calcitic Marble

The dominant gangue mineral in veins hosted by calcitic marble in the Onguati study area is milky quartz, but in smaller veins, calcite can also make up a substantial part of the vein. Small amounts of biotite, chlorite and muscovite may also be present. Sulphide mineralization is best developed along quartz vein margins, in fractures that cross-cut veins perpendicular to their margins, in open spaces in brecciated veins, and in vugs or fissures that divide veins along their lengths.

7.2.1. Onguati Mine

At Onguati Mine, the bulk of the mineralization is hosted by deformed, 1 to 3 metre-thick quartz veins. However there are places adjacent to some thick, well-mineralized quartz veins (e.g. area around 10N/180E) where massive sulphide mineralization has extended into, and replaced, metre-scale regions of the calcitic marble. The sulphides have since oxidized to thick gossan units that retain the original layering and folding of the marbles they replaced. The mineralized quartz veins at Onguati Mine are composed of 5% to 60% (large veins average ≈ 40%) sulphide, including substantial amounts of chalcopyrite and pyrrhotite with lesser amounts of pyrite, sphalerite, bornite and chalcocite, and traces of arsenopyrite and cobaltite.

Arsenopyrite grains in the Onguati Mine ore samples can contain trace amounts of Bi, Co and Ni (Table 7.1), the last two of which, may substitute in small quantities for Fe (Deer *et al.*, 1992). Cobaltite inclusions in chalcopyrite may also have anomalous Bi contents (Table 7.2), and many pyrrhotite, chalcopyrite, pyrite and sphalerite grains (Tables 7.4, 7.5, 7.6 and 7.7 respectively) contain trace amounts of Se. Some chalcopyrite (Table 7.5, sample ONG13-1) and pyrite grains (Table 7.6, sample 46-1) also contain anomalous Au contents, but these are thought to be due to minute inclusions of Au or some other Au-bearing phase. No native gold was observed in the numerous polished ore sections examined and analysed in this study. The chalcopyrite sample 13-4 (Table 7.5) is worthy of note because it contains significant amounts of Se, As, Zn, Ag and Bi. While minor amounts of both As and Se can replace S, and Zn can substitute for Cu or Fe in chalcopyrite (Deer *et al.*, 1992, p.595), the relatively large amounts of Se, Bi and Ag suggest these elements are present as minor phases within the chalcopyrite. Steven (1993, p.121) has reported a number of minor exsolved phases in massive chalcopyrite ore which include a Co-rich pyrrhotite, Se-bearing hessite, a Bi-selenide (Bi_4Se), costibite and native bismuth.

The veins in the Onguati Mine area (and elsewhere) show various textures and proportions of hydrothermal mineralization that are related to 2 successive stages of filling: (i) a pre-ore stage in which large amounts of quartz±carbonate were precipitated and (ii) a later ore-stage in which sulphides were deposited and incompatible elements collected and exsolved. In the Onguati Mine veins, chalcopyrite and pyrrhotite were the first sulphides to be deposited and in places replaced the quartz and carbonate gangue. It is common to find concave re-entrants of pyrrhotite replacing chalcopyrite (i.e. cusp and carie texture), but there are also a few examples where the reverse is true, and chalcopyrite replaces an earlier pyrrhotite. Massive chalcopyrite ore often contains abundant inclusions of pyrrhotite and sphalerite, the latter of which frequently possess 'chalcopyrite disease'. Arsenopyrite may have been deposited shortly after chalcopyrite and pyrrhotite in the Onguati study area because a number of examples contain cores of these two minerals. Small grains of sphalerite with numerous inclusions are common and replace both chalcopyrite and

Table 7.1: Representative analyses of arsenopyrite from veins in the Onguati study area. The Onguati Mine samples have Fe:As:S ratios very close to 1:1:1. The Brown Mountain arsenopyrites analysed fit better to a $FeAs_{0.9}S_{1.1}$ formula unit. BDL = Below detection limit (see Appendix B for analytical procedure).

Element wt%	Onguati Mine area (FeAsS)			Brown Mountain area ($FeAs_{0.9}S_{1.1}$)			
	46-1a	46-1b	46-1c	13-1	13-2a	13-2b	13-2c
Se	BDL	BDL	BDL	BDL	BDL	BDL	BDL
As	44.41	44.66	44.95	47.30	47.79	47.40	46.72
Au	BDL	BDL	BDL	BDL	BDL	BDL	BDL
Zn	BDL	BDL	BDL	BDL	BDL	BDL	BDL
Cu	BDL	BDL	BDL	BDL	BDL	BDL	BDL
Ni	0.25	0.07	0.11	BDL	BDL	BDL	BDL
Co	1.85	BDL	1.22	0.66	0.70	0.61	0.54
Fe	33.62	35.75	34.04	33.86	33.28	34.15	34.36
Mn	BDL	BDL	0.04	BDL	0.04	BDL	0.06
Sb	BDL	BDL	BDL	BDL	BDL	BDL	BDL
Ag	BDL	BDL	BDL	BDL	BDL	BDL	BDL
S	18.42	18.99	17.87	16.38	16.91	16.56	17.29
Mo	BDL	BDL	BDL	BDL	BDL	BDL	BDL
Bi	1.01	0.91	0.99	0.99	0.87	0.85	0.85
Total	98.56	100.38	99.22	99.19	99.59	99.57	99.82

Table 7.2: Representative analyses of cobaltite, (Co,Fe)AsS, from veins in the Onguati Mine area.

Element wt%	Onguati Mine Area		
	25-1	25-2	25-3
Se	BDL	BDL	BDL
As	41.75	42.77	42.52
Au	BDL	BDL	BDL
Zn	BDL	BDL	BDL
Cu	BDL	0.19	0.14
Ni	BDL	BDL	BDL
Co	34.91	33.69	34.55
Fe	1.23	2.46	1.76
Mn	0.05	0.04	BDL
Sb	BDL	BDL	BDL
Ag	BDL	BDL	BDL
S	19.18	18.35	18.85
Mo	BDL	BDL	BDL
Bi	0.88	0.80	0.76
Total	98.00	98.30	98.58

Table 7.3: Representative analyses of digenite, $(Cu_{(9-x)}S_5)$, from veins in the Brown Mountain area. BDL = Below detection limit.

Element wt%	Brown Mountain area		
	8-1	8-2	8-3
Se	0.24	0.19	0.28
As	BDL	BDL	BDL
Au	BDL	BDL	0.10
Zn	BDL	BDL	BDL
Cu	76.52	77.25	79.36
Co	BDL	BDL	BDL
Fe	4.16	2.50	1.97
Sb	BDL	BDL	BDL
Ag	BDL	BDL	BDL
S	22.64	22.55	22.70
Bi	BDL	0.05	BDL
Hg	BDL	BDL	0.04
Te	BDL	BDL	BDL
Total	103.56	102.54	104.45

Table 7.4: Representative analyses of pyrrhotite, $Fe_{(x-1)}S$, from veins in the Onguati Mine and Brown Mountain areas. BDL = Below detection limit (see Appendix B for electron probe operating conditions, standards and average lower levels of detection).

Element wt%	Onguati Mine area						Brown Mountain area											
	13-5a	13-5b	13-5c	27-1	46-1a	46-1b	10-1	10-2a	10-2b	10-3a	10-3b	10-3c	13-1a	13-1b	13-2	15-1	15-2	15-3
Se	**0.20**	**0.18**	**0.12**	**0.20**	BDL	BDL	BDL	**0.12**	BDL	BDL	BDL	BDL	BDL	BDL	BDL	BDL	BDL	**0.11**
As	BDL	BDL	BDL	BDL	BDL	**0.20**	BDL	BDL	BDL	BDL	BDL	BDL	BDL	BDL	BDL	BDL	BDL	BDL
Au	BDL	BDL	BDL	BDL	BDL	BDL	BDL	BDL	BDL	BDL	BDL	BDL	BDL	BDL	BDL	BDL	BDL	BDL
Zn	BDL	BDL	BDL	**0.83**	BDL	BDL	BDL	BDL	BDL	BDL	BDL	BDL	BDL	BDL	BDL	BDL	BDL	BDL
Cu	BDL	BDL	BDL	**0.11**	BDL	BDL	BDL	BDL	BDL	BDL	BDL	BDL	BDL	BDL	BDL	BDL	BDL	BDL
Ni	BDL	BDL	BDL	BDL	BDL	**0.10**	BDL	**0.04**	BDL	BDL	BDL	BDL	BDL	BDL	**0.04**	**0.08**	BDL	BDL
Co	BDL	BDL	BDL	BDL	BDL	BDL	BDL	BDL	BDL	BDL	BDL	BDL	BDL	BDL	BDL	BDL	BDL	BDL
Fe	**60.68**	**61.02**	**60.44**	**59.59**	**60.81**	**61.18**	**60.01**	**59.54**	**60.66**	**60.06**	**60.00**	**59.45**	**60.66**	**60.42**	**61.03**	**60.69**	**61.70**	**61.36**
Mn	BDL	BDL	BDL	BDL	BDL	BDL	BDL	BDL	BDL	BDL	BDL	BDL	BDL	BDL	BDL	BDL	BDL	BDL
Sb	BDL	BDL	BDL	BDL	BDL	BDL	BDL	BDL	BDL	BDL	BDL	BDL	BDL	BDL	BDL	BDL	BDL	BDL
Ag	BDL	BDL	BDL	BDL	BDL	BDL	BDL	BDL	BDL	BDL	BDL	BDL	BDL	BDL	BDL	BDL	BDL	BDL
S	**38.89**	**39.67**	**39.99**	**38.79**	**38.55**	**39.83**	**40.90**	**38.73**	**39.24**	**38.66**	**38.87**	**39.00**	**37.60**	**38.40**	**38.14**	**38.39**	**37.50**	**38.09**
Mo	**0.20**	BDL	BDL	BDL	BDL	BDL	BDL	BDL	BDL	BDL	BDL	BDL	BDL	BDL	BDL	BDL	BDL	BDL
Bi	BDL	BDL	BDL	BDL	BDL	BDL	BDL	BDL	BDL	BDL	BDL	BDL	BDL	BDL	BDL	BDL	BDL	BDL
Total	**99.97**	**100.87**	**100.55**	**99.52**	**99.36**	**101.31**	**100.91**	**98.43**	**99.90**	**98.72**	**98.87**	**98.45**	**98.26**	**98.82**	**99.21**	**99.16**	**99.20**	**99.56**

Table 7.4: Representative analyses of pyrrhotite, $Fe_{(x-1)}S$, from veins in the Onguati Mine and Brown Mountain areas. BDL = Below detection limit (see Appendix B for electron probe operating conditions, standards and average lower levels of detection).

Element wt%	Onguati Mine area						Brown Mountain area											
	13-5a	13-5b	13-5c	27-1	46-1a	46-1b	10-1	10-2a	10-2b	10-3a	10-3b	10-3c	13-1a	13-1b	13-2	15-1	15-2	15-3
Se	**0.20**	**0.18**	**0.12**	**0.20**	BDL	BDL	BDL	**0.12**	BDL	BDL	BDL	BDL	BDL	BDL	BDL	BDL	BDL	**0.11**
As	BDL	BDL	BDL	BDL	BDL	**0.20**	BDL	BDL	BDL	BDL	BDL	BDL	BDL	BDL	BDL	BDL	BDL	BDL
Au	BDL	BDL	BDL	BDL	BDL	BDL	BDL	BDL	BDL	BDL	BDL	BDL	BDL	BDL	BDL	BDL	BDL	BDL
Zn	BDL	BDL	BDL	**0.83**	BDL	BDL	BDL	BDL	BDL	BDL	BDL	BDL	BDL	BDL	BDL	BDL	BDL	BDL
Cu	BDL	BDL	BDL	**0.11**	BDL	BDL	BDL	BDL	BDL	BDL	BDL	BDL	BDL	BDL	BDL	BDL	BDL	BDL
Ni	BDL	BDL	BDL	BDL	BDL	**0.10**	BDL	**0.04**	BDL	BDL	BDL	BDL	BDL	BDL	**0.04**	**0.08**	BDL	BDL
Co	BDL	BDL	BDL	BDL	BDL	BDL	BDL	BDL	BDL	BDL	BDL	BDL	BDL	BDL	BDL	BDL	BDL	BDL
Fe	**60.68**	**61.02**	**60.44**	**59.59**	**60.81**	**61.18**	**60.01**	**59.54**	**60.66**	**60.06**	**60.00**	**59.45**	**60.66**	**60.42**	**61.03**	**60.69**	**61.70**	**61.36**
Mn	BDL	BDL	BDL	BDL	BDL	BDL	BDL	BDL	BDL	BDL	BDL	BDL	BDL	BDL	BDL	BDL	BDL	BDL
Sb	BDL	BDL	BDL	BDL	BDL	BDL	BDL	BDL	BDL	BDL	BDL	BDL	BDL	BDL	BDL	BDL	BDL	BDL
Ag	BDL	BDL	BDL	BDL	BDL	BDL	BDL	BDL	BDL	BDL	BDL	BDL	BDL	BDL	BDL	BDL	BDL	BDL
S	**38.89**	**39.67**	**39.99**	**38.79**	**38.55**	**39.83**	**40.90**	**38.73**	**39.24**	**38.66**	**38.87**	**39.00**	**37.60**	**38.40**	**38.14**	**38.39**	**37.50**	**38.09**
Mo	**0.20**	BDL	BDL	BDL	BDL	BDL	BDL	BDL	BDL	BDL	BDL	BDL	BDL	BDL	BDL	BDL	BDL	BDL
Bi	BDL	BDL	BDL	BDL	BDL	BDL	BDL	BDL	BDL	BDL	BDL	BDL	BDL	BDL	BDL	BDL	BDL	BDL
Total	**99.97**	**100.87**	**100.55**	**99.52**	**99.36**	**101.31**	**100.91**	**98.43**	**99.90**	**98.72**	**98.87**	**98.45**	**98.26**	**98.82**	**99.21**	**99.16**	**99.20**	**99.56**

Table 7.5: Representative analyses of chalcopyrite, $CuFeS_2$, from veins in the Onguati study area. BDL = Below detection limit (see Appendix B for electron probe operating conditions, standards and average lower levels of detection).

Element wt%	Onguati Mine area									Brown Mt. Area			Western Workings Area					
	25-1	25-2	25-3	13-1	13-2	13-4	13-5	27-1	27-2	10-1a	10-1b	13-2	6-1a	6-1b	6-1c	5-1a	5-1b	5-2
Se	BDL	BDL	BDL	BDL	0.12	5.42	0.09	0.14	0.19	BDL	BDL	BDL	0.34	0.38	0.37	0.37	0.34	0.40
As	BDL	BDL	0.09	BDL	BDL	1.10	BDL	BDL	BDL	BDL	BDL	0.24	BDL	BDL	BDL	0.08	BDL	BDL
Au	BDL	BDL	BDL	0.16	BDL	BDL	BDL	BDL	BDL	BDL	BDL	BDL	BDL	BDL	BDL	BDL	BDL	0.12
Zn	BDL	BDL	BDL	BDL	BDL	0.16	BDL	BDL	BDL	BDL	BDL	BDL	BDL	BDL	BDL	BDL	BDL	BDL
Cu	33.84	34.91	34.26	34.31	34.46	28.73	34.14	34.45	34.44	34.08	34.28	34.42	34.49	34.18	33.86	33.74	34.56	34.23
Ni	BDL	BDL	BDL	BDL	BDL	BDL	BDL	BDL	BDL	BDL	BDL	BDL	BDL	BDL	BDL	BDL	BDL	BDL
Co	BDL	BDL	BDL	BDL	BDL	BDL	BDL	BDL	BDL	BDL	BDL	BDL	BDL	BDL	BDL	BDL	BDL	BDL
Fe	30.70	30.73	30.27	30.05	30.08	25.52	30.42	30.88	30.85	30.25	30.44	31.21	30.02	30.17	30.20	30.87	31.14	31.15
Mn	BDL	BDL	BDL	BDL	BDL	BDL	BDL	BDL	BDL	BDL	BDL	BDL	BDL	BDL	BDL	BDL	BDL	BDL
Sb	BDL	BDL	BDL	BDL	BDL	BDL	BDL	BDL	BDL	BDL	BDL	BDL	BDL	BDL	BDL	BDL	BDL	BDL
Ag	BDL	BDL	BDL	BDL	BDL	1.81	BDL	BDL	BDL	BDL	BDL	BDL	BDL	BDL	BDL	BDL	BDL	BDL
S	34.36	34.34	33.98	35.99	35.82	32.11	35.89	34.28	34.06	34.12	35.64	32.94	35.00	34.24	34.24	35.11	34.79	34.00
Mo	BDL	BDL	BDL	BDL	0.20	BDL	0.14	BDL	BDL	BDL	BDL	BDL	BDL	BDL	BDL	BDL	BDL	BDL
Bi	BDL	BDL	BDL	BDL	BDL	4.73	BDL	BDL	BDL	BDL	BDL	BDL	BDL	BDL	BDL	BDL	BDL	BDL
Total	98.90	99.98	98.60	100.51	100.68	99.58	100.68	99.75	99.54	98.45	100.36	98.81	99.85	98.97	98.67	100.17	100.83	99.90

Table 7.6: Representative analyses of pyrite, FeS_2, from veins in the Onguati study area. BDL = Below detection limit (see Appendix B for electron probe operating conditions, standards and average lower levels of detection).

Element wt%	Onguati Mine area			Brown Mt. area			Western Workings area						
	13-1	46-1	46-2	13-1a	13-1b	13-2	5-1	5-2	5-3	5-4	5-5	6-1	6-2
Se	0.13	BDL	BDL	BDL	BDL	BDL	0.84	0.70	0.31	0.30	0.41	0.63	BDL
As	BDL	0.51	BDL	BDL	BDL	BDL	BDL	BDL	BDL	BDL	BDL	BDL	BDL
Au	BDL	0.10	BDL	BDL	BDL	BDL	BDL	0.21	0.34	BDL	BDL	BDL	BDL
Zn	BDL	BDL	BDL	BDL	BDL	BDL	BDL	BDL	BDL	BDL	BDL	BDL	BDL
Cu	BDL	BDL	BDL	BDL	BDL	BDL	BDL	0.06	0.24	0.06	0.05	0.24	0.10
Ni	BDL	0.12	BDL	BDL	BDL	BDL	0.05	BDL	BDL	0.06	BDL	0.05	BDL
Co	BDL	BDL	BDL	BDL	BDL	BDL	BDL	BDL	BDL	BDL	BDL	BDL	BDL
Fe	45.63	47.34	47.86	46.98	47.36	48.04	46.78	46.95	46.03	47.26	47.65	45.83	47.39
Mn	BDL	BDL	BDL	BDL	BDL	BDL	BDL	BDL	BDL	BDL	BDL	BDL	BDL
Sb	BDL	BDL	BDL	BDL	BDL	BDL	BDL	BDL	BDL	BDL	BDL	BDL	BDL
Ag	BDL	BDL	BDL	BDL	BDL	BDL	BDL	BDL	0.18	BDL	BDL	BDL	BDL
S	55.86	52.76	52.86	52.43	52.75	51.39	51.88	52.39	52.36	53.69	51.57	53.87	52.39
Mo	BDL	BDL	BDL	BDL	BDL	BDL	BDL	BDL	BDL	BDL	BDL	BDL	BDL
Bi	BDL	BDL	BDL	0.17	BDL	BDL	0.98	BDL	BDL	BDL	BDL	BDL	0.10
Total	101.62	100.83	100.72	99.58	100.11	99.43	100.53	100.31	99.46	101.37	99.68	100.62	99.98

Table 7.7: Representative analyses of sphalerite, ZnS, from veins in the Onguati Mine and Western Workings areas. BDL = Below detection limit (see Appendix B for electron probe operating conditions, standards and average lower levels of detection).

Element wt%	Onguati Mine area											Western Workings area						
	25-1	13-1	13-2a	13-2b	13-4a	13-4b	13-5a	13-5b	13-5c	27-1	27-2	6-1a	6-1b	6-2	6-3	6-4	6-5	6.7
Se	0.12	0.14	0.36	0.39	0.53	0.34	0.16	0.10	0.12	BDL	0.18	0.40	0.30	0.22	0.31	1.36	0.33	0.36
As	BDL	BDL	BDL	BDL	BDL	BDL	BDL	BDL	BDL	BDL	BDL	BDL	BDL	BDL	BDL	BDL	BDL	BDL
Au	BDL	BDL	BDL	BDL	BDL	BDL	BDL	BDL	BDL	BDL	BDL	BDL	BDL	BDL	BDL	BDL	0.23	0.19
Zn	55.07	55.28	55.45	56.10	52.60	53.47	55.30	54.94	55.61	56.08	51.70	53.41	54.21	55.46	53.07	54.80	55.23	55.29
Cu	0.15	0.16	0.05	0.18	1.93	1.59	BDL	BDL	BDL	0.12	3.63	1.24	0.57	0.10	1.62	0.36	0.33	0.31
Ni	BDL	BDL	BDL	BDL	BDL	BDL	BDL	BDL	BDL	BDL	BDL	BDL	BDL	BDL	BDL	BDL	BDL	BDL
Co	BDL	BDL	BDL	BDL	BDL	BDL	BDL	BDL	BDL	BDL	BDL	BDL	BDL	BDL	BDL	BDL	BDL	BDL
Fe	10.80	9.73	10.04	9.80	10.59	10.45	10.81	11.06	10.29	10.25	11.98	10.70	10.58	10.20	10.53	9.96	10.48	11.21
Mn	0.13	BDL	BDL	BDL	BDL	BDL	BDL	BDL	BDL	0.13	0.07	BDL	BDL	BDL	BDL	BDL	BDL	BDL
Sb	BDL	BDL	BDL	BDL	BDL	BDL	BDL	BDL	BDL	BDL	BDL	BDL	BDL	BDL	BDL	BDL	BDL	BDL
Ag	BDL	BDL	BDL	BDL	BDL	BDL	BDL	BDL	BDL	BDL	BDL	BDL	BDL	BDL	BDL	BDL	BDL	BDL
S	33.29	33.68	33.98	33.97	33.67	34.02	33.80	33.82	33.97	32.08	32.46	34.30	34.61	34.24	33.24	32.49	32.31	33.48
Mo	BDL	0.15	BDL	0.17	BDL	BDL	BDL	BDL	BDL	BDL	0.14	BDL	BDL	BDL	BDL	BDL	BDL	BDL
Bi	BDL	BDL	BDL	BDL	BDL	BDL	BDL	BDL	BDL	BDL	BDL	BDL	BDL	BDL	BDL	BDL	BDL	BDL
Total	99.56	99.14	99.88	100.61	99.32	99.87	100.07	99.92	99.99	98.66	100.16	99.65	100.27	100.22	98.77	98.97	98.91	100.84

pyrrhotite. Pyrite can be common in some veins and formed late in the paragenetic sequence. 'Bird's eye' textures are present in many of the polished ore sections and result from the alteration of early pyrrhotite to marcasite-pyrite intergrowths.

On the surface, vein sulphides have oxidized to form gossan. Ferruginous gossan frequently fills cracks and open spaces in the quartz veins and mainly consists of haematite and limonite. Malachite is often well-developed along the margins of the very large quartz veins and may extend outwards along fractures or layering in the calcitic marble (Fig. 6.15). Minor amounts of chrysocolla, jasper and chalcedony may also be found in places.

7.2.2. Brown Mountain

Veins in the calcitic marbles of the Brown Mountain area are characterized by their abundant haematite±goethite gossan and by their lack of malachite staining. Weathering of iron sulphides in the near surface environment, due in part to karstic activity in the region, resulted in the widespread staining of marble surfaces at Brown Mountain. Fresh ore samples collected from mineralized quartz veins are almost always dominated by pyrrhotite, and may contain lesser, variable amounts of the following sulphide minerals: pyrite, chalcopyrite, sphalerite and arsenopyrite. Trace amounts of digenite (Table 7.3) were found in one section, associated with pyrrhotite and chalcopyrite.

Compared with Onguati Mine and Western Workings, sulphides in the Brown Mountain vein array are noticeably deficient in Se. Only digenite, a relatively rare sulphide phase, contains similar levels of Se to the sulphides in the other areas. Analyses of Brown Mountain arsenopyrites consistently fit better to a $FeAs_{0.9}S_{1.1}$ formula unit. This is in stark contrast to the usual 1:1:1 ratio of Fe:As:S observed for arsenopyrites at Onguati Mine. The sulphides in the Brown Mountain veins show a distinct lack of contained Au or Ag, but arsenopyrite and pyrite can have trace amounts of Bi.

As with the Onguati Mine area there was an initial pre-ore stage of quartz±carbonate filling, and a later ore-stage when the bulk of the sulphides were deposited in quartz vein fractures and open spaces. The paragenetic sequence at Brown Mountain is relatively simple because only a few sulphides phases were deposited. Textural relationships show that pyrrhotite and chalcopyrite were precipitated at an early stage (most samples show chalcopyrite replacing pyrrhotite), followed by deposition of minor sphalerite and then pyrite. Numerous late calcite±quartz veinlets cut through the sulphides and quartz gangue in many of the sections studied.

7.2.3. Western Workings

The vein mineralization in the Western Workings area shows many similarities to the mineralization found in the Onguati Mine area. Large, deformed quartz veins host the bulk of the sulphide mineralization, and as a consequence, were exploited for their Cu contents. The major sulphide phases are chalcopyrite and pyrrhotite, with smaller, variable quantities of pyrite, sphalerite and marcasite-pyrite intergrowths. In one ore section considerable amounts of scheelite were found in association with sulphide phases. Many of the chalcopyrite, pyrite and sphalerite grains that were analysed (Tables 7.5-7.7 respectively) contained trace amounts of Au. One pyrite grain (sample WW5-3) also contained trace quantities of Ag. The Au may occur as tiny inclusions either in its native state or associated with other elements such as Bi (e.g. maldonite) or Ag. As with the Onguati Mine vein mineralization, the sulphide phases at Western Workings nearly always possess trace amounts of Se which probably substituted for S.

After quartz vein formation, the paragenetic sequence involved early precipitation of chalcopyrite followed closely by pyrrhotite deposition. Massive chalcopyrite ore frequently contains large inclusions of sphalerite and pyrrhotite, which sometimes occur as aggregates. Many of the sphalerite grains exhibit 'chalcopyrite disease'. In several ore sections the quartz gangue, and large chalcopyrite grains with their sphalerite inclusions, are cut and partially replaced by pyrrhotite veinlets ('islands' of the host sulphide are preserved in the veinlets). In one section (sample WW5), scheelite replaced earlier chalcopyrite and possibly pyrrhotite. Numerous scheelite pseudomorphs after cubic pyrite were also discovered in this section. Late pyrrhotite veinlets cut the scheelite pseudomorphs and extend into the quartz gangue. Supergene enrichment may have occurred in the Western Workings deposit, where it led to the formation of bornite, chalcocite and covelite replacement rims around many of the primary chalcopyrite grains. On the surface, fractures in many of the veins are filled by haematite. Malachite and minor azurite staining is best developed along vein margins or in late fractures or joints that lead away from the veins into the calcitic marbles.

7.3. Mineralization in Veins Hosted by Dolomitic Marble

The quartz veins in the dolomitic marbles of the Brown Mountain and Western Workings area commonly possess tremolite-rich margins. The tremolite 'skarn' developed due to the reaction of siliceous H_2O-bearing hydrothermal fluids with the dolomitic wall rocks. The vein arrays are best developed close to the boundary with the underlying calcitic marble package, but in most cases they do not appear to contain significant sulphide mineralization. Recently these veins have been the focus of renewed interest because similar, sulphide-poor veins at Grid A and Otjimbojo have been found to contain appreciable, if somewhat irregular, amounts of Au (Steven, 2000, p.5).

The quartz-tremolite veins hosted by dolomitic marbles in the northwestern parts of the Brown Mountain mapping area show few signs of mineralization. Only limited amounts of gossan are associated with these veins and there is a distinct absence of malachite or azurite along the vein margins (i.e. small amounts of pyrrhotite±pyrite may be present but chalcopyrite is absent).

In the dolomitic marbles to the north of Western Workings, the veins are more abundant and appear to be better mineralized than those at Brown Mountain. The thicker quartz-tremolite veins (~5 cm) contain gossan-filled fractures and may show abundant malachite staining along their wall rocks. These veins may contain small amounts of Cu sulphides such as chalcopyrite.

7.4. Discussion

A number of authors (e.g. Petzel, 1988a; Pirajno *et al.*, 1991) have noted the distinct Cu+Fe+As±Bi±W–strong Au metal association at Onguati Mine and Western Workings (similar to that at Navachab Mine) compared to the Fe+As±Cu–weak Au association at Brown Mountain. This difference has been explained as a metal zonation effect away from an underlying granitic heat source (Gray, 1988; Petzel, 1988a; Pirajno *et al.*, 1991; Pirajno & Jacob, 1991), as a result of different fluid pressure regimes in the vein systems (Gray, 1988), or as a consequence of two episodes of mineralization involving a high temperature Cu-Au event and a later Fe-As±Au event (Steven, 2000). In addition to differences in the ore assemblages and exsolution phenomena, the analyses of sulphides in this study show that subtle differences exist in sulphide trace element composition (e.g. Se content) between Brown Mountain and the other areas. These results can be most simply explained as the result of at least 2 separate mineralizing events, as advocated by Steven (2000). Each event could have been associated with different composition hydrothermal fluids that were derived and equilibrated with differing source rocks. The Onguati Mine and Western Workings deposits may have developed at a similar time from the same regional hydrothermal fluids, and involved fluids with a more complex chemistry (e.g. exsolution of a variety of Bi-, Se- and Co-minerals). Brown Mountain sulphides may have been deposited at a different times to the other areas, and may have accessed more local ore fluids.

8. FRACTAL ANALYSIS OF VEINS IN THE ONGUATI STUDY AREA

8.1 Fractal Geometry and Fracture Systems

The study of fracture systems, including filled fractures or veins, has received increasing attention over the last few decades. This is largely as a result of the many areas of potential application, especially in the safe siting of underground nuclear and toxic waste repositories, and in the oil and geohydrology industries where fluids must be extracted from naturally fractured reservoirs (Chilès, 1988; Gillespie *et al.*, 1993). A full understanding of fracture systems is also required in mine development where fractures play an important part in determining the stability of slopes and underground workings (La Pointe, 1988), or where veins (i.e. filled fractures) may host mineralization. There is frequently an additional need to fully characterize entire fracture fields, and to model their development (Chilès, 1988).

Traditional geostatistics have been widely used in the study of various fracture attributes such as orientation, trace length, aperture, density and spacing (Chilès, 1988). These simple parameters have proved adequate for many geotechnical applications because there is frequently good 3D exposure and the methods are cost effective and easy to implement during development (La Pointe, 1988). Nevertheless there are cases, such as in the exploration of oil and mineral deposits or in the initial stages of mine development, where there is a lack of large underground exposure. Interpretation may rely solely on data collected from available surface outcrop or borehole core where only part of the fracture scale range may be observed (La Pointe, 1988; Gillespie *et al.*, 1993). With such spatially limited data, conventional geostatistical methods frequently struggle to characterize the complex form of the fracture network, and neither allow extrapolation to other scales nor provide reliable predictions of fracture properties such as permeability or stability in target volumes (La Pointe, 1988). Loriga (1999, p.57) and others have pointed out that the unsuitability of traditional geostatistics to many fracture applications is primarily a result of geometric problems rather than probabilistic ones.

In the last ten years there has been a "fractal revolution" in structural geology (Lonergan *et al.*, 1999, p.3). It has been suggested that fractal analysis can be applied to the study of fracture spatial distribution (e.g. La Pointe, 1988; Velde *et al.*, 1990; Gillespie *et al.*, 1993; Stowell *et al.*, 1999), and to various aspects of faulting (i.e. fracturing with displacement), including earthquake magnitude-frequency analysis (e.g. Gutenberg & Richter, 1954; Turcotte, 1986b, 1989), sizes of comminuted rock and fault gouge (e.g. Sammis *et al.*, 1986; Turcotte, 1986b) and to fault displacements, lengths and aperture (e.g. Aviles *et al.*, 1987; Scholz & Cowie, 1990; Walsh *et al.*, 1991; Knott *et al.*, 1996; Needham *et al.*, 1996; Nicol *et al.*, 1996; Pickering *et al.*, 1997). Along with dynamic system or Chaos theory, fractal geometry has also proved useful in modelling the complex processes of fracturing and fracture system development (Chilès, 1988; Kruhl, 1994a; Kupková & Krišťáková, 1994; Silberschmidt & Silberschmidt, 1994; Turcotte, 1997).

Fractal geometry has lingered in theoretical mathematics since the turn of the last century, and it was only through the innovative work of Mandelbrot (1967, 1975, 1977, 1983) that it was finally introduced to the sciences as a powerful tool for describing irregular form and pattern. Due to its varied use in the mathematical and natural sciences (see Mandelbrot, 1983) some ambiguity has arisen when phenomena are labelled "fractal". Fundamentally, a fractal geometry is one that is scale-invariant or self-similar at all scales between upper and lower fractal limits, such that any portion of the system is a scaled down version of the whole (Gillespie *et al.*, 1993). The concepts of scale-invariance and self-similarity are not new to the geosciences, and it is well known that many geological structures are identical over several, but not infinite, orders of magnitude (e.g. fold form can be extrapolated from the hand sample to outcrop- or tens of kilometre-scales). A broader definition of fractals, to include those which have a weaker scale-invariant property known as self-affinity, is also useful in the analysis of many natural phenomena (Mandelbrot, 1983). The so-called self-affine fractals involve patterns that invoke systematic transformations in geometry with scale change, so that when such systems are analysed, they appear to have different fractal dimensions at each scale and require additional parameters to fully describe their scaling properties (Gillespie *et al.* 1993; Turcotte, 1997).

Phenomena with fractal properties also possess a power-law dependence because this is the only distribution that does not include a characteristic length scale (Turcotte, 1997). It is the exponent of the power law function, commonly referred to as the "D-value" or "fractal dimension" in geology, that provides a numerical index to describe the self-similarity of complex shapes (Wei & Pengda, 2002). The quantitative characterization of complex form, such as found in fracture systems, facilitates comparison and allows models of pattern formation to be established and tested. Readers with little knowledge of fractal geometry can refer to *Appendix C* for more information on the development of fractals, their formal definition and applicability to the geosciences, and for details of their many unique features.

8.2. Vein Thickness Distributions

Many properties of veins (i.e. mineral-filled extensional fractures) are fractal, and there have been numerous recent investigations into vein thickness (McCaffrey *et al.*, 1993; Kruhl, 1994b; Sanderson *et al.*, 1994; Clark *et al.*, 1995; Roberts *et al.*, 1998; Gillespie *et al.*, 1999; Loriga, 1999; Roberts *et al.*, 1999; Gillespie *et al.*, 2001; Monecke *et al.*, 2001) and spacing distributions (Manning, 1994; McCaffrey & Johnston, 1996; Stowell *et al.*, 1999), as well as in the relationship between vein aperture and length (Vermilye & Scholz, 1995; Johnston & McCaffrey, 1996; Stowell *et al.*, 1999).

Vein-thickness data from the Onguati study area were analysed for fractal distribution, by testing the validity of the following power-law relationship (Roberts *et al.*, 1999, p.7):

$$N/m = Ct^{-D} \qquad [1]$$

where N/m is the number of veins with a thickness ≥t per metre (m) transect (i.e normalized cumulative number per metre), C represents the frequency of veins ≥ unit thickness (in this study ≥1 metre), and the exponent -D is the fractal dimension. On a plot of log N/m vs. log t, only a power-law distribution (i.e. fractal) will yield a straight line (Roberts et al., 1999). The straight line in log-log space will have a gradient which is equal to the negative power-law exponent, or the D-value of the vein-thickness distribution (Loriga, 1999). The closer the line to horizontal, the lower the D-value (Roberts *et al.*, 1999). The D-value reflects the rate of size change across scale, so that steeper slopes will have more small veins relative to large veins. Alternatively the lower the D-value, the higher the proportion of large veins in the population. It is important to note that when distributions are power-law, the relative proportions of small and large veins remain the same at all scales over which the veins are found (Gillespie *et al.*, 1993).

If the vein thicknesses measured in the calcitic and dolomitic marbles of the Onguati Mine, Brown Mountain and Western Workings areas conform to a power-law distribution, then the determination of D-values will reflect the overall geometry of each vein network. This is useful because it facilitates quantitative comparison between the vein systems of each rock type and area, and may help in determining some of the deposit-scale controls on hydrothermal mineralization in the Karibib area.

8.2.1 Sampling Procedure

A variety of techniques have been developed to sample fracture and vein characteristics with power-law distributions (Gillespie *et al.* 1993). In this project, a simple 1-dimensional line or transect sampling technique was employed. There are a number of reasons for this choice:

1. Line sampling is simple to undertake in areas of uneven ground or patchy exposure.
2. Where there is patchy outcrop it is possible to lay out a number of small traverses. Data obtained in this manner can be safely combined to provide a 'multi-line' sample (e.g. Walsh *et al.*, 1991; Pickering *et al.*, 1995; Loriga, 1999) although steep right-hand fall-off can occur. The result is almost equivalent to finite range effect *(see 8.2.2. below)* and can normally be corrected in the same manner to provide statistically valid D-values (Pickering *et al.*, 1996).
3. Line sampling provides 1-dimensional data, which can be combined or compared with other forms of commonly available data (e.g. drill core data).
4. Traverses can be oriented in different directions over the 2-dimensional vein array to take account of different vein sets (Velde *et al.*, 1991).
5. Sampling error is less severe and better understood in line sampling than in 2-dimensional methods (Pickering *et al.*, 1996).
6. Two-dimensional sampling techniques such as the box-counting methods, have been, to date, far too insensitive to yield a statistically representative D-value (Gillespie *et al.*, 1993), or in the case of the gliding box method, are very complicated and still in their infancy (e.g. Cheng, 1997).

In this study, a series of transects were positioned approximately normal to the dominant SE-dipping vein set, in close proximity to the Western Workings and Onguati Mines, and on the slopes of Brown Mountain. The orientations of veins, intersected along each of the transects, have been plotted as poles-to-planes in *Figs. 8.1, 8.2 and 8.3.* Where reasonably well-developed areas of veining occur in both the calcitic and dolomitic marbles, separate line samples were undertaken. In addition to recording true vein thickness and vein orientation data along each transect, description was made of vein spacing, morphology, gangue and mineralization. A lower limit on vein thickness and spacing measurement was set at 1 mm for veins from all areas. This permits a reliable test of power-law thickness distribution to be made from millimetre to metre scale, and hence over several orders of magnitude (Loriga,

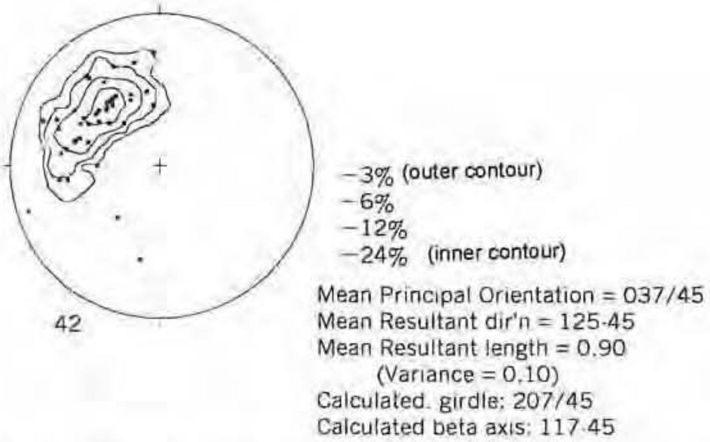

Mean Principal Orientation = 037/45
Mean Resultant dir'n = 125-45
Mean Resultant length = 0.90
(Variance = 0.10)
Calculated. girdle: 207/45
Calculated beta axis: 117-45

Fig. 8.1: Poles to quartz±carbonate veins intersected along the Onguati Mine line surveys (lower hemisphere, equal area projection).

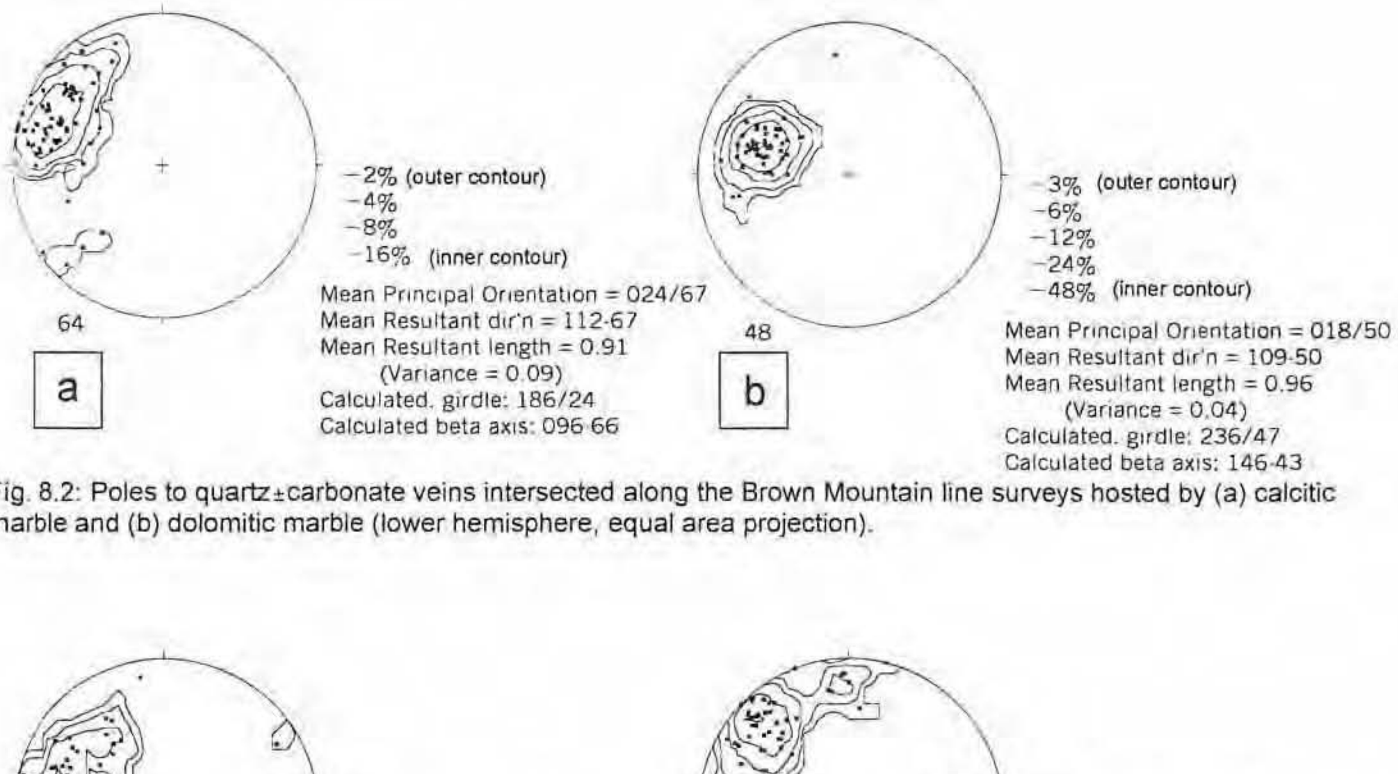

a: Mean Principal Orientation = 024/67
Mean Resultant dir'n = 112-67
Mean Resultant length = 0.91
(Variance = 0.09)
Calculated. girdle: 186/24
Calculated beta axis: 096-66

b: Mean Principal Orientation = 018/50
Mean Resultant dir'n = 109-50
Mean Resultant length = 0.96
(Variance = 0.04)
Calculated. girdle: 236/47
Calculated beta axis: 146-43

Fig. 8.2: Poles to quartz±carbonate veins intersected along the Brown Mountain line surveys hosted by (a) calcitic marble and (b) dolomitic marble (lower hemisphere, equal area projection).

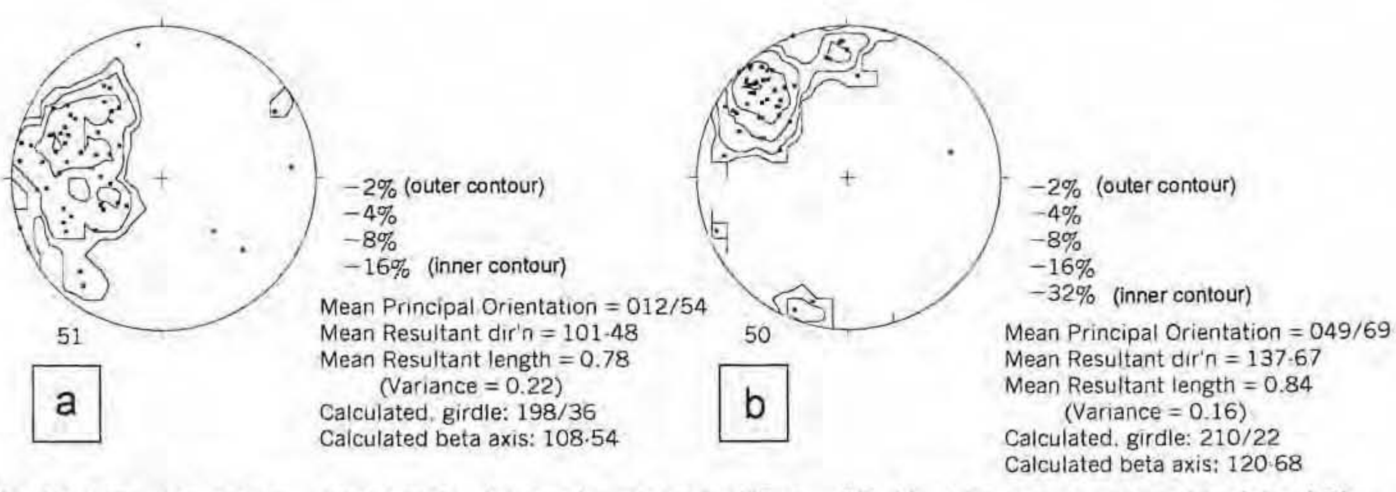

a: Mean Principal Orientation = 012/54
Mean Resultant dir'n = 101-48
Mean Resultant length = 0.78
(Variance = 0.22)
Calculated. girdle: 198/36
Calculated beta axis: 108-54

b: Mean Principal Orientation = 049/69
Mean Resultant dir'n = 137-67
Mean Resultant length = 0.84
(Variance = 0.16)
Calculated. girdle: 210/22
Calculated beta axis: 120-68

Fig. 8.3: Poles to quartz±carbonate veins intersected along the Western Workings line surveys hosted by (a) calcitic marble and (b) dolomitic marble (lower hemisphere, equal area projection).

1999). In the dolomitic marbles great care had to be taken because late fractures are often filled with small amounts of secondary carbonate and quartz. For this reason, only veins that exceeded 3 mm in thickness were recorded.

Loriga (1999) has estimated that, on average, a minimum of 50 vein thickness measurements are required to form a useful data set, and that a sample of greater than 100 measurements should be statistically robust. Over many parts of the Onguati study area it was difficult to collect samples where n>50 due to a combination of poor outcrop and low-vein density. Single line sampling was found to be especially inappropriate for veins hosted by the calcitic marbles at Onguati Mine, and in the dolomitic marbles of Western Workings. In these areas a number of parallel transects had to be made over several outcrops, and the line transect data combined. A statistically ideal multi-line sample would require equally spaced traverses, but this requirement is not crucial, and could not be achieved (Loriga, 1999). *Table 8.1* indicates the line samples combined and the number of measurements (n) recorded. In addition, a regularly 'stepped' line transect was made over an elongate outcrop of veined, calcitic marbles at Western Workings. Transects were oriented perpendicular to the main vein set and when calcrete or mine dumps were encountered, the tape measures were simply shifted sideways by a small amount, and distance measurements resumed from where they had been left off.

8.2.2 Sampling Error

Most of the vein thickness data collected in this study shows significant deviation from the expected straight line at both the small and large scale in log-log plots of cumulative number versus vein thickness. These types of deviations from ideal behaviour are typical for samples collected from geological power-law distributions and have been traditionally attributed to short-comings in the sampling procedure (e.g. Sanderson *et al.*, 1994; Roberts *et al.*, 1998, 1999; Monecke *et al.*, 2001). In fracture and vein studies, deviation from the power-law relationship is normally related to sample truncation effects and to a lesser degree, by censoring (Pickering *et al.*, 1994, 1995). It is essential to note that in some cases large-scale deviation could be quite unrelated to problems of sampling, and may be a consequence of vein linkage as discussed later *(section 8.5)*. As per Pickering *et al.* (1995, p.5) the difference in value between the t_{max} and t_{min} of the vein thickness sample is referred to as the *scale range*, but in this account the number of values within the sample is called the *sample size*.

Table 8.1: Summary of line transect data from the Onguati study area.

Sample	*Host Rock*	*Mean Vein Orientation*	*n*	*Traverse Length (m)*	*Thickness (mm)*		*Thickness per metre (mm/m)*	*Density (veins/m)*	*C*	*D*	*Confidence Interval*		*Standard Deviation (σ)*
					Min.	*Max.*					*68%*	*95%*	
Onguati – 1	Calcitic Marble	–	13	31.00	1	90	5.19	0.42	–	–	–	–	–
Onguati – 2	Calcitic Marble	–	12	26.80	2	20	3.06	0.45	–	–	–	–	–
Onguati – 3	Calcitic Marble	–	11	31.60	20	3000	192.72	0.35	–	–	–	–	–
Onguati – 4	Calcitic Marble	–	6	13.00	8	80	10.54	0.46	–	–	–	–	–
Onguati – combined	Calcitic Marble	037°/45°SE	42	69.15	1	3000	63.18	0.41	0.0307	**0.4056***	±0.07	±0.13	±0.11
Brown Mountain	Calcitic Marble	024°/67°SE	64	31.50	2	380	74.16	2.03	0.0790	**0.6035***	±0.08	±0.16	±0.12
Brown Mountain	Dolomitic Marble	018°/50°SE	48	69.15	1	32	6.90	0.69	0.0027	**0.9940***	±0.15	±0.30	±0.27
Western Workings	Calcitic Marble	012°/54°SE	51	167.7	1	1000	21.81	0.3	0.0306	**0.3701***	±0.05	±0.11	±0.09
Western Workings – 1	Dolomitic Marble	–	11	13.15	5	36	13.69	0.84	–	–	–	–	–
Western Workings – 2	Dolomitic Marble	–	30	18.20	3	70	29.23	1.65	–	–	–	–	–
Western Workings – 3	Dolomitic Marble	–	9	5.30	3	40	23.77	1.69	–	–	–	–	–
W. Workings – combined	Dolomitic Marble	049°/69°SE	50	36.65	3	70	22.86	1.36	0.0045	**1.1244***	±0.17	±0.34	±0.33
W. Workings – BM2 Borehole	Calcitic Marble	NA	49	143.12	1	80	3.28	0.34	0.0004	**1.1590**	NA	NA	NA

** D-values corrected using the cumulative frequency method of Pickering et al. (1995, p.5); confidence intervals calculated according to Pickering et al. (1994, p.109); approximation of standard deviation as per Pickering et al. (1995, p.10). See text and **Appendix C** for details on correction procedure.*

(a)Truncation

Samples collected from fractal populations where power-law distributions characteristically span many orders of magnitude, are commonly truncated because only limited parts of the scale range can be covered by single sampling methods. For example, fault displacement data collected from borehole core can only show small-scale displacements, usually measuring from a few millimetres to several tens of centimetres at most. Seismic methods though, are generally only capable of distinguishing displacements greater than ~20 metres and up to a maximum of a few kilometres in size (Pickering *et al*, 1994). Truncation can thus occur at both the small- and large-scale ends of a data set, but importantly, does not always result in sample bias. If the truncated sample is self-similar to the original population then it will retain the same power-law relationship without deviation (e.g. curve A in Fig. 8.4).

Small-scale or left-hand truncation (LHT) is normally related to the lower limit of the measurement method employed (Pickering *et al.*, 1995). In the example above, the size of the smallest fault displacement that can be recognized by seismic methods is directly proportional to the bandwidth of the signal used (Pickering *et al.*, 1994). LHT is frequently associated with small-scale data loss which leads to "LHT fall-off" (see Fig. 8.4), a type of small-scale deviation from the straight line in cumulative frequency graphs (Pickering *et al.*, 1995, p.4). All of the Onguati data sets show LHT which is related to observational limits (i.e. only veins ≥1 mm in thickness can be reliably measured), but display varying degrees of LHT fall-off. This fall-off may be due to an under-sampling effect that occurs as the lower limit of measurement is approached. Millimetre-scale veins, which are often dominated by a carbonate fill, can become very difficult to distinguish from their layered marble host rocks. Some veins could also have been incorrectly regarded as being smaller than the 1 mm lower threshold. In the Onguati data sets this effect is relatively minor and is easily countered by applying selective curve-fitting procedures (i.e. in most cases only points where $t \geq 5$ mm were used in curve-fits). As this approach is successful in all the Onguati vein thickness data, there is no need to apply small-scale corrections as proposed by Barton & Zoback (1992).

Large-scale or right-hand truncation (RHT) is thought to be just as prevalent in natural data sets as LHT but is less frequently considered, probably because it is very difficult to determine the upper fractal limits of geological power-law distributions (Pickering *et al.*, 1995, 1996). In many natural samples, even in populations that are ideally power-law distributed, there is often significant deviation at the large scale. The right-hand fall-off of data on cumulative frequency graphs such as in Fig. 8.4, has been attributed to the very low probability of intersecting the larger, more scarce members of a power-law population

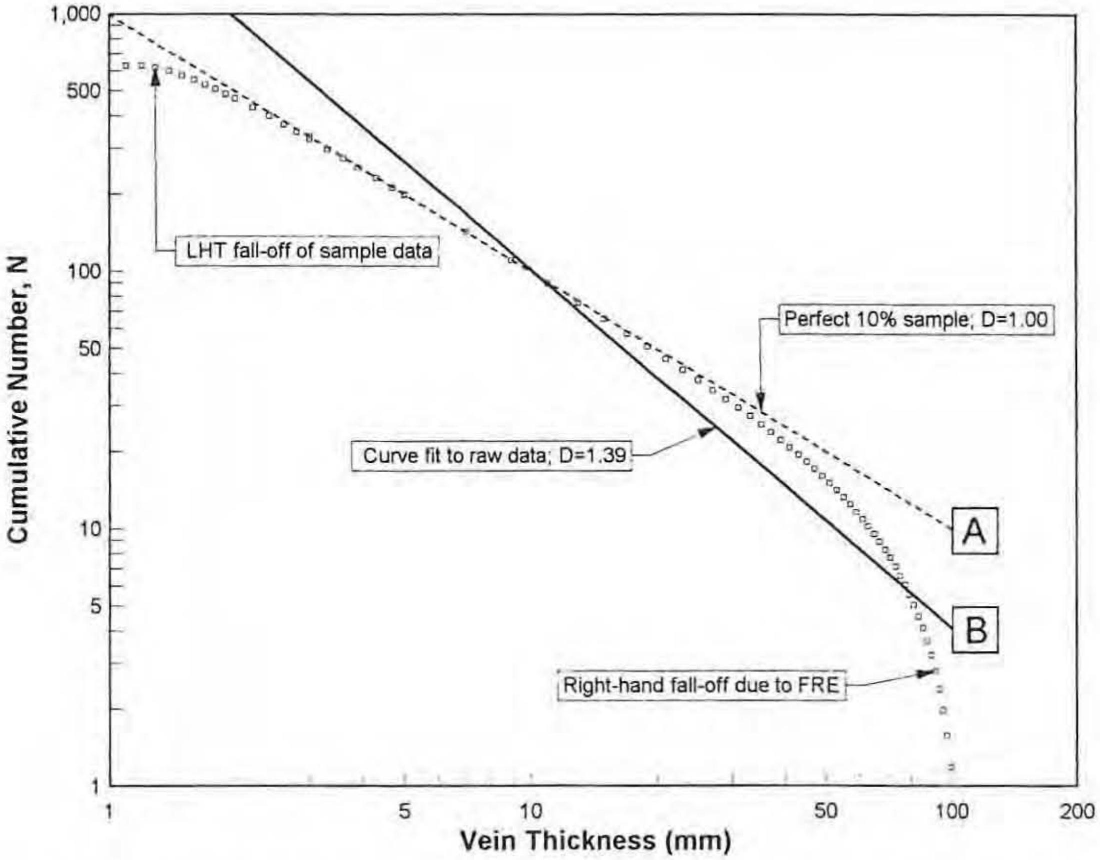

Fig. 8.4: Log-log plot of cumulative number, N(≥t) versus vein thickness, t for two idealized samples 'collected' from a synthetic power-law population. The population (not shown) has 10 000 values, a scale range that extends from 1 mm up to 10 m and a D-value of 1.00. Both samples contain 100 values and show large scale truncation (i.e. RHT) because they include a reduced scale range from 1 mm to 10 cm. Curve A shows a perfect sample that retains a D-value of 1.00, with no deviations at the small or large scales (i.e. self-similar to population). Sample B shows both LHT fall-off and right-hand fall-off, and a curve fit to the affected data yields a highly biased D-value of 1.39. In natural data, LHT fall-off is related to the lower limit of resolution in the measurement method employed, and can simply be dealt with by ignoring the affected points during curve-fitting procedures. Right-hand fall-off is normally the result of finite range effect (FRE) and requires correction to yield statistically valid D-values (see text). Refer to Appendix C, especially Figs. C.3 and C.4, for more detail on the creation of the synthetic power-law population, and the simulation and correction of induced sampling error.

(Pickering *et al.*, 1995). The resulting under-sampling of the large values reduces the rank of all the values in the data set, but has the most profound effect on values approaching the maximum. Previously this deviation was defined as a type of censoring (e.g. Jackson & Sanderson, 1992; Pickering *et al.*, 1994), but Pickering *et al.* (1995, 1996) believe that this effect is introduced largely by the RHT of the sample. To avoid further confusion with other sampling techniques, Pickering *et al.* (1995, p.5) have proposed that this large-scale fall-off be called "finite range effect".

The vein thickness data recorded in the calcitic and dolomitic marbles of the Onguati Mine, Brown Mountain and Western Workings areas are not thought to be severely truncated from the full vein thickness ranges of their populations. However in most plots, large scale deviation due to finite range effect can be quite severe and causes over-estimation of the D-value if correction is not undertaken. In this project, the finite range correction of Pickering *et al.* (1994, 1995, 1996) was adopted over more recent alternative strategies (e.g. Monecke *et al.*, 2001) because it has been applied to a wide range of geological phenomena with proven success (eg. vein-thickness distributions, Roberts *et al.*, 1998, 1999; fault displacement data, Pickering *et al.*, 1994). The procedure has also been thoroughly tested on synthetic data and the results have been used to calibrate methods for estimating the confidence intervals of corrected sample D-values. Details of this corrective technique and methods for assessing D-value quality can be found in Appendix C. In addition, the appendix contains a simulation that illustrates and tests the iterative correction procedure on a simple synthetic power-law distribution created for this study.

(b) Censoring

Censoring related bias is incurred when parts of the sample are systematically under- or over-estimated (Pickering *et al.*, 1995). Pickering *et al.* (1995) define several types of censoring common to fracture length studies that are related to the areal limitations of sample surveys, but these are thought to have little relevance to the Onguati vein studies. The line samples employed in the Onguati study area were always in excess of the widths of the thickest veins, and were made as long as was required to span the breadth of each vein system. Consequently a large part of the vein thickness distribution was encountered without any sampling-imposed limitations. A type of censoring may have been incurred in the borehole data used at Western Workings, and may be related to problems in the orientation of the hole relative to the vein system. This is discussed in more detail in the results section that follows.

8.2.3. Results

D-values of vein thickness distribution were obtained for vein arrays hosted in the calcitic marbles of the Onguati Mine area, and for veins found in both the dolomitic and calcitic marbles of the Western Workings and Brown Mountain areas. Vein characteristics and D-values for all the line samples are summarized in *Table 8.1*. Log-log plots are presented for each vein system, and show the vein thickness distributions as collected, and after finite range correction *(Figs. 8.5-8.7, 8.10-8.12)*.

(a) Onguati Mine Area

Veining with an average orientation of 037°/45° (strike/dip, right-hand rule notation; n=42, variance, σ^2=0.10) is best developed in the calcitic marbles of the Onguati Mine area. In the thin dolomitic marbles preserved on the southern slopes of the Onguati hill, there is only minor evidence of hydrothermal activity as millimetre-thick veinlets. Fig. 8.5[a] shows that the vein-thickness distribution in the calcitic marbles conforms to a power-law distribution, but that it has been affected at the large scale by slight fall-off. A least-square linear regression to the raw data yields a D-value of 0.4500 (n=42, r=0.9845) which has a small bias due to 2 outliers. After applying 2 iterative corrections (Fig. 8.5[b]) the D-value is 0.4056 (r= 0.9951) with a standard deviation (σ) of 0.11, one of the lowest D-values of all the vein systems.

The Onguati Mine area has a vein thickness per metre value of 63.18 mm/m, mainly as a result of a few very large veins along the transect. The largest vein recorded along the transect was 3 metres in thickness. Although veins in the calcitic marbles of Brown Mountain have a similar vein thickness per metre value (74.16 mm/m), this is generally due to a high density of smaller veins. The vein density at Onguati Mine is 0.41 veins per metre which is comparable to Western Workings (0.30 veins/m). The Onguati Mine veins have a C value of 0.0307 (i.e. every 100 metres of transect, there is a probability that ~3 veins with a $t \geq 1$ metre will be intersected) which is almost identical to the vein system hosted by calcitic marbles at Western Workings (0.0306).

(b) Brown Mountain

Low-grade hydrothermal mineralization has occurred extensively in the calcitic and dolomitic marbles of the Brown Mountain region. Veins in both rock types dip towards the southeast. Veins hosted by calcitic marbles have a mean vein orientation of 024°/67° (strike/dip, right-

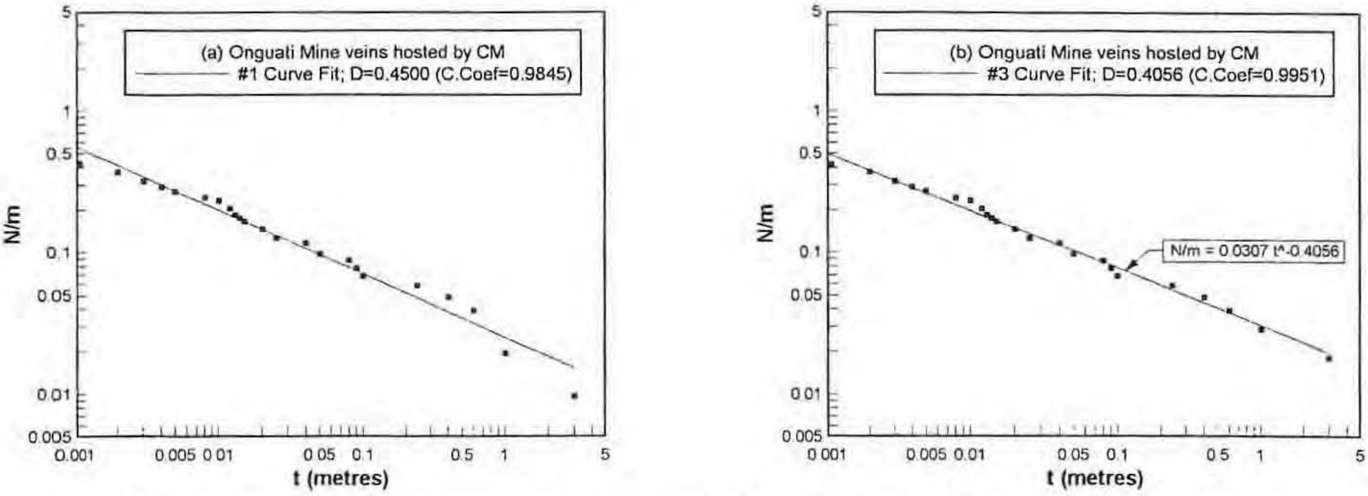

Fig. 8.5: Onguati Mine vein thickness distribution sampled from calcitic marbles (CM) of the Navachab Member. Diagrams show (a) log cumulative number, N(≥t) and (b) corrected log cumulative number, N(≥t) [both normalized per metre] versus vein thickness, t. Corrected plot yields a D-value of 0.4056±0.11.

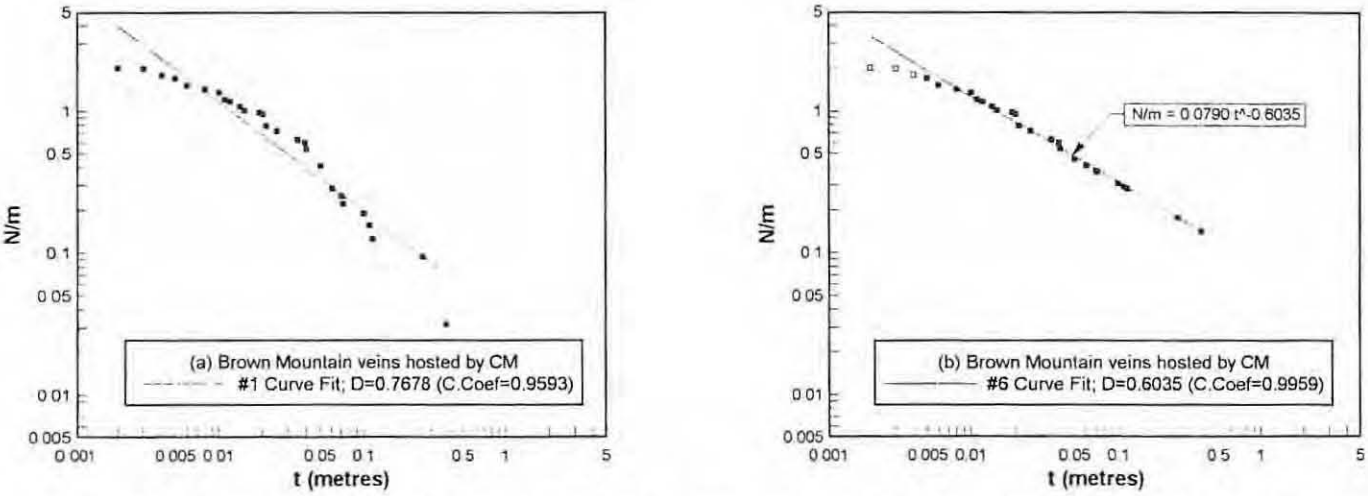

Fig. 8.6: Brown Mountain vein thickness distribution sampled from calcitic marbles (CM) of the Navachab Member. Diagrams show (a) log cumulative number, N(≥t) and (b) corrected log cumulative number, N(≥t) [both normalized per metre] versus vein thickness, t. Corrected plot yields a D-value of 0.6035±0.12.

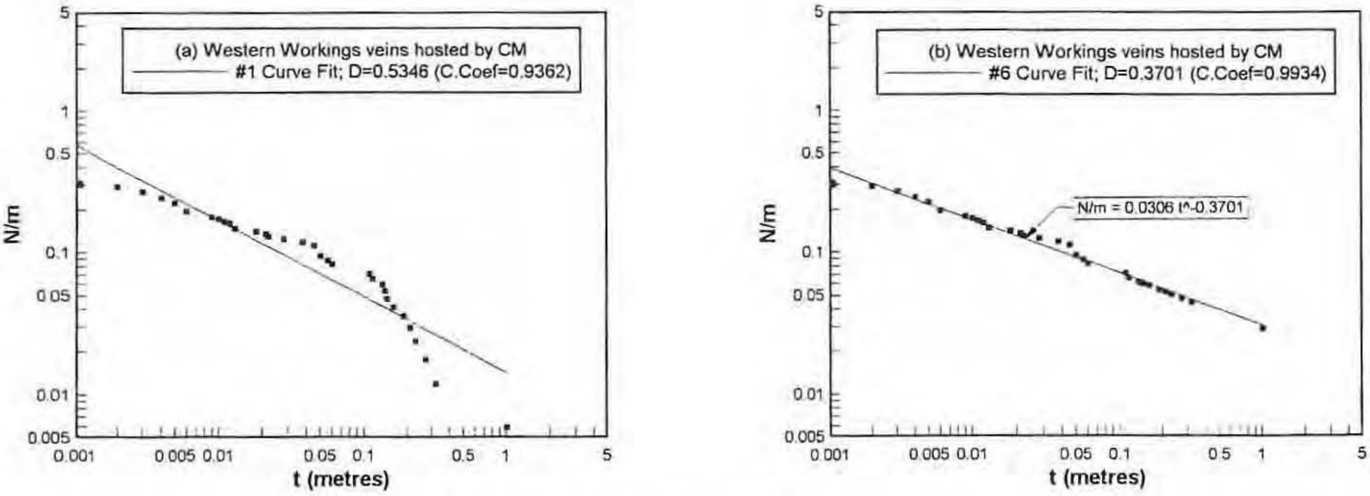

Fig. 8.7: Western Workings vein thickness distribution sampled from calcitic marbles (CM) of the Navachab Member. Diagrams show (a) log cumulative number, N(≥t) and (b) corrected log cumulative number, N(≥t) [both normalized per metre] versus vein thickness, t. Corrected plot yields a D-value of 0.3701±0.09.

hand rule; n=64, σ^2=0.09), while veins hosted by dolomitic marbles possess a mean orientation of 018°/50° (strike/dip, right-hand rule; n=48, σ^2=0.04).

The vein-thickness distribution in the calcitic marbles shows a significant deviation away from a power-law array (Fig. 8.6[a]) and this is thought to be the combined result of LHT "fall-off" and finite range effect associated with RHT. Points significantly affected by LHT "fall-off" (open-squares in Fig. 8.6[b]) were ignored in regression. The straight central segment between 5 mm and 5 cm in Fig.8.6[a] is likely to be the least biased remnant of the power-law distribution. Fall-off at the large scale can be accounted for by progressive under-sampling of the more rarely found, larger veins. A curve-fit to the affected data gave a D-value of 0.7678 (n=64, r=0.9593), but after successive correction the D-value converged at 0.6035 (r=0.9959) with a standard deviation of 0.12. Brown mountain veins hosted by calcitic marbles are characterized by their high vein density (2.03 veins/m), C-value (vein density at $t \geq 1$ metre is 0.0790) and thickness per metre values (74.16 mm/m), but have a much smaller scale range (2 - 380 mm) than the other areas. The cumulative vein thickness and frequency curves (Fig. 8.8) have regular but very steep gradients (indicative of small veins of high density) compared to veins hosted by calcitic marbles at Onguati Mine (not shown) and Western Workings (Fig. 8.9).

In the dolomitic marbles (Fig. 8.10[a]), the first approximation of the D-value for the vein size distribution is 1.4979, but as the correlation coefficient (0.9416) indicates, the least-square linear regression is a poor fit to the spread of data. This is probably due to combined finite range effect and severe LHT "fall-off". The pronounced small-scale "fall-off" is likely to be the result of problems in distinguishing veinlets from late, healed joints with a carbonate±quartz fill. Values recorded at vein thicknesses of 1 to 2 mm are severely biased and were excluded from further regression (open squares in Fig. 8.10[b]). After 8 iterative corrections (Fig. 8.10[b]) the D-value does not change significantly and is calculated at 0.9940 (n=48, r=0.9909). A gradient of this value is comparable with a line-fit to the array of data points between 4 mm and 2 cm, excluding the 'step' caused by an under-valued vein thickness.

Unfortunately it is difficult to assess whether this distribution data unequivocally conforms to a power-law relationship, and if so, whether the D-value is truly valid. Additional vein thickness data is required to resolve these reliability issues. An ideal source of vein thickness data could come from borehole core drilled perpendicular to the main vein set (i.e. 288°/40°, trend/plunge) in the dolomitic marbles. An uninterrupted sample could be taken and compared with the line sample, and if similar, combined to form a more robust data set. It is

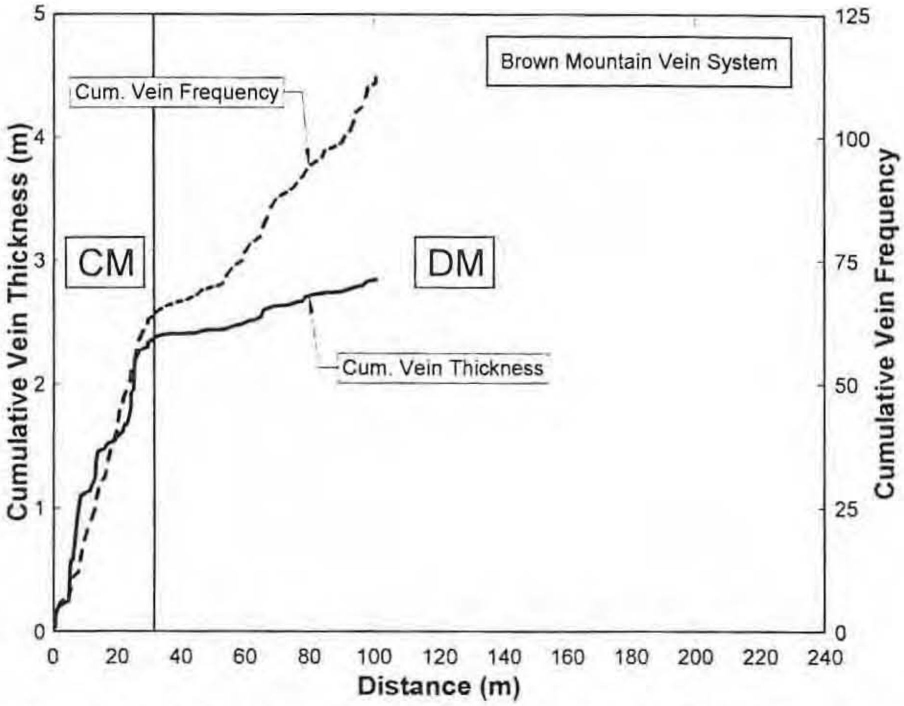

Fig. 8.8: Cumulative vein thickness (m) and vein frequency over the 2 line transects positioned on the calcitic (CM; left of vertical line) and dolomitic marbles (DM; right of vertical line) of the Brown Mountain area. Note the marked decrease in cumulative vein thickness and vein frequency in the dolomitic marbles compared to veins in the calcitic marbles.

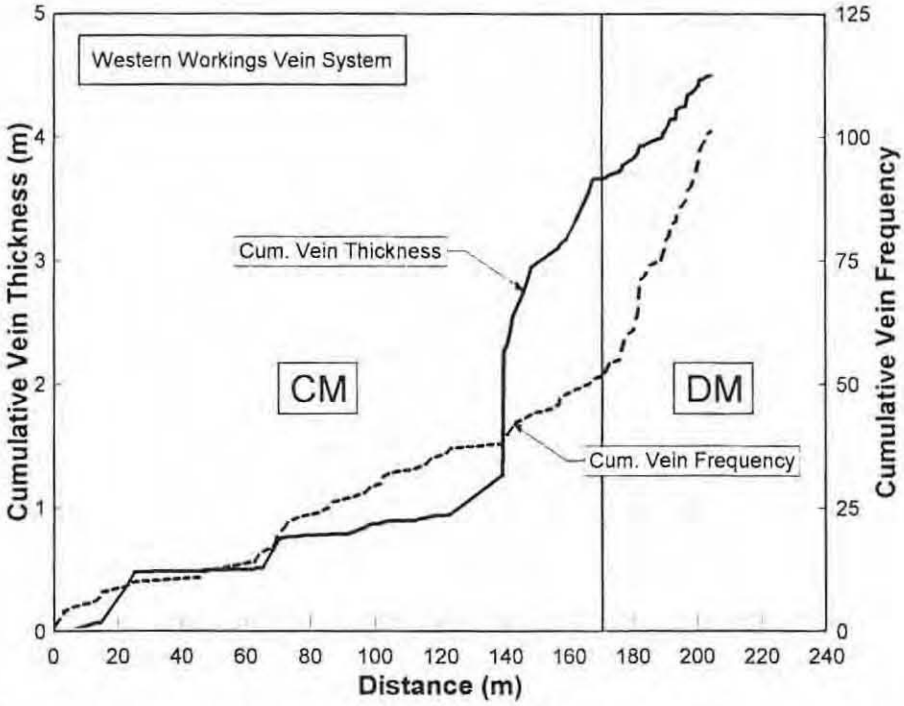

Fig. 8.9: Cumulative vein thickness (m) and vein frequency over the 4 line transects positioned over the calcitic (CM; left of vertical line) and dolomitic marbles (DM; right of vertical line) of the Western Workings area. Note the marked increase in cumulative vein frequency in the dolomitic marbles and the more gradual increase in cumulative vein thickness compared with the step-like pattern developed in the calcitic marbles.

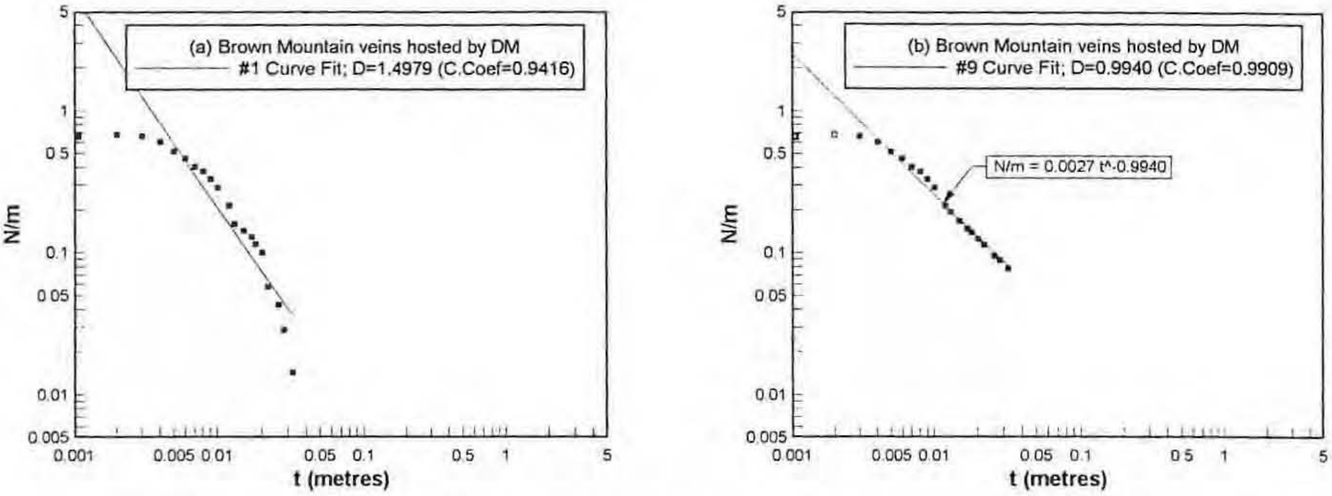

Fig. 8.10: Brown Mountain vein thickness distribution sampled from dolomitic marbles (DM) of the Navachab Member. Diagrams show (a) log cumulative number, N(≥t) and (b) corrected log cumulative number, N(≥t) [both normalized per metre] versus vein thickness, t. Corrected plot yields a D-value of 0.9940±0.27.

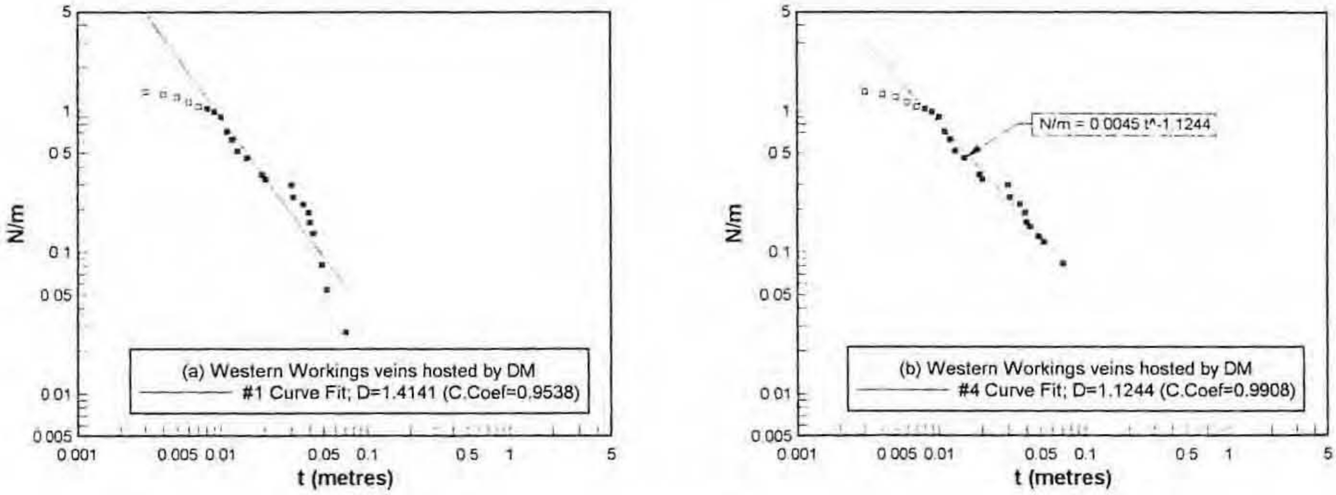

Fig. 8.11: Western Workings vein thickness distribution sampled from dolomitic marbles (DM) of the Navachab Member. Diagrams show (a) log cumulative number, N(≥t) and (b) corrected log cumulative number, N(≥t) [both normalized per metre] versus vein thickness, t. Corrected plot yields a D-value of 1.1244±0.33.

pertinent to note that the D-value obtained for veins in the dolomitic marbles at Brown Mountain (and Western Workings - see later) must be significantly higher than for veins occurring in calcitic marbles elsewhere, because their scale range is at least an order of magnitude smaller. With large numbers of small veins and an absence of metre-scale veins, the data must yield higher gradients and therefore higher fractal dimensions for their vein thickness distribution.

Brown Mountain veins hosted by dolomitic marbles have a low thickness per metre value (6.90 mm/m), a small scale range (1 - 32 mm), and a low vein density (0.69 veins/m) only slightly higher than in the calcitic marbles of the Onguati Mine area (0.41 veins/m). The cumulative vein frequency and vein thickness curves for veins in the Brown Mountain dolomitic marbles (Fig. 8.8) have lower gradients than their calcitic counterparts (i.e. smaller veins at lower vein densities). A comparison of the dolomitic marble (DM) portions of Figs. 8.8 and 8.9 also illustrates that the Brown Mountain veins are generally smaller (i.e. gentle cumulative vein thickness curve) and have lower vein densities (i.e lower gradient cumulative frequency curve) than veins hosted by dolomitic marbles at Western Workings.

(c) Western Workings

At Western Workings two distinct vein systems can be recognized. The first is hosted by calcitic marbles and contains well-mineralized veins, several of which are of metre thickness or more. The other vein system is extensively developed in the dolomitic marbles to the north of the mined area but is characterized by a much smaller vein thickness range (3 - 40 mm). Veins in the calcitic marbles were sampled along a 'stepped' transect to avoid mine dumps while intersecting an uninterrupted vein distribution. Vein thicknesses measured along this line survey were in the 1 mm to 1 metre scale range, and are distinguished by their very low vein density (0.3 veins/m) and thickness per metre values (21.81 mm/m). The presence of very thick veins, such as in the calcitic marbles of the Onguati Mine area, gives rise to a cumulative vein thickness curve that increases in large, irregular steps (Fig. 8.9). Mean vein orientation in the calcitic marbles is 012°/54° (strike/dip, right-hand rule; n=51), but can be quite variable (σ^2=0.22), so that dip directions can range from ENE to SE.

In Fig. 8.7[a] the vein thickness distribution shows an abrupt inflection at 0.1 m and this results in a heavily biased regression where D is 0.5346 (n=51, r=0.9362). This distribution is not thought to be multi-fractal or self-affine. Deviation from a straight line power-law fit may be the result of progressive under-sampling of veins, especially at vein thicknesses$\geq$0.1 m (finite range effect). This interpretation is supported by the corrected D-value of 0.3701 (r=0.9934; σ= 0.09) which is close to that obtained for the mineralized Onguati Mine vein system hosted by calcitic marble (D=0.4056). As veins in the calcitic marbles of both the Western Workings and Onguati Mine areas share similar values of C (0.0306-0.0307), so their vein thickness distributions can also be described by nearly identical power-law relationships (see Figs. 8.5[b] and 8.7[b]).

Veins hosted by the dolomitic marbles of the Western Workings area have an average orientation of 049°/69° (strike/dip, right-hand rule; n=50, σ^2=0.16), but there are a few outliers which have near vertical dips towards either the north or south. The vein thickness per metre value is 22.86 mm/m and the vein density is 1.36 veins/m, which are both significantly higher than veins hosted by dolomitic marbles in the Brown Mountain locale (also refer to Figs. 8.8 and 8.9). The D-value from veins in the dolomitic marbles of the Western Workings area is 1.1244 (n=50, r=0.9908) after 3 corrective iterations (Fig. 8.7[b]). The vein-thickness data have experienced LHT "fall-off" and finite range effect at the large scale. Large scale deviation could also have been accentuated in the multi-line surveys because larger members of the vein population would have been repeatedly under-sampled in each line making up the combined data set. As with the D-values for the dolomitic marble-hosted veins of the Brown Mountain area, more data is required to ensure that this result is valid, ideally from a borehole drilled perpendicular to the dominant vein set (i.e 319°/21°, trend/plunge).

The D-values for veins hosted by dolomitic marbles in the Western Workings and Brown Mountain areas are significantly higher (i.e. 2σ either side of the corrected vein thickness D-values) than those obtained for veins hosted by calcitic marbles at all three localities studied. A D-value close to 1 appears realistic because the maximum vein thicknesses seldom exceed 10 cm in the dolomitic marbles of the two sites.

Vein thickness data was also collected from borehole core (stored at the GSN core store, Windhoek) drilled in calcitic marble close to the contact with overlying dolomitic marbles of the Western Workings area. The diamond drill hole BMD-2, was drilled by Goldfields Namibia Ltd. and deepened an existing percussion hole BMP-11 from 100 m to a depth of 250 m (Petzel & Roesener, 1988). The hole was positioned at 090S/2040W with an orientation of 325°/60° (trend/plunge), to intersect an induced polarization, geophysical anomaly (Petzel & Roesener, 1988). Fig. 8.12 compares the vein thickness distributions of line samples taken in the calcitic and dolomitic marbles (as detailed above) with that of the core. The borehole data shows a distinctly different distribution to the corrected vein thickness data obtained from surface transects over the calcitic marbles of Western Workings. It shares a similar D-value to veins hosted by the Western Workings dolomitic

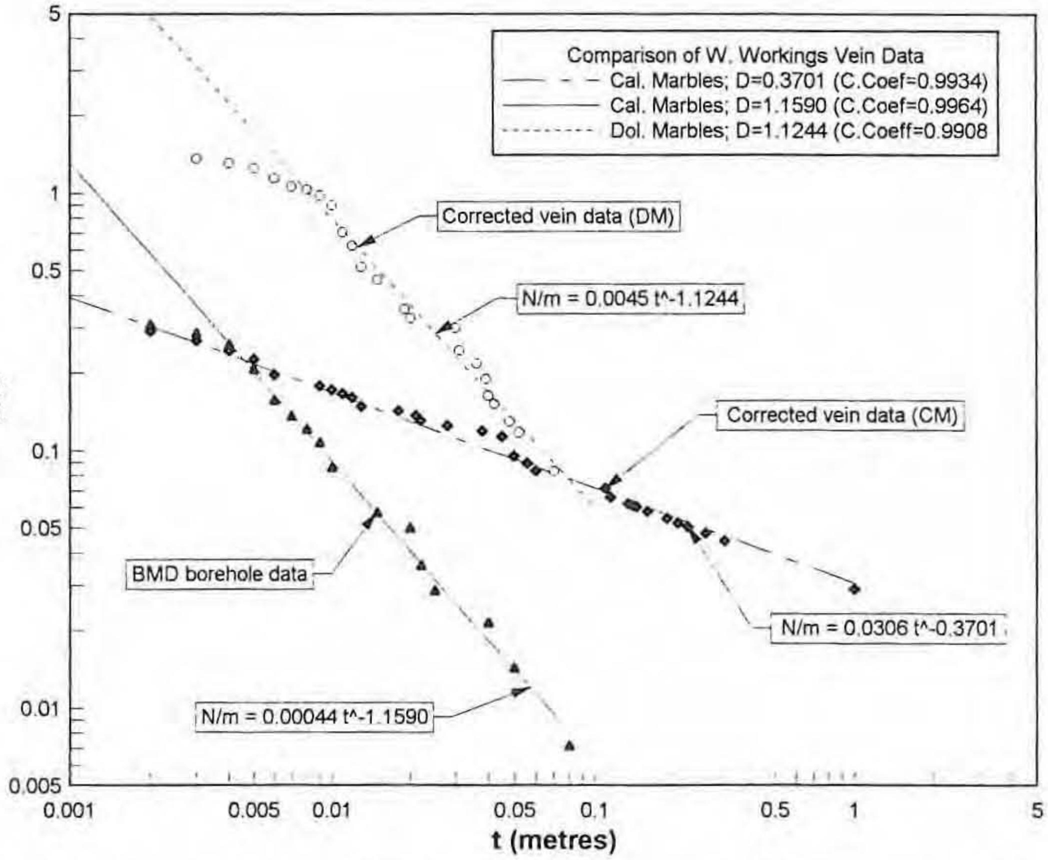

Fig. 8.12: Log-log plot of the cumulative number of veins per metre, N/m(≥t) versus vein thickness, t for various vein data collected in the Western Workings area. Corrected line survey data for veins in calcitic (bold diamond symbols) and dolomitic marbles (open circles), as well as vein data from the BMD-2 borehole core (filled triangle) are presented. Note the similarity in D-value between the borehole core which intercepts veins in calcitic marbles to veins in the nearby dolomitic marble, but the marked difference in their density (i.e. relative 'height' of curves in log-log space as indicated by the value of C). Veins hosted in calcitic marble yield a corrected D-value of 0.3701±0.09; veins in dolomitic marbles yield a corrected D-value of 1.1244±0.33; borehole vein data yields a D-value of 1.1590 (no correction apparently required).

marbles but a much lower density at all scales (i.e. veins in the core yield a C of 0.0004 compared to 0.0045 for veins in the dolomitic marbles).

The disparity between the data collected along surface transects and from borehole core in the calcitic marbles may occur for a number of reasons. Firstly, the borehole data may be sub-standard because BMD-2 is not ideally oriented to intersect veins with an average orientation of 012°/54° (strike-dip, right-hand rule). The optimum borehole should have been positioned closer to 282°/36° (trend-plunge) and not at 325°/60°. In addition, the veins intersected by the borehole only cover 2 orders of magnitude (the line survey spans more than 3) and so may be heavily truncated at the large scale. The results indicate the importance of correct borehole orientation so the majority of vein intersections are approximately perpendicular to the core, and that there is optimum chance of intersecting a wide thickness range right up to the t_{max} in the best case scenario.

A marked disparity between the two data sets could also occur if the BMD-2 borehole sampled marginal parts of the vein system in the calcitic marbles because of its very steep plunge (i.e. 60°). Veins in the upper parts of the calcitic marbles could have developed in a similar way to veins in the dolomitic marbles because of their close proximity, and hence share high D-values >1. These veins could represent a transition between the low D-value vein system of the calcitic marbles and the higher D-value vein system hosted by dolomitic marble. The low value of C may be a result of the poor positioning of the borehole or may indicate a decrease in veining towards the margin with the dolomitic marbles.

8.3. Vein Length-Width Relationships

In addition to collecting vein-thickness data in the Onguati study area, vein length (apparent) and width (maximum) measurements were taken from well-exposed examples. The relationship between vein length and width is often fractal and can provide useful information on growth history and possibly even the stresses of formation of the veins (Vermilye & Scholz, 1995). When plotted on log-log graphs, length-width data often lie in a linear array, which can be described by a power-law relationship of the form (Johnston & McCaffrey, 1996; Stowell *et al.*, 1999):

$$L = kW^a \qquad [4]$$

where L is length in mm, W is width in mm, k is a constant of proportionality, and the exponent *'a'* determines the rate of change in aspect ratio with scale. Johnston & McCaffrey (1996) relate the constant k to wallrock strength and strain field, so that ideally, simple shear in soft rocks leads to a small value of k and low aspect ratio (i.e. length/width value) veins, while pure extension in hard rocks results in a large k and veins with a high aspect ratio.

As is shown in Fig. 8.13[a] when a is 1, veins increase in length at the same rate at which they grow in thickness (i.e. they maintain a constant aspect ratio) and are therefore self-similar over a range of scales (Stowell *et al.*, 1999). In most geological settings though $a \neq 1$, so that either $a>1$, or more commonly $a<1$ (Johnston & McCaffrey, 1996). In situations where $a>1$ or $a<1$, the veins are termed self-affine because vein geometry changes exponentially as a function of the scale (Johnston & McCaffrey, 1996; Stowell *et al.*, 1999).

In this study, the length-width data for veins were combined from all the localities because it was difficult to find sufficient numbers of fully-exposed veins at each locality alone. The data have been plotted in Fig. 8.13[b], and yield the average relationship $L = 2011\ W^{0.55}$ ($n=25$, $r=0.8970$). The veins from the Onguati study area are self-affine ($a=0.55$), and because $a<1$, grow in thickness and inflate faster than they grow in length. Longer veins will consequently be relatively wider than shorter veins in the population (Stowell *et al.*, 1999). The value of k (2011 mm) simply represents the approximate length of a 'unit', 1 mm-thick vein in the combined sample for the 4 veins systems studied. The k-value can be a useful parameter in comparison to other millimetre-scale, vein width-to-length plots.

Although more vein data needs to be collected, this preliminary work indicates that at all of the sites in the calcitic marbles, veins follow the same self-affine scaling laws so that their axial ratios change in a similar manner across scale. This observation could be significant in the calcitic marbles because it means that while the Brown Mountain vein system contains a smaller thickness range (i.e. larger D-value) to those hosted at Onguati Mine and Western Workings, they all grew by the same mechanism. If some of the Brown Mountain veins had continued to grow to large sizes they would have ultimately developed the same vein geometries as the thickest veins in the other two areas.

A basic application of defining the relationship between vein length and aperture is the ability to estimate length, within certain maximum and minimum limits, by simply measuring the true thickness of veins where their full extents are obscured by cover. This could be useful if veins of economic interest were intersected along diamond drill holes during future exploration of the Onguati region because at least minimum estimates of vein length could be made, and the volume of vein material calculated for ore resource evaluation.

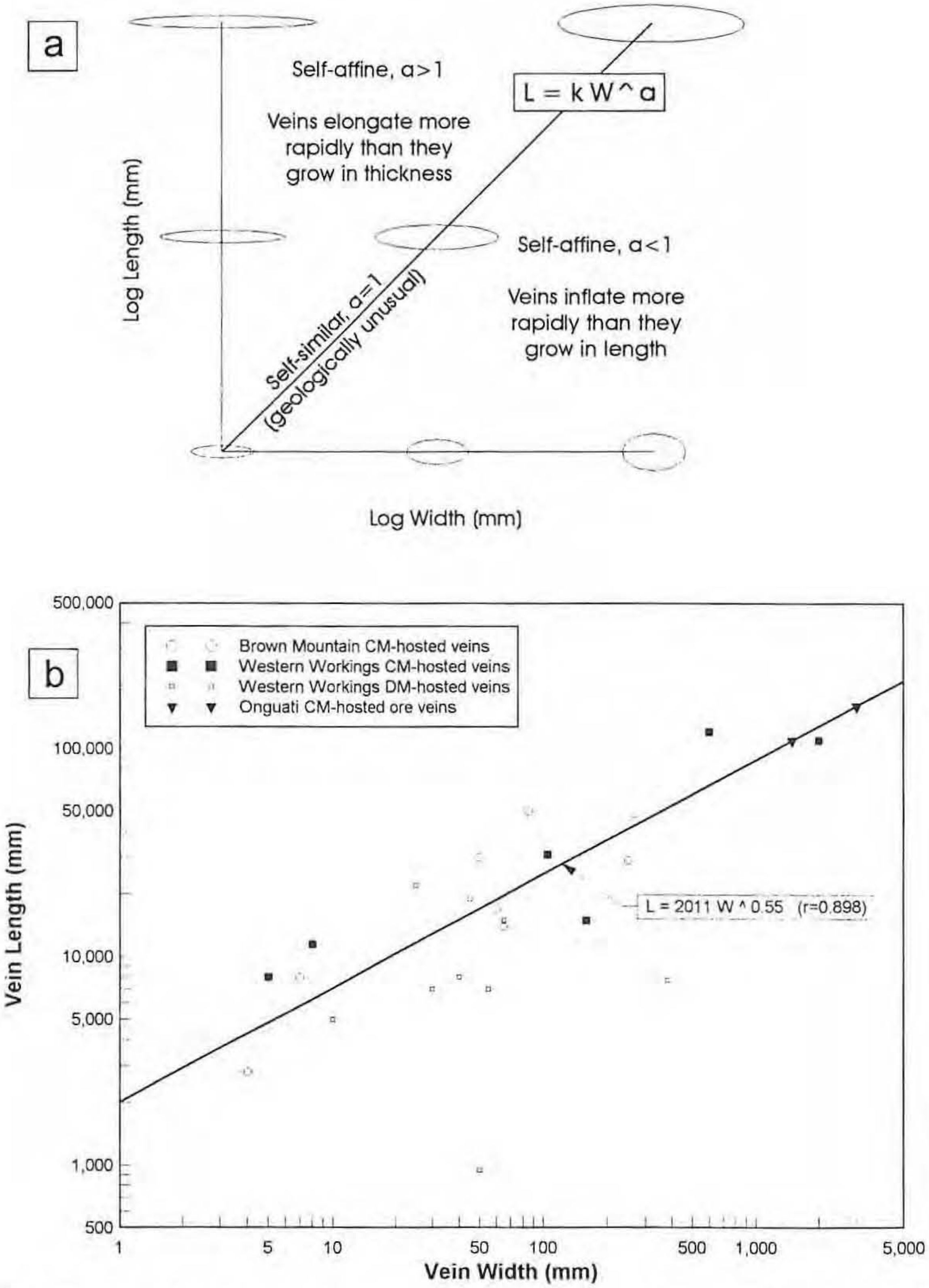

Fig. 8.13: Log-log plots of apparent vein length (mm) versus vein width (mm). (a) Plot after Johnston & McCaffrey (1996, Fig. 5, p.355) showing the form of the straight line fit and the fields for self-similar veins (a=1) and self-affine veins (a≠1); (b) Combined vein data for calcitic and dolomitic marbles of the Onguati Mine, Brown Mountain and Western Workings areas yields an average relationship: L = 2011 W^0.55 (n=23, r=0.898).

8.4. Discussion of Fractal Concepts

While vein systems provide a final 'snapshot' of the dynamic processes that resulted in their formation, it is almost impossible to reconstruct their development from field evidence alone. Model simulations for the development of various vein thickness distributions have been of particular use in this regard. They have allowed vein system evolution to be tracked over time and have permitted simple relationships between the fractal D-value and processes of vein growth to be determined and tested. This section summarizes the main results of models proposed in the available literature. Section 8.5 discusses the significance of these results to the vein systems found in the Onguati study area and accounts for differences in array style and mineralization.

How does a fractal vein thickness distribution result?

The size distribution of any natural phenomena is ultimately controlled by the birth rate, growth rate and death rate of the objects within a population (Clark *et al.*, 1995). Vein thickness distributions are no exception, but unlike other phenomena, veins are not commonly annihilated after formation (i.e. death rate is effectively zero). Vein systems are particularly useful to study because they are a permanent record of the results of different vein nucleation and growth rates. For vein thicknesses to exhibit a power-law distribution it is necessary to couple a constant vein nucleation rate with a proportional growth rate (Clark *et al.* 1995).

How is a constant vein nucleation rate achieved and maintained?

In view of the fact that rocks have innumerable imperfections over many orders of scale, it is not difficult to envisage constant vein nucleation in a heterogeneous rock mass undergoing deformation. Although favourable imperfections at any scale can result in failure (Paterson, 1978), Griffith (1921, 1924) discovered that fracturing in rocks was most strongly influenced by minute flaws at the grain-scale. These microfractures are commonly referred to as Griffith cracks and are ubiquitous and inherent features of all rocks that are activated, but not created by deformation (Paterson, 1978; Cladouhos & Marrett, 1996). Griffith cracks measure between 1 and 1000 microns in length and have apertures of a few microns (Davis & Reynolds, 1996). They occur particularly at grain boundaries as intergranular microfractures, or within and between grains as intra- and trans-granular microfractures respectively (Paterson, 1978).

Griffith cracks almost always cause rocks to be significantly weaker than their theoretical strength (Paterson, 1978). They reduce resistance to fracturing by focussing and amplifying very low remote stresses into high magnitude, local stresses which can exceed the interatomic cohesion at microcrack tips (Davis & Reynolds, 1996). Griffith's theory (1924) envisages failure when the vulnerably oriented microcracks in a population of randomly arranged features, begin to extend under the applied stress (Paterson, 1978). The implication for rocks undergoing deformation is that it should be relatively easy to maintain a steady-state, vein nucleation rate. There are an almost infinite number of flaws to 'seed' fracturing as long as deformation is long-lived and there is an abundance of fluids to fill the newly formed fractures.

Are fractures initially seeded with a power-law distribution in size or spacing?

The orientation and distribution of Griffith cracks in rocks varies quite considerably, but because they are made up of a whole combination of different flaws (e.g. mineral cleavage, grain boundaries, tectonic micro-cracks etc...) it is very unlikely that they will show an initial power-law distribution in size or spacing. Where pre-existing microfractures show fractal distributions (e.g. Wong *et al.*, 1989), it is possible that they represent some of the smallest-scale remnants of a previous deformation that utilized yet earlier Griffith cracks. In all probability, vein systems develop power-law distributions irrespective of the original distribution or arrangement of Griffith cracks. Numerical models of fault development by Cladouhos & Marrett (1996) demonstrate that it is possible to create power-law fault length distributions from microfracture populations with initially unimodal distributions. This finding strengthens the notion that it is the nature of the growth processes (i.e. birth and growth rates) and not the starting conditions (e.g. size or spacing distributions of Griffith cracks in the host rock) that determines whether the vein system develops a fractal size distribution or not.

How is a proportional growth rate achieved?

Proportional vein growth can only be achieved in natural systems by positive feedback processes (Clark *et al.*, 1995). Positive feedback refers to a run-away effect where a change to some variable results in mechanisms that amplify the change. In vein systems where growth rate is a function of vein size, positive feedback is a consequence of the interplay between deformation and the planar anisotropy introduced to the rock mass by veining. Just as Griffith microfractures reduce the strength of rocks considerably, so newly nucleated veins represent sites of discrete weakness that localize strain. As more strain is accommodated by a growing vein so its growth rate accelerates and the larger it becomes in a positive feedback process.

The growth of veins by a positive feedback process can be simplified and interpreted in terms of the 3D stresses acting around each vein in the developing array, assuming elastic rheology (Gillespie *et al.*, 1999). Veins possess two important zones with respect to stress. One is an extensive zone of low tensile effective stress perpendicular to each vein wall, known as the stress shadow. The other is a small zone of enhanced effective stress at the vein tip, referred to as the process zone, in which new fractures may grow even when the remote stress is compressive (Price & Cosgrove, 1990). Because larger veins have proportionally higher growth rates they easily outpace the growth of nearby smaller veins, often trapping them in their ever expanding stress shadows (Gillespie *et al.*, 1999). At the same time the process zone of the large, growing vein will exert an increasing influence on more distant veins (Gillespie *et al.*, 1999). Put another way, the biggest members of the vein system would accommodate larger amounts of the available strain and would leave less energy for the nucleation and growth of other veins. This scenario allows for the development of a power-law vein thickness distribution (i.e. strongly skewed distribution) where there are exponentially greater numbers of small veins (low growth rates, large numbers) compared to thick veins (high growth rates, small numbers).

Does layering have an effect on vein thickness distribution?

Studies of synthetic and natural vein systems by Gillespie *et al.* (1999) indicate that profound differences exist between stratabound and non-stratabound vein systems. In stratabound arrays, individual veins are confined to the thickness of discrete mechanical units such as individual beds, and seldom display power-law distributions in size or spacing (Gillespie *et al.*, 1999). Regular vein spacing is the norm in stratabound arrays and is thought to develop because veins often have stress shadows proportional to their width, at least in elastic rheologies (Gillespie *et al.*, 1999, p.53). Only so many veins can form in each mechanical unit (i.e vein density is related to layer thickness) before the stress shadows of the veins begin to repel one another and saturation ensues (Gillespie *et al.*, 1999).

Vein arrays in non-layered rocks tend to be clustered (i.e. fractal spacing) and commonly display power-law vein thickness distributions (Gillespie *et al.*, 1999). In such systems the size of the localized stress field is proportional to vein size as detailed above (e.g. thickness as in Clark et al., 1999, and Monecke *et al.*, 2001; or length as per Gillespie *et al.*, 1999), and there is little influence from the host rock. Non-layered rocks present fewer "crack-stopping discontinuities" to the growing vein and allow the development of power-law size and spacing distributions (Gillespie *et al.*, 1999. p.53). Consequently there is no characteristic size or spacing scale to the vein system. Clustering of veins can result in non-layered rocks because large veins outpace and encroach on smaller veins without being repulsed by their much weaker stress shadows (Gillespie *et al.*, 1999).

While the calcitic marbles of the Onguati study area have a well developed banding (S_0/S_1 foliation) individual layers have not constrained the growth of individual veins (i.e. veins cross-cut the layering). The lack of significant vein diffraction or termination at layer interfaces, even where thin calc-silicate laminations occur, indicates that there is little rheological contrast between the marble bands and that the layering in the calcitic marbles does not impede the growth of the majority of veins. While large calc-silicate units may impose significant crack-stopping mechanical barriers they do not occur everywhere in the calcitic marbles and thus do not appear to have had a profound effect on the distribution of vein thicknesses. Although individual veins are not limited by layer thickness, it is evident that whole vein systems are constrained to rock type in the Onguati study area, so that veins in adjacent dolomitic and calcitic marble packages belong to two separate vein systems, each with a distinct D-value.

Can numerical models provide insight into the development of vein systems with power-law vein thickness distributions?

The power-law relationship $N = C\ t^{-D}$ does not describe the formation of veins or fractures, but quantifies the scale-invariant process by which country rocks undergo brittle extension (Kruhl, 1994b). An early attempt to mimic vein system formation with a power-law thickness distribution was based on a Cantor-dust model (Kruhl, 1994b). Cantor dusts are one of the oldest fractal sets known to mathematics (see Mandelbrot, 1977 for details), and have previously been used to describe fracture patterns in geological materials (e.g. Velde *et al.*, 1990). In the Cantor-dust model, the continuous broadening of veins leads "to successively thinner veins and an escalating irregularity in the regional stress field" (Kruhl, 1994b, p.102). The formation of veins of different thickness results in local decreases in the stress field around each vein (Kruhl, 1994b). The D-value in such a model can thus be related to the rate at which vein thickness decreases with successive formation, or the rate at which the stress field becomes more irregular (Kruhl, 1994b, p.102). The D-value additionally indicates the probability of finding a vein of certain thickness within the vein system (Kruhl, 1994b). While the model successfully captures the fractal pattern of vein thickness distribution, it does not provide insight into the ultimate mechanism(s) responsible. The Cantor-dust model may also over-simplify vein evolution because it relies on the growth of successively thinner veins only after the formation of very large veins in the system.

Clark *et al.* (1995, p.976) present an insightful stochastic model of vein system evolution that relies on a positive feedback process where larger veins grow thicker at a rate proportional to thickness. The following assumptions were made: (1) new veins with a minimum thickness t_0 are introduced at a constant nucleation rate, so a constant ratio A between the number of birth and refracturing events is maintained; (2) the probability P of any given vein refracturing and growing thicker is the same (i.e. $[P \propto 1] \div$ number of veins); and critically for a proportional growth model, (3) once a vein refractures, it continues to grow for as long as required until it has grown to some proportion B of its thickness (i.e. after refracturing, vein of thickness t grows to thickness $[1+B]t$). The model of Clark *et al.* (1995) incorporates a crack-seal process of vein growth which is thought to be common in natural systems.

Monecke *et al.* (2001) have developed an analytical model, which like that of Clark *et al.* (1995), attempts to quantify the relationship between the D-value and the nucleation and growth of veins. A simple interpretation of the fractal dimension is given as follows (see Monecke *et al.*, 2001, p.412 for details):

$$D = \frac{\alpha V}{\beta N} \qquad [5]$$

where D is the fractal dimension, α is the nucleation rate which is held constant during a specific geological time interval, V is the volume in which veining occurs, β is the growth rate constant (so that the growth rate, $\gamma = \beta t$), and N is the number of veins between t_{min} and t_{max} (in volume V). Monecke *et al.* (2001, p.412) propose that the D-value is the quotient of the amount of material consumed in vein nucleation over a certain period of time, over the amount of material incorporated during vein growth during that same time.

In log-log plots of cumulative number versus vein thickness, results from both the models of Clark *et al.* (1995) and Monecke *et al.* (2001) conform to a power-law distribution. Although A and B in Clark *et al.* (1995) are not exactly equivalent to α and β in Monecke *et al.* (2001), it is possible to make the same generalisations from both models. Namely, the slope shallows (i.e. lower D-values) in log-log space with a decreasing nucleation rate and increasing proportional growth-rates, so that a smaller D-value simply reflects the greater prevalence of thicker veins in the vein population. Simulations by Clark *et al.* (1995) show that if all steps are birth events ($A=1/0$) then veins will have the same thickness and the slope will be vertical, but if all the steps are growth events ($A=0$), D approaches 0. These observations are in agreement with Monecke *et al.* (2001), whose model predicts that vein systems with lower α/β ratios (i.e. high nucleation rates) will have larger D-values and be dominated by thinner veins. Conversely, when the α/β ratios are higher (i.e. very high proportional growth rates), the scale range of vein thicknesses will increase exponentially and D will tend towards smaller values.

How realistic are the above models and is the development of power-law size distribution compatible with vein linkage?

Field studies and simulations of fracture system formation both show that linkage is a common and necessary process by which veins can substantially increase in length, and so in turn thicken, to produce vein arrays with fractal properties (Cladouhos & Marrett, 1996). Examples of multi-segment veins, where veins are composed of tip-to-tip linked elements, and sets of intersecting or branching veins have been found in many vein systems, especially those with power-law vein thickness distributions (e.g. Sanderson *et al.*, 1994; Vermilye & Scholz, 1995; Johnston & McCaffrey, 1996; Roberts *et al.*, 1998, 1999, Stowell *et al.*, 1999). Additional evidence of linkage can also be found in log-log plots of comprehensive vein length-width data where significant length scatter may be found for each vein width recorded (e.g. Johnston & McCaffrey, 1996, Figs. 2 and 6; Stowell *et al.*, 1999, Fig. 11). The plots show that for each vein width there may be a range of possible lengths, so that a transition exists between short veins that have grown by simple tip propagation with little or less linkage, and very long veins produced by multiple vein linkage.

The models of Clark *et al.* (1995) and Monecke *et al.* (2001) can be referred to as single-vein growth models (analogue of the single-fault growth model of Cladouhos & Marrett, 1996) because each vein in the population grows by simple tip propagation, at a rate proportional to size. The models discussed above do not take linkage of individual veins into account, so while they can successfully simulate power-law vein thickness distributions and provide insight into vein system evolution, they probably represent the simplest possible scenarios for doing so. In particular the mechanism/s by which proportional growth rates are achieved may be somewhat over-simplified when vein linkage is considered. Because single-vein growth models do not reproduce the dynamic interaction of veins they can not be fully realistic. After all, it is the competition between vein nucleation and growth processes amongst members of the vein population that leads to the development of power-law size distributions and to vein systems with differing D-values.

The fault growth studies of Cladouhos & Marrett (1996, p.284) have demonstrated that single growth models require enormous growth increment exponents to produce power-law distributions, and that these values far exceed the possible range for geological systems. These findings strongly point to the action of other processes of fracture propagation in addition to simple tip growth, the most likely of which is linkage (Cladouhos & Marrett, 1996). Vein linkage models (Zhang & Sanderson, 1994; Roberts *et al.*, 1998, 1999) and their fault linkage analogues (Cladouhos & Marrett, 1996) share a number of similar concepts and procedures, namely:

1. The models consist of a simulated model region of finite size which contains a population of Griffith-like microcracks. The configuration of these flaws varies considerably between the different models so that they can be seeded with random or unimodal spacing distributions, and lengths that are either power-law or normal in distribution. The initial population can also consist of single or multiple sets of flaws that may show random or normal deviation about the mean orientation of each microfracture set.
2. On model activation, favourably oriented microfractures dilate and begin to grow by one of two mechanisms: (a) incremental tip growth of individual veins where growth rate is directly proportional to vein size, or (b) if two vein tips are in close proximity they link to form a multi-segment vein.
3. The distance at which linkage occurs between two fracture tips depends on the size of each of the veins involved (e.g. when the larger process zone of a longer vein intersects the smaller process zone of a shorter vein, then veins can "elastically feel each other" (Cladouhos & Marrett, 1996, p.285) and attract one another to link). In many models this is simplified so that two fractures link when the distance between their tips is some proportion of the combined length of both veins.
4. All of the models assume that the vein linkage is a scale invariant process so that veins of all sizes can link to form larger structures.
5. In the models of Roberts *et al.* (1998, 1999) vein thickness is proportional to vein length (i.e. $L=kW^a$), so once two veins link the multi-segment vein grows in thickness to some proportion of its new length.

The vein linkage models are sampled at regular intervals during the simulation so that the progress of vein linkage can be monitored in relation to the evolving vein thickness or length distributions of the model region. The results from all the simulations show that power-law size distributions can be quickly attained for fractures that have linked, regardless of the initial flaw distribution (Sanderson *et al.*, 1994; Zhang & Sanderson, 1994; Cladouhos & Marrett, 1996, Roberts *et al.*, 1998, 1999). Unlinked flaws grow at proportional growth rates and thus retain the original size distributions defined by each model (Cladouhos & Marrett, 1996).

The vein thickness distributions become power-law distributed because linkage provides an effective mechanism for veins to grow unevenly in the population (Cladouhos & Marrett, 1996). Linked veins may cannibalize smaller veins (Cladouhos & Marrett, 1996) or may trap such veins in their exponentially larger stress shadows (Gillespie *et al.*, 1999). Either way, linkage provides a stop to high initial nucleation rates after a short model time (Monecke *et al.*, 2001). In common with the models of Clark *et al.* (1995) and Monecke *et al.* (2001), linkage allows larger veins to accommodate more strain and dilation, and hence to concentrate more hydrothermal material at the expense of newly formed veins.

What is the effect of vein linkage on D-value?

One of the most significant findings of the linkage simulations is that there is a systematic decrease in D-value as vein linkage becomes more widespread in the model region (Zhang & Sanderson, 1994; Cladouhos & Marrett, 1996, Roberts *et al.*, 1998, 1999). In fact Cladouhos & Marrett (1996) suggest that the D-value does not evolve to a constant value. Instead they predict the power-law exponent D will continue to decrease as long as the model region does not constrain the length of the growing fractures. If the longest veins are allowed to approach the dimensions of the simulated model region then the decrease in D-value slows and becomes limited. Increasing either the initial flaw density or reducing the tip distance for linkage in the model results in more efficient vein linkage and causes a more rapid decrease of the power-law exponent D (Cladouhos & Marrett, 1996).

As an increasing proportion of the flaws become linked to form a multi-segment vein population, so the power-law thickness and length distributions will come to have decreasing D-values that are ultimately defined by the smaller, more numerous veins of that population. The result is that the larger veins have to grow at ever increasing rates (exponential?) to maintain the evolving power-law size distribution. A point is reached in the models where these increasing rates of growth can no longer be sustained because the model region imposes limits on the lengths of fractures that can link and grow (Cladouhos & Marrett, 1996). A multi-segment vein can only attain the dimension of the simulated model region, and as a consequence, its thickness can only grow to some proportion of this constrained length. The larger veins in such data sets thus deviate from the power-law distribution (e.g. Cladouhos & Marrett, 1996; Roberts *et al.*, 1998, 1999) in an effect known as "roll-over" (Cladouhos & Marrett, 1996, p.288).

Cladouhos & Marrett (1996) speculate that this roll-over effect could occur in natural systems because fracture arrays are always finite in size, either constrained by stratigraphic or structural boundaries. Therefore, roll-over can provide an alternative interpretation of the large-scale fall-off seen on many log-log plots of cumulative number versus thickness or length (Cladouhos & Marrett, 1996). Traditionally this deviation is explained as finite range effect related to the RHT of the sample (e.g. Pickering et al., 1995, 1996). In the Onguati Mine and Western Workings areas, the largest veins can be several metres thick and have lengths of a hundred metres or more, and could have been limited in their growth by the thickness of the calcitic marble package which hosts them. As a consequence the large-scale fall-off seen in these plots (Figs. 8.5 and 8.7) could indicate the onset of large-scale vein linkage and the break-down of the power-law vein thickness relationship. In the other areas though, the thickness of the calcitic and dolomitic packages would have had little to do with the large-scale fall-off because the veins in these systems are generally much smaller in size.

8.5. Implications for Mineralization in the Onguati Study Area

From previous studies, there appears to be growing evidence that a relationship exists between the D-value of the fractal vein thickness distribution and vein mineralization. Analysis of vein thicknesses and gold grades in drill core from the La Codosera region of western Spain demonstrates that vein systems with low D-values have systematically higher gold grades and are associated with more extensive hydrothermal alteration (Sanderson *et al.*, 1994; Roberts *et al.*, 1999). The same relationship, where lower D-values are associated with more intense mineralization, is seen in Sn-W–bearing veins of the Central Iberian Peninsula (Roberts *et al.*, 1998; 1999) and for sulphide-bearing veins in the Hellyer VHMS deposit of Australia (Monecke *et al.*, 2001).

In the Onguati study area, vein systems hosted by calcitic marbles of the Western

Workings (D=0.3701) and Onguati Mine (D=0.4056) areas have the lowest vein thickness D-values and show the best indications of mineralization. Both sites have been previously mined for their Cu-sulphide mineralization and have produced appreciable quantities of Au as a by-product (see Appendix A for detail on the mining history). This is in stark contrast to veins hosted by calcitic marbles of the Brown Mountain area, where the D-value for surface veins is significantly higher (0.6035) and the vein system does not host Cu or Au mineralization. The highest D-values in the Onguati study area are found in the dolomitic marbles of the Brown Mountain (0.9940) and Western Workings (1.1244) sites. Although the veins have extensive tremolite, skarn-like margins with minor malachite staining, previous exploration in these systems has failed to find economic mineralization. The relationship between D-value and mineralization is not simply related to any of the commonly measured vein parameters such as vein density or vein thickness per metre values. For example, veins hosted by calcitic marbles at Brown Mountain appear to be poorly mineralized even though they have a higher vein density (2.03 veins/m) and a similar vein thickness per metre value (74.16 mm/m) to those at Onguati Mine (0.41 veins/m and 63.18 mm/m respectively).

In the previous section detailing fractal concepts, it was emphasized that vein linkage is an important process by which veins can achieve uneven growth, initiate positive feedback mechanisms of propagation and thus evolve to have power-law vein thickness or length distributions. Linkage may also be key to understanding the apparent relationship between the intensity or quality of hydrothermal vein mineralization and the D-value at the different prospects in the Onguati study area, and elsewhere where fractal vein distributions are encountered. Well connected arrays of veins, and other fracture phenomena such as faults, provide high permeability pathways for hydrothermal fluid flow in otherwise impermeable mediums (Cox, 1999). As such, linked vein systems have been interpreted as types of percolation phenomena that may belong to much larger percolation networks (Sahimi, 1994). This is fully compatible with modern ideas of mesothermal vein mineralization (see Cox, 1999) where deposits are often found in close proximity to faults and shear zones that form part of a larger, crustal-scale system of shears (Chapter 3 highlights regional structures in and around the Onguati surrounds that may be part of such a system).

Insights from percolation theory (see Sahimi, 1994, for a comprehensive review) have been used to interpret vein system evolution and mineralization in the Onguati study area. In this regard, the percolation cluster models of vein linkage developed by Sanderson *et al.* (1994), Zhang & Sanderson (1994) and Roberts *et al.* (1998, 1999) have been of particular use. At the start of vein system formation in the Onguati region, it is envisaged that all of the veins would have been small and poorly connected (Roberts *et al.*, 1999). The veins would have had characteristically narrow thickness ranges and very high D-values (≫1). Continued vein nucleation and growth would have resulted in increasing vein density and this would have forced an increasing proportion of veins to interact. In many instances smaller veinlets would have been cast into the stress shadows of larger veins and would not have grown further (i.e. stop to high vein nucleation rates). Other veins would have linked and this would have initiated the formation of veins "clusters" (Sahimi, 1994, p.10). Vein clusters allow effective fluid passage between their interconnected members but are always bound by vacant or 'dead-end' elements (Sahimi, 1994). Models show that both vein clusters and unlinked veins would have only allowed the ingress of locally-derived fluids that would have flowed over small distances (Sanderson *et al.*, 1994; Roberts *et al.*, 1998, 1999). Present-day evidence for limited fluid flow is commonly found away from the most intensely veined areas of the Onguati study area, where thin, isolated veins are dominated by a carbonate fill which is sourced from the adjacent marble host rocks.

As deformation proceeded in the Onguati region, the vein clusters would have grown considerably in extent by linking with nearby veins and other fracture clusters. Models predict that the D-values would have dropped rapidly with increasing vein linkage (Cladouhos & Marrett, 1996; Roberts *et al.*, 1998, 1999). With time a larger proportion of the veins in the Onguati study area would have become interconnected, until eventually, the largest vein clusters in each of the vein systems would have linked with nearby faults or shear zone networks. Thus each of the Onguati vein arrays represents a branching or "dangling" element off a much larger, crustal-scale percolation network (Cox, 1999, p.132). As the network became more intricately linked across scale, a percolation threshold would have eventually been reached (Cox, 1999; Roberts *et al.*, 1999). The whole fracture system would have then suddenly switched from a macroscopically disconnected structure to a connected one, in the same manner as a phase change (Sahimi, 1994). "Sample-spanning" (Sahimi, 1994, p.11) of the network by the largest group of connected elements, known as the "infinite cluster" (Roberts *et al.*, 1999), would have resulted in the onset of fluid flow across the entire width of the hydrothermal system (Cox, 1999). Hence, a large potential source area of metals and fluids would have been made available to downstream parts of the network, such as the vein deposits in the Onguati region.

Differences in D-value and mineralization potential between the vein systems in the Onguati study area may simply be related to the efficiency of fluid flow through fracture networks of differing connectivity. At Onguati Mine and Western Workings, the calcitic marbles may host vein arrays with high connectivities because their vein thickness distributions are characterized by very low D-values ($\ll 1$). These intensely veined areas would have been able to tap high fluid fluxes from the nearby backbone faults and shear zones of the infinite cluster, and consequently would have become better mineralized than less well connected systems in the dolomitic marbles. The ingress of externally-derived fluids into the Onguati vein arrays is shown by the presence of large volumes of quartz gangue and sulphides which could not have been extracted from the marbles alone.

The vein systems in the calcitic marbles of all three areas are generally better connected than those in dolomitic marble because strong strain partitioning occurred between the host rocks. During deformation, the calcitic marbles would have been considerably more ductile than the adjacent dolomitic marbles and would have accommodated much more strain. Consequently, veins in the calcitic marbles would have localized more dilation as is shown by the steeper cumulative vein thickness curves in Figs. 8.8 and 8.9. These veins would have also grown to greater lengths and in a more clustered fashion to their dolomitic counterparts. The greater range of thicknesses developed, and the higher likelihood of linkage is reflected in the low D-values (0.4 - 0.6) of these systems. In the competent dolomitic marbles, the veins would have been partially shielded from regional stresses and would not have developed the connectivity required to localize fluid flow and concentrate mineralization.

The higher D-value of the vein array in calcitic marbles of the Brown Mountain area (~0.6) suggests that it was not as well connected to the regional hydrothermal system as its counterparts were at Onguati Mine and Western Workings (both have D-values of ~0.4). Brown Mountain has a higher D-value because a larger proportion of its mineral precipitates were incorporated into smaller veins, and thus its fluid flow was more dispersed. It appears that this area had a higher vein nucleation rate than vein systems at Onguati Mine or Western Workings, where nucleation was suppressed and more vein material was concentrated into small numbers of very large veins. Aerial photographs (see chapter 3) show that the Brown Mountain area is associated with a NNE-trending linear structure (same orientation as a nearby thrust or reverse fault) which could represent a large shear zone. If this is the case, then higher strain rates may have been accommodated in the calcitic marble package at Brown Mountain. A higher vein density may have resulted in the shear zone and dilation could have been more evenly distributed throughout the rock mass to produce a high D-value vein thickness distribution. Although there is considerable field evidence of intersection and linkage in these veins, the Brown Mountain vein array would have contained a large fraction of sealed veins because of their generally smaller thicknesses. This would have impeded efficient fluid flow throughout the vein system. Smaller veins also provide a larger surface area of rock for cooling and reaction to occur with hydrothermal fluids, and as a result the Brown Mountain veins contain more disseminated, non-economic mineralization. It is also possible that Cu±Au deposition could have occurred at an earlier stage and that better mineralization could be encountered at depth in the Brown Mountain vicinity.

Onguati Mine and Western Workings contain much thicker veins in the calcitic marbles (reflected in the lower D-value) and these would have remained open to flow for longer periods of time. The thicker veins of these two areas, would have allowed extremely focussed fluid flow within restricted parts of the vein system and would have provided smaller surface areas, possibly even armoured vein margins, that would have prevented premature fluid-rock reaction (Roberts *et al.*, 1999). While the hydrothermal fluids may have only contained very small amounts of metals (e.g. ppm or even ppb range), the high fluid fluxes concentrated along limited parts of the vein network could have resulted in slow but continuous metal deposition over an extended time period to produce economic Cu±Au deposits in the Onguati Mine and Western Workings areas.

The determination of D-values for power-law vein thickness distributions could be useful in further exploration of the Onguati region for a number of reasons:

1. The D-value reflects mechanisms responsible for vein system formation and provides insight into the percolation properties of the network. Contrasting D-values between mineralized and barren vein systems indicate that vein systems can develop in entirely different ways (Roberts *et al.*, 1998, 1999; Monecke *et al.*, 2001).

2. The D-value provides a powerful descriptive parameter that could be used to quantitatively characterize and compare vein arrays in the Karibib region. For example, higher D-values may be associated with more disseminated, stockwork-style deposits, while lower exponents may indicate the development of thick vein-style systems (Monecke *et al.*, 2001).

3. The D-value is a potential exploration tool that can be used to make predictions of vein properties such as connectivity from spatially limited data, commonly collected from 1D borehole core or line transects. In addition, the D-value can be easily calculated in the field, and may provide preliminary indications of mineralization potential before assay results can be made available.

4. Once the D-value has been measured, the power-law relationship allows more reliable up- and down-scale extrapolation of vein thickness to be made than traditional vein parameters (Monecke *et al.*, 2001). This could help better constrain resource calculation and guide further exploration.

The fractal analysis of the Onguati vein arrays suggests that while favourable physical and chemical conditions are provided in the calcitic and dolomitic marbles of all the areas studied, that economic mineralization will only occur in these rocks when vein systems are well connected to a suitable source area, with a sufficiently focussed fluid flow.

9. ORE GENESIS IN THE ONGUATI STUDY AREA

9.1. Review of Genetic Models

A thorough understanding of the genesis of hydrothermal deposits in the Karibib region is of great economic interest, and could help to refine predictive exploration models for Au in this part of the Damaran Belt. In order to develop a successful ore genesis model for the Onguati vein deposits the following principal problems must be addressed:

(a) the source/s of metals, sulphur and fluids;
(b) the means of transporting ore components in the hydrothermal solutions;
(c) the regional fluid transport and focussing structures that link source to sink;
(d) the driving force for moving fluids through these crustal structures; and
(e) the physical and/or chemical mechanisms that result in economic and sub-economic Cu-Au mineralization.

Current models of hydrothermal deposit formation in this region of the SCZ, differ mainly in their proposed source rocks. Until recently little emphasis was placed on crustal- or deposit-scale structures that may have facilitated the passage or trapping of mineralizing fluids. In the first section of this chapter, a brief overview of the existing models will be presented, including the multi-stage model of Petzel (1988a), Pirajno & Jacob (1991) and Pirajno *et al.* (1991); and the differing source area hypotheses of Steven (1993) and Jacob *et al.* (2000a; b). In the second part, an integrated ore genesis model is detailed for the development of mineralization in the Onguati study area. This model may have wider application to hydrothermal mineralization in the northern parts of the Damaran Belt, and could provide useful input and geological control on future Au exploration programmes.

9.1.1. Multi-Stage Model of Ore Formation

The multi-stage ore genesis model (Petzel, 1988a; Pirajno & Jacob, 1991; Pirajno *et al.*, 1991) is the most comprehensive and integrated model to date, and is based on observations made in the Onguati region. The discovery of disseminated sulphides and elevated Au (up to 990 ppb) and metal contents in the mafic meta-volcanic rocks of the Daheim Member, close to the Onguati hydrothermal mineralization, sparked interest in a possible genetic relationship between the two (Petzel, 1988a, b; Pirajno *et al.*, 1991). In this region of the SCZ, the Daheim Member (Arandis Formation) is situated directly below the marbles of the Navachab Member (Karibib Formation) that host Cu±Au vein mineralization.

The first stage of this model involves submarine extrusion of alkaline basalts and pyroclastic material along normal faults bounding regional-scale grabens. The submarine volcanism may have been accompanied by extensive hydrothermal and exhalative activity. Convecting fluids could have leached magmatic sulphides and base metals from underlying mafic rocks. Disseminated sulphides and minor Au mineralization may then have precipitated within the volcanic sequence, and in the calcareous muds and limestones surrounding volcanic centres (Pirajno & Jacob, 1991; Pirajno *et al.*, 1991). This process would have formed a protore for subsequent hydrothermal activity in the SCZ (Pirajno *et al.*, 1991).

The second stage is related to Damaran orogeny and is characterized by high temperature metamorphism (approximately 580°C and 3.3 kbar) and widespread metamorphic dehydration (Pirajno *et al.*, 1991). The devolatilization reactions resulted in the creation of a metamorphic hydrothermal fluid which circulated through the mafic volcanic rocks of the Daheim Member, where it scavenged Mg and ore-forming constituents. It is thought that these fluids could have resulted in hydrothermal dolomitization of marble units in close proximity to the Daheim ortho-amphibolites (Petzel, 1998a; Pirajno & Jacob, 1991). Metals would have then precipitated in suitable traps in the overlying Karibib Formation marbles, possibly as disseminated mineralization or as thin veinlets and stockworks (Pirajno *et al.*, 1991).

In the final stage of this model, the intrusion of syn- to post tectonic Damaran granitoids led to a large input of heat and regional-scale hydrothermal convection was initiated. Metals were remobilized and concentrated into quartz veins in the marble and calc-silicate rocks of the Karibib Formation (Petzel, 1988a; Pirajno & Jacob, 1991). Early mineralization may have occurred mainly in stockwork systems, such as at Brown Mountain or Navachab Mine. In the later stages of hydrothermal mineralization, Au and Cu could have been remobilized from these stockworks into the larger 'vein-type' deposits of Onguati Mine or Western Workings (Pirajno *et al.*, 1991). The similar Cu-Au-Bi-W metal association at Onguati Mine, Western Workings and Navachab Mine compared to Fe-As±Cu±Au at Brown Mountain may be explained as a metal zonation effect away from a granitic heat source. In these models Brown Mountain is interpreted as being higher up within the magmato-hydrothermal system (Pirajno *et al.*, 1991).

While the multi-stage model provides a mechanism by which Au and ore-forming metals can be leached from a suitable source and concentrated by magmato-hydrothermal processes to form vein and skarn deposits, there are several problems associated with this model, namely:

1. The Daheim Member does not form a volumetrically significant part of the SCZ stratigraphy (Badenhorst, 1992). Meta-volcanic rocks of this unit vary considerably in thickness and are often confined to small lenses in the Karibib area, possibly bound by the faults along which they were intruded (Pirajno & Jacob, 1991). Although these rocks contain anomalous metal values and sulphide, it is unlikely that they could have supplied all of the vast quantity of metals required to form the economic Navachab Au deposit (ore reserve of ~12 Mt at an average grade of 2.17 g/t).

2. There is little evidence of ductile shearing, veining or fracturing that would have permitted widespread circulation of hydrothermal fluids and efficient scavenging of Au and sulphides from the mafic meta-volcanic rocks. Rocks of the Daheim Member experienced less severe deformation than surrounding, less competent lithologies (especially calcitic marbles) and preserve many original volcanic features such as pillows, lapilli and volcanic bombs (Mullin, 1989).

3. There is no obvious evidence of widespread leaching and alteration of the meta-volcanic rocks (Steven, 1993). Intense leaching would be required to produce sufficiently mineralized hydrothermal fluids, especially if the Daheim Member is limited in extent.

4. The multi-stage model invokes "regional-scale selective hydrothermal alteration" (Pirajno & Jacob, 1991, p.308) and "extensive dolomitization" that "destroyed earlier structures in the carbonate rocks" (Pirajno *et al.*, 1991, p.98), but field observations do not support this. While dolomitization may have occurred in marbles adjacent to the meta-volcanic rocks of the Daheim Member (Petzel, 1988b), and in parts of the upper calcitic marble package at Western Workings, its extent is very minor. The Daheim Member simply does not contain enough Mg to result in the extensive dolomitization envisaged (see Steven, 1993, p.125, for mass balance calculations). The small pockets of hydrothermal dolomitic marble at Western Workings are associated with

dense quartz veinlets and are relatively late features. The overlying DM unit on the other hand, was formed before deformation took place (i.e. different styles of folding and deformation are observed between the CM and DM units). The DM unit is also a homogeneous rock type, in many places is devoid of the stockwork-type veining required for effective Mg-fluid infiltration, and occurs at the same stratigraphic position over the entire Onguati study area. In the upper parts of the TM unit and in the lowermost parts of the DM unit, thin, well-defined calcitic and dolomitic marble laminations intercalate and could not have formed by selective hydrothermal alteration.

5. The different metal associations between Brown Mountain and Onguati Mine-Western Workings rely on metal zonation away from underlying granitic heat sources, but there is little evidence (e.g. aeromagnetic or gravity data) to support the presence of hidden granites in the Onguati-Kranzberg anticlinorium. Steven (2000) prefers to interpret the Cu-Au mineralization at Onguati Mine and Western Workings as a high T event that formed at a different time to the Fe-As-weak Au mineralization at Brown Mountain.

9.1.2. Magmatic Source of Gold and Ore-Forming Metals

Although Navachab Mine is viewed as a distal, exoskarn deposit because it is not spatially related to a particular intrusive rock type (Meinert, 1998), there are several lines of evidence which point to a possible genetic relationship between hydrothermal mineralization and granitoid plutons in the Karibib region. Firstly, pyrite at Onguati Mine has $\delta^{34}S$ values of +1.93 to +3.76‰ (Petzel, 1988a), and together with the S isotope values of pyrrhotite at Navachab Mine, suggest a possible igneous source of sulphur (Moore *et al.*, 1999). In addition C and O isotope values for calcites in the Navachab veins and skarn give a typical 'magmatic' signature (Moore *et al.*, 1999). Steven (1993) noted that the Au-Bi-As-Te-S association found in many of the hydrothermal deposits of the Karibib region is similar to felsic intrusion-related mineralization in other orogenic belts. Consequently, Steven (1993) proposed that mineralizing fluids could have originated from late- to post-tectonic felsic intrusions hidden below the mineralized marbles of the Karibib area. However such a metal association is not conclusive evidence of a genetic link to a granitoid source as a similar Au-Ag ± As ± B ± Bi ± Sb ± Te ± W association is common to orogenic gold deposits that do not have a specific or proximal relationship to a given intrusion or intrusive suite (Groves *et al.*, 2003).

Jacob *et al.* (2000a, b) believe that dioritic rocks of the Goas Magmatic Suite, which are exposed to the south of Navachab Mine, could provide a viable source of Au and other metals. A porphyritic member of the Goas Magmatic Suite on the farm Ukuib 84, just NW of the Okahandja Lineament, is associated with veins, skarn and small zones of alteration that contain minor sulphide mineralization (Jacob, *pers. comm.*, 2003). SHRIMP geochronology was employed by Jacob *et al.* (2000a, b) to ascertain if an age relationship exists between granitoid emplacement and Navachab mineralization. Zircons in nearby granitoids, namely the Mon Repos dioritic-granodioritic member of the Goas Magmatic Suite and the Rotekuppe monzogranite yielded ages of ~550 Ma and ~540 Ma respectively. Titanites in mineralized quartz veins of the Navachab Mine were dated at ~500 Ma (Jacob *et al.*, 2000b). The results are inconclusive and can be interpreted in at least two ways. The first possibility is that the zircon ages constrain the ages of both granitoid intrusion and mineralization to about 550 Ma, so that the titanite age represents cooling through the titanite closure temperature at a later time. Alternatively, the titanite age could represent the age of mineralization near closure temperatures, in which case these igneous rocks are not temporally related to Karibib hydrothermal mineralization (Jacob *et al.*, 2000b).

The main problems with a dioritic source area for ore-forming metals are:

1. The Goas Magmatic Suite has a limited extent and is only found in the southernmost parts of the SCZ. Commonly great distances separate dioritic members from areas of mineralization, as in the case of deposits found in the Onguati region. A high volume of fluids would be required to transport metals from their magmatic source along crustal-scale structures to suitable sink areas.

2. Plutonic bodies of the Goas Magmatic Suite are commonly emplaced along, or close to, the Karibib Formation–Kuiseb Formation interface. As a result the dioritic rocks are situated at a higher stratigraphic level than the mineralization at Navachab Mine (Dirks & Mikhailov, 2000). The Onguati deposits are found at a higher level in the Karibib Formation but are still situated below the level of dioritic magmatism.

3. Dirks & Mikhailov (2000) believe that dioritic rocks of the Goas Magmatic Suite were emplaced as sheet-like bodies before doming and mineralization occurred. If these field observations are correct, then this would support the age interpretation of the

Mon Repos diorite/granodiorite emplacement at ~550 Ma and unrelated hydrothermal mineralization at ~500 Ma.

9.1.3. Abbabis Metamorphic Complex as a Potential Source of Au and Metals

In the Abbabis Inlier, Steven (1993) discovered anomalous amounts of Au (>300 ppb) in ENE-trending shear zones, chlorite-magnetite rocks and cupriferous quartz veins (see sections 3.2.1 and 3.3.1). Evidence from basement shear zones in other parts of the Damara Belt (e.g. Kamanjab Inlier) suggest that there was a widespread, pre-Damara gold-mineralizing event. Steven (1993) calculates that the main shear zone on the Abbabis and Narubis farms, which is approximately 10 m wide by 6 km long and which may extend 1 km in depth, may contain in excess of 810 000 ounces of Au, assuming an average grade of 150 ppb Au. Some Cu-Au–bearing quartz veins cut undeformed pegmatites and this suggests they are very late Damaran at the oldest (Steven, 1993).

Viljoen (2002) proposed a metamorphic devolatilization model where the basement provided the source of both hydrothermal fluids and ore-forming metals during Damaran orogeny, but there is a serious problem with this scenario. The Abbabis Metamorphic Complex underwent pre-Damara metamorphism and dehydration, and many of the lithologies are dominated by anhydrous mineral assemblages. While basement rocks may contain a substantial metal resource they could not have developed high volumes of metamorphic hydrothermal fluid during Damaran lower amphibolite metamorphism. However, fluids derived from overlying volatile-rich Damaran source rocks could have circulated into the basement and scavenged available metals if a long-lived convective system was in operation.

9.2. Integrated Genetic Model for Cu-Fe±Au Vein Mineralization in the Onguati Study Area

In the Karibib region of the SCZ there are several lines of evidence to suggest the operation of a crustal-scale hydrothermal system during late Damaran orogeny:

1. *There is laterally extensive hydrothermal activity:* Cu±Au mineralization is common in deformed veins and/or skarn that cross-cut Damaran structure in the northeastern parts of the SCZ. As is the case for gold deposits in other metamorphic terranes, there are a large number of non-economic showings in the Karibib district, a lesser number of sub-economic Cu±Au hydrothermal deposits (e.g. Onguati deposits), and only one known, world-class Au deposit (Navachab Mine with 140 t or 4.5 Moz Au).

2. *There is vertically extensive hydrothermal activity:* Epigenetic Cu±Au mineralization occurs throughout the SCZ supracrustal pile, although the best mineralization is confined to the marbles and calc-silicate rocks of the Okawayo Member (Arandis Formation) and Karibib Formation.

3. *There are abundant regional-scale (~100 km) and deposit-scale (<10 km) lineaments:* A number of the faults and shear zones in the SCZ may belong to a regional fracture network that was kinematically active during late Damaran orogeny. Many of the hydrothermal mineral showings are found in close proximity to such structures (e.g. Onguati deposits are bound by a system of faults).

If such a hydrothermal system was in existence, then this necessitates an ore genesis model for the Onguati vein deposits that has general applicability to all other epigenetic Cu±Au occurrences in the region. A metamorphic ore genesis model, similar to those outlined by Groves & Phillips (1987) and Williams (1990) for the formation of gold deposits, fulfils this requirement and provides a viable means of producing hydrothermal Cu±Au deposits such as those in the Onguati study area. The suggested model does not address all problems associated with mineralization in metamorphic terranes, as will be detailed later in section 9.2.1, but it does provide a basic framework for understanding SCZ metallogenesis and hence has application to regional Au exploration.

(a) Source of fluids and metals:

It is envisaged that the entire package of Damaran metasedimentary and metavolcanic rocks in the Karibib region, including any syngenetic mineralization that it may contain, could have provided a large potential source of ore-forming constituents and fluid. Metamorphic devolatilization reactions, such as dehydration and decarbonation, would have occurred extensively throughout the rock sequence during orogeny. High T-low P metamorphism with a high geothermal gradient of 55-65°C/km (Hawkesworth *et al.*, 1986; Steven, 1993) and the absence of significant crustal melting in this part of the SCZ would have promoted metamorphic dehydration (e.g. $Ms+Qtz \rightleftharpoons Sill+Kfs+H_2O$; see Fig. 5.7) and the generation of large volumes of metamorphic fluid with metal and Au-transporting capability (Groves & Phillips, 1987). Due to the grain-scale nature of the devolatilization reactions, the developing metamorphic fluids would have come into contact with a large portion of the source area rocks (Groves & Phillips, 1987). This would have permitted efficient Au and metal extraction.

(b) Metal transporting mechanisms:

Dissolution and transportation of the metals in the metamorphic fluids would have occurred via complexing agents, the most important being chlorine and sulphur species (Skinner, 1997). The applicability of various complexes to the hydrothermal mineralization in the Karibib region requires a sound knowledge of the original concentrations of the ligands (S, Cl etc.) and the temperature, pressure, pH and oxidation state of the hydrothermal fluids (Seward & Barnes, 1997). The exact nature of the ore fluids at Onguati or at the nearby Navachab Mine is still unknown, but studies from other orogenic gold deposits show that the mineralizing fluids are commonly CO_2-H_2O-rich with low salinities (Groves & Phillips, 1987; Groves *et al.*, 2003). In such fluids, reduced sulphide complexes (e.g. $Au(H_2S)^+$, $Au(HS)^{2-}$, $Cu(HS)^{2-}$, $Zn(HS)_3^-$) tend to be the dominant metal carriers if S is present in excess, and in many orogenic gold deposits Au-thiosulphide complexes ($Au(HS)_2$) are invoked (e.g. Phillips *et al.*, 1984). Although chlorine complexes are less favoured in orogenic gold mineralization (i.e. Cl-poor fluids), they are nevertheless efficient metal transporters (e.g. $AuCl_2^-$, $CuCl$, $CuCl_3^{2-}$, $CuCl_3^-$, $FeCl^+$, $FeCl_3^-$) and cannot be ruled out before comprehensive fluid inclusion work is carried out. The role of Bi as a potential gold carrier, especially if Au-undersaturated conditions existed (Douglas *et al.*, 2000), also needs to be assessed because of the Au-Bi correlation at Onguati Mine (Pirajno *et al.*, 1991). A strong Au-Bi association is also known at Navachab Mine where maldonite (Au_2Bi), native bismuth and bismuthinite are found in the ore assemblage (Moore *et al.*, 1999).

(c) Fluid flow and focussing structures:

At elevated temperatures and confining pressure, the metamorphic pore fluids in the lower parts of the Damaran Sequence may have developed near-lithostatic to transiently supra-lithostatic fluid pressures (Etheridge, 1984). The large resulting fluid pressure gradients would have provided a strong driving force for the upward migration of ore-bearing metamorphic fluids (Cox, 1999). Thermally driven convection (i.e. buoyancy effects) could also have resulted locally and/or regionally with the emplacement of hot intrusive bodies in the source rocks (Cox *et al.*, 2001).

Ongoing deformation would have been crucial in creating and maintaining permeability (e.g. microcrack growth) at all stages of fluid flow, and would have facilitated further fluid-source rock interaction (Cox, 1999). The migration of metamorphic pore fluids into high permeability microcrack pathways and successive localization into connected fractures, shear zones and faults in the upstream parts of the regional hydrothermal system would have allowed sufficient volumes of fluid and metal to be extracted. Focussing of these regionally-derived fluids into a very small fraction of the percolation network (i.e. fluid flow along a major crustal-deep structure or 'fluid backbone') would have maximized fluid-rock ratios thus preventing premature ore deposition (Cox, 1999).

(d) Local structural control and vein connectivity:

The location of many Cu-Au deposits in SCZ domes and antiforms (e.g. Navachab Mine, Onguati deposits) may reflect the favourable combination of chemically reactive marbles and calc-silicate rocks with regional structural 'highs' that encouraged the upward migration of ore-bearing metamorphic fluids. Schists of the overlying Kuiseb Formation could have further enhanced mineralization in the underlying lithologies of these domes if they acted as an impermeable barrier to the hydrothermal system. The Riedel-type arrangement of faults and/or shear zones developed on the Onguati-Kranzberg anticlinorium, closely associated with the vein deposits of the Onguati study area, may represent a lower-order structure that accessed fluids from a yet unknown, crustal-deep fluid conduit. The thrusts and reverse faults that lie in the R shear position exploited a major competency contrast between the Navachab and Onguati Members on either limb of the Onguati-Kranzberg anticlinorium, and may have been particularly effective fluid pathways. Fluid would have been transferred from this fault system into the vein arrays at Onguati Mine, Brown Mountain and Western Workings at depth.

In the Onguati study area there was intense strain partitioning between the less competent calcitic marble package and the overlying dolomitic marble unit. As a consequence the best-developed veining is hosted by calcitic marble, although weak vein networks do occur in the lowermost parts of the dolomitic marbles. The dolomitic marbles could have further aided veining by acting as an impermeable cap to fluid migration at the deposit-scale. High fluid pressures could have been localized in the underlying calcitic marbles, and this may have facilitated hydraulic fracturing and the formation of vein breccias.

Vein systems with the highest connectivities, as predicted by vein thickness distributions with low D-values, would have promoted the ingress of large volumes of externally-derived fluids such as at Onguati Mine or Western Workings. The few, very large veins in these systems would have remained open to fluids for longer periods of time than their smaller counterparts, and would have further focussed fluid flow at the local level. Such vein configurations would have provided the high fluid fluxes necessary for the deposition and accumulation of appreciable quantities of Cu and Au from metamorphic fluids that contain very low metal concentrations.

(e) Mechanisms of ore deposition:

A number of ore deposition mechanisms, in addition to general temperature and pressure decreases, could have operated in the Onguati vein systems (see Mikucki, 1998 for review of common depositional processes). Good evidence for the role of fluid-rock reactions in Onguati ore deposition is seen from the preferential mineralization of the chemically reactive carbonate and calc-silicate lithologies throughout the region. Fluid-marble wall rock reactions could have resulted in pH changes and/or reduction of ore-bearing fluids in the Onguati vein arrays. This could have caused significant destabilization of the aqueous complexes of Cu, Fe and Au. Differences in Cu±Au grades between the Onguati Mine, Brown Mountain and Western Workings vein areas could be related to the wall-rock surface areas presented for fluid reaction. For example, in the higher D-value vein systems of the Brown Mountain area there would have been much more efficient wall-rock reaction than in the lower D-value Onguati Mine and Western Workings systems where fluids were localised into a few, very large veins. The vein configuration at Brown Mountain could have resulted in premature fluid-rock interaction at depth and together with inefficient, intermittent fluid flow, may have resulted in the disseminated, non-economic vein mineralization observed.

Fluid-mixing reactions could have been important in the initial stages of ore deposition at Onguati. During early vein and vein cluster development, fractures would have contained only locally-derived and equilibrated, carbonate-rich fluids. As the vein arrays became better connected and linked to the percolation network, externally-derived fluids would have rushed into the fracture system where they would have mixed and reacted with the local fluids (Cox, 1999). Such fluid interactions could have destabilized metal-complexes causing early sulphide precipitation. Back-mixing (Cox *et al.*, 1995) of reacted ore fluids with fresh, incoming fluids could have aided ore deposition throughout vein mineralization in the Onguati study area.

Additional ore deposition mechanisms may have operated in the Onguati vein deposits. Pressure fluctuations due to sealing and re-opening of veins in the fracture networks could have led to phase separation and precipitation of various ore minerals if the changes were severe (Sibson *et al.*, 1988). The adsorption of charged Au complexes to sites of increased charge density on semi-conducting sulphide grain surfaces (Starling *et al.*, 1989) could provide a mechanism to explain the anomalous Au contents of some pyrite, sphalerite and chalcopyrite grains in the Onguati Mine and Western Workings areas. The gold could occur as minute blebs or inclusions (chemical absorption of gold or sulphide overgrowth) in these sulphide minerals. Such a process could be a particularly effective means of extracting and concentrating gold from the relatively Cu-Fe-rich, Au-poor ore-fluids that are thought to have mineralized the Onguati study area. The general lack of pyrite, sphalerite and chalcopyrite in the vein arrays hosted by calcitic marbles at Brown Mountain and dolomitic marbles elsewhere, could provide an explanation for the lack of a Au association if such a process was in operation.

9.2.1 Current Knowledge Gaps and Future Research

A number of aspects in the ore genesis model proposed for the Onguati study area are poorly constrained or unknown and require further study. The more serious of these include: (i) the precise timing of mineralization; (ii) the exact nature of the ore-bearing fluids; (iii) the complex/s by which ore components were transported and the exact means of ore deposition; (iv) the regional-scale controls on mineralization in the Karibib district, especially the location and configuration of the major fluid conduits; (v) the deposit-scale controls on mineralization at the other Cu±Au deposits found in this part of the SCZ; and (vi) at the geodynamic scale, the tectonic setting in which Au mineralization occurred.

(i) Timing of mineralization:

Precise dating (e.g. SHRIMP U-Pb dating; Re-Os analysis of ore sulphides and gold) of the vein mineralization in the Onguati study area and elsewhere, and of the main deformational, metamorphic and magmatic events in the SCZ is required. A close temporal relationship between a major period of metamorphic devolatilization and mineralization is critical in the model suggested above. Precise dating of the hydrothermal deposits in the Karibib region could determine if there were single or multiple episodes of Cu-Au hydrothermal mineralization during Damaran orogeny. The precise age/s of the various ore deposits relative to the emplacement of particular intrusives could also test the magmatic source hypothesis (e.g. Jacob *et al.*, 2000b).

(ii) Fluid source and composition:

The nature of the mineralizing fluids in the Onguati vein arrays and at other Cu±Au hydrothermal deposits in the Karibib region could be addressed by studying fluid inclusions in the ore-related minerals. The geochemistry and stable isotope compositions of fluid inclusions together with radiogenic and stable isotope compositions of the ore-related minerals could be useful tracers (Groves *et al.*, 2003). This could indicate whether a metamorphic fluid source is feasible and if there are other fluid contributions (e.g. magmatic).

(iii) Transport and deposition of ore components:

The means by which Cu, Au and other metals were transported in the fluids that mineralized the Onguati deposits or the nearby Navachab Mine is poorly understood. The relative importance of S- and Cl-complexes or other complexing agents (e.g. Bi, As) in transporting metals and gold and the related mechanisms of ore deposition can only be fully assessed when the nature and composition of the Onguati hydrothermal fluid is known.

(iv) Regional-scale controls on mineralization:

The broad controls on Cu-Au mineralization in the Karibib district remain poorly constrained. An effective means of addressing this problem would be to create a comprehensive geographical information system (GIS) for the region, as recommended by Dirks & Mikhailov (2000). Such a system would include all the available lithostratigraphic, metamorphic, structural, geophysical and geochemical data for the Karibib region. Possible relationships could be statistically tested (eg. do regional relationships exist between mineralization and various lineaments, domal features, particular intrusive bodies or complexes, lithostratigraphic units etc.) and this would help determine the factors which, in concert or in various combinations, control the siting, style and intensity of mineralization in the SCZ.

The crustal-scale faults and/or shear zones that could have channelled large fluid fluxes in the SCZ remains unresolved (e.g. NNE-trending ABL[i] swath). An appreciation of these structures is important because they could have strongly controlled the extent of mineralization in the region. Detailed structural analysis of the numerous SCZ lineament zones and sets is long overdue, and should concentrate on the definition of these structures (i.e. fault, shear zone, dyke etc.) and their kinematic timing relative to Damaran orogeny and mineralization. High-resolution magnetic, gravity and seismic reflection data may be particularly useful in determining the depth extents of faults and shear zones, and could facilitate the selection of structures that are most likely to have been major fluid conduits.

(v) Deposit-scale controls on mineralization:
While deposit-scale structural control on mineralization has been assessed in the Onguati study area, more research is required at the other deposits. Study of the Navachab Au deposit may be particularly insightful because very large systems normally develop in zones where a large number of favourable physical and chemical conditions coincide (Groves *et al.*, 2003). In smaller, sub-economic deposits only some of the necessary conditions for optimal ore deposition are met (i.e. one or two dominant factors are present) and consequently there is weaker mineralization.

(vi) Tectonic setting of Cu-Au mineralization in the Damara Belt:
The geodynamic evolution of the Damaran Orogen remains poorly constrained and is highly contentious, but its understanding could prove beneficial to future Au exploration. For example, the occurrence of significant Au mineralization in the northern tectonostratigraphic zones of the Damara Belt may be broadly similar to the location of both orogenic and intrusion-related Au deposits in the over-riding margins of continental arc settings (see Groves *et al.*, 2003).

9.2.2 Significance to Exploration

The widespread occurrence of epigenetic gold mineralization in the Damara Belt, the presence of the world class Navachab Au Mine in the SCZ and the recent discovery of the potentially large Otjikoto Au prospect in the NZ (Wilton *et al.*, 2002), all suggest that this region has a substantial gold potential. If the metamorphic devolatilization model is valid in explaining the development of mineralization in the Onguati study area and elsewhere in the

CZ or NZ, then it may have great significance to future Au exploration. Firstly the refinement of the metamorphic ore genesis model (see section 9.2.1) would provide improved understanding of the controls on economic Au mineralization, and this in turn, would improve exploration models. In addition a genetic 'concept-driven' exploration methodology for Au could be employed as recommended by Foster *et al.* (2001). Such an approach relies on a systematic process in which the focus of exploration narrows from selection of suitable metamorphic source regions, to identification of major fluid conduits in the overall fracture architecture, and finally to ground selection based on the conjunction of favourable structural and lithological conditions. A series of basic steps could be implemented (and supplemented as more geological information is gathered) in the search for new Au deposits in the northern tectonostratigraphic zones of the Damara Belt:

Investigation of the northern Damara Belt (several 100's of km scale)

<u>Step 1:</u> The first step in the genetic exploration methodology is to delineate areas of the northern Damaran Belt that have experienced high T-low P metamorphism (i.e. geothermal gradients of 35-65°C/km) without widespread anatexis. The central to northeastern parts of the CZ (i.e. lower amphibolite metamorphism), and large parts of the NZ (greenschist facies metamorphism) may be particularly favourable in this regard. The southwestern region of the CZ does not present ideal metamorphic conditions and has low Au exploration potential because there has been extensive *in situ* partial melting. Metamorphic dehydration and migmatization were probably broadly contemporaneous in this region, and as result the developing melts would have scavenged much water devolatilizing from the metasedimentary rock pile. This would have hindered the generation of ore-bearing metamorphic fluids and may explain the lack of significant Cu-Au hydrothermal mineralization in the southwestern parts of the CZ.

Terrane-scale investigation (100's of km scale)

<u>Step 2:</u> Within suitable parts of the northen Damaran Belt, emphasis should shift to the identification of crustal-deep faults and/or shear zones that were kinematically active during late Damaran orogeny. Such structures could have accessed the base of the metamorphic pile and acted as mega-scale fluid conduits. The selection process could rely on quantitative analysis of existing GSN high-resolution aeromagnetic data. From the review of SCZ crustal

structure (section 3.4.1) and high-resolution aeromagnetic image interpretation (section 3.5.2), NNE-trending regional lineaments (e.g. ABL[i]) may hold the greatest potential as fluid 'backbone' structures, especially where they intersect NE- to ENE-trending faults, such as at the tectonostratigraphic zone boundaries (e.g. OL, OML), but this requires further study.

District-scale investigation (10's of kilometre scale)

Step 3: Identification of lower-order dilational and contractional structures that could have accessed the primary conduits (as selected above) forms the first step of district-scale analysis (aeromagnetic and remote sensing data may be particularly useful). Second- or third-order Riedel shear zone systems, intersections of faults/shears, fault splays, jogs or bends in faults/shear zones, or stress shadows developed about granitoid or other rigid bodies of rock could have diverted fluids from the primary fault/shear zone with which they connect and could prove highly prospective (Foster, 1996; Groves *et al.*, 2003). At the prospect-scale, NNE- and/or ENE-trending faults and shear zones appear particularly favourable for enhanced local fluid flow and are often associated with Cu-Au mineralization (e.g. Onguati deposits, Sandamap Noord prospect - see Steven *et al.*, 1993, Steven, 1999).

Step 4: Areas where first and/or lower-order fluid transporting structures are found adjacent to or intersect favourable rock types should be delineated and rated (see Table 9.1). Existing

Table 9.1: Basic system for ranking the mineralization potential of various Damaran host rocks, based on known Cu±Au deposit occurrences in the northern parts of the Damaran Belt.

Most Favourable	carbonate/calc-silicate lithologies, especially of the Okawayo Member and Karibib Formation.	*e.g. Navachab Au Mine and Onguati area Cu±Au vein deposits, both in the SCZ*
	albitites and hornfelsed Bt-schists of the Karibib Formation (NZ).	*e.g. Otjikoto Au deposit in the NZ (Wilton et al., 2002)*
	Bt-schists of the Kuiseb Formation, (especially if graphite-rich?).	*e.g. Sandamap Noord Au prospect in the NCZ*
Less favourable	quartzites and quartzofeldspathic rocks of the Etusis Formation.	*e.g. Nordenberg Au prospect in the SCZ*

geological maps and high-resolution airborne radiometric and magnetic data (both available from the GSN) should be merged in a GIS environment to aid the effectiveness of this study.

Step 5: Once district-scale ground is selected in which suitable lower-order structures are found with chemically reactive host rocks, high-resolution aeromagnetic data (either GSN data or customized aerial surveys) should be reassessed at this scale. Au mineralization could be associated with strong positive magnetic highs due to its association with pyrrhotite mineralization (e.g. Navachab Mine, Otjikoto Au prospect). Preliminary mapping of selected district-scale ground could be undertaken with emphasis on the basic lithostratigraphy, and the nature of the superficial cover (e.g. autochthonous/allochthonous soils, calcrete/ferricrete cover, alluvium etc.). After thorough landscape analysis and orientation studies, geochemical soil surveys could be carried out to search for suitable pathfinder element anomalies (e.g. As, Cu, Zn) in the selected areas.

Prospect-scale investigation (km scale)

Step 6: On the basis of the district-scale investigation, more detailed structural and lithological mapping could be undertaken at prospect-scale targets. Follow-up geochemical soil programmes and ground-based magnetic, electromagnetic and induced polarization surveys could be employed at this stage to better delineate areas of potential mineralization, especially if there is poor outcrop due to calcrete cover. If obvious signs of mineralization occur (e.g. veins, skarn, gossan), samples should be collected for ore petrography and geochemical analysis. Fractal analysis could also be used as a standard exploration tool by implementing simple transect sampling over exposed parts of vein arrays. The calculated D-value for the vein thickness distribution could be used to evaluate the permeability and consequent mineralization potential of each vein system encountered, before expensive drilling programmes are implemented.

10. ACKNOWLEDGEMENTS

I dedicate this thesis to my Grandfather, ***David Llewelyn Lewis****, who passed away shortly after I had returned from my fieldwork in Namibia. I wish I could have show him the finished product.*

A special word of appreciation is directed to my supervisor, Professor Roger Jacob, who stuck with me during my MSc. Thank you so much for all the discussions, advice, proof-reading and helpful criticism. I am forever in your debt!

I would like to thank Navachab Mine for their generous logistical and financial support.

Thank-you to Frik Badenhorst for all his help during the course of my fieldwork and for his patience in the years that followed. A big thank-you is also due to the Badenhorst family for their hospitality during my stays at their 'farm'.

Thanks is due to the Geological Survey of Namibia, especially Mr. V. Petzel, for assistance over the years and for access to their high-resolution geophysical imagery.

To Willie van Vyk thank-you for all your time spent digitizing the Onguati maps.

To my parents a special thank-you for your love and generosity. Thanks for not giving up on me even when I was ready to throw in the towel this year.

Brendan Viljoen for being my 'rock' during our time at Rhodes University. Thanks for your sound advice and for you great sense of humour – I could not have done it without you!

To Steffen Büttner thanks for the discussions on structure and for the many practical suggestions.

Siksha Bramdeo and Ronel August thanks for all help with the electron microprobe analyses.

A big thank-you to John Hepple for his direction during the cutting, slide-making and ore section polishing stages of my MSc, and especially for the chats.

To Leon Brits thank-you for recovering important parts of my thesis from a Windows 98 disaster.

To Jenny and Ashley, thanks for your friendliness and helpfulness over the many years.

Janet, thanks for all the coffee!

Finally, a big thank you to everyone in the Geology department who made studying here such an enjoyable and rewarding experience.

11. REFERENCES

Anovitz, L.M. & Essene, E.J. (1987). Phase equilibria in the system $CaCO_3$-$MgCO_3$-$FeCO_3$. *Journal of Petrology*, **28**, 389-414.

Aviles, C.A., Scholtz, C.H. & Boatwright, J. (1987). Fractal analysis applied to characteristic segments of the San Andreas Fault. *Journal of Geophysical Research*, **92**, 331-344.

Badenhorst, F.P. (1987). Lithostratigraphy of the Damara Sequence in the Omaruru area of the northern Central Zone of the Damara Orogen and a proposed correlation across the Omaruru Lineament. *Communications of the Geological Survey of S.W.A./Namibia*, **3**, 3-8.

Badenhorst, F.P. (1988). The lithostratigraphy of the Chuos mixtite in part of the southern Central Zone of the Damara Orogen, South West Africa. *Communications of the Geological Survey of S.W.A./Namibia*, **4**, 103-110.

Badenhorst, F.P. (1992). *The lithostratigraphy of area 2115B and D in the Central Zone of the Damara Orogen, Namibia: with emphasis on facies changes and regional correlation*. Masters Thesis (unpubl.), University of Port Elizabeth, 124 pp.

Badenhorst, F.P. (1993). The Navachab Gold Mine in central Namibia. *Conference on Mining Investment in Namibia, Windhoek, 17th-19th March*. Ministry of Mines Publication, 1993, p.33-34.

Barnes, J.F.H. (1981). *Some aspects of the tectonic history of the Khan-Swakop region of the Damara Belt, Namibia*. PhD thesis (unpubl.), University of Leeds, U.K., 348 pp.

Barnes, S.-J. & Sawyer, E.W. (1980). An alternative model for the Damara Mobile Belt: ocean crust subduction and continental convergence. *Precambrian Research*, **13**, 297-336.

Barton, C.A. & Zoback, M.D. (1992). Self similar distribution and properties of macroscopic fractures at depth in crystalline rock in the Cajon Pass Scientific borehole. *Journal of Geophysical Research*, **97**, 5181-5200.

Beck, A. (2003). *http://www.glyphs.com/art/fractals/what_is.html*. Glyphs, last updated 2003.

Bessinger, G. (1994). *The geology and industrial potential of an area northeast of Karibib, Namibia*. Honours Thesis (unpubl.), Rhodes University, 56 pp.

Bickle, M.J. & Powell, R. (1977). Calcite-dolomite geothermometry for iron-bearing carbonates: the Glockner area of the Tauern Window, Austria. *Contributions to Mineralogy and Petrology*, **59**, 281-292.

Blenkinsop, T.G. (1995). Fractal measures for size and spatial distributions of gold mines: economic applications, 177-185. *In:* Blenkinsop, T.G. & Tromp, P.L., Eds., *Sub-Saharan economic geology*. A.A. Balkema, Rotterdam, 301 pp.

Blenkinsop, T.G. & Sanderson, D.J. (1999). Are gold deposits in the crust fractals? A study of gold mines in the Zimbabwean craton, 141-151. *In:* McCaffrey, K.J.W., Lonergan, L. & Wilkinson, J.J., Eds., *Fractures, fluid flow and mineralization*. Geological Society, Special Publications, **155**, 330 pp.

Botha, P.J.V. (1979). *The stratigraphy of the Khomas Subgroup west of the Spitzkoppe, South West Africa*. Transactions of the Geological Society of South Africa, **82**, 329-333.

Brandt, R. (1985). Preliminary report on the stratigraphy of the Damaran Sequence and the geology and geochemistry of Damaran granites in an area between Walvis Bay and Karibib. *Communications of the Geological Survey of S.W.A./Namibia*, **1**, 31-43.

Brandt, R. (1987). Granitic magmatism in the Damaran Orogenic Belt, Namibia. *Revista Brasileira de Geociências*, **17**(4), 459-463.

Burger, A.J. & Walraven, F. (1976). Summary of age determinations carried out during the period April 1975 to March 1976. *South African Geological Survey Annals*, **11**, 323-

329.

Carlson, C.A. (1991). Spatial distribution of ore deposits. *Geology*, **19**, 111-114.

Cheng, Q. (1997). Multifractal modelling and lacunarity analysis. *Mathematical Geology*, **29**(7), 919-932.

Cheng, Q., Atgerberg, F.P. & Ballantyne, S.B. (1994). The separation of geochemical anomalies from background by fractal methods. *Journal of Exploration Geochemical*, **51**(2), 109-130.

Chilès, J.P. (1988). Fractal and geostatistical methods for modelling of a fracture network. *Mathematical Geology*, **20**(6), 631-654.

Cladouhos, T.T. & Marrett, R. (1996). Are fault growth and linkage models consistent with power-law distributions of fault lengths? *Journal of Structural Geology*, **18**, 281-293.

Clark, M.B., Brantley, S.L. & Fisher, D.M. (1995). Power-law vein-thickness distributions and positive feedback in vein growth. *Geology*, **23**, 975-978.

Corner, B. (1983). An interpretation of the aeromagnetic data covering the western portion of the Damara Orogen in South West Africa/ Namibia. *Special Publication of the Geological Society of South Africa*, **11**, 339-354.

Corner, B. (2000). Crustal framework of Namibia derived from magnetic and gravity data. *Communications of the Geological Survey of Namibia*, **12**, 13-19.

Coward, M.P. (1981). The junction between Pan-African mobile belts in Namibia: its structural history. *Tectonophysics*, **76**, 59-73.

Coward, M.P. (1983). The tectonic history of the Damara Belt. *Special Publication of the Geological Society of South Africa*, **11**, 409-421.

Cox, S.F. (1999). Deformational controls on the dynamics of fluid flow in mesothermal gold systems, 123-140. *In:* McCaffrey, K.J.W., Lonergan, L. & Wilkinson, J.J., Eds., *Fractures, fluid flow and mineralization*. Geological Society, Special Publications, **155**, 330 pp.

Cox. S.F., Knackstedt, M.A & Braun, J. (2001). Principles of structural control on permeability and fluid flow in hydrothermal systems. *Reviews in Economic Geology*, **14**, 1-24.

Cox, S.F., Sun, S.S., Etheridge, M.A., Wall, V.J. & Potter, T.F. (1995). Structural and geochemical controls on the development of turbidite-hosted gold quartz vein deposits, Wattle Gully mine, central Victoria, Australia. *Economic Geology*, **90**, 1722-1746.

Davis, G.H. & Reynolds, S.J. (1996). *Structural geology of rocks and regions* (2nd Ed.). John Wiley & Sons, Inc., New York, 776 pp.

De Wit, M.J. (1998). On Archean granites, greenstones, cratons and tectonics: does the evidence demand a verdict? *Precambrian Research*, **91**, 181-226.

Deer, W.A., Howie, R.A. & Zussman, J. (1992). *An introduction to the rock forming minerals* (2nd Ed.). Addison Wesley Longman Limited, Harlow, Essex, 696 pp.

Dirks, P.H.G.M., & Mikhailov, A. (2000). *An assessment of the structural controls on gold mineralisation at Navachab Mine and related Au occurrences: implications for regional exploration*. Report to Anglogold Ltd. (unpubl.), 53 pp.

Douglas, N., Mavrogenes, J., Hack, A. & England, R. (2000). The liquid bismuth collector model: an alternative gold depositional mechanism. *Geology Society of Australia, Abstract No. 59*, 135 (Abstract).

Downing, K.N. & Coward, M.P. (1981). The Okahandja Lineament and its significance for Damaran tectonics in Namibia. *Geologische Rundschau*, **70**, 972-1000.

Eberle, D. & Hutchins, D.G. (1996). The regional magnetic data set of Namibia: comments on compilation and geological overview. *Geological Survey of Namibia Bulletin*, **2**, 40 pp.

Edgar, G.A. (1995). *Measure, topology, and fractal geometry*. Springer-Verlag, New York, 231 pp.

Engelder, T. & Peacock, D.C.P. (2001). Joint development normal to regional compression during flexural-flow folding: the Lilstock buttress anticline, Somerset, England. *Journal of Structural Geology*, **23**, 259-277.

Essene, E.J. (1982). Geologic thermometry and barometry. *Reviews in Mineralogy*, **10**, 153-206 pp.

Essene, E.J. (1983). Solid solutions and solvi among metamorphic carbonates with applications to geologic thermobarometry. *Reviews in Mineralogy*, **11**, 77-96 pp.

Essene, E.J. (1989). The current status of thermobarometry in metamorphic rocks, 1-44. *In:* Daly, J.S., Ed., *Evolution of metamorphic belts*. Geological Society, Special Publication, **43**.

Etheridge, M.A., Wall, V.J., Cox, S.F. & Vernon, R.H. (1984). High fluid pressure during regional metamorphism and deformation: implications for mass transport and deformation mechanisms. *Journal of Geophysical Research*, **89**, 4344-4358.

Evans, A.M. (1993). Ore geology and industrial minerals: an introduction (3rd Ed.). Blackwell Science Limited, London, 389 pp.

Feder, J. (1989). *Fractals*. Plenum Press, New York, 283 pp.

Foster, R.P. (1996). Gold in the year 2000: a global overview. *Australian Journal of Earth Sciences*, **43**, 1-14.

Foster, R.P., Leahy, K., Hunns, S.R., Pelham, D.A., Lawrence, S.R. & Harrison, A.E. (2001). Pan-African terranes: realizing the metal potential. *Transactions of the Institution of Mining and Metallurgy* (Sect. B: Appl. earth sci.), **110** (January-April), B15-B23.

Frommurze, H.F., Gevers, T.W. & Rossouw, P.J. (1942). *The geology and mineral deposits of the Karibib area, South West Africa*. Explanation Sheet 79 (Karibib, S.W.A), Geological Survey of South Africa, 180 pp.

Gevers, T.W. (1931). An ancient tillite in South West Africa. *Transactions of the Geological Society of South Africa*, **34**, 1-17.

Gillespie, P.A., Howard, C.B., Walsh, J.J. & Waterson, J. (1993). Measurement and characterisation of spatial distributions of fractures. *Tectonophysics*, **226**, 113-141.

Gillespie, P.A., Johnston, J.D., Loriga, M.A., McCaffrey, K.J.W., Walsh, J.J. & Watterson, J. (1999). Influence of layering on vein systematics in line samples, 35-56. *In:* McCaffrey, K.J.W., Lonergan, L. & Wilkinson, J.J., Eds., *Fractures, fluid flow and mineralization*. Geological Society, Special Publications, **155**, 330 pp.

Gillespie, P.A., Walsh, J.J., Watterson, J., Bonson, C.G. & Manzocchi, T. (2001). Scaling relationships of joint and vein arrays from The Burren, Co. Clare, Ireland. *Journal of Structural Geology*, **23**, 183-201.

Gleick, J. (1988). *Chaos: making a new science*. Penguin Books, New York, 352 pp.

Goldfarb, R.J. Groves, D.I. & Gardoll, S. (2001). Orogenic gold and geological time: a global synthesis. *Ore Geology Reviews*, **18**, 1-75.

Goldsmith, J.R., Graf, D.L. & Heard, H.C. (1961). Lattice constraints of the calcium-magnesium carbonates. *The American Mineralogist*, **46**, 453-457.

Goldsmith, J.R. & Heard, H.C. (1961). Subsolidus phase relations in the system $CaCO_3$ – $MgCO_3$. *Journal of Geology*, **69**, 43-61.

Goldsmith, J.R. & Newton, R.C. (1969). P – T – X relations in the system $CaCO_3$ – $MgCO_3$ at high temperatures and pressures. *American Journal of Science*, **267-A**, 160-190.

Goodwin, A.M. (1991). *Precambrian geology: the dynamic evolution of the continental crust*. Academic Press Ltd., London, 666 pp.

Graf, D.L. & Goldsmith, J.R. (1955). Dolomite-magnesian calcite reactions at elevated temperatures and CO_2 pressures. *Geochimica et Cosmochimica Acta*, **B**, 109-118.

Gray, D. (1988). *The geology of Onguati Mine and Brown Mountain, Karibib District, Damara*

Orogen, S.W.A./Namibia. Honours Thesis (unpubl.), Rhodes University, 26 pp.

Griffith, A.A. (1921) The phenomena of rupture and flow in solids. *Royal Society of London Transactions*, **221**, p.163-198.

Griffith, A.A. (1924). The theory of rupture, 55-63. *In:* Biezeno, C.B. & Burgers, J.M., Eds., *Proceedings of the First International Congress on Applied Mechanics*. J. Waltman, Delft.

Groves, D.I. & Phillips, G.N. (1987). The genesis and tectonic control on Archaean gold deposits of the Western Australian Shield – a metamorphic replacement model. *Ore Geology Reviews*, **2**, 287-322.

Groves, D.I., Goldfarb, R.J., Robert, F. & Hart, C.J.R. (2003). Gold deposits in metamorphic belts: overview of current understanding, outstanding problems, future research, and exploration significance. *Economic Geology*, **98**, 1-29.

Gutenberg, B. & Richter, C.F. (1954). *Seismicity of the Earth and associated phenomena*. Princeton University Press, Princeton, NJ, 310 pp.

Haack, U. & Martin, H. (1983). Geochronology of the Damara Orogen - a review, 839-846. *In:* Martin, H. & Eder, F.W., Eds., *Intracontinental fold belts: case studies in the Variscan belt of Europe and the Damara belt in Namibia*. Springer-Verlag, Berlin, 945 pp.

Hamilton, W.B. (1998). Archaean magmatism and deformation were not products of plate tectonics. *Precambrian Research*, **91**, 143-179.

Harker, R.I. & Tuttle, O.F. (1955). Studies in the system CaO – MgO – CO_2, Part 2: limits of the solid solution along the binary join $CaCO_3 - MgCO_3$. *American Journal of Science*, **253**, 274-282.

Hartmann, O., Hoffer, E. & Haack, U. (1983). Regional metamorphism in the Damara Orogen: interaction of crustal motion and heat transfer. *Special Publication of the Geological Society of South Africa*, **11**, 233-241.

Hartnady, C.J. (1978). Tectonic evolution of the southeastern part of the Hakos-Auas Mountain Zone in the Damara orogenic belt. *Precambrian Research Unit, Annual Report*, University of Cape Town, **14/15**, 171-182.

Hastings, H.M. and Sugihara, G. (1993). *Fractals: a user's guide for the natural sciences*. Oxford University Press, Oxford, 235 pp.

Haughton, S.H., Frommurze, H.F., Gevers, T.W., Schwellnus, C.M. and Rossouw, P.J. (1939). *The geology and mineral deposits of the Omaruru area, South West Africa*. Explanation Sheet 71 (Omaruru, S.W.A.), Geological Survey of South Africa, 151 pp.

Hawkesworth, C.J., Gledhill, A.R., Roddick, J.C., Miller, R.McG. & Kröner, A. (1983). Rb-Sr and $^{40}Ar/^{39}Ar$ studies bearing on models for the thermal evolution of the Damara Belt, Namibia. *Special Publication of the Geological Society of South Africa*, **11**, 323-338.

Hawkesworth, C.J., Menzies, M.A. & van Calsteren, P. (1986). Geochemical and tectonic evolution of the Damara Belt, Namibia, 305-319. *In:* Coward, M.P. & Ries, A.C., Eds., *Collision tectonics*. Geological Society, Special Publication, **19**, 415 pp.

Henry, G., Stanistreet, I.G. & Maiden, K.J. (1986). Preliminary results of a sedimentological study of the Chuos Formation in the Central Zone of the Damara Orogen: Evidence for mass flow processes and glacial activity. *Communications of the Geological Survey of S.W.A./Namibia*, **2**, 75-92.

Henry, G., Clendenin, C.W., Stanistreet, I.G. & Maiden, K.J. (1990). Multiple detachment model for the early rifting stage of the Late Proterozoic Damara orogen in Namibia. *Geology*, **18**, 67-71.

Hirsch, M.F.H. & Genis, G. (1992). *The Mineral Resources of Namibia - Gold (1st Ed.)*, Section 4.1. Ministry of Mines and Energy/ Geological Survey, Windhoek, 18 pp.

Hodgson, C.J. (1989). The structure of shear-related, vein-type gold deposits: a review. *A* *review: Ore Geology Reviews*, **4**, 231-273.

Hoffmann, K.-H. (1983). Lithostratigraphy and facies of the Swakop Group of the southern Damara belt, S.W.A./Namibia. *Special Publication of the Geological Society of South Africa*, **11**, 43-63.

Hoffmann, K.-H. (1990). Sedimentary depositional history of the Damara Belt related to continental breakup, passive to active margin transition and foreland basin development. *Abstracts of Geocongress 1990: Earth Science Congress of the Geological Society of South Africa*, 250-253 (Abstract).

Jackson, P. & Sanderson, D.J. (1992). Scaling of fault displacements from the Badajoz Cordoba shear zone, SW Spain. *Tectonophysics*, **210**, 179-190.

Jacob, R.E. (1974). Geology and metamorphic petrology of part of the Damara Orogen along the lower Swakop River, South West Africa. *Precambrian Research Unit, Bulletin*, University of Cape Town, **17**, 201 pp.

Jacob, R.E., Kröner, A. & Burger, A.J. (1978). Areal extent and first U-Pb age of the pre-Damara Abbabis Complex in the central Damara belt of South West Africa (Namibia). *Geologische Rundschau*, **67**, 706-718.

Jacob, R.E., Moore, J.M. & Armstrong, R.A. (2000a). SHRIMP dating and implications for the timing of Au mineralisation, Navachab, Namibia. Geocongress 2000: 27th Earth Science Congress of the Geological Society of South Africa, *Journal of African Earth Science*, **31**(1A), 32-33 (Abstract).

Jacob, R.E., Moore, J.M. & Armstrong, R.A. (2000b). Zircon and titanite age determination from igneous rocks in the Karibib District, Namibia: implications for Navachab vein-style gold mineralization. *Communications of the Geological Survey of Namibia*, **12**, 157-166.

Jacob, R.E., Snowden, P.A. & Bunting, F.J.L. (1983). Geology and the structural development of the Tumas basement dome and its cover rocks. *Special Publication of the Geological Society of South Africa*, **11**, 157-172.

Jaques, A.L., Wellman, P., Whitaker, A. & Wyborn, D. (1997). High-resolution geophysics in modern geological mapping. *AGSO Journal of Australian Geology & Geophysics*, **17**(2), 159-173.

Johnston, J.D. & McCaffrey, K.J.W. (1996). Fractal geometries of vein systems and variation of scaling relationships with mechanism. *Journal of Structural Geology*, **18**, 349-358.

Joubert, B. (1989). *The structure and volcanic history of the Daheim area, Namibia*. Honours Thesis (unpubl.), Rhodes University, 40 pp.

Jung, S., Hoernes, S. & Mezger, K. (2000a). Geochronology and petrogenesis of Pan-African, syn-tectonic, S-type and post-tectonic A-type granite (Namibia): products of melting of crustal sources, fractional crystallization and wall rock entrainment. *Lithos*, **50**, 259-287.

Jung, S., Hoernes, S. & Mezger, K. (2000b). Geochronology and petrology of migmatites from the Proterozoic Damara Belt: importance of episodic fluid-present disequilibrium melting and consequences for granite petrology. *Lithos*, **51**, 153-179.

Jung, S., Mezger, K. & Hoernes, S. (2001). Trace element and isotopic (Sr, Nd, Pb, O) arguments for a mid-crustal origin of Pan-African garnet-bearing S-type granites from the Damara orogen (Namibia). *Precambrian Research*, **110**, 325-355.

Kagan, Y.Y. & Knopoff, L. (1980). Spatial distribution of earthquakes: the two-point correlation function. *Royal Astronomical Society Geophysical Journal*, **62**, 303-320.

Kasch, K.W. (1983a). Regional P-T variations in the Damara Orogen with particular reference to early high-pressure metamorphism along the southern margin. *Special Publication of the Geological Society of South Africa*, **11**, 243-253.

Kasch, K.W. (1983b). Tectonothermal evolution of the southern Damara Orogen. *Special*

Publication of the Geological Society of South Africa, **11**, 255-265.

Kasch, K.W. (1983c). Continental collision, suture progradation and thermal relaxation: A plate tectonic model for the Damara Orogen in Central Namibia. *Special Publication of the Geological Society of South Africa*, **11**, 423-429.

Kasch, K.W. (1987). Metamorphism of pelites in the Upper Black Nossob River area of the Damara Orogen. *Communications of the Geological Survey of Namibia*, **3**, 63-82.

Kennedy, W.Q. (1964). The structural differentiation of Africa in the Pan-African (± 500 m.y.) tectonic episode. *Research Institute of African Geology*, University of Leeds, **8**, 48-49.

Klein, J.A. (1980). *Geological report on area 2115A*. Geological Survey of S.W.A/Namibia (unpubl.), Windhoek, 39 pp.

Knott, S.D., Beach, A., Brockbank, P.J., Brown, J. L., McCallum, J.E. & Welbon, A.I. (1996). Spatial and mechanical controls on normal fault populations. *Journal of Structural Geology*, **18**, 359-372.

Kröner, A. (1980a). Chronologic evolution of the Pan African Damara belt in Namibia, south western Africa, 221-224. *In:* Closs, H. *et al.*, Eds., *Mobile Earth: final report of the geodynamics project, Federal Republic of Germany*. Harald Boldt Verlag, Boppard.

Kröner, A. (1980b). Pan African crustal evolution. *Episodes, International Union Geological Sciences*, **2**, 3-8.

Kröner, A. (1981a). Evolution of the Damara belt and Pan-African plate tectonics. *Geocongress '81, South African Geodynamic Project abstracts*, 131-132 (Abstract).

Kröner, A. (1981b). Precambrian plate tectonics, 57-90. *In:* Kröner, A., Ed., *Precambrian plate tectonics*. Elselvier, Amsterdam, 781 pp.

Kröner, A. (1982). Rb-Sr geochronology and tectonic evolution of the Pan-African Belt of Namibia, Southwestern Africa. *American Journal of Science*, **282**, 1471-1507.

Kröner, A. (1984). Domes structures and basement reactivation in the Pan-African Damara belt of Namibia, 191-206. *In:* Kröner, A. & Greiling, R., Eds., *Precambrian tectonics illustrated*. E., Schweizerbart'sche Verlagsbuchhandlung (Nägele u. Obermiller), Stuttgart, 419 pp.

Kröner, A., Retief, E.A., Compston, W., Jacob, R.E., Burger, A.J. (1991). Single-grain age and conventional zircon dating of remobilised basement gneisses in the central Damara belt of Namibia. *South African Journal of Geology*, **94**, 379-387.

Kruhl, J.H. (1994a). Preface, V-V1. *In:* Kruhl, J.H., Ed., *Fractals and dynamic systems in geoscience*. Springer-Verlag, Berlin, 425 pp.

Kruhl, J.H. (1994b). The formation of extensional veins: an application of the Cantor-Dust model, 95-104. *In:* Kruhl, J.H., Ed., *Fractals and dynamic systems in geoscience*. Springer-Verlag, Berlin, 425 pp.

Kukla, P.A. & Stainstreet, I.G. (1991). Record of the Damaran Khomas Hochland accretionary prism in central Namibia: refutation of an "ensialic" origin of a late Proterozoic orogenic belt. *Geology*, **19**, 473-476.

Kupková, M. & Krišťáková, Z. (1994). Fracture dimension of fracture patterns: a computer simulation, 87-94. *In:* Kruhl, J.H., Ed., *Fractals and dynamic systems in geoscience*. Springer-Verlag, Berlin, 425 pp.

La Pointe, P.R. (1988). A method to characterize fracture density and connectivity through fractal geometry. *Int. J. Rock Mech. Min. Sci. & Geomech. Abstr.*, **25**(6), 421-429.

Lehtonen, M.I., Manninen, T.E.T. & Schreiber, U.M. (1996). Report: lithostratigraphy of the area between the Swakop, Khan and lower Omaruru Rivers, Namib Desert. *Communications of the Geological Survey of Namibia*, **11**, 65-75.

Lesmoir-Gordon, N., Rood, W & Edney, R. (2000). *Fractal geometry*. Icon Books Ltd., Cambridge, 176 pp.

Lisle, R.J. (1992). Strain estimation from flattened buckle folds. *Journal of Structural Geology*,

14, 369-371.

Lonergan, L., Wilkinson, J.J. & McCaffrey, K.J.W. (1999). Fractures, fluid flow and mineralization: an introduction, 1-6. *In:* McCaffrey, K.J.W., Lonergan, L. & Wilkinson, J.J., Eds., *Fractures, fluid flow and mineralization*. Geological Society, Special Publications, **155**, 330 pp.

Loriga, M.A. (1999). Scaling systematics of vein size: an example from the Guanajuato mining district (Central Mexico), 57-67. *In:* McCaffrey, K.J.W., Lonergan, L. & Wilkinson, J.J., Eds., *Fractures, fluid flow and mineralization*. Geological Society, Special Publications, **155**, 330 pp.

Lubbe, B.L. (1988a). *Geophysical report No. 2115DD-1: Ground magnetic interpretation on the Brown Mountain Claims, Karibib Area.* Gold Fields Namibia Internal Report (unpubl.), 4 pp.

Lubbe, B.L. (1988b). *Geophysical report No. 2115DD-2: Induced Polarization and Resistivity Interpretation on the Brown Mountain claims area, Karibib District.* Gold Fields Namibia Internal Report (unpubl.), 5 pp.

Mandelbrot, B.B. (1967). How long is the coast of Britian? Statistical self-similarity and the fractional dimension. *Science*, **156**, 636-638.

Mandelbrot, B.B. (1975). Stochastic models for the Earth's relief, the shape and fractal dimension of the coastlines, and the number-area rule for islands. *Proc. Nat. Acad. Sci. USA*, **72**, 3825-3828.

Mandelbrot, B.B. (1977). *Fractals: form, chance, and dimension*. W.H. Freeman and Company, San Francisco, 365 pp.

Mandelbrot, B.B. (1983). *The fractal geometry of nature* (updated and augmented 2nd Ed.). W.H. Freeman, San Fransisco, CA, 468 pp.

Mandelbrot, B.B. (1989). Multifractal measure, especially for geophysicists. *Pure and Applied Geophysics*, **131**(1), 5-42.

Manning, C.E. (1994). Fractal clustering of metamorphic veins. *Geology*, **22**, 335-338.

Martin, H. (1965). The Precambrian geology of South West Africa and Namaqualand. *Precambrian Research Unit*, University of Cape Town, 159 pp.

Martin, H. (1978). The mineralization of the ensialic Damara orogenic belt. *Special Publication of the Geological Society of South Africa*, **4**, 405-415.

Martin, H. (1983a). Overview of the geosynclinal, structural and metamorphic development of the intracontinental branch of the Damara Orogen, 473-501. *In:* Martin, H. & Eder, F.W., Eds., *Intracontinental fold belts: case studies in the Variscan belt of Europe and the Damara belt in Namibia*. Springer-Verlag, Berlin, 945 pp.

Martin, H. (1983b). Alternative geodynamic models for the Damara Orogeny: a critical discussion, 913-945. *In:* Martin, H. & Eder, F.W., Eds., *Intracontinental fold belts: case studies in the Variscan belt of Europe and the Damara belt in Namibia*. Springer, Berlin, 945 pp.

Martin, H. & Porada, H. (1977). The intracontinental branch of the Damara Orogen in South West Africa: discussion of geodynamic models. *Precambrian Research*, **5**, 311-338.

McCaffrey, K.J.W., Johnston, J.D. & Feely, M. (1993). Use of fractal statistics in the analysis of Mo-Cu mineralization at Mace Head, County Galway. *Irish Journal of Earth Sciences*, **12**, 139-148.

McCaffrey, K.J.W. & Johnston, J.D. (1996). Fractal analysis of a mineralized vein deposit: Curraghinalt gold deposit, County Tyrone. *Mineralium Deposita*, **31**(1-2), 52-58.

McWilliams, M.O. (1981). Palaeomagnetism and Precambrian tectonic evolution of Gondwana, 649-687. *In:* Kröner, A., Ed., *Precambrian Plate Tectonics*. Elselvier, Amsterdam, 781 pp.

McWilliams, M.O. and Kröner (1981). Paleomagnetism and tectonic evolution of the Pan

African Damara belt, southern Africa. *Journal of Geophysical Research*, **86**, 5147-5162.

Meinert, L.D. (1998). A review of skarns that contain gold, 359-414. *In:* Lentz, D.R., Ed., *Mineralized intrusion-related skarn systems*. Mineralogical Association Of Canada, Short Series Course, **26**, 664 pp.

Merceron, T. & Velde, B. (1991). Application of Cantor's method for fractal analysis of fractures in the Toyoha Mine, Hokkaido, Japan. *Journal of Geophysical Research*, **96**(B10), 16,641-16,650.

Mikucki, E.J. (1998). Hydrothermal transport and depositional processes in Archean lode-gold systems. *A review: Ore Geology Reviews*, **13**, 307-321.

Miller, R.McG. (1974). Some economic aspects of the crystallisation of the Damara granites, South West Africa. *Precambrian Research Unit, Bulletin*, University of Cape Town, **15**, 184-192.

Miller, R.McG. (1980). Geology of a portion of central Damaraland, South West Africa/Namibia. *Memoirs of the Geological Survey of South Africa, S. W. Afr. Ser.*, **6**, 78 pp.

Miller, R.McG. (1983b). Economic implications of plate tectonic models of the Damara Orogen. *Special Publication of the Geological Society of South Africa*, **11**, 385-395.

Miller, R.McG. (1983c). The Pan-African Damara Orogen of South West Africa/ Namibia. *Special Publication of the Geological Society of South Africa*, **11**, 431-515.

Miller, R.McG. (1992). *The Mineral Resources of Namibia - Mineral exploration targets in Namibia (1st Ed.)*, Section 1.1. Ministry of Mines and Energy/ Geological Survey, Windhoek, 5 pp.

Miller, R.McG. and Burger, A.J. (1983). U-Pb zircon ages of members of the Salem Granitic Suite along the northern edge of the central Damaran granite belt. *Special Publication of the Geological Society of South Africa*, **11**, 273-280.

Miller, R.McG. & Hoffmann, K.-H. (1981). *Guide to the excursion through the Damara Orogen*. Geocongress '81, Geological Society of South Africa, 103 pp.

Misiewicz, J.E. (1988). The geology and metallogeny of the Otavi Mountain Land, Damara Orogen, SWA/Namibia, with particular reference to the Berg Aukas Zn-Pb-V deposit - a model of ore genesis. Masters (Exploration Geology) Dissertation (unpubl.), Rhodes University, 135 pp.

Monecke, T., Gemmell, J.B. & Monecke, J. (2001). Fractal distributions of veins in drill core from the Hellyer VHMS deposit, Australia: constraints on the origin and evolution of the mineralizing system. *Mineralium Deposita*, **36**, 406-415.

Moore, J.M. & Jacob, R.E. (1998). The Navachab sheeted-vein/ skarn Au-deposit, Namibia. *GAC-MAC Joint Congress, Quebec 1998*, A125-126 (Abstract).

Moore, J.M., Jacob, R.E., Harris, C. & Armstrong, R.A. (1999). The Navachab gold deposit, Namibia: a mesothermal sheeted-vein/ skarn system related to the Pan-African Damara Orogen. GSA 11: Earth Resources for Africa, *Journal of African Earth Science*, **28**(4A), 50-51 (Abstract).

Mullin, G. (1989). *The geology, metamorphism and hydrothermal alteration of the Swakop Group on Daheim farm in the Karibib District of Namibia*. Honours Thesis (unpubl.), Rhodes University, 55 pp.

Nash, C.R. (1971).Metamorphic petrology of the S.J. Area, Swakopmund District, South West Africa. *Precambrian Research Unit, Bulletin*, University of Cape Town, **9**, 77 pp.

Needham, T., Yielding, G. & Fox, R. (1996). Fault population description and prediction using examples from the offshore U.K. *Journal of Structural Geology*, **18**, 155-167.

Nicol, A., Walsh, J.J., Watterson, J. & Gillespie, P.A. (1996). Fault size distributions: are they really power-law? *Journal of Structural Geology*, **18**, 191-197.

Nicolas, A. (1987). *Principles of rock deformation*. D. Reidel Publishing Company, Dordrecht, 208 pp.

Norrish, K. & Hutton, J.T. (1969). An accurate X-ray spectrographic method for the analysis of a wide range of geological samples. *Geochimica et Cosmochimica Acta*, **33**, 431-453.

Nörtemann, M.F.-J., Mücke, A., Weber, K. & Meinert, L.D. (2000). Mineralogy of the Navachab skarn deposit, Namibia: an unusual Au-bearing skarn in high grade metamorphic rocks. *Communications of the Geological Survey of Namibia*, **12**, 149-156.

Oliver, G.J.H. (1994). Mid-crustal detachment and domes in the central zone of the Damara orogen, Namibia. *Journal of African Earth Science*, **19**, 331-344.

Oliver, G.J.H. (1995). The Central Zone of the Damara Orogen, Namibia, as a deep metamorphic core complex. *Communications of the Geological Survey of Namibia*, **10**, 33-41.

Oliver, G.J.H. & Kinnaird, J.A. (1996). The Rössing-SJ Dome, Central Zone, Damara Belt, Namibia: an example of mid-crustal extensional ramping. *Communications of the Geological Survey of Namibia*, **11**, 53-64.

Passchier, C.W. (2001). Flanking structures. *Journal of Structural Geology*, **23**, 951-962.

Passchier, C.W. & Trouw, R.A.J. (1998). *Microtectonics* (corrected 2nd Ed.). Springer-Verlag, Berlin, 289 pp.

Paterson, M.S. (1978). *Experimental rock deformation - the brittle field*. Springer-Verlag, Berlin, 254 pp.

Peitgen, H.-O., Jürgens, H. and Saupe, D. (1992). *Chaos and fractals: new frontiers of science*. Springer-Verlag, New York, 984 pp.

Perkins, D., III, Essene, E.J. & Marcotty, L.A. (1982). Thermometry and barometry of some amphibolite–granulite facies rocks from the Otter Lake area, southern Quebec. *Canadian Journal of Earth Sciences*, **19**, 1759-1774.

Petzel, V.F.W. (1988a). *Geological progress report on the Brown Mountain claims, Karibib District*. Gold Fields Namibia Internal Report (unpubl.), 75 pp.

Petzel, V.F.W. (1988b). *Progress report on geological exploration conducted on the farms Spes Bona 105 and Daheim 106, Grant M46/3/1631*. Gold Fields Namibia Internal Report (unpubl.), 48 pp.

Petzel, V.F.M. & Roesener, H. (1988). *Memorandum on diamond drilling conducted in the Brown Mountain claim area*. Gold Fields Namibia Internal Report (unpubl.), 9 pp.

Phillips, G.N., Groves, D.I. & Martyn, J.G. (1984). An epigenetic origin for Archean banded iron-formation hosted gold deposits. *Economic Geology*, **79**, 162-171.

Pickering, G., Bull, J.M. & Sanderson, D.J. (1995). Sampling power-law distributions. *Tectonophysics*, **248**, 1-20.

Pickering, G., Bull, J.M. & Sanderson, D.J. (1996). Scaling of fault displacements and implications for the estimation of sub-seismic strain. In: Buchanan, P.G. & Nieuwland, D.A., Eds., *Modern developments in structural interpretation, validation and modelling*. Geological Society, Special Publication, **99**, 11-26.

Pickering, G., Bull, J.M., Sanderson, D.J. & Harrison, P.V. (1994). Fractal fault displacements: a case study from the Moray Firth, Scotland, 105-119. *In:* Kruhl, J.H., Ed., *Fractals and dynamic systems in geoscience*. Springer-Verlag, Berlin, 425 pp.

Pickering, G., Peacock, D.C.P., Sanderson, D.J. & Bull, J.M. (1997). Modelling tip zones to predict the throw and length characteristics of faults. *American Association of Petroleum Geologists Bulletin*, **81**, 82-99.

Pickford, M. & Senut, B. (2001). *Namibia palaeontology expedition (27th June to 2nd July, 2001)*. Report (unpubl.), Collège de France/ UMR 8569, CNRS, 17pp.

Piper, J.D.A. (1982). The Precambrian palaeomagnetic record: the case for the Proterozoic Supercontinent. *Earth and Planetary Science Letters*, **59**, 61-89.

Pirajno, F. & Jacob, R.E. (1991). Gold mineralisation in the intracontinental branch of the Damara Orogen, Namibia: a preliminary survey. *Journal of African Earth Science*, **13**, 305-311.

Pirajno, F., Jacob, R.E. & Petzel, V.F.W. (1991). Distal skarn-type gold mineralization in the Central Zone of the Damara Orogen, Namibia. In: Ladeira, E.A., Ed., *Brazil Gold'91*. Balkema, Rotterdam, 823 pp.

Poli, L.C. & Oliver, G.J.H. (2001). Constrictional deformation in the Central Zone of the Damara Orogen, Namibia. *Journal of African Earth Science*, **33**, 303-321.

Porada, H. (1979). The Damara–Ribeira orogen of the Pan-African–Brasiliano cycle in Namibia (Southwest Africa) and Brazil as interpreted in terms of continental collision. *Tectonophysics*, **57**, 237-265.

Porada, H. (1983). Geodynamic model for the geosynclinal development of the Damara Orogen, Namibia/South West Africa, 503-541. *In:* Martin, H. & Eder, F.W., Eds., *Intracontinental fold belts: case studies in the Variscan belt of Europe and the Damara belt in Namibia*. Springer-Verlag, Berlin, 945 pp.

Porada, H. (1985). Stratigraphy and facies in the Upper Proterozoic Damara orogen, Namibia, based on a geodynamic model. *Precambrian Research*, **29**, 235-264.

Porada, H. (1989). Pan-African rifting and orogenesis in southern to equatorial Africa and eastern Brazil. *Precambrian Research*, **44**, 103-136.

Poulsen, K.H. & Robert, F. (1989). Shear zones and gold: practical examples from the Southern Canadian Shield, 239-266. *In:* Bursnall, J.T., Ed., *Mineralization and shear zones*. Geological Association of Canada, Short Course Notes (1989 Montréal GAC Annual Meeting), **6**, 299 pp.

Price, N.J. & Cosgrove, J.W. (1990). *Analysis of geological structures*. Cambridge University Press, Cambridge, 502 pp.

Puhan, D. (1976). Metamorphic temperature determined by means of the dolomite-calcite solvus geothermometer: examples from the Central Damara Orogen (South West Africa). *Contributions to Mineralogy and Petrology*, **58**, 23-28.

Puhan, D. (1983a). Temperature and pressure of metamorphism in the Central Damara Orogen. *Special Publication of the Geological Society of South Africa*, **11**, 219-223.

Puhan, D. (1983b). Metamorphism of siliceous dolomites of the Central and Southern Part of the Damara Orogen, 767-784. *In:* Martin, H. & Eder, F.W., Eds., *Intracontinental fold belts: case studies in the Variscan belt of Europe and the Damara belt in Namibia*. Springer-Verlag, Berlin, 945 pp.

Rantitsch, G. (2001). The fractal properties of geochemical landscapes as an indicator of weathering and transport processes. *Journal of Geochemical Exploration*, **73**(1), 27-42.

Rice, J.M. (1977). Contact metamorphism of impure dolomitic limestone in the Boulder Aureole, Montana. *Contributions to Mineralogy and Petrology*, **59**, 237-259.

Robert, F. & Poulsen, K.H. (2001). Vein formation and deformation in greenstone gold deposits. *Reviews in Economic Geology*, **14**, 111-155.

Roberts, R.G. (1988). Archean lode gold deposits, 1-19. *In:* Roberts, R.G. & Sheahan, P.A., Eds., *Ore Deposit Models*. Geoscience Canada (Reprint 3 Series), Ottawa, 194 pp.

Roberts, S., Sanderson, D.J. & Gumiel, P. (1998). Fractal analysis of Sn-W mineralization from Central Iberia: Insights into the role of fracture connectivity in the formation of an ore deposit. *Economic Geology*, **93**, 360-365.

Roberts, S., Sanderson, D.J. & Gumiel, P. (1999). Fractal analysis and percolation properties of veins, 7-16. *In:* McCaffrey, K.J.W., Lonergan, L. & Wilkinson, J.J., Eds., *Fractures,* *fluid flow and mineralization*. Geological Society, Special Publications, **155**, 330 pp.

Robinson, E.S. & Çoruh, C. (1988). *Basic exploration geophysics*. John Wiley & Sons, New York, 576 pp.

Sahimi, M. (1994). *Applications of percolation theory*. Taylor & Francis Ltd., London, 258 pp.

Sammis, C.G., King, G. & Biegel, R.L. (1986). The kinematics of gouge deformation. *Pure and Applied Geophysics*, **125**, 777-812.

Sanderson, D.J., Roberts, S. & Gumiel, P. (1994). A fractal relationship between vein thickness and gold grade in drill core from La Codosera, Spain. *Economic Geology*, **89**, 168-173.

Sawyer, E.W. (1981). Damaran structural and metamorphic geology of an area south-east of Walvis Bay, SWA/Namibia. *Memoirs of the Geological Survey of S.W. Africa/Namibia*, **7**, 94 pp.

Scholle, P.A., Bebout, D.G. & Moore, C.H. (1998). *Carbonate depositional environments*. AAPG Memoir 33 (4th reprint), USA, 708 pp.

Scholz, C.H. & Cowie, P.A. (1990). Determination of total strain from faulting using slip measurements. *Nature*, **346**, 837-839.

Seward, T.M. & Barnes, H.L. (1997). Metal transport by hydrothermal ore fluids. *In:* Barnes, H.L., Ed., *Geochemistry of hydrothermal ore deposits (3rd Ed.)*. John Wiley & Sons, Inc., New York, 972 pp.

Sibson, R.H., Robert, F. & Poulsen, K.H. (1988). High-angle reverse faults, fluid-pressure cycling, and mesothermal gold deposits. *Geology*, **16**, 551-555.

Silberschmidt, V.V. & Silberschmidt, V.G. (1994). Multi-scale model of damage evolution in stochastic rocks: fractal approach, 53-64. *In:* Kruhl, J.H., Ed., *Fractals and dynamic systems in geoscience*. Springer-Verlag, Berlin, 425 pp.

Skinner, B.J. (1997). Hydrothermal mineral deposits: what we do and don't know, 1-29. *In:* Barnes, H.L., Ed., *Geochemistry of hydrothermal ore deposits (3rd Ed.)*. John Wiley & Sons, Inc., New York, 972 pp.

Smith, D.A.M. (1965). The geology of the area around the Khan and Swakop Rivers in SW Africa. *Geological Survey of South Africa, Memoir*, S.W. Afr. Ser., **3**, 1-113.

South African Committee for Stratigraphy (SACS), (1980). The Damara Sequence, 415-438. *In:* Kent, L.E., Ed., *The stratigraphy of the Republic of South Africa, South West Africa/Namibia, and the Republics of Bophuthatswana, Transkei and Venda*. Handbook of the Geological Survey of South Africa, **8**, 690 pp.

Stanistreet, I.G., Kukla, P.A. & Henry, G. (1991). Sedimentary basinal responses to a Late Precambrian Wilson Cycle: The Damara Orogen and Nama Foreland, Namibia. *Journal of African Earth Science*, **13**, 141-156.

Starling, A., Gilligan, J.M., Carter, A.H.C., Foster, R.P & Saunders, R.A. (1989). High-temperature hydrothermal precipitation of precious metals on the surface of pyrite. *Nature*, **340**, 298-300.

Steven, N.M. (1993). A study of epigenetic mineralisation in the Central Zone of the Damara Orogen, Namibia, with special reference to gold, tungsten, tin and rare earth elements. *Memoir of the Geological Survey of Namibia*, **16**, 166 pp.

Steven, N.M. (1999). Evaluation of the Sandamap Noord turbidite-hosted gold prospect, central Namibia, for a heap-leach gold operation: implications for regional gold exploration in the Navachab district. *University of Witwatersrand, Economic Geology Research Unit Information Circular No. 337*, 1-14.

Steven, N.M. (2000). *Onguati, Karibib District Review*. Rockwater Consulting cc. (unpubl.), 13 pp.

Steven, N.M., Armstrong, R.A. & Moore, J.M. (1993). The Sandamap Noord Gold Prospect, Central Namibia: discovery of a new style of turbidite-hosted gold mineralization.

International Geology Reviews, **35**, 840-854.

Steven, N.M., Badenhorst, F.P. & Petzel, V.F.W. (1994). A review of gold occurrences in the Northern and Central Zones of the Damara Orogen and the underlying mid-Proterozoic basement, central Namibia. *Communications of the Geological Survey of Namibia*, **9**, 63-77.

Stowell, J.F.H., Watson, A.P. & Hudson, NFC (1999). Geometry and population systematics of a quartz vein set, Holy Island, Anglesea, North Wales, 17-23. *In:* McCaffrey, K.J.W., Lonergan, L. & Wilkinson, J.J., Eds., *Fractures, fluid flow and mineralization*. Geological Society, Special Publications, **155**, 330 pp.

Talbot, C.J. (1970). The minimum strain ellipsoid using deformed quartz veins. *Tectonophysics*, **9**, 47-76.

Tankard, A.J., Jackson, MPA, Erickson, K.A., Hobday, D.K., Hunter, D.R., Minter, W.E.L. (1982). *Crustal evolution of Southern Africa: 3.8 billion years of Earth history*. Springer-Verlag, New York, 523 pp.

Tsitos, Y. (1992). *Interim report on the ground geophysical surveys carried out over the Brown Mountain, KR-48 and Chuos grids*. Genmin Mineral Resources Division - Springs Metals and Minerals Department Internal Report (unpubl.), 10 pp.

Turcotte, D.L. (1986a). A fractal approach to the relationship between ore grade and tonnage. *Economic Geology*, **81**, 1528-1532.

Turcotte, D.L. (1986b). Fractals and fragmentation. *Journal of Geophysical Research*, **91**, 1921-1926.

Turcotte, D.L. (1989). Fractals in geology and geophysics. *Pure Applied Geophysics*, **131**, 171-177.

Turcotte, D.L. (1991). Earthquake prediction. *Annual Reviews of Earth and Planetary Science*, **19** , 1921-1926.

Turcotte, D.L. (1994). Crustal deformation and fractals, a review, 7-23. *In:* Kruhl, J.H., Ed., *Fractals and dynamic systems in geoscience*. Springer-Verlag, Berlin, 425 pp.

Turcotte, D.L. (1997). *Fractals and chaos in geology and geophysics* (2nd Ed.). Cambridge University Press, Cambridge, 398 pp.

Twiss, R.J. & Moores, E.M. (1992). *Structural geology*. W.H. Freeman & Co., New York, 532 pp.

Valley, J.W. & O'Neil, J.R. (1981). $^{13}C/^{12}C$ exchange between calcite and graphite: a possible thermometer in Grenville marbles. *Geochimica et Cosmochimica Acta*, **45**, p.411-419.

Vearncombe, J.R. (1993). *MSc workshop: deformation and mineralisation*. T. Nutt and Associates (unpubl.), Harare, 121 pp.

Velde, B., Dubois, J., Moore, D. & Touchard, G. (1991). Fractal patterns of fractures in granites. *Earth and Planetary Science Letters*, **104**, 25-35.

Velde, B., Dubois, J., Touchard, G. & Badri, A. (1990). Fractal analysis of fractures in rocks: the Cantor's Dust method. *Tectonophysics*, **179**, 345-352.

Vermilye, J.M. & Scholz, C.H. (1995). Relation between vein length and aperture. *Journal of Structural Geology*, **17**, 423-434.

Viljoen, W.G. (2000). *Remote sensing and geophysical imaging and their relationship to the structural framework of the Etusis-Neikhoes pluton (Damara Belt, Namibia)*. Honours Thesis (unpubl.), Rhodes University, 53 pp.

Viljoen, W.G. (2002). *Copper-gold mineralization in the Onguati area, Karibib District, Southern Central Zone, Namibia*. 11th Quadrennial IAGOD Symposium and Geocongress 2002, Windhoek, 51 pp (Abstract).

Wada, H. & Suzuki, K. (1983). Carbon isotopic thermometry calibrated by dolomite-calcite solvus temperatures. *Geochimica et Cosmochimica Acta*, **47**, 697-706.

Walsh, J.J., Watterson, J. & Yielding, G. (1991). The importance of small scale faulting in regional extension. *Nature*, **351**, 391-393.

Watson, N.I. (1982). *Regional geology of areas 2155C and DC/ &UC*. Report of the Geological Survey of S.W.A./Namibia (unpubl.), Windhoek, 51pp.

Watters, B.R. (1976). Possible Late Precambrian subduction zone in South West Africa. *Nature*, **259**, 471-473.

Webb, K.E. (1992). *Onguati Project - Final report*. Report to Genmin Mineral Resources Division (unpubl.), Gold and Base Metals Section, Windhoek Regional Office, 26 pp.

Wei, S & Pengda, Z. (2002). Theoretical study of statistical fractal model with applications to mineral resource prediction. *Computers & Geosciences*, **28**, 369-376.

Williams, P.J. (1990). Evidence for late metamorphic origin of disseminated gold mineralization in Grenville gneisses at Calumet, Quebec. *Economic Geology*, **85**, 164-171.

Wilson, G. & Cosgrove, J.W. (1982). *Introduction to small-scale geological structures*. George Allan & Unwin, Boston, 128 pp.

Wilton, J., Lombard, P.J.A. & Philpot, H.G. (2002). Discovery of the Otjikoto gold deposit in Namibia, 1-6. *In:* Steven, N., Ed., *Mesothermal gold deposits of the Damara Orogen excursion guidebook (F1)*. 11th Quadrennial IAGOD Symposium and Geocongress 2002, Windhoek.

Winter, J.D. (2001). *An introduction to igneous and metamorphic petrology*. Prentice Hall, New Jersey, 699 pp.

Wong, T.-F., Fredrich, J.T. & Gwanmesia, G.D. (1989). Crack aperture statistics and pore space fractal geometry at Westerly granite and Rutland quartzite: implications for an elastic contact model of rock compressibility. *Journal of Geophysical Research*, **94**, 10267-10278.

Yielding, G., Walsh, J.J. & Watterson, J. (1992). The prediction of small-scale faulting in resevoirs. *First Break*, **10**, 449-460.

Zhang, X. & Sanderson, D.J. (1994). Fractal structure and deformation of fractured rock masses, 37-51. *In:* Kruhl, J.H., Ed., *Fractals and dynamic systems in geoscience*. Springer-Verlag, Berlin, 425 pp.

1:250 000 Geological Map Series, Omaruru Sheet 2114 (1997). Geological Survey of Namibia, Ministry of Mines and Energy, Windhoek.

1:250 000 Geological Map Series, Walvis Bay Sheet 2214 (1995). Geological Survey of Namibia, Ministry of Mines and Energy, Windhoek.

1:50 000 Topocadastral Map Series, South West Africa Sheet 2115DD - KARIBIB (1st Ed.). Office of the Surveyor General, Windhoek.

1:500 000 Geological Map of the Damara Orogen, Southwest Africa/Namibia - Sheet 2 (1998). Geological Survey of Namibia, Ministry of Mines and Energy, Windhoek.

APPENDIX A: HISTORY OF MINE PRODUCTION AND GOLD EXPLORATION IN THE ONGUATI MINE AREA

The Onguati Copper Mine was developed in the late 1950s by the Atlas Mining Company, and began with small scale exploitation of the Onguati gossan (Petzel, 1988a). Production was in the order of 80 tonnes per month, and grade was maintained at about 20% Cu by stringent hand sorting (Petzel, 1988a). The Atlas Mining Company undertook minor exploration to find the downward extension of the Onguati ore body, but due to unfavourable siting their diamond-drill holes intersected no ore (Petzel, 1988a).

Shortly after the closure of Onguati Mine, NV Billiton Maatschappij carried out an electromagnetic survey and a minor drilling programme. The major geophysical anomalies were explored by six shallow diamond-drill holes (total length of 336 metres) but no major mineralisation was intersected and the options for the claims were dropped (Petzel, 1988a). Tsumeb geologists also investigated the Onguati mineralisation at various times during the 1960s, but a detailed exploration programme was never conducted (Petzel, 1988a).

The Onguati Mine was reopened and exploited by Cu Ventures (Pvt.) Ltd. for a short period between1972 and 1973, and produced a chalcopyrite concentrate with a gold credit. It is estimated that almost 67 000 tonnes of ore grading 3 wt% Cu were mined during this time (Steven, 2000). A credit note from the Tsumeb smelters for a 76 tonne batch of concentrate reported metal grades of Cu as 20,495%, Au as 10,20 g/t and Ag as 235,85 g/t (Petzel, 1988a). In later sampling, Pirajno *et al.* (1991) reported low-to-moderate Au-grades ranging from 0.1 to 6 g/t in vein material, with local peak values of up to 80 g/t.

Following the discovery of carbonate-hosted gold as part of an extensive pyrrhotite skarn at the then Anglo American, Navachab Gold Mine, there was a period (1986-1992) of intensive gold exploration in the Karibib district (Webb, 1992). In the mid-1980s, Anglo American Prospecting Services Namibia (AAPSN) entered into agreement with Canbra Holdings who held the prospecting license (M46/3/1556) for the area over the Onguati claims (Steven, 2000). Stream sampling and soil geochemistry were utilized by AAPSN and a number of gold anomalies were identified, but no drilling was ever undertaken.

Gold Fields Namibia (GFN) began exploration for Navachab-type gold mineralisation in the Onguati region in late 1986. A 600 by 3000 metre grid was setup over Western Workings and Brown Mountain, and the area was mapped at a scale of 1:2 500 (Petzel, 1988a). This was followed by more detailed geological mapping of certain parts at a scale of

1:500 by Gray (1988) as part of an Honours research project. At a similar time and a short distance ENE of Onguati Mine, exploration and 1:1 000 mapping was implemented by GFN in an area where several mafic meta-volcanic units (Daheim Formation meta-volcanic rocks) cropped out (Petzel, 1988b; Joubert, 1989, Mullin, 1989).

GFN carried out a stream sediment, orientation survey in the tributaries draining either side of the Western Workings, Brown Mountain and Onguati Mine areas (Petzel, 1988a). A detailed soil sampling exercise identified 5 major Au anomalies with a 100 to 200 ppb Au range, 3 distinct Cu anomalies with a 100 to >1000 ppm Cu range, and 2 anomalous Zn values with a 164 to 235 ppm Zn range (Petzel, 1988a). Lithogeochemical samples taken along transects at Brown Mountain had a Au range from 55 to 410 ppb, with one sample having >1000 ppb Au, and all showed corresponding, anomalous Cu values (Petzel, 1988a). Western Workings lithogeochemical samples yielded values from 60 to >3000 ppb Au (highest values from mineralized vein margins) and Cu values range from 316 to >1000 ppm (Petzel, 1988a).

Goldfields did not follow-up any of the large, soil gold anomalies they identified away from the obvious quartz vein systems, but did carry out percussion drilling along a number of traverses in the Western Workings and Brown Mountain areas (Steven, 2000). A total of 13 boreholes were drilled along four traverses to a depth of 100 m, with a 50 m spacing between holes (Petzel, 1988a). The first traverse, consisting of five holes (BMP-1 to 5), was undertaken on the western side of Brown Mountain and was oriented perpendicular to the main vein set (Petzel, 1988a). A further percussion hole (BMP-13) was drilled 240 m to the SW of this traverse to test the lateral extent of mineralisation. Abundant sulphides were encountered in all the boreholes, associated with zones of veining and ferruginization, and consisted mainly of pyrrhotite with lesser amounts of pyrite, arsenopyrite and chalcopyrite (Petzel, 1988a). Anomalous amounts of Cu (>1000 ppm), Au (highest value, 381 ppb) and As (highest value, 9130 ppm) were also recorded along this traverse. BMP-13 recorded a Au value exceeding 1000 ppb and a Cu value greater than 1000 ppm towards its base (Petzel, 1988a; Steven, 2000).

Traverse 2 consisted of an array of three holes (BMP-6 to 8). The drill holes tested a major thrust zone for mineralisation, as well as the lithological contacts between the calcitic and dolomitic marbles, and the dolomitic and mafic tuffs of the Western Workings region (Petzel, 1988a). Although veins were present, as well as ferruginous and brecciated zones, they had metal contents that were only weakly anomalous (Petzel, 1988a).

Traverse 3 and 4 (BMP-9 to 12) were positioned on the northern and southern flanks of a large antiformal structure, close to the mineralized areas of Western Workings (Petzel, 1988a). Anomalous values for Cu and Au were obtained for the two holes drilled on the northern flank of the antiform, with BMP-10 having two samples with Au values exceeding 3000 ppb (Petzel, 1988a). In addition, zones with anomalous Cu values were commonly found to have anomalous Zn values. BMP-11 and 12, drilled on the southern flank of the Western Workings antiform, intersected zones of abundant sulphide mineralisation (mainly pyrrhotite and pyrite ± chalcopyrite), and a number of samples had highly anomalous Au contents exceeding 1000 ppb (Petzel, 1988a).

A ground magnetic survey was carried out by GFN (Lubbe, 1988a) with the aim of establishing the depth extent and density of vein mineralisation. The magnetic survey indicated that pyrrhotite-bearing veins were still present at a depth of 200 m below Brown Mountain, but was inconclusive in assessing whether vein density increased with depth (Lubbe, 1988a; Petzel, 1988a). An induced polarization and direct current resistivity survey was carried out by Lubbe (1988b) to supplement the previous geophysical work. The survey was conducted across line 960W over Brown Mountain and along line 2040W at Western Workings. The direct current resistivity method met with poor results, but the induced polarization survey detected a number of highly conductive areas (Lubbe, 1988b).

At the recommendation of Lubbe (1988b), two diamond drill holes were sited to intersect the zones identified by the geophysical surveys (Petzel & Roesener, 1988). Diamond drill hole BMD-1 was drilled at Brown Mountain (282,50S/807,00W) with an orientation of 292°/45° (trend/plunge), and had a final length of 450,38 m. All veins and alteration zones were analysed for Cu, Pb, Zn, As, Bi and Au. The Au content of all samples along this hole was very low or below the detection limits. Anomalous As values were encountered, along with low Bi contents which increased with depth (Petzel & Roesener, 1988). The second diamond hole (BMD-2) was drilled at Western Workings (090S/2040W) and deepened an existing percussion hole BMP-11, from a depth of 100 m to 250 m. BMD-2 was oriented at 325°/60° (trend/plunge) to intersect a geophysical anomaly at a depth of 170 m (Lubbe, 1988b; Petzel & Poesener, 1988). While there were numerous Cu values >100 ppm, there were only 2 notable anomalous Au values of 400 ppb and 2100 ppb (Petzel & Roesener, 1988). After these two diamond drill holes failed to intersect any economic mineralisation, the options on the Brown Mountain claims were dropped.

In the period from 1990 to 1992, Genmin undertook a regional exploration programme to identify potential areas of carbonate-hosted pyrrhotite skarn over the farms Onguati 52 and 53, and further west over Kranzberg 59 (Webb, 1992). The Genmin exploration strategy relied from the onset, on regional aeromagnetic, and stream sediment and rock chip geochemical surveys (Webb, 1992). Genmin believed that Navachab-type mineralisation was intimately associated with NW-trending lineaments, and utilized the aeromagnetic surveys to identify the intersections of areas of high magnetic intensity (possibly related to pyrrhotite mineralisation) with these crustal structures (Webb, 1992; Tsitos, 1992).

The stream sampling exercise was carried out at a 500 m spacing along all the main rivers and tributaries draining the areas of interest (Webb, 1992). Together with regional rock chip sampling, several anomalies were identified in the Onguati study area and in the Kranzberg region (Webb, 1992; Steven, 2000). Rock chip analysis from the Onguati study area also confirmed previous work by Gold Fields that Au mineralisation is located within sulphide-bearing quartz veins. A vein sample from Western Workings had 5 g/t Au with 1.27% Cu, 131 ppm Zn, 139 ppm As and 478 ppm Bi (Webb, 1992).

No further exploration was carried out at Onguati Mine or at Western Workings because these deposits are not amenable to open-cast mining (Webb, 1992). A detailed follow-up programme of rock-chip sampling, soil geochemistry, and ground geophysics was conducted at Brown Mountain because of its high tonnage potential. The highest Au values attained from the rock chip samples were in the region of 150 ppb, while As values were as high as 7010 ppm with a Cu maximum value of 119 ppm (Webb, 1992). Although a number of soil geochemical anomalies were identified by Genmin over the Onguati study area, none were drilled. Following ground magnetic and electromagnetic surveys (lines 480W to 1320W), and some induced polarization transects (lines 600W to 1320W) it was concluded that there was a strong, positive magnetic high with southward-dipping EM conductors (Tsitos, 1992). These were interpreted as thrust zones with abundant sulphide mineralization (Tsitos, 1992). Although there were coincident geological, geochemical and geophysical anomalies over Brown Mountain, the claims for this area were dropped. It was thought that if there was significant mineralisation that the previous Goldfields diamond drill holes (i.e. BMD series) should have intersected it (Webb, 1992). Genmin shifted their focus to the Kr 48 (northern parts of Kransberg 59) and Chuos (northern flank of the Groot Rooiberg Mountain) anomalies further along strike.

APPENDIX B: ANALYTICAL PROCEDURE

B.1. Electron Microprobe Mineral Analyses

Mineral grains were analysed using a JEOL Superprobe 733 in the Rhodes University Geology Department. A combination of probe sections (25 x 45 mm) and ore briquettes (26 mm diameter) were polished (1 µm finish) and carbon coated, and used for the analyses. The Probe for Windows NT software package (V5.05) designed by J. Donovan was used to collect and process data from the electron microprobe.

(a) Carbonate minerals - probe operating conditions:

Beam current:	15 nA
Accelerating voltage:	15 kV
Beam size (diameter):	20 µm
Probe Scan:	Off (some attempts with probe scan on)

Calibration standards:

Elements		Standards	Count times		Crystals	L.L.D.* (elemental wt%)
			On peak (s)	Background (s)		
Ca	Ka	Calcite	20	10	PET	0.052
Mg	Ka	Dolomite	20	10	TAP	0.034
Sr	La	Strontianite	20	10	TAP	0.075
Fe	Ka	Siderite	20	10	TAP	0.063
Mn	Ka	Rhodonite	20	10	LIF	0.112
C	0	NAF	-	-	-	-

** L.L.D. = lower level of detection*

(b) Sulphide minerals - probe operating conditions:

Beam current:	30 nA
Accelerating voltage:	25 kV
Beam size (diameter):	2 µm

Calibration standards:

Elements		Standards	Count times		Crystals	L.L.D. (elemental wt%)
			On peak (s)	Background (s)		
Se	Ka	130 Silver Bismuth Selenide	20	10	LIF	0.091
As	Ka	129 Palladium arsenide 472	10	5	LIF	0.078
Au	La	15 JEOL Gold metal	40	20	LIF	0.100
Zn	Ka	125 Sphalerite 20	10	5	LIF	0.043
Cu	Ka	121 Chalcopyrite (NAT)	10	5	LIF	0.037
Ni		Ni-oxide	10	5	LIF	0.032
Co	Ka	527 Cobalt metal	10	5	LIF	0.055
Fe	Ka	121 Chalcopyrite (NAT)	10	5	LIF	0.035
Mn		Willemite	10	5	LIF	0.036
Sb		127 Palladium Antinomide 297	10	5	PET	0.163
Ag	La	Silver Bismuth Selenide	40	20	PET	0.179
S	Ka	125 Sphalerite 20	10	5	PET	0.062
Mo		Mo-metal	10	5		0.131
Bi	Ka	Silver Bismuth Selenide	40	20	LIF	0.139
Hg*		128 Palladium Mercury Telluride	40	20	LIF	0.84
Te*		128 Palladium Mercury Telluride	40	20	PET	0.88

* detection of Hg and Te was only carried out on a few select grains (not routinely analysed for in bulk of sulphide samples).

B.2. XRD Mineral Determination

Powdered rock samples were analysed by X-ray diffraction (XRD) in the Chemistry Department of Rhodes University and in the Department of Geology at the University of Cape Town (UCT). A small quantity of powdered quartz was added as an internal standard to the calcitic marble samples used for preliminary XRD calcite-dolomite solvus geothermometry.

(a) Rhodes University - XRD operating conditions:

Model:	Philips powder diffractometer (vertical goniometer)
Tube:	Copper tube
Filter:	Nickel filter
Radiation:	Cu K-alpha

Wavelength: 1.5404 Å

(b) University of Cape Town - XRD operating conditions:

Model: Philips PW1390 powder diffractometer
Software package: Philips X'Pert Graphic and Identify
Tube: Copper tube
Radiation: Cu K-alpha
Wavelength: 1.54056 Å

B.3. XRF Whole-rock Geochemical Data

Samples were analysed by X-ray fluorescence (XRF) spectrometry on a Philips 1480 machine in the Geology Department of Rhodes University.

(a) Sample preparation:

Several-kilogram hand specimens and drillcore samples of the main rock types were collected. Samples were washed, then crushed in a Mn-steel jaw crusher and milled, and a small portion finally ground to –300# in an automatic agate mortar. Quartzitic samples were run through the jaw crusher and steel milling vessel after each sample to ensure machine cleanliness.

(b) Major oxide analysis (total rock):

The procedure of Norish & Hutton (1969) was used to produce glass disks by fusing sample powders with a lithium tetraborate + lithium carbonate + lanthanum oxide flux. The glass disks were analysed in duplicate using the K-alpha line for each of the major rock-forming oxides. When both analyses were acceptable (sums 100±1%) and in close agreement, the reported analyses are the average of the duplicates.

(c) Selected trace element analysis (total rock):

XRF analysis of zinc, copper and nickel was carried out on pressed powder briquettes and relied on the K-alpha spectral line. The XSO7 programme of the Rhodes Geology Department was used to calculate Zn, Cu and Ni in the analysed samples.

APPENDIX C: FRACTAL GEOMETRY AND CORRECTION OF SAMPLED POWER-LAW DISTRIBUTIONS

C.1. Fractal Geometry as a Tool to Characterize Complex Form

The form of the natural world has been explained in terms of Euclid's ideal shapes and commonly invokes the concept of symmetry. The geometry of natural objects, scaling from atomic size to the universe, is central to the models we make in order to 'understand' nature (Feder, 1989). Euclidean ideals are fuelled by the human desire to find simplicity and order in nature, but in reality, the natural world is fashioned with irregularity and abounds with asymmetry (Hastings & Sugihara, 1993). In this regard, mathematics has failed to describe nature's form without oversimplification to common shapes (Lesmoir-Gordon *et al.*, 2000). Science has embraced a geometry that only rarely, if ever, describes shapes found in the real world (Lesmoir-Gordon *et al.*, 2000).

An important breakthrough was made by Mandelbrot (1967, 1975) when he discovered that fractal geometry could be used as a tool to describe irregular form. Mandelbrot (1977, p.16) coined the term "*fractal*" to explain sets that were fragmented and more irregular than those considered in classical geometry (Edgar, 1995). Fractals compliment classical geometry by providing a workable new middle ground between the excessive order of Euclidean geometry and true geometric chaos (Mandelbrot, 1989). In the account below, an attempt has been made to explain the fundamental aspects of fractal geometry by methodically building on basic concepts, and also by providing simple examples.

Consider a perfectly straight line of length 1 unit. If four lines, the standard 'building blocks' of Euclidean shapes, were arranged on a plane at right angles to one another, a square would be formed; if eight more lines were used, a 3-dimensional cube could be created with 12 edges, each 1 unit in length (s); both take up space in the relevant dimensions. When working with Euclidean shapes such as these, it is found that the area and volume calculations invoke power laws (Hastings & Sugihara, 1993). For example:

Area of a square 1 unit by 1 unit	$\mathbf{A = 1^2}$	*(or 1 ^ 2)*
(or any square s units by s units)	$A = s^2$	*(or s ^ 2)*
Volume of a cube 1 unit by 1 unit by 1 unit	$\mathbf{V = 1^3}$	*(or 1 ^ 3)*
(or any cube s units by s units by s units)	$V = s^3$	*(or s ^ 3)*

In these simple Euclidean examples the *scaling exponent* is the *dimension* of the object (i.e. a square is a 2-dimensional object; a cube a 3-dimensional object). This intuitive scaling exponent is referred to as the *topological dimension* (D_T) and is *always* an integer. It is possible then to formulate a power-law for the topological dimension where the number of miniature pieces in the final shape N, is equal to the scaling factor S, raised to the power of the topological dimension D_T (i.e. $N = S \wedge D_T$).

To take this one step further, imagine doubling the sides of both the square and the cube (see Table C.1*)*. These shapes would obviously be twice as large as the original square and cube respectively (i.e. sides of 2 units), but in all ways would still resemble the original shapes by having all sides the same length. Put another way, the large square could be made up of 4 copies of the original 1 unit by 1 unit square (i.e. area is $2^2 = 4$ 'square' units); the cube could be made up of 8 copies of the original cube measuring 1 unit by 1 unit by 1 unit (i.e. volume is $2^3 = 8$ 'cubic' units). When shapes like squares or cubes can be made up of reduced copies of the whole they are termed *self-similar* because they look the same over all ranges of scale (Mandelbrot, 1977; Hastings & Sugihara, 1993).

Returning to the topological dimension, it is possible to relate the concepts of dimension and self-similarity as follows: the topological dimension is mathematically defined as "the *scaling dimension* that measures the 'mass' (natural measure) of a *self-similar* set X in terms of the small-scale copies of X" (Hastings & Sugihara, 1993, p.29). So topological dimension relies on finding out how many scaled-down 'unit' copies of the whole are needed to fill the Euclidean shape of interest (Table C.1).

The topological dimension is not the only way of viewing dimension. Another line of reasoning can be employed, and focuses on "the manner in which shapes fill the space *around* them" (Lesmoir-Gordon *et al.*, 2000, p.24). This second take on dimension is known as the Hausdorff-Besicovitch dimension (D), after Hausdorff who first formulated it in 1919, and Besicovitch, who put it in its final form (Mandelbrot, 1977). Hastings & Sugihara (1993, p.27) describe this dimension in mathematical terms: "the Hausdorff-Besicovitch dimension measures the 'mass' (natural measure) of X in terms of Euclidean building blocks: open balls of a given radius". Fig. C.1 illustrates this concept, but in the case of a 1-dimensional, complex line it is more convenient to use 2-dimensional circles rather than spheres.

The most important difference between the topological dimension and the Hausdorff-Besicovitch dimension is that the latter *need not be an integer.* In the case of simple Euclidean shapes, such as the square or cube examined earlier, both definitions of dimension agree, so $D = D_T$, and D is an integer (Hastings & Sugihara, 1993). However, the two

Table C.1: The concept of topological dimension is illustrated in terms of some common Euclidean shapes. Also note how the larger shapes can be made up of a number of *self-similar* 'building blocks' (modified after Lesmoir-Gordon *et al.*, 2000, p.28).

	Building block	**Scaling factor = 2**	**Number of self-similar copies**	**Topological Dimension (D_T)**
Line		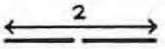	$2 = 2 \wedge 1$	1
Square	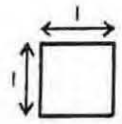	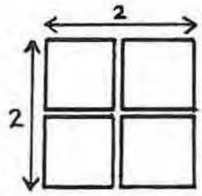	$4 = 2 \wedge 2$	2
Cube	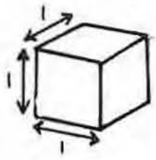	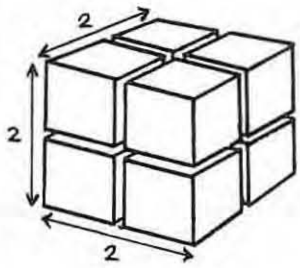	$8 = 2 \wedge 3$	3
General	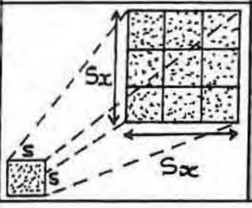	**Power Law relationship:** $N = S \wedge D_T$ $\therefore \log N = D_T \log S$		$D_T = \log N / \log S$

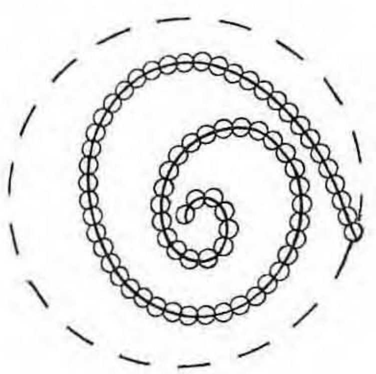

Fig. C.1: The Hausdorff-Besicovitch or fractal (D) dimension utilizes open spheres of a given radius to measure how much space any object takes up in the 3 dimensions of Euclidean geometry. In the case of a complex line we can simply use 2D circles rather than spheres. It takes a minimum of 71 small circles (could also be thought of as mathematical 'sets') to cover the entire length of this line, but only one large circle to completely enclose this complex shape. Obviously the smaller the radius of the circle the more you will need. The relationship between the number of circles it takes to cover the line and the circle size gives an approximation of how much space this line is taking up between the first (i.e. a perfectly straight line) and second (e.g. a circle) dimensions. This relationship turns out to be a power law, and for many natural objects the result of this procedure is a 'fractional dimension', commonly called the fractal dimension (D) (Illustration taken from Edgar, 1995, p.148, Fig. 6.1.2).

dimensions do not always coincide, and for many natural objects they seldom do (Hastings & Sugihara, 1993). If this situation arises, as in the case of more complicated, non-Euclidean forms, then D must be a fraction. The problem that arises though, and one that plagued mathematicians from the time the Hausdorff-Besicovitch dimension was first formulated, is how can an object have a fractional dimension and therefore lie in-between dimensions? It was Mandelbrot (1977) who first realized that most objects in nature have fractional dimension, and he called these non-Euclidean forms *fractal* (Lesmoir-Gordon *et al.*, 2000).

This realization led Mandelbrot (1977, p.15) to define a fractal "as a set for which the Hausdorff-Besicovitch dimension strictly exceeds the topological dimension" (i.e. $D>D_T$). To expand, fractals always possess self-similarity (strictly speaking) and scale-invariance. For practical purposes, these properties are useful because they can be measured. Mathematical sets with fractal geometry have some additional peculiarities: they have infinite detail, infinite length but finite area, and are devoid of smoothness or derivative (Lesmior-Gordon *et al.*, 2000).

When the Hausdorff-Besicovitch dimension is fractional, Mandlebrot (1977) suggested calling this scaling exponent, the *fractal dimension* (still denoted by D). The fractal dimension denotes sets where $D>D_T$ and avoids ambiguity with Hausdorff topological concepts (Mandlebrot, 1977). In practical application the fractal dimension is incredibly useful because it measures the degree of irregularity solely on the basis of self-similarity (Wei & Pengda, 2002). The power of using self-similarity is the ability to cut across scale, to look at the complexity of the whole without simplification (Gleick, 1988). In fractal geometry, complexity arises from the original self-similar, building blocks rather than the pattern building process itself (Hastings & Sugihara, 1993). This is in stark contrast to Euclidean geometry which utilizes simple building blocks but extremely complicated 'construction' mathematics to mimic complex form (Hastings & Sugihara, 1992). As Beck (2003, p.1) notes "infinity is implicit and invisible in the computations of calculus" but "explicit and graphically manifest in fractals."

In terms of a natural example, the irregular shape of any coastline is fractal and can be measured using fractal geometry. With increasing magnification, traditional Euclidean patterns would resolve into shapes that look more and more like straight lines in the limit. In fractal geometry zooming in on a particular stretch of coastline will result in ever increasing detail, but the degree of irregularity remains constant, whatever the scale of observation (Hastings & Sugihara, 1993). The irregular line defining the form of the coastline lies somewhere between the first and second dimensions because it fills more space than a straight 1-dimensional line, but less space than a 2-dimensional rectangle. As a result the shape of any coastline can be quantitatively described by its fractal dimension (e.g. the coastline of Britain has D = 1.26), and has an 'infinite' length (at least down to the atomic scale) which 'crowds' into a finite area (Gleick, 1988; Lesmoir-Gordon *et al.*, 2000).

The key to fractal geometry is using the right 'building blocks', scaled-down copies of the irregular fractals themselves (i.e self-similarity). It is possible to measure the irregularity of a shape or distribution through power laws, just as easily as measuring the dimension of regular objects in Euclidean geometry (Hastings & Sugihara, 1993). Wei & Pengda (2002, p.370) show that a general fractal model can be represented as a power-law relation in terms of a *discrete frequency distribution* of the following form:

$$Y \propto X^{F(D)} \qquad [1]$$

where X and Y are variables with different meaning; $\propto$ is proportionality and F(D) is the fractal dimension function. A simpler statistical fractal model is commonly employed in fractal analysis as follows (Wei & Pengda, 2002, p.370):

$$N(r) = Cr^{\pm D} + \varepsilon, \quad r > 0 \qquad [2]$$

where C is the constant of proportionality (prefactor parameter), r is a characteristic linear measure, D the fractal dimension, $N(r) = N(\leq r)$ [number of objects with characteristic linear measure $\leq r$] or $N(r) = N(\geq r)$ [number of objects with characteristic linear measure $\geq r$], and ε is a random variable. Thus equation [2] can be divided into two sub-models (Wei & Pengda, 2002, p.370) :

$$N(\leq r) = Cr^{+D} + \varepsilon, \quad r > 0 \qquad [2']$$

$$N(\geq r) = Cr^{-D} + \varepsilon, \quad r > 0 \qquad [2'']$$

It must be noted that the formal mathematical definition of a fractal (Mandelbrot, 1977) has been problematic, and even Mandelbrot (1983) has admitted that his definition may be too restrictive. A multitude of potentially useful 'borderline' fractals are excluded. Attempts have been made to repair the original definition but perhaps the most pragmatic suggestion has been to define fractals simply as "shape[s] made up of parts similar to the whole in some way"

(Feder, 1989, p.11). This definition captures the essential feature of scale independence, but is also broad enough to include the so called 'borderline' fractals with their weaker scale-invariant property of self-affinity. Self-affine fractals differ from standard fractals because they are not made up of simple scale-downed versions of the whole, but rather of components that require some systematic transformations in their geometry with scale change (Mandelbrot, 1983). The result when these types of fractals are analysed, is that the system appears to have different fractal dimensions at each scale, and so a description of the scaling properties requires additional parameters (Turcotte, 1997; Gillespie *et al.*, 1993). Gillespie *et al.* (1993, p.114) loosely define self-affine fractals "as consisting of a number of independent attributes, each of which may be scale independent with its own fractal dimension, but which combine to render the system scale dependent." Unless otherwise stated, fractal in this account is defined in the strict sense and infers self-similarity.

One of the other implications of the second more relaxed definition is that while fractals were originally defined with respect to dimension (i.e. $D>D_T$), the term fractal is now widely used to describe any system with a power-law distribution (e.g. Gutenberg-Richter relation for the frequency-magnitude statistics of earthquakes), even where there is no spatial reference (Turcotte, 1997; Gillespie *et al.*, 1999). In many modern-day applications the fractal dimension (D) does not only describe how a shape fills space but also how phenomena are *arranged* in space, so it is the *distribution* of elements that have *statistical self-similarity* across scale (e.g. size distribution).

The common theme of all fractals is that they result from dynamic 'growth' processes (Peitgen *et al.*, 1992). Although fractal patterns are frequently observed as static features, they provide clues to the dynamic nature of the system in which they formed and evolved (Kruhl, 1994a). Fortunately, most fractals result from very basic processes, but these simple "engines of change" result in elaborate and infinite complexity (Beck, 2003, p.2). Whether generated by computers or natural processes, fractal propagation is always the result of positive feedback. An input goes in one side, undergoes some form of slight modification (e.g. scaling and mapping), and comes out the other side as output. A fractal results when the output is fed back as input over and over again (i.e. recursion). A good natural example of this occurs during the dynamic process of faulting. The input is tectonic stress, the output is faulting, and the positive feedback loop develops during the course of deformation. Larger faults within the population and areas of higher fracture density become the loci of increased strain over time because they represent ever weakening and therefore more and more deformable portions of the brittle crust. The larger faults or fault zones grow at the expense of their smaller neighbours, and as a result, a fractal distribution in fault properties (e.g. spacing, size etc.) develops.

In the last decade, fractal geometry has increasingly penetrated into the everyday work of scientists and mathematicians (Lesmoir-Gordon *et al.*, 2000). Not least of all, fractal geometry has turned out to be an incredibly powerful tool for the geosciences (Kruhl, 1994a). Describing the form of the Earth has been a preoccupation of geologists for hundreds of years and it is common in geology to want to interpret macroscopic or microscopic events from observations made at different scales (Merceron & Velde, 1991). Fractals expand our ability to characterize, and importantly, to compare and extrapolate the complex structures and patterns that are so commonly displayed in the natural world, over very large scales.

Fractal theory has been applied to a wide range of geological phenomena (see Turcotte, 1997 for an overview), including mineral resource prediction (e.g. Turcotte, 1986a, 1989; Carlson, 1991; Blenkinsop, 1995; Blenkinsop & Sanderson, 1999; Wei & Pengda, 2002); geochemical and geophysical anomaly separation from background (e.g. Cheng *et al.*, 1994; Rantitsch, 2001); epicentre distribution and earthquake magnitude-frequency analysis and prediction (e.g. Kagan & Knopoff, 1980; Turcotte, 1991, 1994); and importantly for the oil industry, fault spacing and size frequency distributions below the limit of conventional seismic methods (Turcotte, 1986b, 1989; Yielding *et al.*, 1992).

C.2. Finite Range Correction in Power-Law Distributions

Simulations of data sets with "finite range effect" (e.g. Fig. 8.4), attributed to large-scale truncation of the sample, show that curve-fits in log-log space always yield D-values which are an overestimate of the true value (Pickering *et al.*, 1994, p 5). The correction method of Pickering *et al.* (1994, 1995) was employed in this study, for plots of the cumulative frequency function $N = C\, t^{-D}$, and is as follows:

$$\log N_C \approx \log N_E - D_E(\log t_{\max} - \log t_{\min}) \qquad [3]$$

[*in the basic form:* $y = c - m(x_{\max} - x_{\min})$]

where N_C is the number of veins with a thickness greater than t_{max} (i.e. in this case after finite range correction); N_E is an estimate of N_T, the number of veins with a thickness greater than the t_{min}; and where t_{max} and t_{min} are the vein-thickness range of the sample as shown in Fig. C.2 below. N_T can be estimated as N_E, as long as the condition $N_E >> N_C$ holds true. Because the fractal dimension D_T of the real vein-thickness population is unknown, an approximate estimate D_E must be made from the gradient of the line fitted to the affected data.

The method allows N_C to be estimated for each of the vein-thickness classes affected by finite range effect, and corrects for much of the bias incurred on log-log plots. In reality, the true distribution D-value is unknown, and so the correction is approximate and becomes increasingly more inaccurate as N_E and D_E become poor estimates of N_T and D_T respectively (Pickering *et al.*, 1994, 1995). Pickering *et al.* (1995) have proposed an iterative approach to estimating these parameters, and solve the potential problem of large starting inaccuracies in estimates of N_E and D_E.

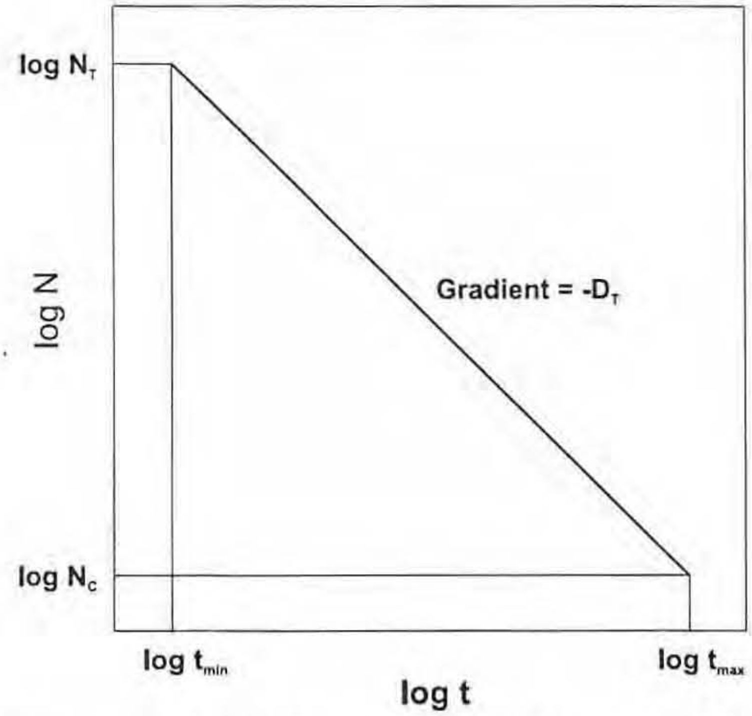

Fig. C.2: Log-log cumulative graph of a self similar sample from a power-law population with exponent D_T. The plot illustrates the parameters used in the Pickering *et al.* (1994, 1995) correction, where t is thickness in metres and N is cumulative number. In the correction of censored sample data, N_T and D_T must be estimated from the best-fit, straight line to the affected data, and are referred to as N_E and D_E respectively. If a sub-sample from t_{max} to t_{min} is taken, then N must take values from N_C to N_T. The geometry of the plot is used to estimate N_C as detailed in the text (modified after Pickering *et al.*, 1995, Fig. 4, p.7).

The iterative approach involves fitting a straight line to the affected data on a log-log plot, reading off the value of N_E at the t_{min}, and calculating the negative gradient D_E. These values are used in correction [3] to adjust all the data which lies below the original best-fit curve. A second curve is then fitted to the data points and refined estimates of N_E and D_E are gained.

These data are used as input in the next correction, and so on until completion. Once the majority of the bias has been removed, the correction will converge rapidly. The change in gradient D_E after each correction becomes increasingly smaller and has little effect on the value of N_C as the correlation coefficient (r) tends towards 1 (i.e. all data points lie perfectly along a straight line).

C.2.1. Synthetic Data Creation and Correction Procedure Testing

The true D-value of a vein thickness distribution in nature is always unknown. Consequently it is difficult to test the reliability of correction methods designed to yield accurate estimates of the fractal dimension. A synthetic data set was created in this study to test the cumulative frequency correction of Pickering *et al.* (1994, 1995), and so indirectly, assess the method when applied to real data.

A data set involving a population of 10,000 values with a vein thickness range from 1 to 10,000 mm, was generated in this study by using the following convenient power-law:

$$N = 10000 \times t^{-1.00} \qquad [4]$$

For each value of t between 1 and 10,000 mm a corresponding cumulative number, N, was calculated to yield a statistically ideal, fractal distribution with a D-value of -1.00 (see Fig. C.3; Table C.2 at end). A 10% sample was then taken from this population and only part of the vein-thickness range included (i.e. $1 \leq t \leq 100$ mm). The sample thickness range is effectively 2 orders of magnitude less than the population (i.e. truncated), but still yields a representative D-value of -1.

A simulation was then carried out to mimic finite range effect in the sample and incur right-hand fall-off in log-log space (Fig. C.4). In this study it is assumed that there is a greater probability for larger veins to be missed along a line transect of limited length during sampling. The effect on the large scale is profound because the cumulative number of larger veins is exponentially smaller than for very small veins. Only a linear increase in the rate of under-sampling with vein thickness, is required to produce severe right-hand fall-off. This relationship is illustrated in Fig. C.5 (below) and is expressed as follows:

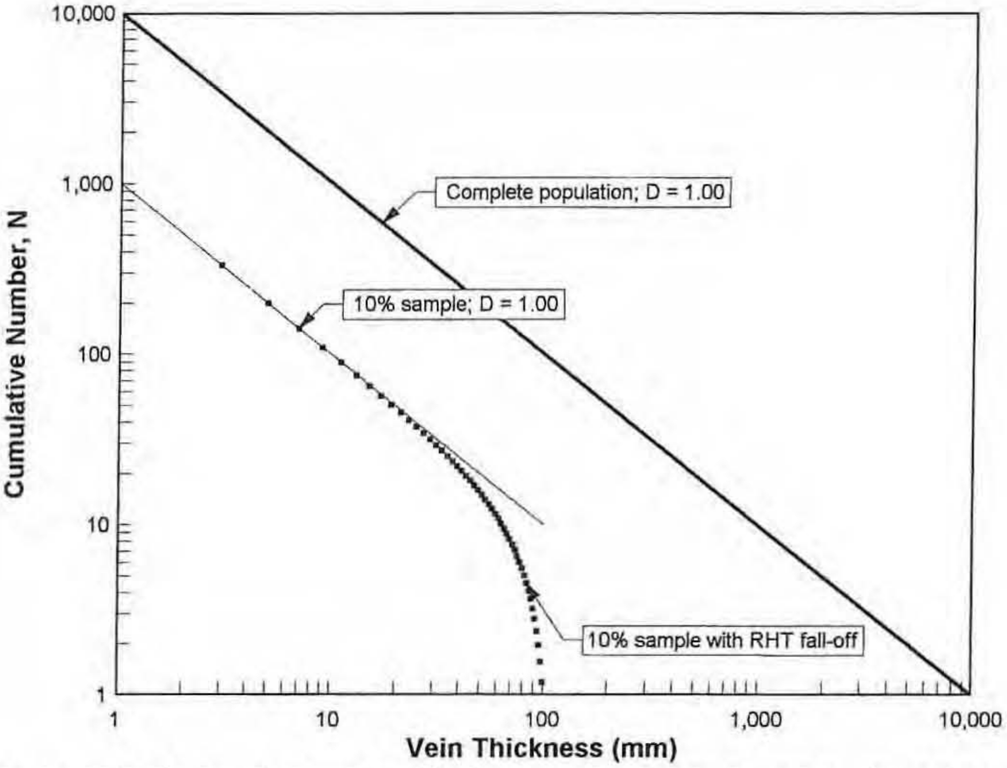

Fig. C.3: Log-log plots of cumulative number (N) versus vein thickness (t) for a synthetic data set showing a power-law distribution. The population has 10 000 values and a D-value of 1.00. The 10% sample without sampling error has a D-value of 1.00, although it only contains 1000 values and has a scale range of 1-100 mm. The sample has been affected by censoring at the large scale and shows right-hand fall-off of data which will bias least-squares, linear regression and hence D-value. The sample with censoring is equivalent to the unaffected sample with the 9 largest values removed.

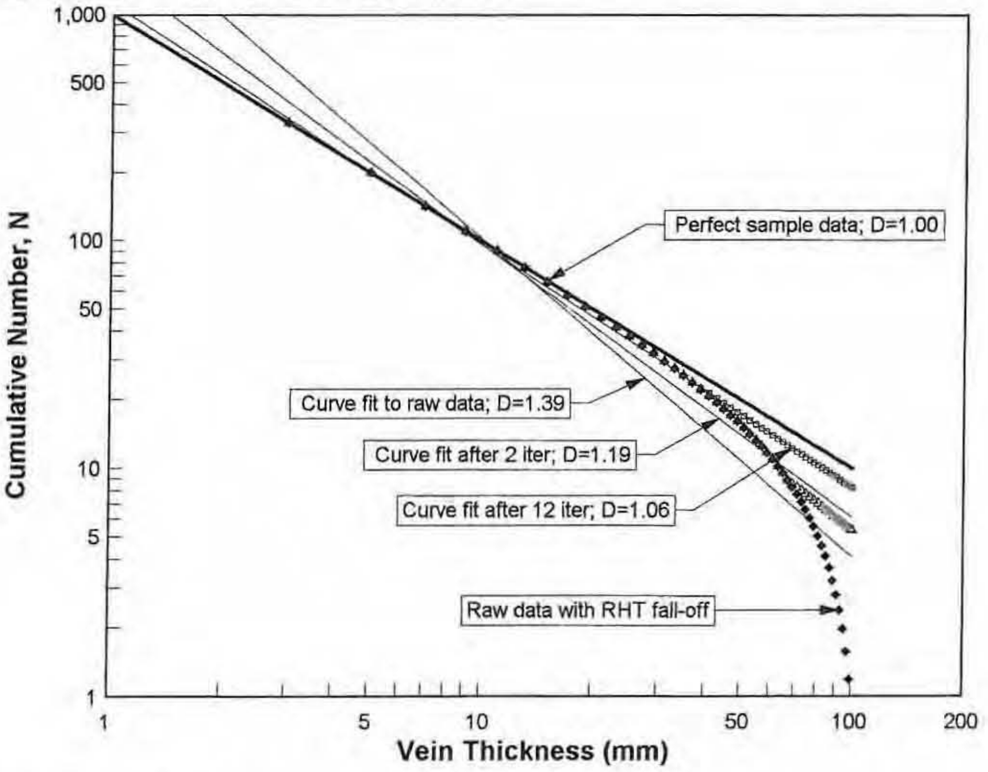

Fig. C.4: A series of plots for the 10% sample taken from Fig. C.3 above, showing successive correction for censoring. The line-fit to the raw data gave a D-value of 1.39, compared to the original population D-value of 1.00. After 12 iterations the correction converges and yields a D-value of 1.06.

$$y = \left(\frac{9}{99} \times t\right) - \frac{9}{99} \qquad [5]$$

[*in the basic form:* $y = mx + c$]

where y is the value of the under-sample and t is vein thickness. The value of y is subtracted from N for each of the vein thickness classes, and the data progressively affected as follows:

$$N_{righthand\ fall-off} = N_{unaffected} - \left(\frac{9}{99} \times t\right) - \frac{9}{99} \qquad [6]$$

When this method is applied to the synthetic sample, the desired right-hand fall-off of the data points is achieved (see Figs. C.3 and C.4; also Fig. 8.4).

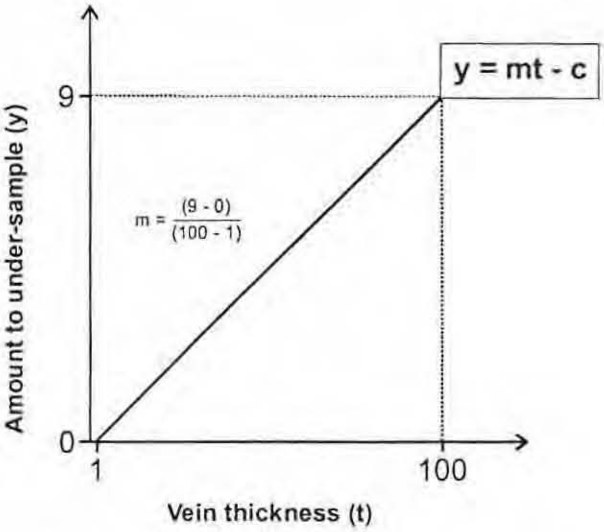

Fig. C.5: Linear relationship between the amount to under-sample, y, and vein thickness, t.

Fig. C.4 shows how the approach of Pickering *et al.* (1995) was used in a consecutive manner to correct the artificially biased sample, derived from the synthetic population with a fractal vein-thickness distribution. The first uncorrected estimate of D (1.39) is heavily biased compared to the population (1.00). However after only 12 iterations, the correction converges on a D-value of 1.06 (r=0.999687) with a standard deviation of 0.04. There is still slight bias in the D-value (i.e. D is a conservative estimate), but the fractal dimension is much closer to the true value of the population. It thus appears that the cumulative frequency correction method of Pickering *et al.* (1995) provides a reasonable estimate of the D-value when power-law data has been affected by finite range effect.

C.2.2. Quality of Power-Law Data after Finite Range Correction

Methods proposed to measure the quality of corrected power-law distributions rely on the results of comprehensive computer simulations, such as those carried out by Pickering *et al.* (1994,1995), because in natural studies the absolute D-value of a fractal population is always unknown. The simulations involve repeatedly taking samples of different size and scale range from a large artificial power-law distribution with a known D; if necessary correcting for finite range effect using the cumulative frequency method of Pickering *et al.* (1994, p.109); and then assessing the quality of the estimated sample D-values. The results of such simulations can be used to estimate:

(i) the *bias* in the corrected mean D-values of the samples compared to the known D-value of the artificial population (i.e. measure of accuracy); and

(ii) the *spread* of corrected D-values from their mean (i.e. measure of precision). The D-value spread has been assessed in two ways and involves either measuring confidence intervals (Pickering *et al.*, 1994, p.109), or the standard deviation of the D-value sample distribution (Pickering *et al.*, 1995, p.10).

The simulations have demonstrated that the mean bias in corrected D-values is always less than 5% (i.e. acceptable) when the cumulative frequency correction method is successful (i.e. correction converges), no matter what the sample size or scale range (Pickering *et al.*, 1995, p.11). From synthesis of the results of these simulations it was also possible to derive empirical relationships that link the confidence intervals or standard deviation of the D-value distribution to the sample size and population D-value as follows:

(a) Confidence Intervals

$$68\%\ Interval \approx \pm 0.075\sqrt{\frac{200}{sample\ size}} \times D \qquad [7a]$$

$$95\%\ Interval \approx \pm 0.15\sqrt{\frac{200}{sample\ size}} \times D \qquad [7b]$$

(b) Standard deviation

$$D \geq 1: \quad \sigma = kD\sqrt{\frac{1}{sample\ size}} \qquad [8a]$$

$$D < 1: \quad \sigma = k\sqrt{\frac{D}{sample\ size}} \qquad [8b]$$

Table C.3: Estimates of k value at different scale ranges for the cumulative frequency correction method of Pickering *et al.* (1995, Table 1, p.11).

Orders of magnitude covered by scale range of sample data	One order	Two orders	Three orders
Cumulative frequency method (finite range correction)	**k = 1.9**	**k = 1.2**	**k = 1.1**

In the simulations of Pickering *et al.* (1995), distributions were found to be approximately normal so that the 68% and 95% confidence limits corresponded to the values of $\pm\sigma$ and $\pm 2\sigma$ respectively. However in this study the relationship did not appear to hold and so both measures of spread were presented (see Table. 8.1). The estimates of standard deviation are probably a better gauge of the quality of the corrected D-value distribution than the confidence intervals because equations 8a and 8b include the additional variable k (Table C.3) which is dependent on the scale range of the sample.

Table C2: A synthetic vein-thickness data set was created to yield a D-value of 1 . A 10% sample was taken from this population but only part of the vein-thickness range was included (i.e. veins betweeen 1 and 100 mm in thickness). The sample data was then systematically adjusted (see text for details) to yield severe right-hand fall-off. The correction process of Pickering *et al.* (1995) was employed on this affected data and after 12 iterations the D-value converged on 1.06 (std. dev. = 0.04), close to that of the population.

N = C * t ^ -D	C =	10000
	D =	-1

	#1 SAMPLE CORR		#2 SAMPLE CORR		#3 SAMPLE CORR	
C =		2540.664		1793.972		1531.768
D =		1.395073		1.262347		1.199677
r		0.949056		0.985874		0.993315
threshold		t = 79mm		t = 69mm		t = 61mm

POPULATION		SAMPLE		SAMPLE W CENSOR		#1 SAMPLE CORR		#2 SAMPLE CORR		#3 SAMPLE CORR	
		10% of population (Range 1-100 mm)		*N values with simulated right-hand fall-off*							
t	N	t	N	t	N	t	N	t	N	t	N
1	10000	1	1000	1	1000	1	1000	1	1000	1	1000
3	3333.333	3	333.3333	3	333.1515	3	333.1515	3	333.1515	3	333.1515
5	2000	5	200	5	199.6364	5	199.6364	5	199.6364	5	199.6364
7	1428.571	7	142.8571	7	142.3117	7	142.3117	7	142.3117	7	142.3117
9	1111.111	9	111.1111	9	110.3838	9	110.3838	9	110.3838	9	110.3838
11	909.0909	11	90.90909	11	90	11	90	11	90	11	90
13	769.2308	13	76.92308	13	75.83217	13	75.83217	13	75.83217	13	75.83217
15	666.6667	15	66.66667	15	65.39394	15	65.39394	15	65.39394	15	65.39394
17	588.2353	17	58.82353	17	57.36898	17	57.36898	17	57.36898	17	57.36898
19	526.3158	19	52.63158	19	50.99522	19	50.99522	19	50.99522	19	50.99522
21	476.1905	21	47.61905	21	45.80087	21	45.80087	21	45.80087	21	45.80087
23	434.7826	23	43.47826	23	41.47826	23	41.47826	23	41.47826	23	41.47826
25	400	25	40	25	37.81818	25	37.81818	25	37.81818	25	37.81818
27	370.3704	27	37.03704	27	34.6734	27	34.6734	27	34.6734	27	34.6734
29	344.8276	29	34.48276	29	31.9373	29	31.9373	29	31.9373	29	31.9373
31	322.5806	31	32.25806	31	29.53079	31	29.53079	31	29.53079	31	29.53079
33	303.0303	33	30.30303	33	27.39394	33	27.39394	33	27.39394	33	27.39394
35	285.7143	35	28.57143	35	25.48052	35	25.48052	35	25.48052	35	25.48052
37	270.2703	37	27.02703	37	23.7543	37	23.7543	37	23.7543	37	23.7543
39	256.4103	39	25.64103	39	22.18648	39	22.18648	39	22.18648	39	22.18648
41	243.9024	41	24.39024	41	20.75388	41	20.75388	41	20.75388	41	20.75388
43	232.5581	43	23.25581	43	19.43763	43	19.43763	43	19.43763	43	19.43763
45	222.2222	45	22.22222	45	18.22222	45	18.22222	45	18.22222	45	18.22222
47	212.766	47	21.2766	47	17.09478	47	17.09478	47	17.09478	47	17.09478
49	204.0816	49	20.40816	49	16.04453	49	16.04453	49	16.04453	49	16.04453
51	196.0784	51	19.60784	51	15.06239	51	15.06239	51	15.06239	51	15.06239
53	188.6792	53	18.86792	53	14.14065	53	14.14065	53	14.14065	53	14.14065
55	181.8182	55	18.18182	55	13.27273	55	13.27273	55	13.27273	55	13.27273
57	175.4386	57	17.54386	57	12.45295	57	12.45295	57	12.45295	57	12.45295
59	169.4915	59	16.94915	59	11.67643	59	11.67643	59	11.67643	59	11.67643
61	163.9344	61	16.39344	61	10.9389	61	10.9389	61	10.9389	61	11.0503
63	158.7302	63	15.87302	63	10.23665	63	10.23665	63	10.23665	63	10.63079
65	153.8462	65	15.38462	65	9.566434	65	9.566434	65	9.566434	65	10.23959
67	149.2537	67	14.92537	67	8.925373	67	8.925373	67	8.925373	67	9.874003
69	144.9275	69	14.49275	69	8.310935	69	8.310935	69	8.561492	69	9.531653
71	140.8451	71	14.08451	71	7.720871	71	7.720871	71	8.258186	71	9.210456
73	136.9863	73	13.69863	73	7.153176	73	7.153176	73	7.973612	73	8.908562
75	133.3333	75	13.33333	75	6.606061	75	6.606061	75	7.706144	75	8.624329
77	129.8701	77	12.98701	77	6.077922	77	6.077922	77	7.45434	77	8.356293
79	126.5823	79	12.65823	79	5.567319	79	5.722936	79	7.216909	79	8.103145
81	123.4568	81	12.34568	81	5.072952	81	5.526769	81	6.992698	81	7.863712
83	120.4819	83	12.04819	83	4.593647	83	5.341869	83	6.78067	83	7.636939
85	117.6471	85	11.76471	85	4.128342	85	5.167339	85	6.579894	85	7.421876
87	114.9425	87	11.49425	87	3.676071	87	5.002376	87	6.389528	87	7.217662
89	112.3596	89	11.23596	89	3.235955	89	4.846251	89	6.208811	89	7.02352
91	109.8901	91	10.98901	91	2.807193	91	4.698308	91	6.037054	91	6.838743
93	107.5269	93	10.75269	93	2.389052	93	4.557953	93	5.873629	93	6.662688
95	105.2632	95	10.52632	95	1.980861	95	4.424645	95	5.717967	95	6.494768
97	103.0928	97	10.30928	97	1.582006	97	4.297893	97	5.569545	97	6.334449
99	101.0101	99	10.10101	99	1.191919	99	4.17725	99	5.427889	99	6.181239
100	100	100	10	100	1	100	4.11909	100	5.35946	100	6.107159
200	50										
300	33.33333										
400	25										
500	20										
600	16.66667										
700	14.28571										
800	12.5										
900	11.11111										
1000	10										
2000	5										
3000	3.333333										
4000	2.5										
5000	2										
6000	1.666667										
7000	1.428571										
8000	1.25										
9000	1.111111										
10000	1										

C = 1397.888
D = 1.16231
r 0.996167
threshold t = 57mm

#4 SAMPLE CORR

t	N
1	1000
3	333.1515
5	199.6364
7	142.3117
9	110.3838
11	90
13	75.83217
15	65.39394
17	57.36898
19	50.99522
21	45.80087
23	41.47826
25	37.81818
27	34.6734
29	31.9373
31	29.53079
33	27.39394
35	25.48052
37	23.7543
39	22.18648
41	20.75388
43	19.43763
45	18.22222
47	17.09478
49	16.04453
51	15.06239
53	14.14065
55	13.27273
57	12.72333
59	12.22342
61	11.75885
63	11.32609
65	10.92205
67	10.54403
69	10.18964
71	9.856791
73	9.543613
75	9.248455
77	8.969838
79	8.706441
81	8.457079
83	8.220684
85	7.996293
87	7.783035
89	7.58012
91	7.386831
93	7.202515
95	7.026575
97	6.858465
99	6.697687
100	6.619902

C = 1316.704
D = 1.137274
r 0.997547
threshold t = 53mm

#5 SAMPLE CORR

t	N
1	1000
3	333.1515
5	199.6364
7	142.3117
9	110.3838
11	90
13	75.83217
15	65.39394
17	57.36898
19	50.99522
21	45.80087
23	41.47826
25	37.81818
27	34.6734
29	31.9373
31	29.53079
33	27.39394
35	25.48052
37	23.7543
39	22.18648
41	20.75388
43	19.43763
45	18.22222
47	17.09478
49	16.04453
51	15.06239
53	14.40501
55	13.81079
57	13.26102
59	12.75099
61	12.27661
63	11.83435
65	11.42112
67	11.03419
69	10.67118
71	10.32999
73	10.00873
75	9.705756
77	9.419567
79	9.148836
81	8.892367
83	8.649085
85	8.418017
87	8.198284
89	7.989088
91	7.789703
93	7.59947
95	7.417783
97	7.244091
99	7.077889
100	6.997449

C = 1262.281
D = 1.119227
r 0.998314
threshold t = 49 mm

#6 SAMPLE CORR

t	N
1	1000
3	333.1515
5	199.6364
7	142.3117
9	110.3838
11	90
13	75.83217
15	65.39394
17	57.36898
19	50.99522
21	45.80087
23	41.47826
25	37.81818
27	34.6734
29	31.9373
31	29.53079
33	27.39394
35	25.48052
37	23.7543
39	22.18648
41	20.75388
43	19.43763
45	18.22222
47	17.09478
49	16.19729
51	15.48805
53	14.8354
55	14.23293
57	13.67517
59	13.1574
61	12.67553
63	12.22601
65	11.80575
67	11.41203
69	11.04246
71	10.69491
73	10.3675
75	10.05857
77	9.766612
79	9.490297
81	9.228419
83	8.979895
85	8.743746
87	8.519085
89	8.305109
91	8.101086
93	7.906349
95	7.72029
97	7.54235
99	7.372019
100	7.289559

C = 1223.269
D = 1.105543
r 0.998781
threshold t = 47mm

#7 SAMPLE CORR

t	N
1	1000
3	333.1515
5	199.6364
7	142.3117
9	110.3838
11	90
13	75.83217
15	65.39394
17	57.36898
19	50.99522
21	45.80087
23	41.47826
25	37.81818
27	34.6734
29	31.9373
31	29.53079
33	27.39394
35	25.48052
37	23.7543
39	22.18648
41	20.75388
43	19.43763
45	18.22222
47	17.33591
49	16.55534
51	15.8391
53	15.17964
55	14.57058
57	14.00643
59	13.48248
61	12.99463
63	12.53933
65	12.11348
67	11.71436
69	11.33955
71	10.98695
73	10.65465
75	10.34098
77	10.04445
79	9.763699
81	9.497526
83	9.24484
85	9.004657
87	8.776085
89	8.558315
91	8.350611
93	8.152301
95	7.962772
97	7.781462
99	7.607855
100	7.523792

C = 1193.915
D = 1.094787
r 0.999084
threshold t = 45mm

#8 SAMPLE CORR

t	N
1	1000
3	333.1515
5	199.6364
7	142.3117
9	110.3838
11	90
13	75.83217
15	65.39394
17	57.36898
19	50.99522
21	45.80087
23	41.47826
25	37.81818
27	34.6734
29	31.9373
31	29.53079
33	27.39394
35	25.48052
37	23.7543
39	22.18648
41	20.75388
43	19.43763
45	18.49513
47	17.63526
49	16.84877
51	16.12677
53	15.46173
55	14.84726
57	14.27789
59	13.74887
61	13.25614
63	12.79612
65	12.36571
67	11.96217
69	11.5831
71	11.22637
73	10.89008
75	10.57256
77	10.27229
79	9.987927
81	9.718254
83	9.462177
85	9.218708
87	8.986951
89	8.766091
91	8.555389
93	8.354169
95	8.161815
97	7.97776
99	7.801486
100	7.716117

C = 1171.089
D = 1.086106
r 0.99929
threshold t = 43mm

#9 SAMPLE CORR

t	N
1	1000
3	333.1515
5	199.6364
7	142.3117
9	110.3838
11	90
13	75.83217
15	65.39394
17	57.36898
19	50.99522
21	45.80087
23	41.47826
25	37.81818
27	34.6734
29	31.9373
31	29.53079
33	27.39394
35	25.48052
37	23.7543
39	22.18648
41	20.75388
43	19.70014
45	18.75103
47	17.88602
49	17.09453
51	16.36768
53	15.69795
55	15.07894
57	14.50518
59	13.97192
61	13.47509
63	13.01112
65	12.57689
67	12.16966
69	11.78702
71	11.42685
73	11.08723
75	10.76648
77	10.4631
79	10.17572
81	9.903122
83	9.644215
85	9.398005
87	9.16359
89	8.940153
91	8.72695
93	8.523304
95	8.328593
97	8.142249
99	7.963752
100	7.877295

C = 1152.856
D = 1.078942
r 0.999437
threshold t = 41mm

#10 SAMPLE CORR

t	N
1	1000
3	333.1515
5	199.6364
7	142.3117
9	110.3838
11	90
13	75.83217
15	65.39394
17	57.36898
19	50.99522
21	45.80087
23	41.47826
25	37.81818
27	34.6734
29	31.9373
31	29.53079
33	27.39394
35	25.48052
37	23.7543
39	22.18648
41	20.9737
43	19.92313
45	18.96946
47	18.10001
49	17.30421
51	16.57319
53	15.89944
55	15.27654
57	14.69902
59	14.16214
61	13.6618
63	13.19445
65	12.75696
67	12.34658
69	11.9609
71	11.59778
73	11.25533
75	10.93184
77	10.62579
79	10.33584
81	10.06076
83	9.799445
85	9.550901
87	9.314224
89	9.088594
91	8.873264
93	8.667553
95	8.470838
97	8.282549
99	8.10216
100	8.014777

C = 1137.956
D = 1.072917
r 0.999544
threshold t = 39

#11 SAMPLE CORR

t	N
1	1000
3	333.1515
5	199.6364
7	142.3117
9	110.3838
11	90
13	75.83217
15	65.39394
17	57.36898
19	50.99522
21	45.80087
23	41.47826
25	37.81818
27	34.6734
29	31.9373
31	29.53079
33	27.39394
35	25.48052
37	23.7543
39	22.33802
41	21.17102
43	20.11634
45	19.15866
47	18.28533
49	17.48577
51	16.75112
53	16.07386
55	15.44757
57	14.86678
59	14.32675
61	13.82338
63	13.35309
65	12.91277
67	12.49966
69	12.11135
71	11.74569
73	11.40077
75	11.0749
77	10.76656
79	10.47439
81	10.19715
83	9.933754
85	9.683192
87	9.44456
89	9.217034
91	8.999867
93	8.792372
95	8.593926
97	8.403955
99	8.221933
100	8.133751

C = 1125.544
D = 1.067774
r 0.999625
threshold t = 39

#12 SAMPLE CORR

t	N
1	1000
3	333.1515
5	199.6364
7	142.3117
9	110.3838
11	90
13	75.83217
15	65.39394
17	57.36898
19	50.99522
21	45.80087
23	41.47826
25	37.81818
27	34.6734
29	31.9373
31	29.53079
33	27.39394
35	25.48052
37	23.7543
39	22.51467
41	21.34393
43	20.2856
45	19.32438
47	18.44762
49	17.64475
51	16.9069
53	16.22654
55	15.59728
57	15.01362
59	14.47082
61	13.96478
63	13.49193
65	13.04912
67	12.63362
69	12.243
71	11.87511
73	11.52804
75	11.20009
77	10.88973
79	10.59562
81	10.3165
83	10.05128
85	9.798953
87	9.558612
89	9.32943
91	9.110655
93	8.901602
95	8.701642
97	8.510202
99	8.326753
100	8.237873

D-value after finite range correctiom

Best D-value Estimate = 1.063326
Corelation Coefficient = 0.999687

Quality of D-value after correction

Confidence Levels (+/-) based on final D		**Standard Deviation based on final D**
[68%]	**[95%]**	
0.04	**0.07**	**0.04**
[Pickering *et al.*, 1994]		[Pickering *et al.*, 1995]

EXAMINERS' REPORTS

TO WAYNE VILJOEN: Examiners' reports for your attention

Referee's report on MSs thesis
By Viljoen, W. (2005)
Geology, Structure and Mineralization of the Onguati Area, Karibib District, Central Namibia

RECOMMENDATION

The candidate should be congratulated for producing a MSc of high standard, that is well written with some excellent illustrations, revealing a thorough familiarity with the relevant literature. The amount and standard of work presented in this thesis is above and beyond the standard expected of a MSc, and the degree should be awarded *cum laude*. There are some minor editorial corrections with regards to the references, listed below.

Having stated that the MSc should be awarded, rather than graduate with a MSc, **I recommend that the candidate should up-grade to a PhD.** The research presented in this thesis is clearly of PhD standard; with some additional work on certain topics and some changes to existing chapters (listed below), this thesis should be resubmitted for examination as a PhD. I assume that Rhodes University has a mechanism whereby such a process is possible. Obviously such a course of action will require discussions with the candidate and his supervisor, but it would be an academic travesty if the candidate were not to be offered this opportunity.

Some minor corrections

There are some minor corrections with regards to the some of the references:

- → De Wit, 1998 on p. 33. 1996 in references ✓
- → Evans, 1997 on p. 36. Missing from references ✓
- → Hartmann et al, 1983 on p. 31. Missing from references ✓
- → Hawkesworth et al. 1983 on p. 23. 1986 in references ✓
- → Kasch, [illegible] 31. Missing from references ✓
- → Kroner, [illegible] on p. 20 and 24. Not in references (or should it be 1981a?) ✓
- → Mis[illegible]988 on p. 36. Missing from references ✓ M. Sc. THESIS ⇒ CHECK FILES ✓
- → ~~[illegible], 1977 on p. 13. Missing from references (or should it be 1979?)~~ ⇐ EXAMINER'S MISTAKE
- → Webb, 1992: missing author's initials ✓ KE.
- → 1 : 250 000 Omaruru Geological Sheet 2114 1997 on p. 38. 1996 in references ✓
- → 1 : 50 000 topo sheet 2115DD on p. 2. Missing from references ?

check + make corrections

REVIEW OF THE THESIS

Chapter 1 is an introduction to the location of the study area, previous geological work etc. while Chapter 2 is covers the geology and geodynamic evolution of the Damara orogen. The latter chapter is very thorough but could have been shortened by eliminating some of the background to the development of the currently accepted models. This review of the geology is continued in Chapter 3 where it concentrates on the Southern Central Zone. On p. 54, the candidate starts to present his own work, beginning with geophysical interpretation of the Karibib area. If I have one criticism of this MSc, it is that this introduction is slightly too long. However is does reflect his thoroughness in researching all relevant background material before embarking on his own work.

Not as long as it was!

When presenting his own work in Chapters 3 and 4 (the geology of the Onguati study area), he reveals the same thoroughness that he used to review the literature. The text gives detailed explanations, backed-up with maps, photographs and summary tables. Chapter 5 is a short interlude concerning calcite-dolomite solvus geothermometry. When I first read the thesis, this chapter seemed out of place; I would have expected the material in Chapter 6 to have followed on from Chapter 4. However as Chapter 6 leads into Chapter 7 which itself leads into Chapter 8 and then onto the ore genesis in Chapter 9, placing Chapter 5 anywhere else would disturb the later natural flow of the thesis.

Chapter 6 covers the structures at the deposits scale. This is a well illustrated chapter with some beautiful hand-drawn diagram. These reveal that the candidate has a good 3D vision of the structural geology and really understands the progressive deformation of the region. Chapter 7 is a relatively short chapter on hydrothermal vein mineralization providing new observations on field aspects and ore petrography, together with some mineral analyses. The candidate's findings show that, despite the work by previous workers, this is a potential area for further research. The fractal analysis of the veins is the topic of the longer Chapter 8 and is used to explain the development of the mineralised vein systems as well as differences in grades in various areas. This could have been enhanced by the inclusion of a diagram or diagrams schematically illustrating the proposed development of the vein system.

Chapter 9 examines previous models for ore genesis, showing their weaknesses. The candidate then presents a integrated model, utilizing evidence from the earlier chapters in the thesis, and shows its significance for further exploration.

The references are complete and require only some minor corrections. Apndiex A gives a short history of gold mining and exploration in the study area, Appendix B gives an outline of the geochemical analytical procedures used, and Appendix C gives a summary of fractal geometry and correction of sampled power-law distributions. Four geological maps are contained in folders at the back of the thesis.

SUGGESTIONS REGARDING A POSSIBLE UP-GRADE

Wayne – Check thru' this section, but you are not upgrading, therefore you need not make corrections; however there may be a comment that you could make in the thesis about these suggestion

Further research on topics

The candidate covers most of the topics in the thesis very thoroughly, but there are two chapters that offer the opportunity for further work. Chapter 5 on the calcite-dolomite solvus geothermometry could be broadened out into a more general investigation of the PTX conditions associated with the mineralization event or even the regional metamorphism. However, this may not contribute much to the main aims of the thesis. In this respect, it would be better to undertake further work on Chapter 7 which is about the hydrothermal vein mineralization. As it stands, this short chapter contains some new field observations and mineral analyses. It concludes that the veins at Onguati Mine and Western Workings may have developed at a different time and from different fluids to those at Brown Mountain. A more detailed study should produce results that could confirm whether this conclusion is correct. This work could them be integrated into the findings of the next chapter on fractal analysis which revealed differences between the vein systems in different areas.

p 3 of 6

Changes to existing chapter

In Chapter 6, the shape of the folds are analysed from drawings taken from photographs (viz. p. 128, Figs. 6.5 and 6.6). Such analysis requires construction of a fold profile prior to analysing the shape. The methodology of producing fold profiles is set out in Ramsay, J.G. and Huber, M. I. (1987) *The Techniques of Modern structural Geology. Volume 2: Folds and Fractures.* Session 18: Fold sections and profiles. p. 365-383. Academic Press, London.

The profile is a section across a fold that is normal to the fold plunge; this reveals the true shape of the fold. As the candidate has shown (p. 126, Fig. 6.3), the folds he analyses have shallow plunges, so the profiles he should be analysing should be near vertical, not the horizontal sections he actually analyses. A consequence of this is that the folds which are described as being isoclinal or tight may actually be close to open, and the conclusions regarding strain using Lisle's (1992) method are incorrect. Furthermore, very oblique sections through folds give the misimpression of the layering being transposed into the axial planar cleavage.

check

In this chapter the candidate interprets that shear zones and faults in terms of a dextral strike-slip system, using as evidence the angles between the fractures, and relating them to a *stress* direction. He analyses the veins in terms of Talbot's method for obtaining the minimum *strain* ellipsoid, referring to the veins being folded and boudinaged. One hand, he is invoking a brittle shear system and on the other hand ductile deformation. Essentially he is relating stress directions with finite strain directions, and he needs to be cautious about this. Apart from anything else, the orientation and angles between the shears in the dextral strike-slip system are those expected in a brittle system; any ductile deformation will result in the shears being rotated and the angles will change.

It would have been useful if the locality and orientations of photographs in Chapter 6 (and other chapters) were given as well as their orientations. This would assist the reader in visualising the orientation of the photographs with respect to the whole area. Also, on some of the excellent summaries of the structures, some of the plates seem to need to be rotated to get the correct perspective (unless I am not seeing them correctly):

Check these points, & modify if necessary

p. 99, plate 4.15: it seems that the plate has to be rotated anticlockwise by 90° to get the correct perspective. X PLATE CORRECT AS IS!

p. 103, plate 4:22: it seems that the plate has to be rotated clockwise by 90° to get the correct perspective. ✓ TRUE – DIFF. TO CHANGE.

p. 131, Fig. 6.11a: it seems that the plate has to be rotated clockwise by 180° to get the correct perspective. (Is there some reason why it is upside down? Is it being orientated with respect to the other plates?)

X PLATE CORRECT AS IS!

p4 of 6

Report on M Sc thesis titled' "Geology, structure and mineralization of the Onguati area, Karibib District, Namibia".

Candidate: Wayne Garreth Viljoen

This thesis is appropriately set out into an abstract, separate chapters, references and appendices that support the main text of the manuscript. The aims of the project as well as reasons for carrying out the work are clearly presented. An adequate number of analyses in the form of determination of minerals in thin section, chemical analyses using the electron microprobe as well as XRD analyses were carried out to show that the candidate is fully conversant with all these research methods and their application to his study area.

Chapters 2 and 3 give an inclusive yet comprehensive account of the Damara Orogen and the regional geology of Namibia, pertaining especially to the geology of the study area. The reader is kept informed of the main aspects of the stratigraphy and evolution of the regional geology, which are especially enhanced by air photo interpretation and the regional magnetic signature of the rock types in the area.

The descriptive account of lithologies and structures in the Western Workings, Brown Mountain and Onguati Mine area are exceptionally good. A big advantage to the reader is that one can clearly relate to the different aspects regarding rock types and structures being referred to in the text, from the Figures in the manuscript. More than an adequate number of readings have been presented on the appropriate stereograms, histograms and rosette diagrams, so as to convincingly give a statistically good average of all the structural data. Evidence from structural measurements in the Onguati area is correctly interpreted in the light of a strike-slip model in which the orientations of structures and veins fit a Riedel shear pattern of fractures. Veins are observed as hosts to copper-gold mineralization, similar to the Navachab Gold Mine, some 20 km to the south-west of the study area. Sketches of small and large-scale structures and their interpretation in the bigger picture are artistically and convincingly presented.

In his application of calcite-dolomite solvus geothermometry on the calcitic and dolomitic marbles of the Onguati area the candidate has impressively shown an understanding of how this system works, as well as being able to make sensible interpretations of the significance of the results in the regional context of the thermal history of the area.

The candidate has applied a fractal analysis to vein outcrops. He has been able to show that the "D-value" (representing the rate of size change across scale) can be attained from thickness and length measurements of veins systems, and applied in the interpretation of the irregular form and pattern of these vein systems. The "D-value" is also shown to be a powerful tool for predicting ore potential when dealing with hydrothermal systems of stockwork or large vein affinities.

p 5 of 6

An acceptable large-scale structural model that could explain hydrothermal activity that accessed a Riedel shear fracture pattern in the Onguati area is proposed by the candidate. Potential economic mineral occurrences were confined to openings in the more competent marble horizons where Cu-Au metals were transported as chloride and sulphide complexes, and precipitated in the vein systems. In a final summation of the work the candidate has proposed an all-embracing metamorphic devolatilization model which takes into account lithologies, structures and metamorphic zones on regional scales, where further potentially economic deposits are likely to occur, preferably in lower grade metamorphic rocks of the Damara Belt.

In my assessment of the thesis as a whole I have to commend the candidate on a job really well done. Not only has he made a very good impression with the quantity and quality of his field work, but he has also presented his data in a clear and unambiguous way. A lot of fundamentally sound, hard work has gone into this thesis. The fact that there are very few spelling or grammatical errors, and that the references are correctly presented warrants special merit, because it has made reading of this thesis so much easier for the examiner. I have no doubt that this thesis merits a distinction.

The following points, however, need attention:

1. Page 111 refers to an Appendix 4, but the manuscript did not include one ✓ ⇒ Appendix 'B'
2. A scale should be included either in the caption or as a bar scale on Figs 5.2 and 5.3 (photomicrographs).

✓ 3. Spelling mistakes – Table 2.3, under Trough infilling, Details – change "conglomeritic" to "conglomeratic". ✓

✓ - Page 32 second para, 5th line change "rang" to "range" ✓

✓ - Plate 4.9 In the caption change"befound" to "be found"

✓ -Page 125. second para 11th line, eliminate "the" from the sentence "Within individual the limbs of these folds…."

✓ -Page 152. In the Figure caption, change "principle" planes to "principal" planes.

✓ · Tectonized should be standardized throughout the text. It is correctly used on e.g. Figs 4.3 and 4.5, but spelt with an "s" in e.g. the second page of "Contents". ✓

· In the caption of the magnificent illustration of quartz veining and folding patterns of Fig. 6.15 and also shown as "a" in the frontal portion of the thesis, the word 'gossaneous" should be changed to"gossanous". This is a personal recommendation, although I have to admit that I cannot locate the word in the Glossary of Geology.

Attend to Correction

Gossanous correct

Dr P W K Booth
Geology Department
Nelson Mandela Metropolitan University,
Port Elizabeth

(9 March, 2005)

RS

p 6 of 6

Table of weighting of marks for MSc thesis, candidate W.G .Viljoen (P Booth)

Areas of consideration	**Weighting**	**Mark given**
Contextualisation, problem definition, planning	20	15
Methodological considerations and procedures	20	18
Knowledge of the field, the discipline and subject being researched (literature study)	40	35
Ability to develop and sustain an argument; strategic follow-through; focus	60	50
Validity and formulation of conclusions	30	25
Style and presentation	30	25
Total	200	168 (84%)

"Arrakis teaches the attitude of the knife – chopping off what's incomplete and saying: 'Now, it's complete because it's ended here'."

– From 'Dune' by Frank Herbert

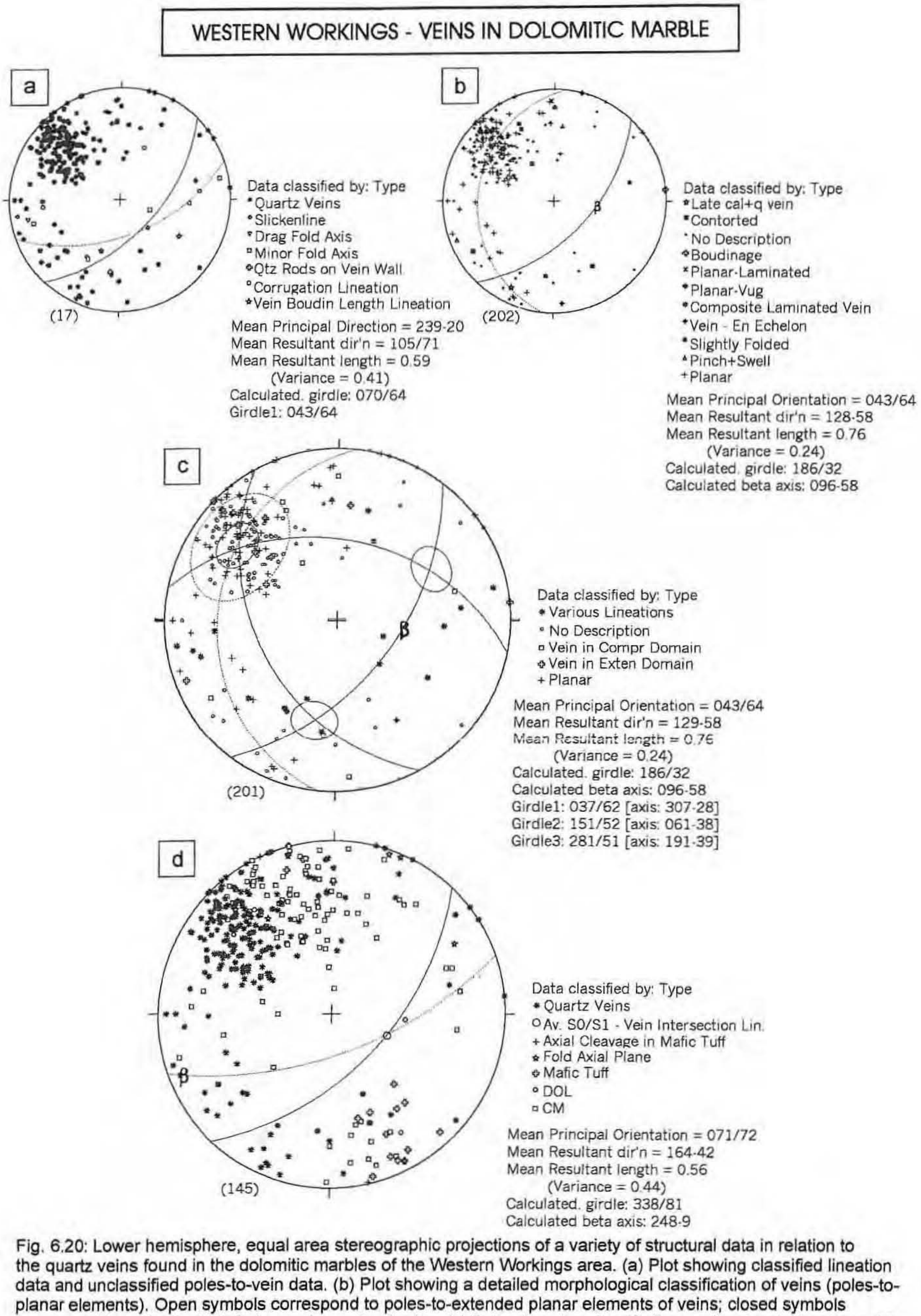

Fig. 6.20: Lower hemisphere, equal area stereographic projections of a variety of structural data in relation to the quartz veins found in the dolomitic marbles of the Western Workings area. (a) Plot showing classified lineation data and unclassified poles-to-vein data. (b) Plot showing a detailed morphological classification of veins (poles-to-planar elements). Open symbols correspond to poles-to-extended planar elements of veins; closed symbols correspond to poles-to-folded planar elements of veins. (c) Poles-to-veins classified according to whether the veins are found in extensional or compressional domains. Minor fold and corrugation fold axes (see plot a) are largely parallel or sub-parallel to the Y-axis. Method of Talbot (1970) used to determine orientation and shape of strain ellipsoid: $\psi_{xz} \approx 23°$, $\psi_{YZ} \approx 23°$; a ≈ 1.00, b ≈ 2.64; X = 061°-38°, Y = 192°-40°, Z = 307°-28° (trend-plunge of axes). (d) Poles-to-veins and poles-to-$S_{0,1}$ foliation defining an average intersection lineation of 108°-62° (trend-plunge).